Forschungszentrum Karlsruhe
in der Helmholtz-Gemeinschaft

Wissenschaftliche Berichte

FZKA 7521

Multi-scale, Coupled Reactor Physics/Thermal-Hydraulics System and Applications to the HPLWR 3 Pass Core

L. Monti

Institut für Kern- und Energietechnik

Oktober 2009

Forschungszentrum Karlsruhe
in der Helmholtz-Gemeinschaft
Wissenschaftliche Berichte
FZKA 7521

Multi-scale, coupled Reactor Physics / Thermal-Hydraulics system and applications to the HPLWR 3 Pass Core

Lanfranco Monti

Institut für Kern- und Energietechnik

von der Fakultät für Maschinenbau der Universität Karlsruhe (TH)
genehmigte Dissertation

Forschungszentrum Karlsruhe GmbH, Karlsruhe
2009

Forschungszentrum Karlsruhe GmbH
Postfach 3640, 76021 Karlsruhe

Mitglied der Hermann von Helmholtz-Gemeinschaft
Deutscher Forschungszentren (HGF)

ISSN 0947-8620

urn:nbn:de:0005-075219

Multi-scale, coupled Reactor Physics / Thermal-Hydraulics system and applications to the HPLWR 3 Pass Core

Zur Erlangung des akademischen Grades
Doktor der Ingenieurwissenschaften
der Fakultät für Maschinenbau
Universität Karlsruhe (TH)

genehmigte
Dissertation
von

Ing. Lanfranco Monti
aus Bologna (Italien)

Tag der mündlichen Prüfung:	9. November 2009
Hauptreferent:	Prof. Dr.-Ing. Thomas Schulenberg Forschungszentrum Karlsruhe Institut für Kern- und Energietechnik
Korreferent:	Prof. Dr.-Ing. Xu Cheng Universität Karlsruhe Institut für Fusionstechnologie und Reaktortechnik

To my family
Carlotta, Francesca, Carla

Zusammenfassung

Die innovativen Reaktorkonzepte, die gegenwärtig im Rahmen des Generation IV International Forum entwickelt werden, haben teilweise Eigenschaften, die sich signifikant von denen existierender Reaktoren unterscheiden. Der Stand der Technik für die Auslegung und die Sicherheitsanalysen ist daher nicht mehr vollständig ausreichend und neue Hilfsmittel werden benötigt.

Der High Performance Light Water Reactor (HPLWR) ist ein Beispiel für solch ein Generation IV Konzept und benötigt fortschrittliche Analyse Programme. Der Reaktor hat ein thermisches Neutronenspektrum und der Kern wird mit überkritischem Wasser gekühlt und moderiert. Die Aufheizung erfolgt in drei Stufen jeweils mit einer Zwischenvermischung des Kühlmittels. Durch die Wärmezufuhr der Aufwärmung verringert sich die Dichte des überkritischen Wassers stark. Deshalb kann die Rückwirkung der Reaktorphysik auf die Thermo-Hydraulik nicht vernachlässigt werden. Die Verteilung der Kühlmitteldichte im Kern verändert sich gemäß der Reaktivität und Verlustwahrscheinlichkeit der Neutronen in den verschieden Zonen des Kerns, während die unterschiedlichen Brennstofftemperaturen und entsprechend der Doppler-Effekt zunimmt, was in einer dreidimensionalen Rückkopplung resultiert, die die Leistungsverteilung im Kern verändert. Die stationären Betriebsbedingungen können nur mit einer Koppelung von Reaktorphysik und Thermohydraulik simuliert werden, so dass neue Hilfsprogramme entwickelt werden müssen.

Die gekoppelte neutronische/thermohydraulische Analyse wird mit eigenständigen Programmen durchgeführt, die nur die entsprechenden Daten miteinander austauschen. Die geplanten stationären Untersuchungen benötigen keine Festlegung des Zeitschrittes. Eine iterative Prozedur, in der die Programme parallel laufen, wurde ausgewählt, um die Kopplung zu ermöglichen. Die in dieser Arbeit vorgestellte Programmschnittstelle wurde in der Programmiersprache Perl geschrieben und dient dem Datenaustausch und der Vorbereitung der Eingabedatei, so dass die iterative Prozedur automatisch ablaufen kann. Die gewählte Programmiersprache ermöglicht eine einfache und flexible Nutzung der Programme, die entsprechend den spezifischen Anforderungen ausgewählt wurden und ausgetauscht werden können, um andere Geometrien des HPLWR oder andere Reaktorkonzepte zu untersuchen. Der untersuchte Reaktorkern benötigt 3D Modelle, die für die ausgewählten eigenständigen Programme entwickelt wurden. Der Quellcode der benutzen Hilfsprogramme wurde hinsichtlich der vorgesehenen Verwendung überprüft und die Simulationsergebnisse der einzelnen Tools wurde mit denen anderer Programme verglichen.

Nach dem Test der Kopplung wurde ein Ansatz ausgewählt, der Ergebnisse für den kompletten Kern liefert. Die gekoppelte Analyse basiert auf einer Auflösung jedes Brennelements im Kern.

Die starken Gradienten des Neutronenflusses im Kern zusammen mit den nicht unerheblichen Veränderungen der Stoffeigenschaften des Wassers während der Aufheizung, erfordern eine genauere Betrachtung als die gemittelte Analyse. Daher wurde der gesamte Kern unterkanalweise aufgelöst. Die Randbedingungen wurden aus der gekoppelten Rechnung verwendet. Dafür wurde die Brennstableistung aus der homogenen Leistungsverteilung rekonstruiert. Die Ergebnisse der Unterkanal-Analyse sind konsistent mit der gemittelten Analyse, liefern jedoch darüber hinaus lokale Hüllrohr- und Brennstofftemperaturen.

Die erbrachten Ergebnisse erscheinen physikalisch sinnvoll und wurden nach bestem Ingenieurverständnis bewertet. Es fehlt jedoc ein abschließender Vergleich mit Experimenten. Die getroffenen Vereinfachungen und Grenzen der Modellierung wurden diskutiert.

Die Ergebnisse zeigen einen neuen Detaillierungsgrad für die Kernauslegung und verringen erheblich die Anzahl der nötigen Annahmen, die im Vorfeld getroffen werden müssen und verbessern dadurch ganz wesentlich die Qualität und Zuverlässigkeit der Auslegungsrechnungen für das untersuchte HPLWR-Konzept.

Abstract

Innovative reactor concepts, currently under investigation within the Generation IV International Forum, present features which may differ significantly from those of existing reactors and may go beyond the current state-of-the-art approach used for design and safety investigations requiring to develop new analyses tools.

The High Performance Light Water Reactor (HPLWR) is an example of such a Generation IV reactor concept with additional requirements for advanced analyses tools; it is a thermal spectrum nuclear reactor cooled and moderated with light water operated at supercritical pressure. The pronounced water density reduction with the heat up, together with the multi-pass core design, results in a pronounced coupling between reactor physics and thermal-hydraulics core analyses which can not be neglected. The water density distribution within the core changes appreciably the reactivity and the leakage probability of the different core regions while the fuel temperature variations, and the associated actinides resonance broadening, results in 3D feedbacks distribution which modifies the power generation within the core. The steady state operative condition can be predicted only with coupled reactor physics / thermal-hydraulics analyses requiring the development of a new computational system.

The coupled reactor physics / thermal-hydraulics analysis has been addressed using available stand-alone codes and expressing the coupling via data exchange among them. The envisioned steady state investigations do not raise any question on the time step selection, and an iterative procedure, in which the codes are run in series, has been chosen to achieve the coupling. The developed code-to-code interfaces, written in Perl language, are devoted to data extraction and input file preparation, they enable automation of the iterative procedure. The selected programming language allows simplicity and high flexibility of these code interfaces which have problem dependencies but can be easily modified to apply this system to a different HPLWR design or even to other reactor concepts. The multi-pass core design demands 3D models which have been built for the available stand-alone codes. The selected tools have been checked for the current applications by means of code-to-code comparison and inspection of the source code.

After the initial testing of the coupled system, an approach to carry out whole core coupled analysis has been proposed and successfully applied obtaining promising results. These coupled analyses are based on a fuel assembly wise spatial representation of the core.

The pronounced neutron flux gradients within the multi-pass core, together with the considerable changes in water properties with the heat up, challenges the accuracy of these average values obtained with the coupled system and hence the whole core has been investigated at sub-channel resolution extracting the boundary conditions from the predicted operative condition. A pin-power reconstruction technique has been introduced to produce reliable input data for the sub-channel investigations. These results are consistent with those obtained by the previous coupled analyses and allow to predict local clad and fuel temperatures.

Physically sound trends have been observed and the results have been analyzed applying engineering judgment, nonetheless the remaining uncertainty of the results, which is affected by the discussed simplifications and limitations of the modeling, has not been verified against experimental data and additional qualification of the coupled system would be needed.

The obtained results represent a new quality in core analyses which drastically reduces the number of a priori assumptions involved in previous core analyses taking into consideration several multi-physics, multi-scale effects.

Acknowledgment

The high number of people I would like to thank for their support, advice and useful discussion is an evidence of how lucky I was in my experience within the Forschungzentrum Karlsruhe.

First of all, I would like to thank Professor Thomas Schulenberg, director of the Institute for Nuclear and Energy Technologies (IKET), for having accepted me as a PhD candidate in his Institute and allowing me to join the HPLWR European Project. I wish to thank him for his attention and continuous guidance during my three year research at the Institute.

I am also very grateful to Dr. Jörg Starflinger, my group leader at the Institute and Coordinator of the HPLWR European Project, for the many useful discussions not only on technical issues but also on professional aspects and organization matter. He always supported my interests for attending international courses and conferences.

I wish to thank Dr. Werner Maschek and all his group, in particular Fabrizio Gabrielli and Dr. Andrei Rineiski, for having treated me as a part of their group speeding up my learning and understanding. Special thanks go to Dr. Edgar Kiefhaber for the useful discussions we had covering all the multi-disciplinary topics that have to be considered simultaneously. In addition, he always provided a careful review of my presentations, papers and also of this manuscript, improving my understanding and also my writing style. It was always a pleasure to justify and defend my results with him.

I would like to mention here also Dr. Victor Hugo Sánchez Espinoza and his colleagues at the Institute for Neutron Physics and Reactor Technology (INR) for the useful and fruitful discussions we had. Special thanks go to Wadim Jäger for having shared with me the interesting topic of TRACE validation for supercritical water. I am also very thankful to Dr. Uwe Imke for his guidance into the sub-channel domain and into the source code of several codes.

I am also very grateful to the colleagues met within the HPLWR European Project. The progress meetings were for me a continuous motivation to advance the status of my research. I would like to thank Jochen Heinecke (AREVA NP GmbH) for sharing with me his experience in core design and analyses, Dr. Annalisa Manera (Paul Scherrer Institut, PSI) for the fruitful discussion on several topics, in particular regarding system codes, and Prof. Gérald Rimpault (Commissariat à l'Énergie Atomique, CEA) for his supervision and advice in the selection of the ERANOS calculation procedures.

I wish to thank all colleagues, PhD candidates, students, scientific researches and secretaries, for the nice and relaxed working atmosphere which was and is within the Institute.

Last but not least, I would like to thank also Professor Xu Cheng for having accepted me as one of his students at a very late status of my activities. His numerous comments were very useful to improve the present manuscript.

Contents

List of Symbols

c_p	specific heat capacity
$\chi(\vec{r}, E, E^\star)$	total fission neutron energy spectrum
d	diameter (clad)
d_H	hydraulic diameter
E	neutron energy
h	convective heat transfer coefficient HTC
k	thermal conductivity
k_∞	infinite multiplication factor
k_{eff}	effective multiplication factor
Nu	Nusselt number $\frac{hd_H}{k}$
$\nu(\vec{r}, E^\star)$	average number of total neutrons per fission
μ	dynamic viscosity of the fluid
$\widehat{\Omega}$	direction
p	fuel rod lattice pitch
$\frac{p}{d}$	lattice pitch to clad outside diameter ratio
$\Phi(\vec{r}, \widehat{\Omega}, E)$	neutron angular flux
$\phi(\vec{r})$	neutron total flux
Pr	Prandtl number $\frac{c_p \mu}{k}$
q''	heat flux
$q'''^\star$	volumetric energy deposition in the coolant
r	relaxation factor
$\vec{r}$	spatial position
Re	Reynolds number $\frac{\rho \vec{v} d_H}{\mu}$
$\rho(\vec{r})$	mass density
$\mathrm{S}(\alpha, \beta)$	scattering law for thermal neutrons
$\Sigma_x(\ldots)$	macroscopic XS for generic reaction x
$\Sigma_f(\vec{r}, E^\star, T)$	fission macroscopic XS
$\Sigma_s(\ldots \rightarrow \ldots)$	scattering kernel
$\Sigma_T(\vec{r}, E, T)$	total macroscopic XS
T	temperature
$\vec{v}$	velocity
V	volume
VR	velocity ratio

Chapter 1

Introduction

1.1 Supercritical water cooled reactors

The growth of the world wide energy demand and the increasing attention to a sustainable usage of the energy resources is resulting in a renaissance of nuclear technology. For this reason the Generation IV International Forum (GIF) [46] was started in July 2001. One of the six innovative reactor concepts proposed and analyzed within the GIF is the SuperCritical Water cooled Reactor (SCWR): a high-temperature, high-pressure water cooled reactor that operates above the thermodynamic critical point of water (647 K, 22.1 MPa).

The main application of SCWRs is efficient electricity production since they have a great potential to fulfill the goals of reducing electricity generation costs and capital cost as well as of better fuel utilization thanks to plant simplifications, reduced size of the components and higher turbine inlet enthalpy, resulting in a higher thermodynamic efficiency, compared to current Light Water Reactors (LWRs) as underlined by Oka and Koshizuka [108]. SCWRs are promising concepts because they rely on two existing technologies: LWRs and fossil fueled power plants operated with water at supercritical pressure [34].

For these innovative kind of reactors, because of both the high heat up and the abrupt changes in water thermophysical properties, the peak clad temperature has been identified as crucial technical issue which should be addressed carefully in the core design stage.

1.2 Brief description of the HPLWR 3 pass core

The object of the current analyses is the High Performance Light Water Reactor (HPLWR) [136, 140] which is a SCWR concept studied in a European framework by different associations [54]. The continuous improvements in core and system plant design are periodically reported by Starflinger et al. [142, 143, 144]. The HPLWR aims to a nominal electric power of 1000 MW. It is envisioned to be a thermal spectrum nuclear reactor cooled and moderated by water operated at a supercritical pressure. To boost the plant thermodynamic efficiency to values comparable to those of modern fossil fueled power plants, the coolant temperature is foreseen to rise of more than 200 K while flowing through the core but, thanks to the nominal pressure of 25 MPa, which is above the critical one of 22.1 MPa, no liquid-steam phase transition occurs while the coolant passes through the core. The issues related to the boiling-crisis, which have been a matter of concern in conventional LWRs, are hence eliminated permitting to aim to an enthalpy rise which is substantially higher than the one of presently operated LWRs.

The large enthalpy rise is a concern for the hottest sub-channel of the core, which can easily have local clad temperatures far beyond any reasonable material limit. The objective of the 3 pass core proposal by Schulenberg et al. [137] is to address this issue presenting a core design which

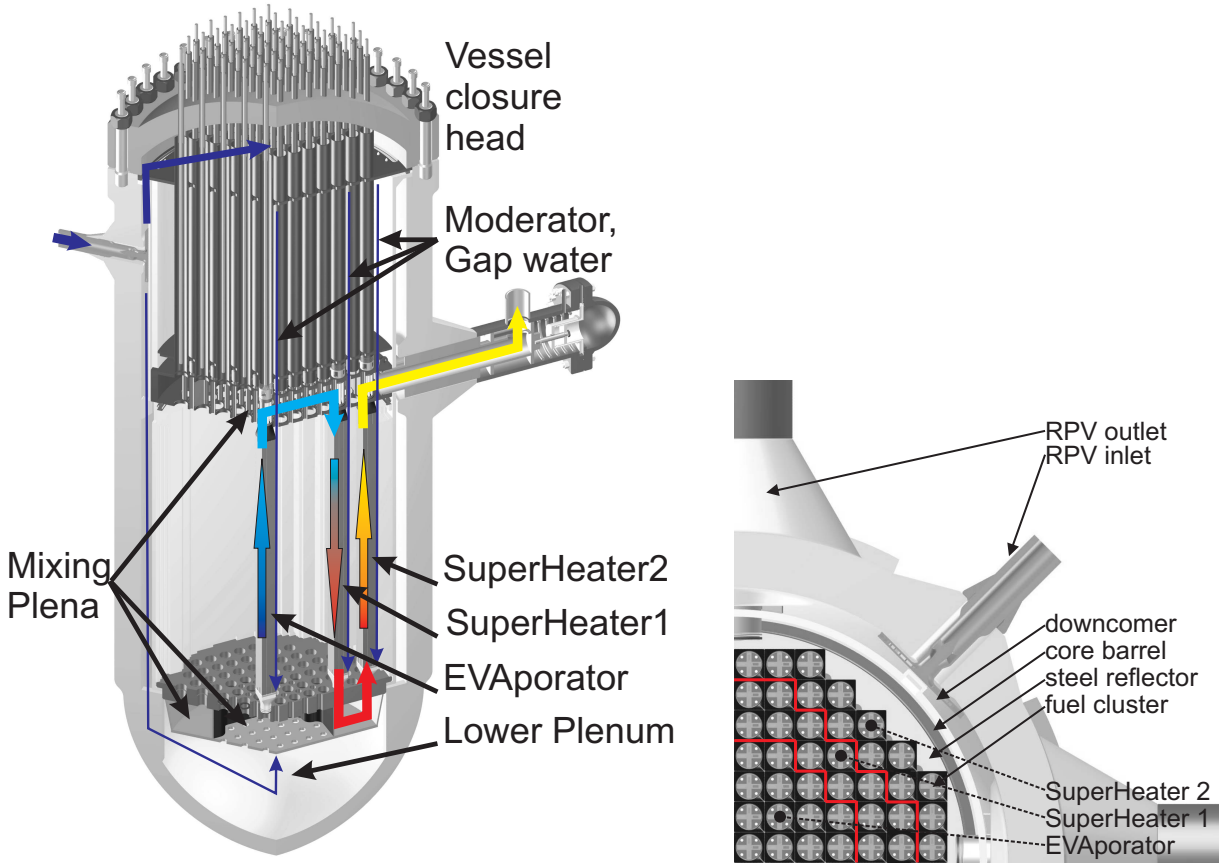

(a) Flow path description (b) Horizontal section

Figure 1.1: HPLWR core

is feasible using cladding materials available today. The basic idea is taken from supercritical fossil fired boilers: there, feed water is heated in a stepwise manner with intermediate mixing to avoid hot spots. In addition, where the water temperature is higher, and the margin to the maximum temperature of the structural material is smaller, the heat flux is reduced. In the HPLWR 3 pass core design the coolant enters the core 3 times in 3 concentric regions – named Evaporator (EVA), SuperHeater 1 (SH1) and SuperHeater 2 (SH2), respectively – which are envisioned to be operated at a different average power level, as described by Schulenberg et al. [137] and depicted in Figure 1.1.

The Reactor Pressure Vessel (RPV) and in-vessel components are already in an advanced design status. A 3D view of the RPV as proposed by Fischer et al. [44] is given in Figure 1.1(a). Also the spatial positioning of the RPV and necessary safety systems within the containment building have been investigated and a preliminary proposal is described with more details by de Marsac et al. [30]. Nonetheless the safety investigations of design basis accident and off normal transients are ongoing within the Working Package 3 of the HPLWR EU-Project [54]. Also the conventional island, the steam cycle and the plant control system are in an advanced design stage, as described by Herbell et al. [52], Schlagenhaufer et al. [135]. The feasibility of the 3 pass core concept is strongly dependent on the effectiveness of the coolant mixing between the heat up steps which should make the inlet temperature of each core region as uniform as possible. Special attention is hence given to the mixing chambers which are investigated with CFD methods by Wank et al. [154].

In order to have homogeneous in-core neutronics characteristics, despite the pronounced variations in water density, which reduces the dynamic complexity of a mixed neutron spectrum,

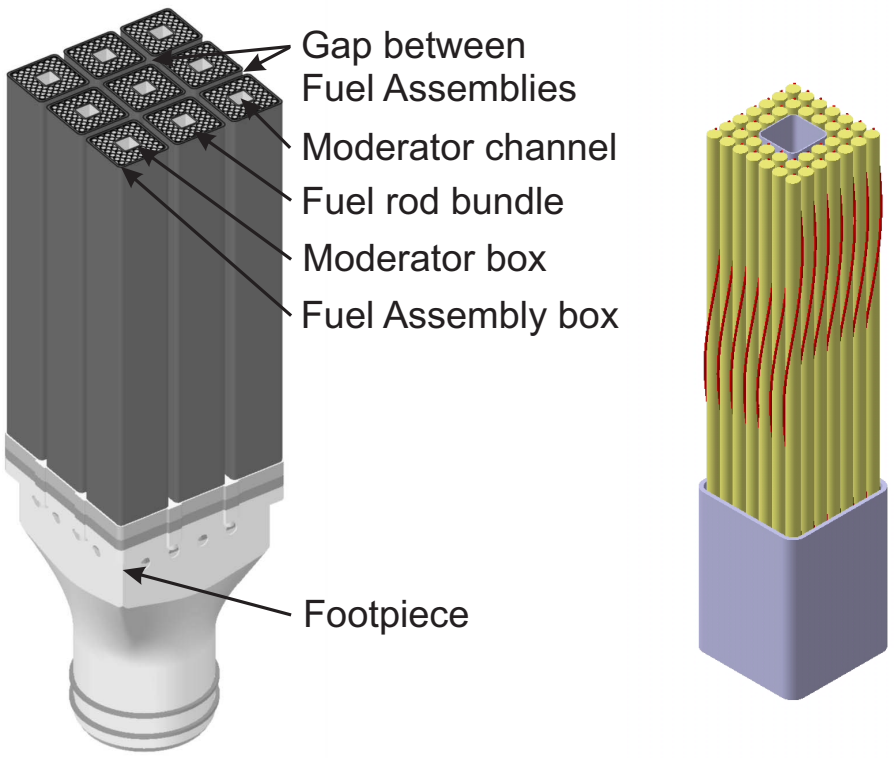

(a) Fuel cluster (CL) (b) Fuel assembly (FA)

Figure 1.2: HPLWR fuel element

loosely coupled core[1], as well as reasonably uniform in-core power distribution, to improve plant economics rising the fuel utilization factor, a thermal neutron spectrum is maintained in the whole HPLWR core with the addition of moderator water. This water at a fairly low temperature flows downward through in-core dedicated paths to rise the average water density, despite the pronounced coolant density reduction associated to the high enthalpy gain, improving neutron thermalization. Part of the RPV inlet water is guided upwards to the vessel closure head and then flows downward within the core. At the bottom of the core the moderator water is collected in the lower plenum through dedicated flow paths in the core support plate and mixed with the remaining fraction of the RPV inlet water to reconstitute the coolant flow rate, as shown in Figure 1.1(a). The coolant inlet temperature is hence determined by the mixing of the downcomer water and of moderator water, which has been heated during its flow through the core. The coolant enters for the first time in the core from the bottom of EVA and flows in upward direction; at the top of the core the coolant is collected in a plenum which is envisioned to homogenize its temperature. It reenters for the second time in the core from the top of SH1 flowing downward to another mixing chamber, located at the bottom of the core, from where it is redistributed to the third core region, SH2, where it flows upward and is finally driven outside of the RPV.

To have physically separated flow paths inside the core, boxes are used to wrap the fuel rods in equivalent channels with common inlet and outlet plena and sealings are envisioned to avoid undesired mixing of cold and hot water. It is desirable to minimize the box thickness because this reduces the mass of structural material inside the core as well as the neutron parasitic absorptions. But these boxes must withstand the pressure difference between moderator water and coolant[2]: to have a tolerable mechanical bending even with reduced wall thickness, the width of these boxes has to be kept short. A small, square, 7×7 fuel rod lattice has been proposed for the

[1] Which may exhibit spatial decoupling due to a small eigenvalue separation [1, 47, 113].

[2] Due to pressure drops during the flow and in the mixing chambers.

HPLWR Fuel Assembly (FA) by Hofmeister et al. [57]. The original design has been recently improved by insulating the boxes and reducing the amount of stainless steel by Herbell et al. [51]: these boxes separate and insulate the coolant, which flows in the fuel rod bundle, from moderator water, which flows downward both in the moderator channel, which occupies the inner 3×3 lattice position, and in the gap between adjacent FAs. Both are marked in Figure 1.2(a).

The tight fuel rod lattice has pitch - to - clad outside diameter ratio equal to 1.18 and allows the usage of wire-wraps as fuel rod spacers, depicted in red in Figure 1.2(b). They have been preferred to conventional grid spacers because of the efficient mixing for both up- and downward flow; the wire revolution is in counter-clockwise direction when observed from the top [55].

To simplify fuel handling, 9 FAs are grouped together with common head- and footpiece in the so called fuel CLuster (CL), as depicted in Figure 1.2(a). In each core region (EVA, SH1, SH2) there are 52 CLs, as shown in Figure 1.1(b), which have common inlet and outlet plena: the mixing chambers. Hence the coolant flow rate in the 468 parallel channels of each core region is physically determined in order to balance the pressure drops due to different heat up and flow velocity and it can be adjusted using adequate orifices dimensioning. Orifices are also necessary to ensure flow stability despite the pronounced density reduction of the coolant during the flow, as underlined by Ortega Gómez et al. [110].

1.3 Thesis objectives

The main purpose of the present thesis is to develop computational simulation tools able to analyze in detail design proposals of the HPLWR 3 pass core in order to provide an evaluation of the peak clad temperature in which only few uncertainties are involved. The prediction of the local temperatures corresponding to the full power, steady state condition is a key issue in answering the question of the feasibility of the HPLWR 3 pass core with currently available cladding materials raised by Schulenberg et al. [137] and such kind of methods are essential to evaluate if the proposed core design meets safety and economics requirements.

The prediction of the local clad temperature requires the knowledge of the power and water temperatures distribution within the core with a fine spatial resolution in which each fuel rod is represented. Due to the complexity of the HPLWR core design and the strong interactions between the reactor physics and thermal-hydraulics characteristics of the core, the numerical methods devoted to a high fidelity evaluation of clad temperatures require multi-physics, multi-scale core analyses as will be underlined in the successive sections and addressed in the whole thesis. The proposed core analyses, offering more realistic simulations, contributes to the reduction of conservatism currently still involved in the core design stage.

The innovative features of the HPLWR concept, beside challenging the available computational tools, require to consider sophisticated physical models while keeping into consideration the limitations of the available computational resources.

1.4 Multi-Physics core analyses

1.4.1 Background

Royer [129] reviewed current approaches for multi-physics simulations of LWRs which are mainly based on coupled Reactor Physics (RP) and Thermal-Hydraulics (TH) investigations, for both core and whole system. They generally include dedicated multi-dimensional RP and TH coupled codes while neglecting the possible interaction with the mechanical behavior of core components (e.g. core clamping systems, fuel assembly or control rod thermal expansion as well as fuel rod bowing and bending). In most cases, these tools have been developed and validated

for analyzing accidental transients of interest for LWRs core and plant safety, as underlined in the Reactor Physics Benchmarks of the Nuclear Energy Agency [105] and by Ivanov et al. [62].

In this section, the main physical reasons which require coupled RP/TH core analyses are explained using steady state equations and the necessity of this kind of analyses for HPLWR design studies is underlined.

RP usually considers criticality calculations to be independent from the thermal power at which the reactor is operated because the steady state linear transport equation (1.1) for the neutron angular flux, $\Phi(\vec{r},\widehat{\Omega},E) = vN(\vec{r},\widehat{\Omega},E)$, is a homogeneous equation and does not explicitly depend on the reactor power [6, 79][3].

$$\widehat{\Omega}\bullet\nabla\Phi(\vec{r},\widehat{\Omega},E)+\Sigma_T(\vec{r},E,T)\Phi(\vec{r},\widehat{\Omega},E) = \iint \Sigma_s(\vec{r},\widehat{\Omega}^\star,E^\star\rightarrow\widehat{\Omega},E,T)\Phi(\vec{r},\widehat{\Omega}^\star,E^\star)\,\mathrm{d}\widehat{\Omega}^\star\,\mathrm{d}E^\star + \frac{1}{k_{\mathrm{eff}}}\iint \chi(\vec{r},E,E^\star)\nu(\vec{r},E^\star)\Sigma_f(\vec{r},E^\star,T)\Phi(\vec{r},\widehat{\Omega}^\star,E^\star)\,\mathrm{d}\widehat{\Omega}^\star\,\mathrm{d}E^\star \quad (1.1)$$

In reality, the geometrical dimensions of the media as well as the macroscopic XSs are functions of the medium temperature T, and hence of the neutron flux introducing non-linearities in the solution of the transport equation. The medium temperature T changes both the *atomic density* and the *thermal motion of the nuclei* originating feedbacks on the neutron transport equation whose complete description is provided in most RP textbooks, e.g. by Stacey [141], and is well beyond the scope of this introductory section. Nonetheless the main physical reasons, which will be considered in the present analyses, are illustrated here:

- the atomic density of the coolant or moderator determines the slowing down of neutrons from the high energy range of the fission source[4] to the low energy range typical of the thermal equilibrium with the medium [5];

- the neutron scattering law, i.e. the energy loss/gain per collision, depends on the medium temperature which determines the mentioned thermal equilibrium, especially for light and chemically bound atoms like hydrogen in water;

- the fuel temperature, modifying the thermal motion of the heavy isotopes, changes the Doppler broadening of the resonances and hence the absorption probability[6].

For these reasons the neutron transport equation is coupled with the steady state energy equations (1.2, 1.3) which determine the temperature distribution of the core components for the given power map, as presented by Todreas and Kazimi [148]. In a heterogeneous nuclear reactor, the heat generated is mainly deposited inside the fuel rods, equation (1.2), from which it is transferred by thermal conduction, convection and radiation to the cooling medium. Neglecting the compressibility, the thermal expansion and the dissipation term, the steady state energy equation for a single phase working fluid, like supercritical water, simplifies to the form given in

[3] The presence of delayed neutrons is not considered in the present analyses.

[4] The average energy of the prompt fission neutrons is around 2 MeV [37].

[5] At a room temperature of 293 K, the thermal energy is 0.0253 eV which corresponds to a neutron velocity of 2200 m/s.

[6] Thermal expansion of the fuel, besides reducing its atomic density and expanding its volume, may result in fuel-clad interactions which change the HTC of the gas-filled gap between fuel pellet and clad. Also geometry modifications can be induced, e.g. fuel rod bowing, requiring additional coupling with mechanical analyses and fuel performance tools [36].

equation (1.3).

$$\nabla \cdot k \nabla T_{\text{fuel}}(\vec{r}) = \bar{E} \Sigma_f \phi(\vec{r}) \tag{1.2}$$

$$\nabla \cdot \vec{v} \rho(\vec{r}) c_p T_{\text{coolant}}(\vec{r}) = q'''^{\star} - \nabla \cdot \vec{q''} \tag{1.3}$$

The left hand side of equation (1.3) represents the spatial change of the fluid enthalpy while the right hand side contains the volumetric energy deposition in the coolant, $q'''^{\star}$, and the heat flux from the fuel rods, q'', which couples the energy equations in the fuel and in the coolant through the definition of the heat transfer coefficient of the boundary layer h:

$$q'' = h\,(T_{\text{clad}} - T_{\text{bulk}}) \tag{1.4}$$

In a nuclear reactor, the volumetric energy deposition in the coolant is mainly due to neutron moderation and gamma ray absorption; since it is only a small fraction of the fission energy deposition, this term is generally neglected.

The temperatures of the various materials within the core are dependent on the in-core power distribution which is actually modified by the change in the material properties requiring a coupled analysis also for the determination of the steady state operative condition. In addition, large temperature gradients may cause mechanical deformations, and hence core geometry changes, adding further complexity to the considered analyses.

For all those cases in which the constituents temperature variations are small and have minor feedbacks, it is possible to neglect this coupling – at least when operative temperatures are used – and to approximate the full power condition with un-coupled reactor physics analyses as defined by Cho [25]. This is the conventional approach for steady state analyses of current LWRs [3, 16, 45, 73] and fast breeder reactors [47, 91] but this assumption is already no longer valid for detailed analyses of conventional BWRs, as underlined by Weber et al. [157], in which the coolant phase change introduces important modifications in the macroscopic XSs resulting in a pronounced bottom peak in the power shape which deviates from the un-coupled solution of PWRs, the well known “cosine” axial power shape [80].

The solution of the criticality and energy equations is hence a coupled problem also for steady state analyses, as described by Duderstadt and Hamilton [37], Chapter 13, which can be tackled with an iterative approach, e.g., at first the neutron transport equation (1.1) is solved assuming the components temperature distribution within the core which is successively recalculated solving the energy equations (1.2, 1.3) with the just calculated core power map and this procedure is iterated until the desired convergence has been reached. A quite comprehensive description of the principles which governs the coupling can be found in [38, 39, 40].

1.4.2 HPLWR core analyses

When considering HPLWR core analyses, since supercritical water behaves as single phase fluid, the coolant density exhibits a continuous, but strongly nonlinear, reduction with its temperature rise – from 553 K to approximately 773 K – while it flows through the core, as shown in Figure 1.3. The density reduction amounts to almost 90% with respect to the inlet condition and modifies substantially the neutron slowing down capabilities of the coolant while it flows through the core. Since the coolant flow path in the HPLWR core consists of a series of successive steps, its properties in the superheaters depend on the experienced heat up, introducing pronounced spatial effects. Also the neutron spectrum will depend on the core position and, since it is desired to operate the 3 core regions (EVA, SH1 and SH2) at different power levels, also the fuel temperature will be position dependent.

For these reasons, detailed studies of the HPLWR core require to go beyond the current state-of-the-art analysis tools used for design and optimization purposes of presently operated

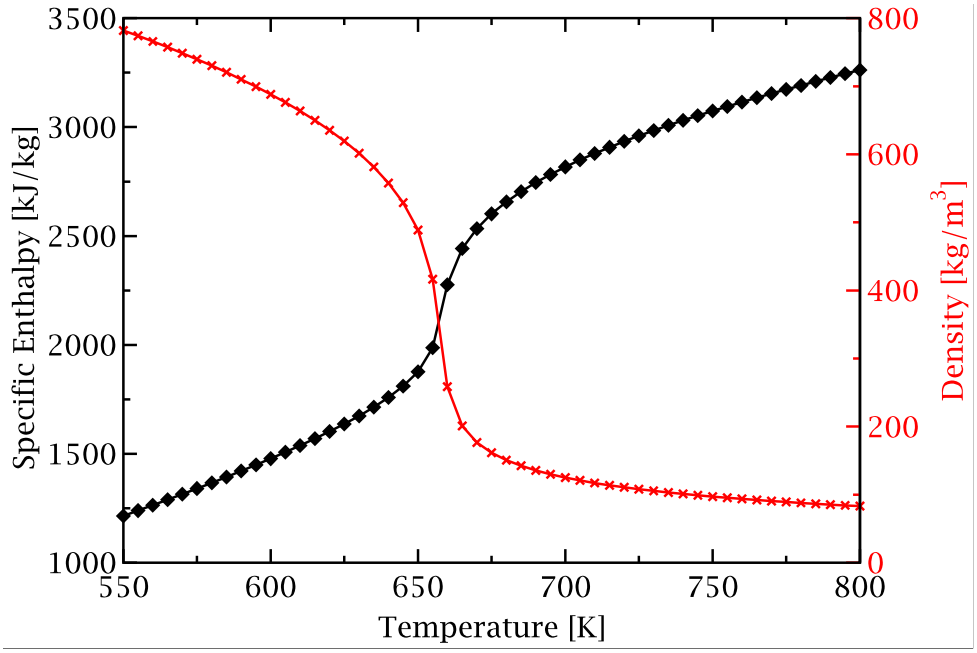

Figure 1.3: Water properties at 25 MPa

LWRs; among these, consistent 3D RP/TH coupled analyses play an important role to model the space dependent TH feedbacks on the full power operative condition, as underlined for other SCWR concepts by Oka [107].

1.5 State-of-the-art: coupled Reactor Physics / Thermal-Hydraulics analyses

1.5.1 3D core analyses for safety and design purposes

Several ambitious projects in the reactor multi-physics analyses field – such as the NUclear REactor SIMulations (NURESIM/NURISP) in Europe [19, 20], the Numerical Nuclear Reactor (NNR) in the framework of a collaboration between United States and Republic of Korea [157, 158] or the Nuclear Energy Advanced Modeling and Simulation (NEAMS)[7] program of the U.S. Department of Energy [36, 106] – have been launched to develop powerful simulation platforms. The main objectives are to enhance the prediction capability of the computations and to provide modern tools for nuclear engineering. The trend is now to use best-estimate approach as much as possible in conjunction with sensitivity and uncertainty analysis for both safety and design analyses.

Ivanov [60] and Royer [129] provided details on the coupling strategies and methodologies finalized to multi-physics analyses of nuclear reactors; here they are briefly summarized.

- The domain of investigation may vary depending on the considered analyses, the quantities of interest and the available computational resources; the main possibilities are:
  - TH plant model and RP core model.
  - RP and TH core models using operating conditions data as boundary conditions.
  - TH plant model (e.g. primary circuit) and RP/TH core model which uses detailed 3D RP model coupled with simplified feedback TH model (generally 1D models for BWRs and 0D for PWRs).

[7] Which include SHARP: coupled RP TH analyses with UNIC and NEK500 [41, 139].

- The coupling between the codes can be realized as internal, merging them in an integrated multi-physics code, or as external, introducing data exchange among the codes by using a coupling software. The latter requires little or no modification of the selected codes facilitating the coupling procedure even if this method may exhibit numerical instabilities and slow convergence especially for dynamic investigations.

- Both one- and two-way coupling approaches have been widely used in the past. The first type is used for zooming or post-processing a given condition, e.g. sub-channel investigations of the hot fuel assembly, while the two-way coupling is desired to represent mutual feedback effects.

- Spatial mesh overlays and time steps algorithms have to be defined, generally by projection techniques, since each model may use its own nodalization and time scale.

- The convergence evaluation requires special attention when considering dynamic analyses with externally coupled codes because a loosely coupled approach, in which each code is fully converged, may result in an unstable solution scheme. Steady state conditions offer the possibility to evaluate the convergence of the calculation by comparing among the iterations and, in practice, relaxation techniques are very useful to speed-up the convergence between TH and RP.

Coupled methods for transient and safety analyses

The state-of-the-art core analyses have generally neglected two-way coupled RP/TH analyses for design of conventional PWRs but the scientific community is aware of the fact that this approximation is no longer valid when considering transients which deviate substantially from the nominal operative condition since the coupling between RP and TH is then more pronounced, e.g. Aniel-Buchheit [2], Ivanov et al. [63]. During the last fifteen years, great efforts have been put in incorporating 3D reactor core models into system transient analysis codes to obtain more realistic safety evaluations of the interactions between the core behavior and the plant dynamics. Various international and national projects were devoted to this purpose e.g. Bousbia-Salah and D'Auria [11], Hu et al. [58], Jackson et al. [66], Kozmenkov et al. [77]. Recent advances in the state-of-the-art coupled analysis finalized to safety evaluation have been collected in two special issues of international journals edited by Ivanov and Sartori [64, 65].

These efforts are mainly dedicated to the investigations of complex transients in which there is a coupled core-plant interaction and are aiming at a best-estimate evaluation of the components temperature for assessment of the whole plant safety, as described by Ivanov and Avramova [61].

Coupled methods for design analyses

The evaluations of steady state multi-physics design conditions are easier to compute because the time-coupling can be ignored and some operating conditions data are directly used as boundary conditions (e.g. RPV inlet mass flow rate and power level).

As underlined in subsection 1.4.2, coupled RP/TH analyses are mandatory for the HPLWR concept not only for safety investigation but also for design purposes and feasibility studies. This additional requirement exceeding the current state-of-the-art core design is shared by other SCWR concepts which have been analyzed both worldwide, e.g. Bae et al. [5], Buongiorno [15], MacDonald et al. [85], Maráczy et al. [87], Reiss et al. [119], Rimpault [123], Yamaji et al. [163], Yoo et al. [166] and within the Forschungszentrum Karlsruhe, e.g. Broeders et al. [12], Mori [98], Vogt et al. [153]. Some of them are reviewed here:

Broeders et al. [12] reported an efficient coupling of the KAPROS system (TWODANT) with RELAP5, in order to model the whole reactor system while using a single channel representation for the core. An on-line generation technique for the necessary multi-group XSs is used. Sensitivity studies to the group structure, ranging from 4 to 69 groups, and to the relaxation factor, used to damp the pronounced oscillations of the power shape in successive iterations, are also presented.

MacDonald et al. [85] reported the feasibility studies of the SCWR project in the US. These studies are focused on multi-physics, multi-scale analyses ranging from whole system behavior to the hot sub-channel investigations but are generally based on a one-way coupling to analyze single fuel assembly and to evaluate peak clad and fuel temperatures. Burn-up studies have also been performed with the MOCUP utility.

Maráczy et al. [87] coupled the 3D, 2 groups diffusion code GLOBUS with the 1D TH code SPROD to analyze the HPLWR 3 pass core with the KARATE program system. The RP model uses a fine spatial resolution in which each fuel assembly is modeled independently. Homogenized tabulated XS are prepared with the MULTICELL transport code as a function of several operating parameters including both TH feedbacks and irradiation history. The GLOBUS nodal code uses interpolated XSs to reduce the computational time needed to perform whole core analyses. A preliminary core loading strategy and control rods positioning schema have been proposed. Concerning the TH analyses, their accuracy is affected by the impossibility to model mass flow redistribution among the various fuel assemblies.

Mori [98] proposed a design for a fast spectrum SCWR on the basis of MCNP core analyses coupled with a TH code capable to generate steady state fuel pin and core TH data.

Reiss et al. [119] coupled MCNP5 with an in-house TH module to determine the steady state equilibrium parameters of a nominal fuel assembly. Additional multi-physics investigations including burn-up effects, evaluated with ORIGEN-S, are also presented.

Rimpault [123] proposed a detailed RP model with the ERANOS system, using both 2D and 3D core calculations for steady state and burn-up investigations together with reactivity equivalence methods for control rods modeling. These accurate RP analyses are coupled with simplified TH calculations based on enthalpy balance, which have been implemented in the ERANOS system to calculate the coolant temperature variations. Cell calculations are performed at the beginning of the analysis to generate the necessary multi-group self-shielded XSs parameterized as function of the coolant temperature, no interpolation scheme has been applied since the closest tabulated temperature is automatically selected.

Vogt et al. [153] developed a 3D coupled RP/TH system, based on the usage of MCNP5 and an in-house TH code, which is able to perform detailed two-way coupling for a reactor concept quite similar to a single pass HPLWR. MCNP5 predicts the 3D core power map which is input into the TH code to determine, together with the mass flow redistribution among the considered parallel channels, the coolant and moderator densities and temperature as well as the fuel temperature variations. In this way the most important TH feedbacks, as described in section 1.4, can be modeled.

Neutron cross-section for coupled calculations

RP/TH coupled calculations generally use 3D neutron kinetics models based on the usage of deterministic tools for the solution of neutron transport or diffusion equation, as described by Ivanov et al. [59], Pautz and Birkhofer [114]. These tools require XS data homogenized on the

assembly level which are generally provided in a set of parameterized 2-group XSs. The usage of these XS lookup tables requires to apply interpolation procedures, at least on a 2D basis as a function of moderator density and fuel temperature. These pre-tabulated XSs must cover the expected range of parameters variations for both nominal and off-nominal conditions.

Watson and Ivanov [155] propose a high order table lookup method to improve the accuracy of the XS modeling for transient applications. Higher order scheme are necessary to overcome the interdependence, i.e. the cross term effect, between different TH feedback parameters which can not be predicted by polynomial fitting procedures.

1.5.2 Multi-scale methodologies for design analyses: from 3D core calculations to pin-by-pin spatial resolution

Since water at supercritical pressure behaves like single phase fluid over the whole operation temperature range, there is no phenomenon associated with the boiling crisis or burnout unlike in current LWRs [148]. For this reason, peak clad surface temperature is a crucial design criterion rather than departure from nucleate boiling, dry out or critical power ratio. Because of the high enthalpy rise and large density change of the coolant, local evaluations of the fuel rod clad temperatures are mandatory to verify and improve the core design, as current approach for other SCWRs [164, 167]. Whole core models used for 3D core analyses may not have sufficient spatial resolution to predict local effects: TH analyses based on equivalent channel approach, generally used at the core design stage, may not be able to predict accurately peak clad temperatures.

For SCWR design, the large changes in the thermophysical properties of water add challenges to whole core analyses requiring finer spatial resolution than used for conventional LWRs, as underlined by Yoo et al. [167]. This necessity is enhanced by the pronounced heterogeneity of the HPLWR FA, depicted in Figure 1.2, which will make precise prediction of core characteristics more difficult from the viewpoint both of RP properties (e.g. non uniform pin-power distribution) and of TH investigations (e.g. coexistence of heating and cooling conditions for the coolant adjacent to the FA walls). These effects will be even more accentuated that those identified by Tada et al. [145] for BWR analyses.

It is hence important to include detailed pin-by-pin investigations also at the present design stage, in order to predict the effects of local power distribution on the maximum clad temperature and to permit design improvements.

For conventional LWRs, whose FAs are well optimized, the effects of spatial flux gradients on the radial pin-power distribution used for sub-channel investigations are not very pronounced and coupled neutronic / sub-channel investigations can be performed at pin level for a single fuel assembly obtaining reasonable results, as the one described by Sánchez Espinoza et al. [132, 133].

Concerning HPLWR applications, since the core will inevitably present pronounced neutron flux gradients at the interface between the 3 core regions (EVA, SH1 and SH2), these have to be taken into consideration to achieve accurate prediction of the power distribution and of the associated *operating* clad temperature. To calculate local quantities, while keeping the computational time reasonably low[8], several techniques have been proposed and are widely used. In the next sections, an approach for obtaining the power distribution in each fuel pin and for performing the refined TH analyses will be presented shortly.

Pin-power reconstruction

Deterministic tools used for RP core analyses employ spatially homogenized XSs for each fuel element and, thus, nodal methods can provide only a smoothly varying flux distribution

[8] As needed for feasibility and design studies.

within each node which are not able to predict the effects of local heterogeneity of the FA, as explained by Rempe and Smith [120]. In contrast, even if Monte Carlo techniques can perform analyses of a heterogeneous core to obtain a pin-wise power distribution, these types of calculations are extremely time consuming, as underlined in [14, 153], mainly because each particle crosses a lot of surfaces before being absorbed, a very high number of histories has to be followed to achieve the desired precision when employing small tally - to - total volume ratios and hundreds of materials have to be defined to accurately model temperature feedbacks.

For these reasons, pin-power reconstruction techniques have been developed to obtain the power distribution at pin level from the one calculated for whole core analyses. Most of the models assume that the detailed pin-by-pin distribution can be approximated by the product of a global homogenized intranodal distribution and a local heterogeneous form function [120]:

$$\phi_{\text{pin-wise}}(\vec{r}) = \phi_{\text{homogeneous}}(\vec{r}) \cdot \phi_{\text{form function}}(\vec{r}) \tag{1.5}$$

where

$\phi_{\textbf{homogeneous}}(\vec{r})$ represents the neutron flux shape obtained from 3D whole core analysis and the associated spatial gradients

$\phi_{\textbf{form function}}(\vec{r})$ represents the local lattice heterogeneity and is predicted with 2D/3D single fuel assembly heterogeneous analysis

In HPLWR applications the form function must account for the pronounced FA heterogeneity, namely for the non uniform neutron thermalization in the coolant/moderator water and for the parasitic absorption in the boxes, in addition to the fuel rod lattice structure.

Examples of the applications of these techniques are widely available in the literature, detailed illustrations are provided by Tohjoh et al. [150], Yamamoto and Ikeno [165].

Sub-channel wise core investigations

Several tools are nowadays available for rod bundle TH analyses [41], among them the most promising are CFD tools to solve the Reynolds averaged Navier-Stokes equation, porous media and sub-channel approaches; the last two are described in more details by Sha [138], Todreas and Kazimi [149].

Traditionally, sub-channel investigations, which are the most widely used for nuclear reactor applications, were limited to selected regions of the core using either nominal flow and power conditions or a one-way coupling approach to zoom in a region of interest. The results obtained were successively corrected by means of the so called “hot channel factor”, which was not rarely even greater than 2 as explained by Carelli and Friedland [17], Chelemer et al. [21]. Nowadays with the rise of the computational power and the optimization of the analysis tools [27, 48], whole core analyses can be performed using the sub-channel approach going towards a best-estimate core analysis which drastically reduce the number of approximations and uncertainties determining the “hot channel factor”.

Detailed sub-channel investigations are generally associated with pin-power reconstruction techniques to have higher confidence in the accuracy of the results, as underlined by Jiménez et al. [72], Wende et al. [159].

1.6 Work plan

1.6.1 Application to HPLWR core analyses

To develop a computational tool capable to predict the local operating clad temperatures with the available computational resources, a multi-step approach, similar to the one discussed by

Yamamoto and Ikeno [165], is proposed:

1. initially, the full power core operative condition should be determined with a two-way coupling between steady state RP and TH calculations which, taking into consideration the main TH feedbacks, predicts FA-wise average parameters;

2. successively the obtained node-average condition should be investigated to sub-channel spatial resolution applying a one-way coupling to zoom in each FA in order to provide local, i.e. pin-wise, clad and fuel temperature distribution necessary to define the critical point of the current design and to suggest improvements.

This implicitly assumes that the effects of local TH properties have negligible impact on whole core RP analyses already coupled with coarse node averaged feedbacks. For the current feasibility study, this assumption is of no concern, especially when considering the additional limitations of the considered methodology, but for future reactor licensing more effort will have to be devoted to the quantification also of the local feedbacks.

Since none of the described tools is able to perform such analysis which aims to achieve a much more detailed spatial resolution than that conventionally obtained for reactor design, a new computational system has to be developed. In the framework of a three year research period, an approach with progressive stages is advisable to guarantee advancement checking and gradual improvements which will be based on the achieved results. For this reason, it was decided to use well-established, stand alone codes for RP and TH analyses and to focus on the new analysis strategies and methodologies which have to be considered and developed.

As a first step, numerical codes have to be selected and verified separately for HPLWR applications. The initial tests, beside allowing the user to gain experience with the codes and with the innovative features of the HPLWR, should concentrate on the key quantities needed for the successive coupled applications and on the verification of their sensitivity and consistency to the input parameters.

The qualification of the stand alone codes and considered models for HPLWR applications is a robust basis on which the coupled system can be developed creating the necessary codes interface and defining a calculation procedure. The coupling is achieved by iterating between static RP and TH calculations until a self-consistent solution is found with a heuristic procedure, similar to that described by Duderstadt and Hamilton [37]. Due to the non-linearity of the considered analyses, a mathematical model of the decoupling between RP and TH has not been developed. Despite the problem complexity, engineering judgment is applied to the inspection of the changes in the physical properties among successive iterations. The coupling of the codes is achieved externally, treating the codes as separate processes, and is expressed by the data exchange between them using external processing functions. The programming effort is finalized to the automation of the iterative procedure including successive codes runs, data extraction (post-processing) and input file preparation (pre-processing) using Bash and Perl languages in a Linux environment. These processing scripts operate by means of uniquely defined key-words in the input files and have been developed considering the format of the output files. Since the majority of CPU time is absorbed by the code runs, an internal coupling is not considered; the coupled system is hence independent from the stand alone code versions[9]. The developed coupling methodology is initially applied to a simplified case to understand in details the various aspects of the coupling. Successively, a methodology is proposed to investigate the whole HPLWR core with the coupled system, covering the first step of the proposed approach obtaining the full power operative condition in which the TH properties and power generation are consistent.

Once that the boundary conditions for whole core investigations are available, the one-way coupling, including pin-power reconstruction and sub-channel analyses of the core, has to be

[9]For example, the update of ERANOS from version 2.0 to 2.1 and successive TRACE v5.0 releases.

derived covering the second step of the proposed approach. Additional mapping scheme have to be introduced to go from the fuel element to the pin resolution and adequate visualization tools for results interpretation are requested. The developed methodology for pin-power reconstruction, based on the theoretical approach mentioned previously, combines the 3D full core analyses at fuel element resolution with detailed heterogeneous investigations of the single fuel elements by using a proper mapping schema. Once the power map at pin level is available, the remaining boundary conditions – such as inlet coolant mass flow and temperature for each FA – can be extracted from whole core TH analyses to complete the input data for the detailed sub-channel investigations.

The development of an independent computational system based on codes not already employed within the HPLWR EU-Project [54, 87, 152] is of particular importance for the analyses of such an innovative reactor concept because it provides the possibility to verify the quality of the obtained results. For the current design stage, since no experimental data are available yet, the assessment of the obtained results has to rely on code-to-code comparisons like the one reported by Rimpault et al. [124] and performed during initial investigations of the HPLWR concept supported by the fifth Framework Programme of the European Commission. For these reasons, a new analysis methodology has been autonomously developed and different computational tools have been selected; they will be described in the following section.

1.6.2 Selected computational tools

As underlined by Jiménez et al. [72], many codes and models have to be used for multi-physics, multi-scale core analyses. The selected computational tools will be introduced and presented in this section, identifying the application domain of each one. More details on these codes will be provided in the dedicated sections.

Reactor Physics codes

MCNP5 The usage of Monte Carlo codes, such as MCNP5 by Brown et al. [13], for neutronic analyses is becoming widespread mainly thanks to its accurate and detailed geometry representation capabilities as well as to a continuous energy treatment but also due to the rise of the available computational resources. This code is a superb tool for detailed investigations of complex geometries for determining local quantities as well as for verification and validation of other codes accuracy. Unfortunately, whole core analyses using a heterogeneous geometry description providing a detailed prediction of the power map, as necessary for HPLWR analyses, are by far too time consuming on a single machine and require complex geometry set up to include detailed TH feedbacks on neutron transport.

ERANOS To easily perform RP analyses of the HPLWR core on a single machine, it is necessary to choose a deterministic approach for the solution of the neutron transport equation. ERANOS [125, 131] has been selected because it is a whole core neutron transport code consisting of various modules which use a common interface and are dedicated to different purposes: this system is capable to perform both XSs processing and 3D core calculations. This allows to go beyond the 2 energy groups structure, i.e. with a fast and a thermal group, most widely used in conjunction with the diffusion approximation [87], and gives the flexibility to choose an independent energy group structure to perform 3D transport calculations.

Although this system of codes was designed for fast reactors, it has already been successfully tested for LWR applications [7, 31, 104] as well as applied to thermal systems [26, 101].

Thermal-Hydraulics codes

TRACE The reference best-estimate reactor systems codes developed by the US NRC for analyzing transient and steady state RP/TH behavior in LWRs, namely TRACE [58, 99, 100], has been selected because of its flexibility and growing applicability. TRACE is the product of a long term effort to combine the capabilities of the NRC's four main systems codes (TRAC-P, TRAC-B, RELAP5 and RAMONA) into one modernized computational tool. It uses a component-based approach to model a reactor system and has automatic steady state and dump/restart capabilities. It offers the possibility to use a steam table for the thermodynamic properties of water in the IAPWS format [147].

TRACE applications to HPLWR analyses may take advantage of the work performed by Jäger et al. [69, 70], Manera and Antoni [86] where the code has been tested to successfully reproduce experimental results obtained using water at supercritical pressure.

MATRA Among the available sub-channel codes for steady state and transient simulations, MATRA [75, 168] has a modern structure and includes a model, originally developed by Rowe [127], to represent the important effect of the wire-wrap fuel rod spacers proposed for the HPLWR FA, as described in Figure 1.2(b). MATRA has been mainly designed for LWRs analyses and hence has several features to represent a two phase fluid but, the hard coded water properties are not suitable for supercritical water and, consequently, code modifications are needed.

1.6.3 Validation of the computational tools

For practical use in industry, numerical simulation tools have to be verified, validated and qualified [62]. For the current feasibility studies of the HPLWR, such a detailed assessment is desirable but not possible since only scarce experimental data are available. Verification and validation of the selected computational tool is a must because of the innovative features of the HPLWR core and can be achieved with code-to-code comparison and with detailed inspections of the models implemented in the codes.

The usage of stand alone codes allows to perform initial un-coupled simulation to gain experience with the codes and to verify separately the models used, as suggested by Royer [129]. Once that each individual code has been considered separately, multi-physics verification can be achieved by checking the correctness of the data exchanges among all the codes. The inspection and analysis of the changes in power map and TH parameters among successive iterations is advisable to control the developed coupling system. This task is facilitated by the selected coupling procedure and by the use of stand alone codes: since each code is run till convergence for the given input data, it is possible and advisable to verify the consistency of the intermediate, not fully coupled[10] solutions for both RP and TH calculations. For the HPLWR studies, the capacity of the model to reproduce reality can not be assessed and hence the results should be carefully examined applying engineering judgment to understand if they are physically sound.

1.7 Outline of the thesis

At the end of this first, introductory chapter, sketching a brief overview of the HPLWR concept followed by the explanation of the reasons requiring the present research work, a brief outline of the thesis is provided.

The independent validation of the selected stand alone codes for HPLWR core applications is summarized in chapter 2 where, in the dedicated sections, ERANOS, TRACE and MATRA will

[10] The intermediate solutions of an iterative procedure may be not physical but, for the selected computational approach, have to be consistent with the input parameters at each iteration.

be applied to uncoupled analyses of the HPLWR to test and verify the used physical models and the considered calculation procedure.

Once the stand alone codes have been qualified for HPLWR core analyses, the two step approach to couple RP and TH core analyses and to investigate the predicted coupled solution at sub-channel resolution is developed as described in chapter 3. ERANOS and TRACE are coupled with a two-way approach which takes into consideration the most important TH feedbacks on RP calculations: variations of coolant, moderator and gap water temperature and density as well as fuel temperature. The coupled system is tested with simple analyses (a single FA) in order to gain experience and insight on the importance of the various parameters as well as to verify the data exchange among the codes. On the basis of these preliminary results a coupling strategy for the successive core analyses is proposed. The multi-scale analyses need an additional, intermediate step in order to provide the power map at fuel rod resolution. It is based on the combination of the mentioned homogeneous intranodal flux distribution calculated by ERANOS and local form functions obtained with MCNP5, as explained in detail in the second part of chapter 3. Having available all the boundary conditions for sub-channel wise core analyses, the developed interfaces for the one-way coupling are described.

The application of the developed multi-scale, coupled RP/TH system to HPLWR core analyses is presented in chapter 4. The ERANOS/TRACE coupled system is able to predict the operative condition of the HPLWR 3 pass core including the most important TH feedbacks on RP analysis. The predicted FA-wise volume averaged TH properties are refined at sub-channel resolution using MATRA which predicts local coolant and clad temperatures taking into account the important effects of the wire-wrap fuel rods spacers. To reproduce both the effects of neutron flux spatial gradients and of local heterogeneity of the FA, a pin-power reconstruction technique has been introduced.

Concluding remarks on the presented methodologies and results are discussed in the last chapter of the thesis.

The appendix includes additional applications of the coupled RP/TH system to HPLWR feasibility studies. They concentrate on the necessity of using a thermal insulation to reduce the heat up of moderator/gap water resulting from the temperature difference to the coolant and underline the pronounced changes of core power map during burn-up which demand detailed 3D optimization of the equilibrium cycle. Proposals for core optimization as well as suggestion for future analyses are also given there.

Documentation and description of the developed coupling interfaces as well as of the considered FA and core models are provided in separate chapters.

Chapter 2

Qualification of the separate fields and models for HPLWR applications

2.1 Validation of ERANOS for HPLWR applications

2.1.1 Whole core neutronic analyses with deterministic tools

At the present time, the solution of the neutron transport equation (1.1) with deterministic methods for reactor core analyses is generally accomplished with a two stages approach:

1. macroscopic XSs are produced in a broad or intermediate energy group scheme for a homogenized fuel element geometry by a cell / lattice code which takes into full account the energy and angular dependence of the neutron flux solving the integral transport equation in the heterogeneous fuel element, e.g. with collision probability;

2. reactor core analysis is performed using a broad energy group scheme and homogenized XSs obtained from the first stage concentrating on the spatial (and time) dependence solving the transport equation, generally in differential form with P_N or S_N theory.

This procedure has been extensively studied and successfully implemented for both thermal and fast reactors. However, the scientific community is going towards the total elimination of homogenization methods, e.g. [83]. In this framework, Monte Carlo methods are widely accepted as powerful tools for verification and validation of these stages and of the multi-group approach.

The current practice has been selected to perform HPLWR core analyses with deterministic methods. A flux weighted spatial homogenization of the heterogeneous fuel element is used to generate self-shielded multi-group homogenized XSs required by the transport code which represents the core with uniform material properties within the fuel element lattice cells. Heterogeneous cell calculations are necessary to determine the neutron flux distribution within the fuel element lattice, which is required for the homogenization procedure to provide a high fidelity representation of the combined space and energy dependent resonance self-shielding effects.

Two main spatial scales are, hence, involved in core analyses: the cell level, at which the homogenized XSs are generated, and the full core 3D or 2D analyses, which employs these XSs.

2.1.2 European Reactor ANalysis Optimized System

The ERANOS system [125, 131] has been selected since it is a tool capable of covering both stages needed for whole core neutron transport analyses and it consists of data libraries, codes and calculation procedures. Recommended calculation procedures to perform whole core

analyses – including representation of control rods, prediction of characteristics quantities[1] and usage of perturbation theory – have been described in details by Rimpault et al. [126] and are based on a multi-scale approach in which different levels of detail have to be considered: from the cell scale to the whole core 2D and 3D model, including burn-up analyses.

In the following sections, the selected calculation procedures for neutronic analyses of the HPLWR core will be presented in more details. Two ERANOS modules have been widely used: European Cell COde (ECCO) [121], to generate multi-group self-shielded microscopic XSs for the homogenized FA geometry, and VARIational Anisotropic Nodal Transport (TGV/VARIANT) [111], to carry out 3D analyses employing the generated homogenized XSs.

ECCO performs 2D cell calculations generating the multi-group self-shielded XSs and P1 scattering matrices required for reactor core calculations. It uses the subgroup method to treat resonance self-shielding effects which is particularly suitable for calculations involving complex heterogeneous structures. ECCO prepares self-shielded XSs and matrices by combining a slowing-down treatment in many groups with the subgroup method within each fine group. The subgroup method takes into account the resonance structure of XSs by means of probability tables and by assuming that the neutron source is uniform in lethargy within a given fine group. Flux calculations in heterogeneous geometry are performed by means of the collision probability method. Effective self-shielded XSs and matrices are obtained by condensation and smearing to match the user required broad group scheme while preserving the neutron balance. The used nuclear data are available in different group structures: in addition to the 1968 fine groups structure based on a lethargy grid of 1/120[2], used as reference master library for the most important isotopes, the XMAS 172-group structure [162] will be considered for HPLWR applications[3] because it is based on the structures formerly used in APOLLO [56] and WIMS [4] and hence is suitable for thermal and intermediate spectra cell calculations. The chosen coarse group structure for core calculations consists of 40 groups selected for thermal systems analyses.

TGV/VARIANT is based on the variational nodal method originally developed by Carrico, Lewis and Palmiotti [32, 82] and solves the 3D multi-group neutron transport equation. This method is based on the second-order form of the even-parity transport equation. A solution is searched in form of expansions for the even and odd parity fluxes in pre-computed angular and spatial basis functions with unknown coefficients. These basis functions are orthogonal polynomials for the spatial variables and spherical harmonics for the angular variables. Scattering anisotropy can be taken into account and both Cartesian (XY or XYZ) and hexagonal (Hex or Hex-Z) geometries are available with TGV/VARIANT. Recommended spatial approximation orders have been selected [151]. A "simplified transport" (SP) option exists, in which the angular developments both within the nodes and at the node boundaries are truncated by neglecting high-order cross terms. This option is rather accurate in practice (large reactors), and less time and memory consuming. Several post-processing functions, as nodal flux reconstruction and flux or power traverses extraction [35, 130], are also included within ERANOS.

The usage of ERANOS for HPLWR applications requires a careful choice of the calculation procedure and its verification with independent MCNP5 analyses, since this reactor has features which were not considered when the code has been developed. The main goal of this section is to present the procedures considered to apply ERANOS to HPLWR analyses as well as the comparison of ERANOS solutions with those of MCNP5 which provide a way to verify the results obtained for this innovative nuclear reactor, since no experimental data are available

[1] e.g., critical mass, delayed neutron fraction, Doppler effect, lattice dilatation, shielding calculations or gamma ray propagation.

[2] The neutron energy loss by scattering is smallest for scattering by heavy nuclides. For ^{238}U, translated into lethargy gain, it is almost constant and is equal to 0.008. This compares well with the fine group width of 1/120 = 0.0083 and explains the fact that 3/4 of the neutrons having a collision in a given fine group escape from that group.

[3] Even if innovative group structures claim to provide better representation of the resonances of both actinides and fission products, e.g. Hfaiedh [53], the well established XMAS has been selected.

yet. The code-to-code comparison is restricted to the differences in the numerical solution algorithms by choosing the same nuclear data basis in both codes: since ERANOS 2.0 data libraries are based on Joint Evaluation File, JEF 2.2 [102], the same set is used also in the MCNP5 calculation [88, 109]. It should be mentioned that MCPN5 does not interpolate between the available temperature dependence of the microscopic XSs neither for thermal scattering nor for resonance-broadening, but both of these are important for accurate calculations and should be modeled properly. Solutions of these limitations include material mixing techniques or XSs generation in a fine temperature mesh, as suggested by Brown et al. [14], but have not yet been considered in the current analyses.

In the following sections, 2.1.3 and 2.1.4, the cell and FA scales will be verified with a direct comparison between ERANOS and MCNP5 results. The developed full core model will be discussed in section 2.1.5, presenting various sensitivity studies to the ERANOS modules selection.

2.1.3 Validation of 2D cell scale

Description of the 2D fuel assembly geometry models

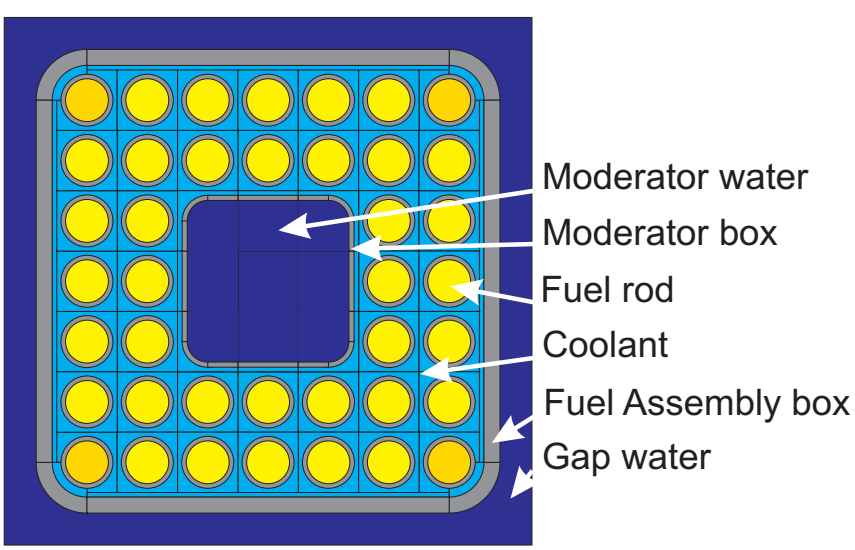

Figure 2.1: Fuel assembly geometry

The original FA design with solid stainless steel boxes [57], shown in Figure 1.2 and 2.1, can be divided in several regions: the moderator water, the moderator box, the fuel rod lattice, the fuel assembly box and the gap water between adjacent FAs. One half of the gap region between adjacent FAs is included in the considered FA cell model whose lateral dimension is 8.2520 cm; the lateral surfaces are assumed to be reflecting. Geometrical details on the fuel rod lattice are given in Table 2.1.

Table 2.1: Fuel rods lattice

lattice pitch	9.44 mm
clad outside diameter	8.00 mm
clad inside diameter	7.00 mm
fuel pellet diameter	6.70 mm
wire diameter	1.34 mm

The fuel used is uranium dioxide with two different enrichments of ^{235}U: 4 wt% for the four pins at the corner of the assembly and 5 wt% for the other 36 pins [57]. The enrichment is constant in axial direction and all FAs in the core have the same enrichment since no core loading strategy is available yet. Both uranium dioxide and water have stoichiometric composition.

The channel for moderator water, which occupies the inner 3×3 lattice position of each FA as depicted in Figure 2.1 and 2.2(a), can not be exactly represented with ECCO capabilities – without going to multiple levels nesting – and hence approximated models have been initially considered. Different modeling possibilities, based on the usage of water rods filled either with coolant or moderator water and on the usage of a homogenized medium, have been developed. They are explained here in more detail, referring to Figure 2.2 (where coolant is light blue, moderator is dark blue and the moderator box is gray):

- **homogeneous cells**: each of the 9 cells is assumed to be composed of a uniform composition material obtained by preserving the volume fraction of coolant, structural material and moderator water in that cell, Figure 2.2(b);

- **moderator rods**: the moderator area in the heterogeneous cells is bigger than that of the maximum diameter rod which can be inserted in the cell as well as that of the coolant is smaller than the minimum value that can be obtained by inserting the maximum diameter rod into the cell. When modeling the moderator box as a ring of moderator water rods, inside the clad and surrounded by coolant, the volume fraction of the moderator and of the coolant can not be preserved. To increase the accuracy of the model, the total mass of the materials must be preserved and hence the density of the coolant and of the moderator are changed in the following way:

$$\rho_{\text{model}} = \rho_{\text{real}} \times \frac{V_{\text{real}}}{V_{\text{model}}}$$

  The rod inner and outer diameters are chosen in order to preserve the structural material volume fraction and hence it is not necessary to adjust its density, Figure 2.2(c).

- **coolant rods**: it is possible to preserve the volume fraction of the three constituents by modeling the moderator box as a ring of coolant rods, inside the clad and surrounded by moderator water, Figure 2.2(d);

- **mixed geometry**: the lattice cells containing the moderator box can be subdivided into two different kinds of cells, Figure 2.2(e):

  1. lateral cells: for these cells both the coolant and structural material volume fraction is very small and hence, to avoid any changes in material density, a coolant rod model with clad and surrounded by moderator geometry is used;
  2. corner cells: for these cells the moderator volume fraction is smaller and hence it is possible to consider a moderator rod model surrounded by a homogeneous mixture of structural material and coolant.

Additional simplifications are introduced for the round corners of the assembly box, which are modeled as rectangular. Independent MCNP5 studies showed that the model accuracy can be increased by preserving the total mass of the constituents slightly changing the dimension of the assembly box. The small water relocations around the assembly box corner are not as important as the change of the structural material mass in determining k_∞.

The wire wrap can not be modeled with ECCO capabilities but it increases the amount of structural material reducing the coolant volume fraction. It has been modeled increasing the clad outside diameter to preserve the correct volume fraction of the various constituents, from 8.0 mm

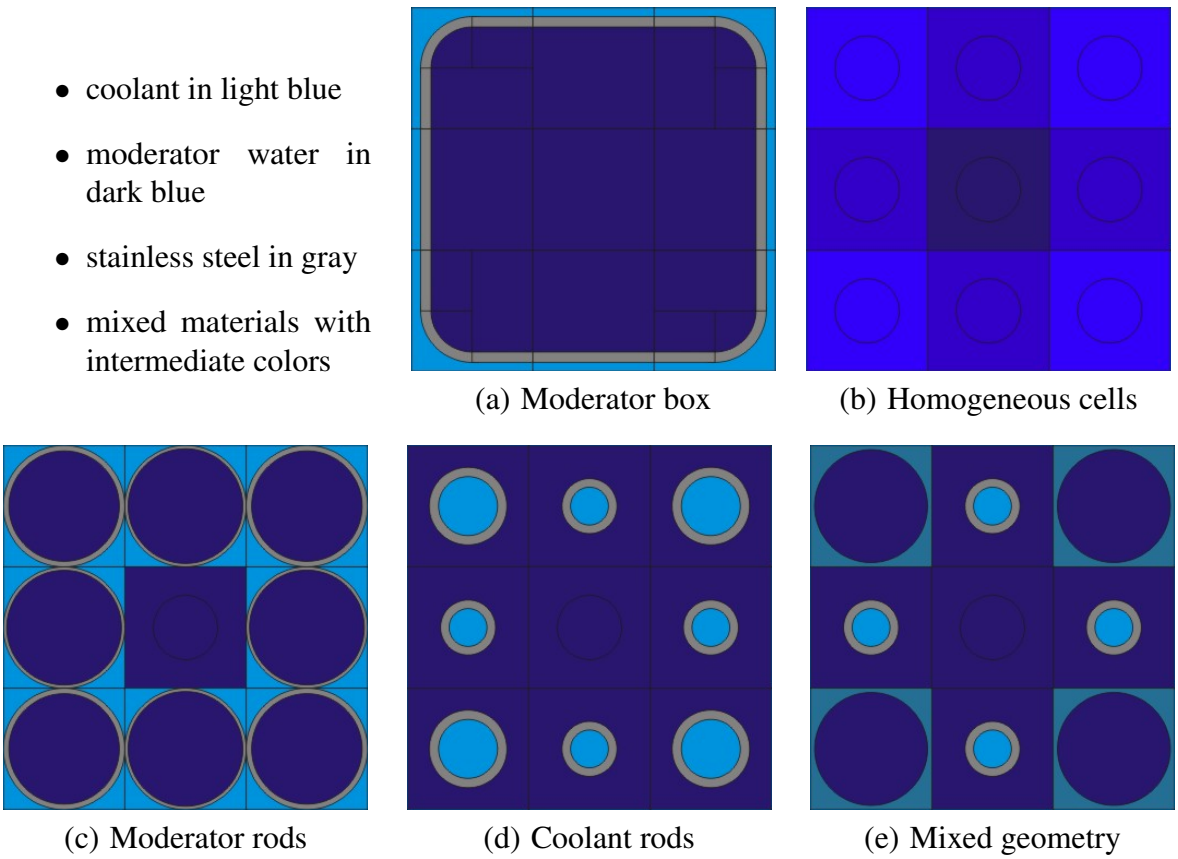

(a) Moderator box (b) Homogeneous cells

(c) Moderator rods (d) Coolant rods (e) Mixed geometry

Figure 2.2: Moderator box and proposed models

to 8.113 mm. The gas-filled gap between fuel pellet and clad is not represented because it should have a negligible effect on RP characteristics hence, the used clad inside diameter coincides with the fuel pellet one and proper clad smear density has been introduced to preserve the structural material mass.

Fuel pellet model For the current analyses, the fuel pellet are represented in ECCO, and in MCNP5, by one single cylinder and not by several concentric ones. This simplification requires to use a proper average value for the fuel temperature which is known to vary parabolically in the fuel rod, [148]. Rather than using a simple volume averaged value, the lumped fuel temperature is evaluated using the formula suggested by Rowlands [128], which has also been recommended by Aniel-Buchheit [2], Bouland et al. [10], de Kruijf and Janssen [29].

$$T_{\text{average}} = \frac{4}{9} T_{\text{centerline}} + \frac{5}{9} T_{\text{surface}} \tag{2.1}$$

Because of the short neutron mean free in a thermal reactor, when considering more advanced design studies it is advisable to verify the sensitivity of characteristic quantities to a more sophisticated model of the fuel pellet. For example, modeling the fuel pellet with several concentric cylinders with different temperatures, an accurate representation of the spatial dependence of the fuel temperature variations in the pellet is obtained and this may influence the combined space and energy dependent resonance self-shielding effect.

Definition of the calculation procedure for HPLWR applications

Description of the reference ECCO calculation procedure ECCO calculations are carried out in a series of steps, the choice of the calculation procedure is highly problem-dependent and

can be selected by the user considering both the desired accuracy and the available computational resources. The reference calculation procedure to generate multi-group XSs, as explained in [122], is considered as a starting point: 5 successive steps are used as described in the following lines and represented in Figure 2.3.

A rough estimation of the solution is obtained at the first step for a volume averaged homogenized geometry using the XMAS 172-group structure, then this solution is used as starting point for step two which considers a heterogeneous cell geometry. This approach is typical of fast reactor calculations [122] but proven to be effective in reducing the computational time also for HPLWR applications. The third step uses a fine energy structure (1968 energy groups) for the most important isotopes and accounts for the resonances self-shielding solving the transport equation in the heterogeneous geometry by means of the collision probability method. The energy group condensation is hence performed: a 40 groups subdivision for the coarse energy structure has been chosen after comparing the results obtained for several thermal systems with various similar group structures by Dr. A. Rineiski (FZK-IKET). Finally, the code performs the flux weighted spatial homogenization of the cell geometry generating the multi-group XS block.

Sensitivity studies pointed out difficulties in performing heterogeneous cell calculations using the Buckling search option, in particular for a cell having a k_∞ less than unity and hence a negative Buckling. This reason suggested to assume a Buckling equal 0 in all the calculation steps. The usage of reflecting boundary conditions, together with a Buckling equal 0, results in a zero-leakage condition which facilitates the direct comparison with MCNP5.

Different collision probability routines [121, 141] for lattice geometries are available in ECCO, among them, two are chosen and compared: `Normal` and `Roth 4`. The first of these routines is the standard one whereas the second is an approximate one; more details on these procedures can be found in [122]. At first, for the results presented in the following paragraph, the approximate technique has been used but successive sensitivity studies suggested to adopt normal collision probability for HPLWR applications since no significant computational time reduction has been found using the approximate method. The difference in k_∞ between them for the selected cases is between 40 and 60 pcm depending on the calculation step whereas the computational time is reduced only by 8%.

Performance of the proposed geometry models k_∞ was chosen as reference parameter to compare the representativeness of the proposed models: the sensitivity of this characteristic quantity to the moderator box representation was considered for selected representative water densities and fuel temperatures.

k_∞ at step 1 is the same in all geometry models, ensuring appropriate representation of the moderator box: the volume averaged homogeneous geometry, being preserved the mass of the constituents, is the same for all models at step 1. For the selected TH parameters, the heterogeneity effect produces a huge difference in k_∞ as expected for a thermal reactor: in step 2, k_∞ is increased of more than 2000 pcm with respect to step 1 depending on the the combination of fuel temperature, coolant and moderator densities. This underlines the importance of performing the calculation with fine energy group structure in heterogeneous geometry. During the successive calculation steps, k_∞ undergoes changes between 150 and 350 pcm when collapsing the energy structure from 1968 to 40 groups and below 1 pcm when performing flux weighted homogenization of the geometry: the generated 40-group library represents sufficiently well the finer group structure. The good agreement found between the last steps with heterogeneous and flux weighted homogenized geometry, compared with the heterogeneity effect of the initial two steps, provides additional assessment of the algorithms used by the code to perform spatial homogenization: these are adequate for the present application.

A graphical representation of k_∞ changes in the successive steps as well as a comparison among the 4 considered models, for a selection of TH parameters, is given in Figure 2.4. The

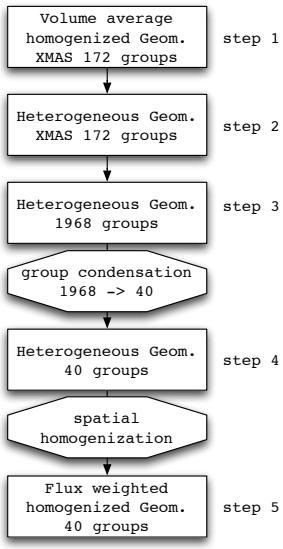

Figure 2.3: ECCO calculation steps

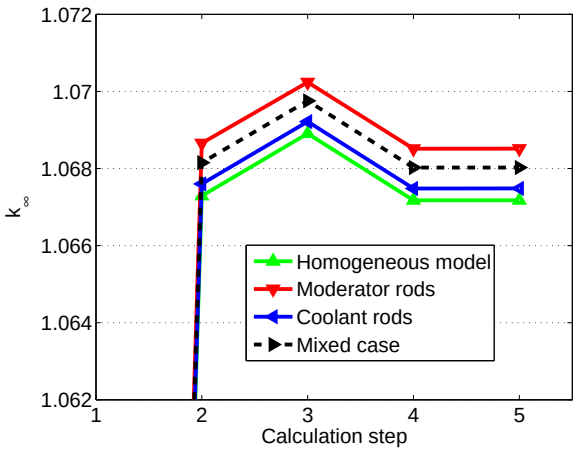

Figure 2.4: Sensitivity of k_∞ to the FA geometry model

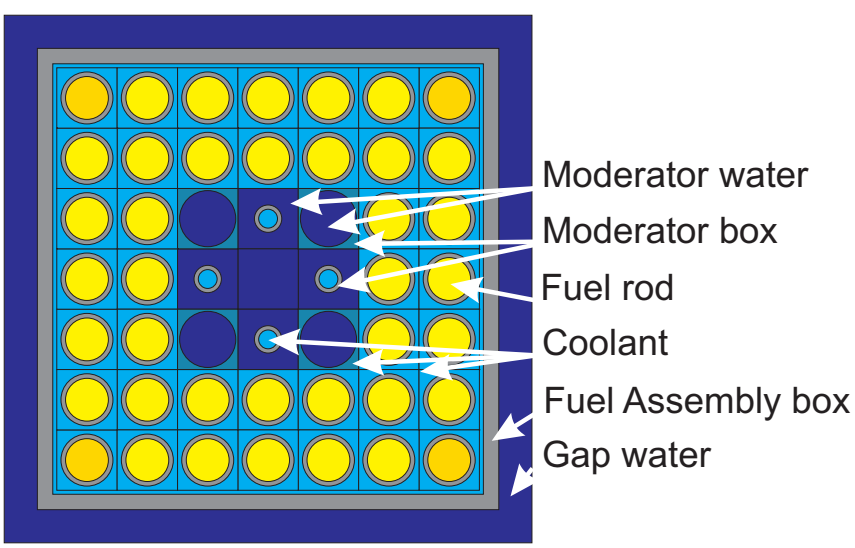

Figure 2.5: Mixed geometry model developed for ECCO

differences among the models are rather small, being of the order of few hundreds pcm, and physical explanations can hardly be verified. Hence they are almost equivalent for the present neutronic analyses. For this reason the "Mixed Geometry", depicted in Figure 2.5, has been chosen as the most suitable one.

The results obtained for the simplified FA geometry are encouraging since a plausible behavior of k_∞ is found when performing energy group condensation and spatial homogenization: k_∞ maintains the value obtained for the heterogeneous geometry with fine energy structure.

At a later stage, a more sophisticated input file has been prepared to verify the possibility of a more accurate representation of the moderator box: subdividing the 7×7 fuel rod lattice into nested regions, a square moderator box can be modeled. The added complexity results in an increase of the computational time by a factor of 2.5 to 3 which suggested to abandon this approach. In addition, this complex geometrical representation induced k_∞ differences during flux weighted homogenization up to 900 pcm, while changing k_∞ for the final step of no more than 300 pcm with respect to the water rods models.

Simplified ECCO calculation procedure The solution of the transport equation using the 1968 energy groups step is extremely time consuming affecting the applicability of the code to HPLWR core analysis: because of the strong heterogeneity both in axial and radial direction, the number of XS blocks that has to be generated is rather high[4]. The goal of this section is to describe the simplifications of the calculation procedures which allow to reduce CPU time needed for ECCO calculations without losing much of the desired accuracy.

When using the described reference calculation procedure, around 10 minutes are necessary on a 2.4 GHz Linux PC with 2 GB of RAM to generate each XS block, the majority of which is spent in the solution of the 1968 energy groups step. Omitting this step and performing the group condensation directly from the 172 groups step, only 1-2 minutes are needed.

This faster procedure requires validation in order to demonstrate that the omission of the fine energy groups step does not appreciably affect the results obtained for HPLWR core analysis. Assuming target values for water densities (coolant 0.498352 g/cm^3, moderator water 0.581175 g/cm^3, gap water 0.566511 g/cm^3) and using XS libraries at room temperature (300 K)[5], k_∞ is used as a parameter to compare the two calculation procedures, Table 2.2. For the first two steps, since the calculation procedure is the same, k_∞ is also the same. k_∞ is increased by roughly 300 pcm by the 1968 energy groups step, this already suggests that the step with the fine energy structure may not justify the high computational time requested. For the last step the difference between the two calculation procedures is only 110 pcm.

Table 2.2: Sensitivity of ECCO k_∞ to the calculation procedure

		5 steps	4 steps
Volume averaged homogenized geometry	172 energy groups	1.06960	1.06960
Heterogeneous geometry	172 energy groups	1.09860	1.09860
Heterogeneous geometry	1968 energy groups	1.10149	omitted
Heterogeneous geometry	40 energy groups	1.09975	1.09865
Flux weighted homogenized geometry	40 energy groups	1.09976	1.09865

Since ECCO calculation is used to generate multi-group XSs, also the sensitivity of the 40 groups neutron spectrum calculated for the flux weighted homogenized geometry to the omission of the 1968 energy groups step is considered. The neutron spectrum obtained for a selected combination of the TH parameters is plotted in Figure 2.6. Since the curves are almost superimposed, the spectrum ratio *sr* is also considered for four cases, that is four combinations of the TH parameters, Figure 2.7. The ratio is close to unity in almost all the 40 energy bins.

$$sr = \frac{\text{40 groups spectrum obtained when condensing from 172 energy groups}}{\text{40 groups one obtained when condensing from 1968 energy groups}} \tag{2.2}$$

The agreement found between the two ECCO calculation procedures both in k_∞ and in the spectra, together with the reduction of more than 70% (often close to 80%) in the calculation time, suggests to use the faster, four steps calculation procedure for HPLWR XSs generation.

Comparison of ECCO versus MCNP5

The selected ECCO model is verified versus MCNP5 for fixed TH parameters (coolant 0.498352 g/cm^3, moderator water 0.581175 g/cm^3, gap water 0.566511 g/cm^3). Besides using

[4]Considering 21 axial nodes times the 22 fuel CLs in 1/8 of the core requires the generation of 462 XS blocks.

[5]The fuel temperature is the main reason for the higher k_∞ with respect to the previous section, for which it was fixed to 1500 K.

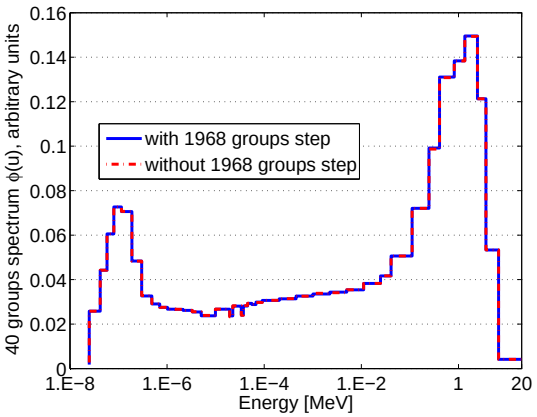

Figure 2.6: Spectrum for the homogenized geometry with different calculation procedure

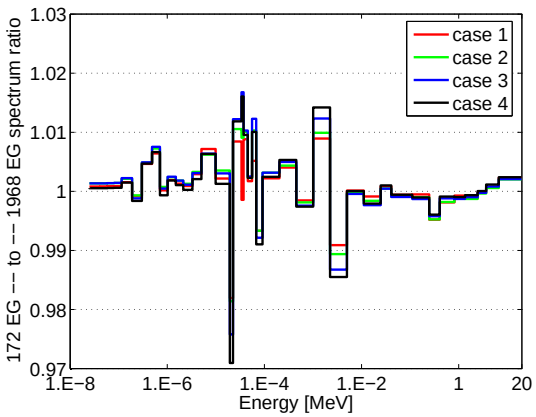

Figure 2.7: 40-group spectrum ratio *sr* corresponding to different TH parameters

Table 2.3: Cell geometry k_∞ calculated by MCNP5

	exact geometry	ECCO geometry	diff [pcm]
MCNP5 k_∞	1.10492 ± 0.00029	1.10243 ± 0.00027	249

the same nuclear data library, all the XSs where chosen at room temperature (300 K) to minimize possible compensation effects restricting the comparison to the geometry model and solution algorithms.

Since MCNP5 is capable to represent both the original geometry and the model developed for ECCO, Figure 2.1 and 2.5, the latter can be verified. The difference between the geometry models is close to 250 pcm, approximately 10 times the Standard Deviation of the Monte Carlo simulation, ensuring sufficient accuracy of the considered geometry model for the current investigations, Table 2.3.

The applicability of ECCO solution algorithms to the HPLWR FA design can be verified by comparing the results of the two codes, Table 2.2 and 2.3: the difference between the k_∞ calculated by ECCO using 1968 energy groups and MCNP5 (when using the same geometry representation) is below 100 pcm. The use of the faster calculation procedure, which removes the 1968 energy groups step, does not significantly affect the accuracy of k_∞ for the last calculation step: in the first case the difference to MCNP5 is 264 pcm whereas in the other it is 375 pcm. This rather small difference is fully acceptable at the current design stage.

These results confirm the applicability of the developed model to the considered FA design as well as the accuracy of the selected calculation procedure for the HPLWR. The multi-group XS blocks can be used for the solution of the multi-group neutron transport equation to evaluate the power shape in 3D FA models.

2.1.4 Validation of 3D fuel assembly scale

In this section attention is given to simple 3D models for which direct comparison with Monte Carlo calculations is possible also on a single machine; in particular a single FA is considered.

Only the active length of the FA (420 cm) is modeled and divided into 21 equal length nodes, as in previous analyses [153]. The horizontal section of the FA has been already described for the cell calculation. Inside the defined axial nodes, the material properties (fuel temperature and water densities) are assumed to be uniform. The boundary condition of the considered geometry are reflective for the four lateral surfaces whereas the neutron flux is assumed to be zero at the upper and lower extrapolated boundaries (in the MCNP5 this condition is replaced by zero

incoming current).

Concerning the angular representation, scattering matrices of order 1 are generated with ECCO while a SP3 flux calculation is performed with VARIANT.

Input data for neutronic analyses

Coolant, moderator and gap water temperature and density variations representative of each one of the 3 core regions have been selected from [87] and adapted to the desired axial subdivision. The selected input data are plotted in Figure 2.8, where only the coolant and moderator densities variations are shown because the considered gap water density axial variation is very similar to that of the moderator water. For this verification, the fuel temperature is assumed to be uniformly distributed to minimize the number of parameters which can influence the power shape, its value is chosen to be 800 K.

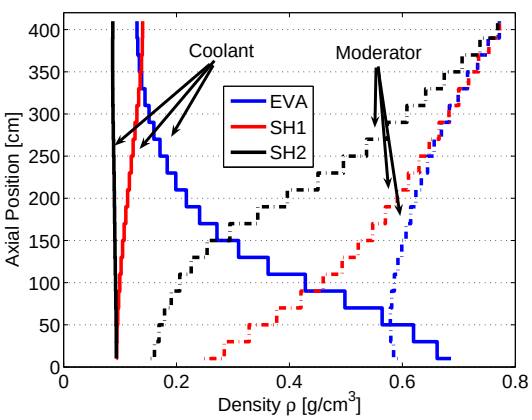

Figure 2.8: Assumed water densities distributions in the 3 core regions (EVA, SH1, SH2) [87]

The modeling of neutron scattering with bound hydrogen in MCNP5 is achieved through the usage of $S(\alpha,\beta)$ data sets produced in IKE, Stuttgart by Mattes and Keinert [88] for the following temperatures: 548.6 / 573.6 / 598.6 / 623 / 643 / 648 / 653 / 663 / 683 / 800 K. MCNP5 does not interpolate between these available temperatures and, since for the "Thermal Treatment Specification" it is not possible to use directly a material mixing technique, a step variation of the XS data set among the available data has been used [14].

ECCO results for fuel assembly calculations

The multi-group XS blocks for each of the 21 axial nodes of the 3 regions were generated with ECCO using the calculation procedure presented in the previous section.

k_∞ obtained for each cell calculation are plotted as a function of the axial position for the 3 core regions in Figure 2.9: the strong coolant density reduction in the SHs causes the drop of k_∞ below unity in the lower half of the active length of SH1 and SH2 where also the moderator density is reduced. This explain the almost zero relative power of the lower part of both SHs shown in Figure 2.11. The TH input data used for these analyses have been extracted from [87] which investigated a quite different HPLWR operating condition, hence they may not be fully representative of the present core design.

k_∞ behavior is quite similar to that of the node-wise volume averaged water density in the 3 regions of the core, plotted in Figure 2.10, having neglected the fuel temperature axial variations. The water densities of coolant, moderator and gap water are weighted with the corresponding volume fractions to calculate the volume averaged water density which is used only for representation purposes. In EVA the volume averaged water density axial variation is not monotonic because there is a compensation between coolant and moderator densities reduction which occurs

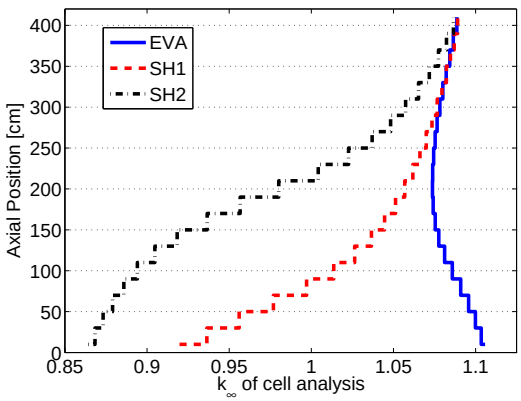

Figure 2.9: ECCO k_∞ in the different core regions for the assumed water properties

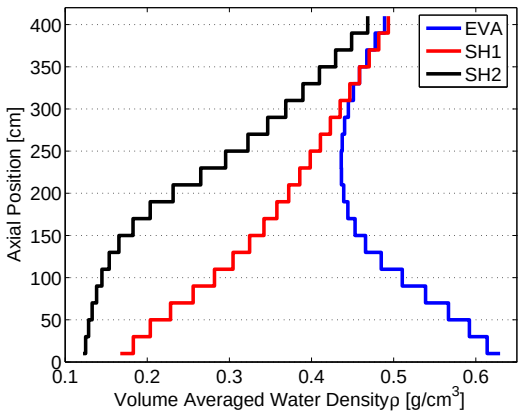

Figure 2.10: Node-wise volume averaged water density distributions

in opposite direction, as shown in Figure 2.8. Combinations of coolant and moderator/gap water densities which give the same volume averaged value lead to different k_∞ values underlining the importance of performing the cell calculation with the detailed heterogeneous FA model. More details are given shortly in Figure 2.15(b)

Multiplication factor

A direct comparison of VARIANT and MCNP5 calculations can be done using k_∞, which, being an integral value, gives an overall evaluation of the codes behavior, Table 2.4.

The two codes use a quite different geometry model: concerning MCNP5, a direct representation of the FA heterogeneity is considered, as shown in Figure 2.1, while with VARIANT the 21 axial nodes are represented with homogeneous composition and the effect of the spatial heterogeneity is included only through the multi-group XS blocks generated with ECCO.

Table 2.4: Comparison of k_∞ for fuel assembly calculations

region	VARIANT	MCNP5	diff [pcm]
EVA	1.07949	1.08601 ± 0.00018	652
SH1	1.06413	1.06906 ± 0.00017	493
SH2	1.04241	1.04669 ± 0.00018	428

Comparison of the power shapes calculated by VARIANT and by MCNP5

The power shape is the result that requires validation because it is the key quantity of the coupling which exists between neutronic and TH analyses of the HPLWR core. The results corresponding to target TH data typical of the 3 core regions are plotted in Figure 2.11 where the ordinate is the axial coordinate, Z, and the abscissa is the normalized value of the power generated in the fuel. The six power shapes were normalized assuming that the 3 FAs are operated at the same power level.

VARIANT can calculate only an average power density for each computational node, since the XY section of the FA is homogenized with ECCO, hence, even if MCNP5 is able to calculate individual power shapes for each fuel rod, an averaged value over the 40 fuel rods of each FA is used for direct comparison with VARIANT. The precision of MCNP5 calculations is checked considering, beside the standard deviation on k_∞ which is below 20 pcm, relative errors on all tally bins for the power densities. The maximum values are less than 0.007 in EVA, 0.022 in SH1

and 0.044 in SH2, but the relative error in the regions of the power peak, which have a better statistic, is well below 0.003 for the 3 FAs.

The power peak is located close to the regions where the volume averaged water density is higher, Figure 2.10, as expected in an under-moderated reactor core: reducing the volume averaged water amount causes a reduction of the thermal neutron flux and, thus, of the power generation. The axial neutron leakage contributes to the shape of the power density. The fuel temperature is here assumed to be constant, neglecting its negative feedback.

The percentage difference in the power shape, $\frac{\text{MCNP5}_{\text{value}} - \text{VARIANT}_{\text{value}}}{\text{MCNP5}_{\text{value}}} \cdot 100$, is used to compare MCNP5 and VARIANT results and is plotted for the 3 cases in Figure 2.12. For all considered water properties variations, the discrepancy between MCNP5 and VARIANT in the regions of higher power density is below 5% and, hence, is not influenced by the statistical uncertainty of MCNP5 calculations.

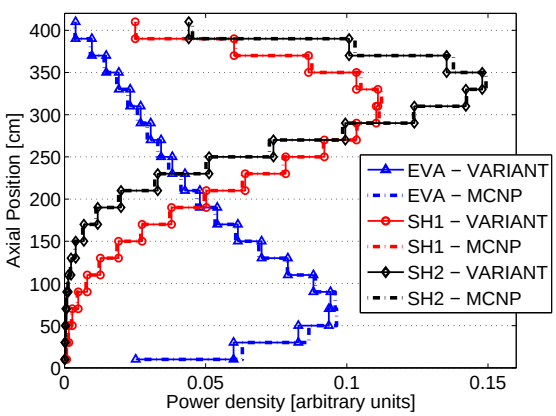

Figure 2.11: Normalized power shape

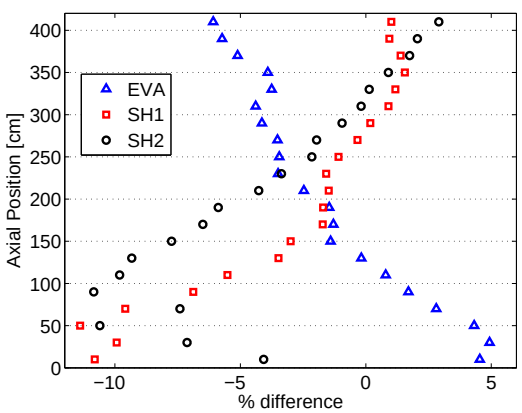

Figure 2.12: Power shape percentage difference

The agreement between the two different calculation approaches is reasonable for the present feasibility study and ensures the accuracy of the developed ERANOS calculation procedure for HPLWR 3D analyses.

Sensitivity studies to the fuel temperature and water densities variations

Before developing the coupled system, a better insight into the physics of the phenomena which govern the coupling between RP and TH analyses of the HPLWR can be achieved by means of sensitivity studies to the fuel temperature and water properties, selecting available axial variations presented by Maráczy et al. [87]. These can be analyzed both separately and individually to investigate possible amplification or compensation effects. For these reasons, four different cases are considered:

1. both fuel temperature and water properties are assumed to be uniformly distributed in the axial direction;

2. the water temperature, plotted in Figure 2.13(a), and the corresponding density vary axially as assumed before for the EVA region whereas the fuel temperature is uniformly distributed in the axial direction;

3. the fuel temperature varies as shown in Figure 2.13(b), these values where selected from those obtained by [87] and have been adapted to the desired axial subdivision using a cubic spline interpolation and averaged using equation (2.1) [128]. The water properties are assumed to be uniform in the axial direction;

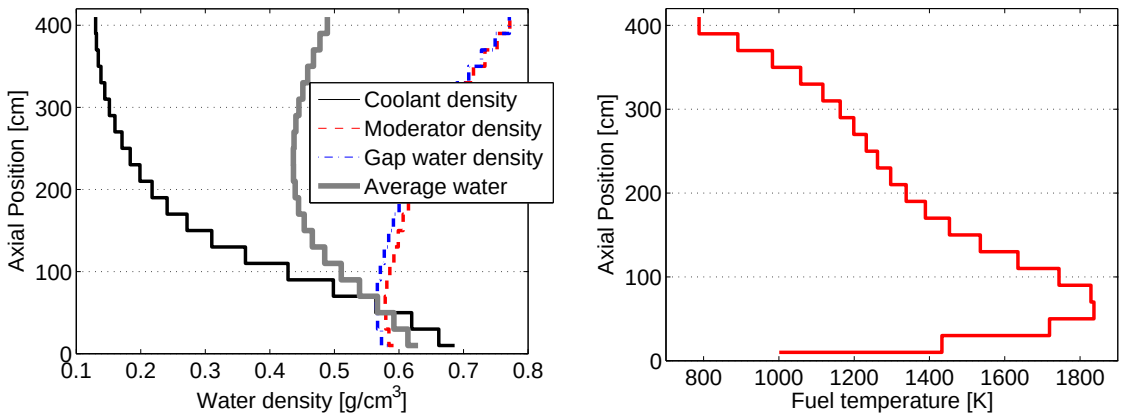

(a) Water densities (b) Node averaged fuel temperature

Figure 2.13: Assumed water densities and fuel temperature axial variations [87]

4. both water properties and fuel temperature vary as described in Figure 2.13.

The strong sensitivity of the power shape to the different input data is evident from Figure 2.14. Each case is separately analyzed in the following lines.

1. Assuming constant material properties in the axial direction, the power shape is a cosine–like function which is the fundamental mode for the considered geometry.

2. When modeling only the axial variation of water properties and assuming uniform fuel temperature, the power peak is shifted from the geometrical center towards regions of higher coolant density, that is the bottom part of the considered geometry, where a better neutron thermalization is achieved.

3. When modeling only the axial variation of fuel temperature with constant water properties, the sensitivity of the power shape to the resonance broadening mainly in ^{238}U (n,γ) XS can be evaluated: this reduces k_∞ of the regions with higher fuel temperature and hence lowers the power generated there, shifting the peak of the power towards the top of the FA where the fuel temperature is lower.

4. The two phenomena act in opposite ways: the former shifts the power peak towards the bottom whereas the second towards the top; when they are considered simultaneously, they partially compensate each other and the resulting power shape is almost flat. Even if the physical reasons are understandable – the fuel temperature acts as a negative feedback which reduces the power generation rate in the region where this is higher – the effect appears to be extremely pronounced and the results are not fully consistent with the input data because the fuel temperature profile should resemble the power shape. These issues will be answered only with a consistent RP/TH coupled analysis.

Also the sensitivity of k_∞ in different regions to both fuel temperature and water densities is considered in Figure 2.15, where the ECCO results are plotted. The axial variation of k_∞ is rearranged as a function of the fuel temperature with constant water properties, Figure 2.15(a), and of the volume averaged water density in the horizontal cross-section of the FA with constant fuel temperature, Figure 2.15(b).

The increase of the fuel temperature reduces k_∞ because of the Doppler effect, mainly in ^{238}U, in an almost linear behavior, as shown in Figure 2.15(a).

Having 3 different waters whose density distribution is changing independently in the axial direction, as shown in Figure 2.13(a), leads to a non monotonic change of the volume averaged

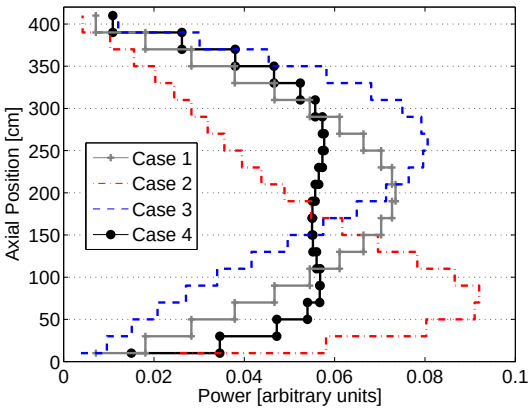

Figure 2.14: Sensitivity of the power shape to the fuel temperature and water densities

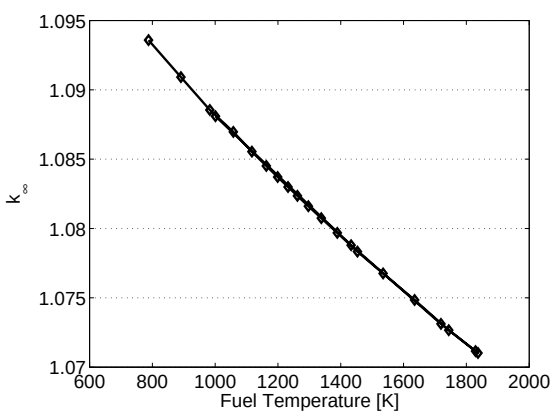

(a) k_∞ as a function of fuel temperature

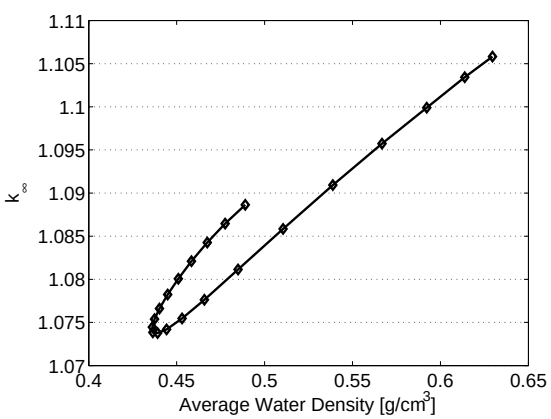

(b) k_∞ as a function of average water density

Figure 2.15: Sensitivity of k_∞ to fuel temperature and average water density axial variation

water density. In general, to an increase of the volume averaged water density correspond a rise of k_∞, Figure 2.15(b), because the reactor is under-moderated. But for axial regions, which have different combinations of coolant, moderator and gap water densities leading to the same volume averaged water density, k_∞ obtained at the last homogeneous step is different as shown in Figure 2.15(b). A region with higher coolant density and a lower moderator density (lower part of the active length) has a lower k_∞ than a region with lower coolant density and higher moderator one (upper part of the active length) which has the same volume averaged water density, Figure 2.13(a). Hence, the importance of the heterogeneous calculation and the capability of ECCO to maintain the differences even when performing the spatial homogenization is evident.

2.1.5 Whole core calculations

The good agreement found between ERANOS and MCNP5 for HPLWR applications, allows proceeding further in developing 3D full core models which are qualified by sensitivity studies to the mesh topology and to the radial reflector model, also comparing the 3D core model with a 2D one which enables exact representation of the radial reflector. Full core heterogeneous representation with MCNP5 is considered to be too expensive on a single machine.

Proposed core model

The assumed symmetry conditions allow to model only one quarter of the core, a horizontal section with regions specifications and CL numbers is plotted in Figure 2.16. Since a core loading strategy is not yet available, all the FAs use the same enrichment described for the cell calculation which is also constant in axial direction. Control rods and other means of reactivity compensation techniques have been omitted.

The core mesh subdivision can be kept coarse using a *nodal* code: sensitivity studies demonstrated that an XY mesh equal to the CL length, 24.7560 cm and a Z mesh equal to 20 cm, gives the same results of finer meshes but reduce the computational time needed. The axial surrounding regions of the core are not yet taken into account, as for FA studies, this topic will be investigated successively. Concerning radially surrounding regions[6], preliminary investigations show that the radial reflector, even if it does not change appreciably k_{eff} (less than 150 pcm), varies the core power map both in radial and axial direction. To minimize the number of computational nodes within the core in order to avoid undesired increase in the computational time, the following assumptions have been introduced: steel reflector and core barrel have been smeared together to occupy the core surrounding ring whereas the remaining region is occupied by downcomer water[7]. To preserve the total mass of water, its density has been modified and to reduce the unphysical relocation of water, the outer region is split into two (symmetrical) regions: in the lateral regions, the downcomer thickness, together with the water density, is preserved whereas in upper right corner (in XY geometry), the water density is reduced to occupy the whole region.

The model presented in Figure 2.16 has been compared with a more detailed one, developed with the purpose of a better fitting of the cylindrical core surfaces with the cartesian nodalization as plotted in Figure 2.17. The results obtained showed a negligible difference in k_{eff} (less than 10 pcm) and very small variation of the core power map (within $\pm 2\%$ with a maximum below 6%), which does not justify the increase by a factor of $\simeq 4$ on the computational time[8]). In addition, since the main purpose of the current neutronic analyses is focused on the core power map, exact representation of the core surrounding regions is not necessary as it would be for other cases, e.g., pressure vessel displacement per atom (DPA) calculations. In the refined model, showed in Figure 2.17, the regions external to the HPLWR core has been modeled preserving their thickness and the void region outside the downcomer has been represented by a strong neutron absorber, made of B_4C with natural enrichment but density increased by a factor of 10, which is almost equivalent to a *zero inlet current* as radial boundary condition. The in-core power distribution showed a limited sensitivity to the smearing of downcomer water or to the usage of B_4C, hence the first approach has been preferred considering that the usage of a black absorber is not exact for the considered "re-entrant" geometry, in which neutrons escaping from the boundary can re-enter in the core without the need to be back-scattered. Verification of the developed model to represent the regions surrounding the core in radial direction is obtained with a 2D RZ analysis described later.

Input data for neutronic analyses

For these core analyses, not yet coupled with TH feedbacks, the same input data already used for previous FA analyses are chosen [87], Figure 2.8. The same water properties are assumed for the different CLs within the 3 core regions – namely EVA, SH1 and SH2 – at each of the

[6]The procedure to calculate multi-group homogenized XSs in non-multiplying medium with ECCO differs from that presented before; it is described in [122, 126].

[7]The variational nodal method is not suitable to represent void regions because in the even-parity transport formulation it is necessary to divide by Σ_{total}, hence the downcomer water is smeared to fill the remaining volume.

[8]from less than 10 to around 40 minutes for SP3 with isotropic scattering (P0 scattering kernel) calculations on a 2.4 GHz Linux PC.

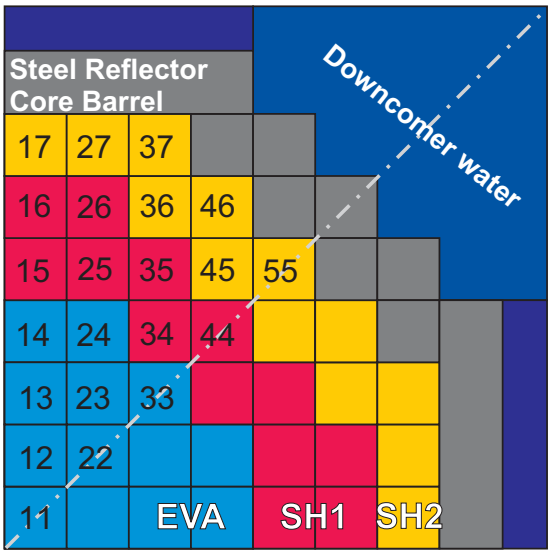

Figure 2.16: XY section of the core model, including clusters numbering

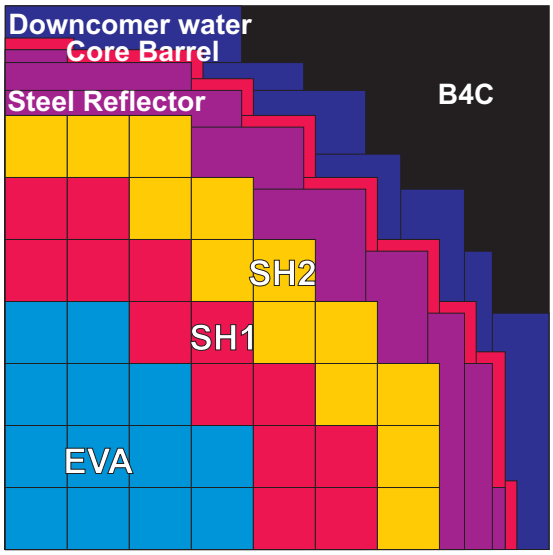

Figure 2.17: Refined core model

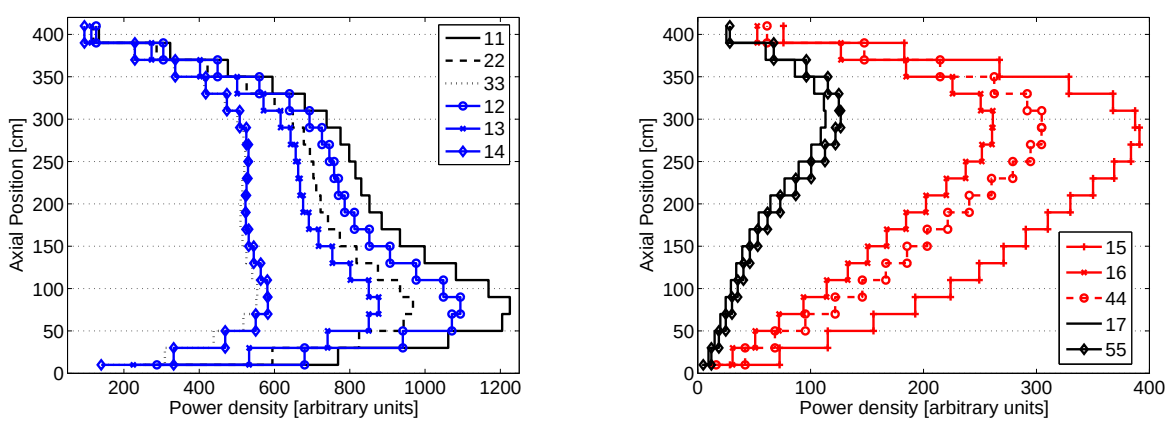

Figure 2.18: Power shape in different clusters

21 axial nodes. The fuel temperature is assumed to be uniform both in the axial and radial, it is equal to 891 K.

Sensitivity studies of in-core power distribution

The axial power shape at different XY positions obtained for core analysis is plotted in Figure 2.18; the reduction in the power generation going from the inner CL (11) to the periphery of the core could be mainly explained by the radial leakage of neutrons from the core. The power gradient is also amplified by the low water densities in the core periphery regions where k_∞ is close to or below unity, as shown in Figure 2.9, and hence a stationary neutron population is maintained only thanks to the neutrons leakage from the inner part of the core. The core loading is not yet optimized in order to provide a more uniform radial power distribution within each core region.

Both water density variations and constant fuel enrichment contribute to the presence of the power peak in the lower third of the central core region where the coolant is at its highest density. The radial coupling between the 3 core regions is useful to reduce the peak - to - average ratio in the power shapes, which shows a smooth transition from a bottom to a top peak shape; the average power generated per CL in the outer regions is substantially lower than the one generated in the central region.

These results are found to be consistent with those presented by Maráczy et al. [87] even if a direct comparison is not possible because of different core loading strategies, fuel burn-up, burnable poisons distribution and control rods positions which have not yet been modeled in the current analysis.

Sensitivity to adjacent regions The spatial coupling effect, due to neutron diffusion among adjacent core regions, changes substantially the axial power shape within the same core region (i.e. EVA, SH1 and SH2), Figure 2.18, where, for these preliminary analyses, all FAs have the same material composition and XS data. Comparing the axial power shapes obtained for FA calculations with those obtained for core analysis, the strong influence of the FA surrounding regions appears evident, Figure 2.11 and 2.18.

- for FA analysis, the lateral surfaces are assumed to be reflecting and hence the geometry corresponds to an infinite lattice of equal composition FAs; this is almost equivalent to the physical condition of one FA at the center of a big conventional LWR core, which, because of the short mean free path of thermal neutrons, is not substantially affected by the description of regions outside the core;

- for HPLWR core analysis, because of the vicinity of the 3 core regions, which have a radically different coolant density variation in the axial direction, each FA has a different environment and, then, different "boundary conditions". This is the reason why the power level and shape at different XY positions is substantially different even if the same multi-group XSs are used.

The radial coupling among the 3 core regions (EVA, SH1, SH2) reduces the amplitude of the power peaks: as evident when comparing the axial shapes shown in Figure 2.11 and 2.18. For single FA analysis, the power peak – physically located closer to the region of maximum water density – is very pronounced as is the one in the water density; for whole core analysis the neutron leakage, from the regions of highest power and coolant density, compensates the inhomogeneity of water density flattening the curves, e.g. CLs 14, 15, 16 and 17.

Core analysis with a 2D model Because of the difficult representation of a cylindrical surface in XYZ geometry, the core 3D model is compared with a 2D one in RZ geometry which guarantees exact representation of the radial boundaries (steel reflector, core barrel and downcomer). The radii of the 3 core regions are obtained preserving their volume. This analysis has been performed with the 2D S_N transport code BISTRO [112] which is included in the ERANOS system. A substantially different core nodalization has been used selecting a $\simeq 5$ cm mesh size in both directions. Using the same P1 XS block generated with ECCO and a S_4 angular representation, k_{eff} calculated by BISTRO is less than 40 pcm above the value obtained by VARIANT when using the SP3 flux angular representation.

Concerning the power shapes, plotted in Figure 2.19, a direct comparison with the 3D model is not considered because it would require to evaluate the equivalent radial position of the XY geometry. The agreement, between RZ and XYZ geometries, at different radial positions is qualitatively good.

The overall behavior of the power shapes is qualitatively similar in the 2D and 3D analyses, and an excellent agreement on k_{eff} is found, the developed 3D XYZ model of the radially surrounding regions is hence suitable for the current analyses.

Sensitivity to the flux angular expansion: diffusion and transport Since in the HPLWR the neutron moderation is achieved mainly by neutron collisions with hydrogen atoms whose scattering dynamic, in the laboratory system, is rather forward peaked especially for high neutron

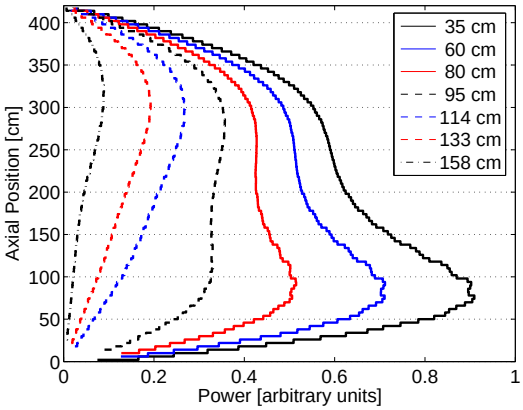

Figure 2.19: Power shapes at different radial position for a 2D (RZ) core model

energy, a sensitivity study of both local and integral characteristics to the angular representation of the neutron flux is considered comparing diffusion and transport 3D core calculations while maintaining a P1 representation of the scattering kernel. Several spherical harmonics order options exist in VARIANT, the default is P3 (or SP3) but also P5 calculations are possible while P1 should be equivalent to diffusion [111] even if it uses an order 1 instead of 0 for the anisotropic scattering approximation. Unfortunately it is not possible to perform cell calculations with ECCO using a P_N order higher than 1 together with a heterogeneous cell geometry representation [122]: P3 and P5 calculations can be performed only using homogeneous geometry. The loss of the heterogeneity effect in the cell calculation would lead to less accurate results, as shown before in Table 2.2, mainly because of the combined space and energy dependent resonance self-shielding[9], and hence it has not been investigated limiting the scattering kernel angular expansion to P1.

These studies, originally performed for the simplified core configuration presented in the previous sections [89], have been repeated at a later stage using a more detailed core composition in which each CL has different TH parameters since the heterogeneity may enhance the effects of a finer angular representation. For this reason, the TH parameters obtained for a coupled RP/TH core analysis [92] are used as input data for the following simulations.

Calculated k_{eff} are summarized in Table 2.5 while axial power shapes in selected CLs are shown in Figure 2.20. The difference in k_{eff} between diffusion and transport are rather small,

Table 2.5: Sensitivity of k_{eff} to the flux angular representation

	diffusion	SP3	P3	P5
k_{eff}	1.12221	1.12307	1.12310	1.12310

less than 100 pcm, and among the transport options are completely negligible. Concerning the power shapes, the P5 transport solution is considered as reference solution to compare point-wise fractional differences with the other calculation options. Diffusion present the biggest values of $\frac{\text{power(P5)} - \text{power(diffusion)}}{\text{power(P5)}}$ which are below 6% but the highest values are mainly located close to the power peak regions giving a higher peak - to - average ratio for transport calculations; the differences between the transport options are fully negligible for the current application, being of the order of 0.1% between P5 and P3 and less than 0.4% between P5 and SP3.

The physical reasons of these small differences may be explained, beside by the core geometry which is big in neutrons mean free paths, by the chosen group structure: the use of 40 energy groups is able to separate the energy range in which the neutron scattering is more anisotropic (the

[9]Together with the resulting different flux amplitude for the fast and thermal neutrons in the fuel and in the water.

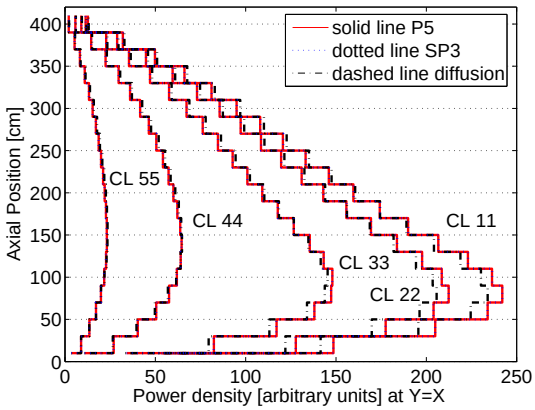

Figure 2.20: Sensitivity of the power shapes to the angular representation of the flux

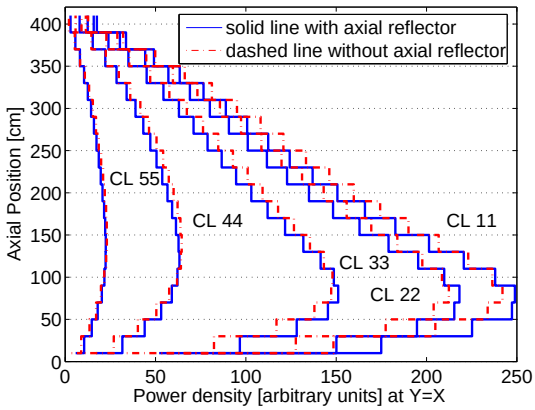

Figure 2.21: Sensitivity of the power shape to the axial boundary conditions

high energy groups) from the thermal ones in which the neutron scattering is not very anisotropic and the neutrons importance is higher ensuring a good scattering dynamics representation also with a lower flux expansion order.

The computational time for SP3 analysis is greater by 1.4 than the one needed for diffusion, the one for P3 by 2.3 and the one for P5 by 5.2. The shown higher peaking factors suggest to use SP3 transport calculations, for whole HPLWR core calculations, as a reasonable compromise between accuracy and CPU time.

Sensitivity to the axial reflector Models which include the axial reflectors are expected to be needed in more advanced design studies which investigate a local maximum of power density possibly located close to the core periphery even if the axial reflector saving should not have a pronounced effect for a core height of 4.2 m neither on k_{eff} nor on the maximum power density. Nonetheless a refined core model which includes both the upper and lower fission gas plenum, 25.5 cm each, has been developed. The model accounts for the different coolant and moderator/gap water densities below and above the active length of the 3 core regions (EVA, SH1, SH2) using different water densities and neutron source for XSs calculation[10]. As expected k_{eff} is almost insensitive to this improvement being raised of around 70 pcm but the core power map exhibits higher sensitivity as shown in Figure 2.21. It is important to underline that, because of the selected axial nodalization, which uses a 20 cm axial node, the local maximum is not visible in Figure 2.21 since only node averaged values are plotted.

Neutron spectrum at cell and 3D core scale

The homogenization process in ECCO preserves the reaction rates in the infinite single assembly lattice geometry, but when the produced XS block is mapped to the reactor core position different boundary conditions result from the solution of the 3D transport equation. When material properties vary greatly, like in the vicinity of control rods, at the core periphery and at interface between the 3 core regions of the HPLWR (EVA, SH1 and SH2), this approximation may lead to a large error since the core environment is very different from the infinite geometry with reflective boundary conditions used for homogenized self-shielded multi-group XS generation. This problem is well known and has been generally assessed introducing assembly discontinuity factors, [155].

Since no experimental data are available for HPLWR applications, it will be extremely

[10]The procedure to calculate multi-group homogenized XSs in non-multiplying medium with ECCO are described in [126].

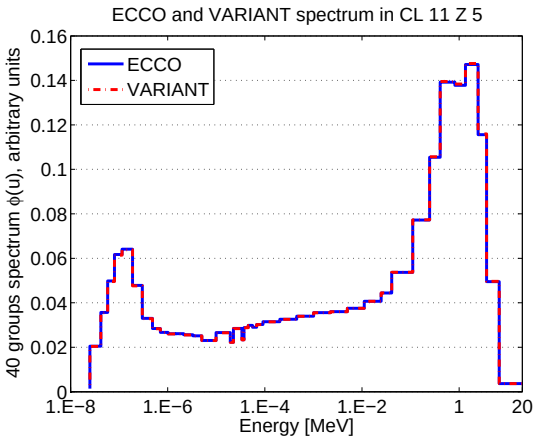

Figure 2.22: Neutron spectrum with ECCO and VARIANT in the power peak region

difficult to quantify this error and hence an alternative procedure has been proposed. The 40-group neutron spectrum

$$\phi(u) = \frac{1}{\int_{0MeV}^{20MeV} \phi(E)\,\mathrm{d}E} \frac{\Delta E_g \phi_g(E)}{\ln\left(\frac{E_g}{E_g+1}\right)}$$

is used to compare the solutions obtained with the lattice code ECCO for the homogenized geometry with that predicted by VARIANT for 3D SP3 core calculation. Initially attention is given to the power peak region, for which the two normalized spectra are plotted in Figure 2.22.

The two spectra are almost identical in the whole energy range, showing that the effect of the neutron leakage from the cell is marginal in determining the spectrum. Since this central region have a small leakage probability, which may influence the spectrum, the comparison is performed also for regions closer to the core periphery which present higher leakage maintaining the good agreement between the two spatial scales, in Figure 2.23. This is probably due to the selected energy groups structure which is adequate for HPLWR applications.

2.2 Verification and improvements of TRACE for HPLWR applications

2.2.1 TRAC/RELAP Advanced Computational Engine

An accurate prediction of water and structural material temperature distributions within the core is of crucial importance to estimate the safety and performance of the HPLWR. The heterogeneity of the HPLWR 3 pass core, together with the pronounced changes in the thermophysical properties of water associated to the high heat up, makes 0D and 1D approaches, used for LWRs design, not sufficiently accurate and demand more detailed investigations. For these reasons, TRACE [58, 99, 100] has been chosen for HPLWR core analyses thanks to its flexibility and growing applications. It is the reference US NRC system code for TH analyses of LWRs and related experimental systems. It was originally designed to cover a wide range of operating conditions typical of LWRs and related experimental systems as well as operational transients such as loss of coolant accidents. It includes a detailed evaluation of the heat transfer coefficient, which is obtained as a function of the flow regime and of the channel geometry. It uses a component-based approach to model a reactor system, i.e. several physical pieces of equipment in a flow loop can be represented as some type of component, and each component can be further nodalized into some number of physical volumes (also called cells) over which the

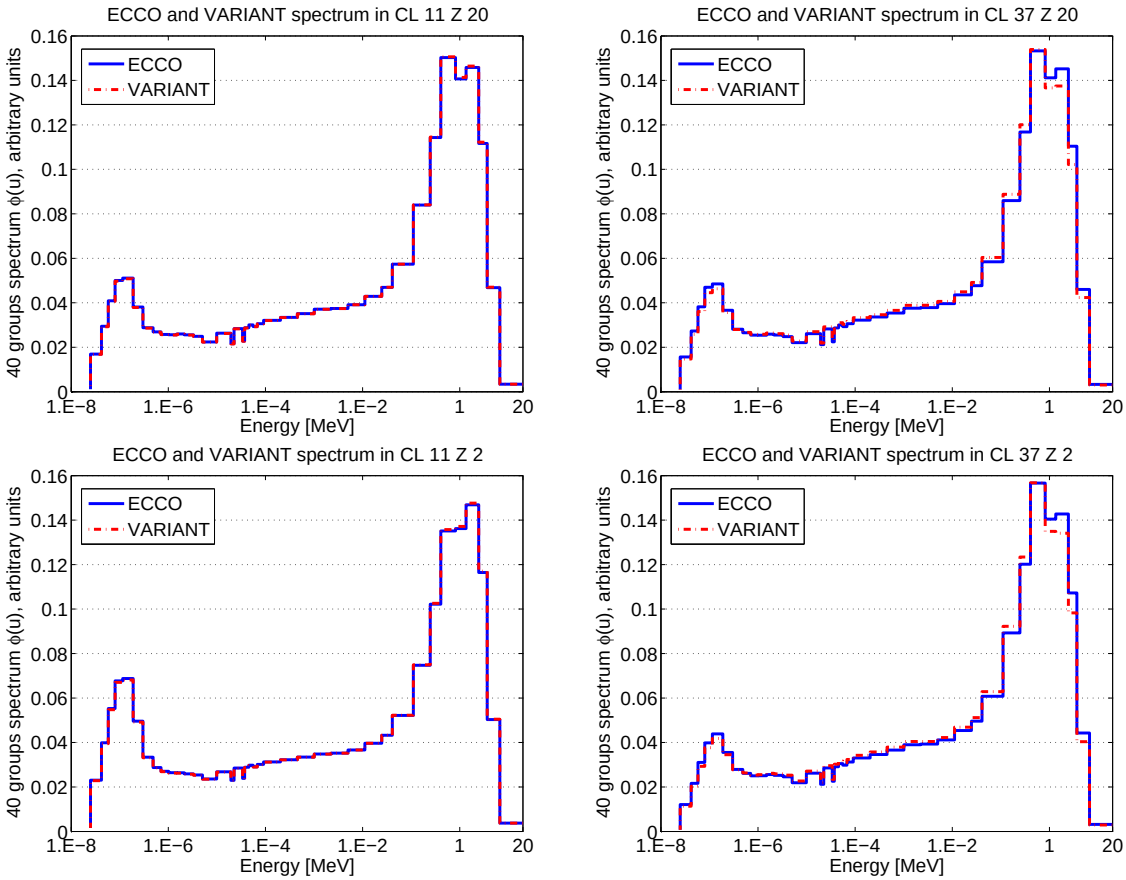

Figure 2.23: Comparison of neutron spectrum in various core regions

fluid, conduction, and kinetics equations are averaged. The present release (version 5.0) has a modular structure and is written in Fortran 90, it is used for all presented applications.

The code was not designed to handle supercritical water and, consequently, the direct application of TRACE to HPLWR core analyses may introduce assumptions which are not adequate neither for supercritical water nor for the unconventional HPLWR core geometry resulting in inaccurate predictions of temperature distributions within the core which may affect the reactor design. For these reasons, a careful check of the physical model hard coded into TRACE source files has been performed, some limitations have been found and improved models have been considered as described in the following.

The heat transfer correlations used in the original TRACE version [100] are based only on fluid bulk properties, but, for supercritical water analyses, the variations of water properties between bulk and wall regions have an important effect in heat transfer prediction, especially in the vicinity of the pseudo-critical point, as summarized in detail by Pioro and Duffey [115]. To be able to model these effects, modifications of the TRACE source code, based on the experimental work of Bishop et al. [8], Jackson and Hall [67], have been introduced and are described in subsection 2.2.3.

2.2.2 Modeling of HPLWR in TRACE

Fuel assembly model

The FA model built for TRACE analysis is described in this section and its graphical representation is given in Figure 2.24. For single FA analysis, a representative EVA FA is considered assuming a coolant inlet temperature of around 580 K and upward flow.

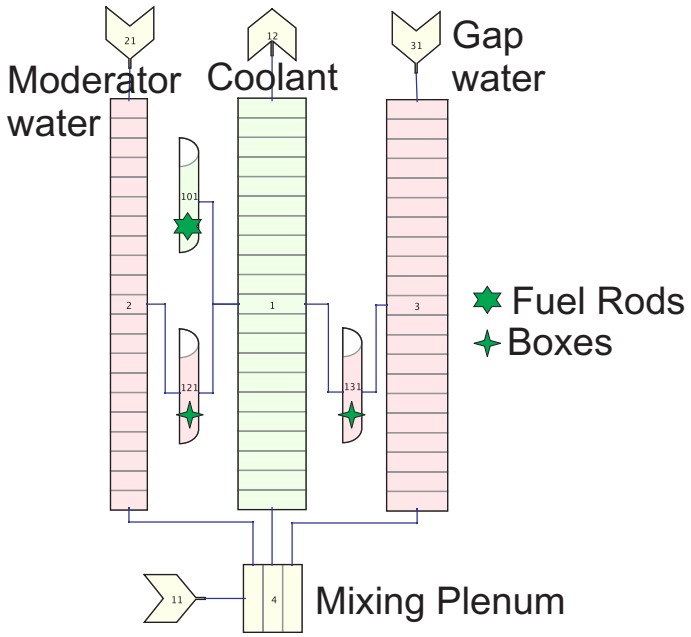

Figure 2.24: Fuel Assembly representation in TRACE

Each FA is composed of 3 parallel flow paths for coolant and moderator water[11], which are represented with equivalent 1D components whose geometry is calculated preserving the hydraulic diameter, the channel flow area and the volume. Only the active length of the fuel rods, 4.2 m, is considered and divided into 21 equal length axial nodes. The inlet effects caused by the real geometry are neglected since they can not be easily represented for the considered pipe geometry and should not affect the temperature distribution.

These three channels are thermally connected using Heat Structures (HSs) which reproduce the 316 stainless steel[12] moderator and FA boxes: the heat flux between moderator water and coolant is calculated according to the temperature differences between the fluids. Two equivalent hollow cylindrical HS are used: the heated areas are specified using heated diameters and the inner and outer surfaces are connected to the different axial cells of the target pipes. This model is hence equivalent to a tube-in-tube heat exchanger: the coolant is flowing in the annular region between two other tubes containing moderator and gap water; the relative flow is counter-current in EVA and SH2 while co-current in SH1.

The fuel rods are modeled using cylindrical HSs which preserve the fuel pellet diameter, gap gas and clad thickness. The gas gap HTC is fixed to 6300 W/(m^2 K) [42, Chapter1] but may require better evaluation. The coolant is heated up by the temperature difference with the clad and no direct heat up of the water, caused mainly by neutron slowing down, is considered in these preliminary analyses which neglect also the axial conductivity of the fuel.

To give a more realistic representation of the FA, the lower mixing chamber is also included. Here the outlet of both moderator and gap channels is mixed with feed water at 550 K to obtain the nominal coolant flow rate and to determine the coolant inlet temperature, corresponding to that of the mixing chamber, which is not an input parameter but is affected, as it will be for core analyses, by the predicted heat transfer to moderator/gap water.

[11] Both the one flowing in the moderator channel and in the gap between adjacent FAs

[12] These calculations have been performed using the original FA [57] without thermal insulation, which will be included only for successive core calculations.

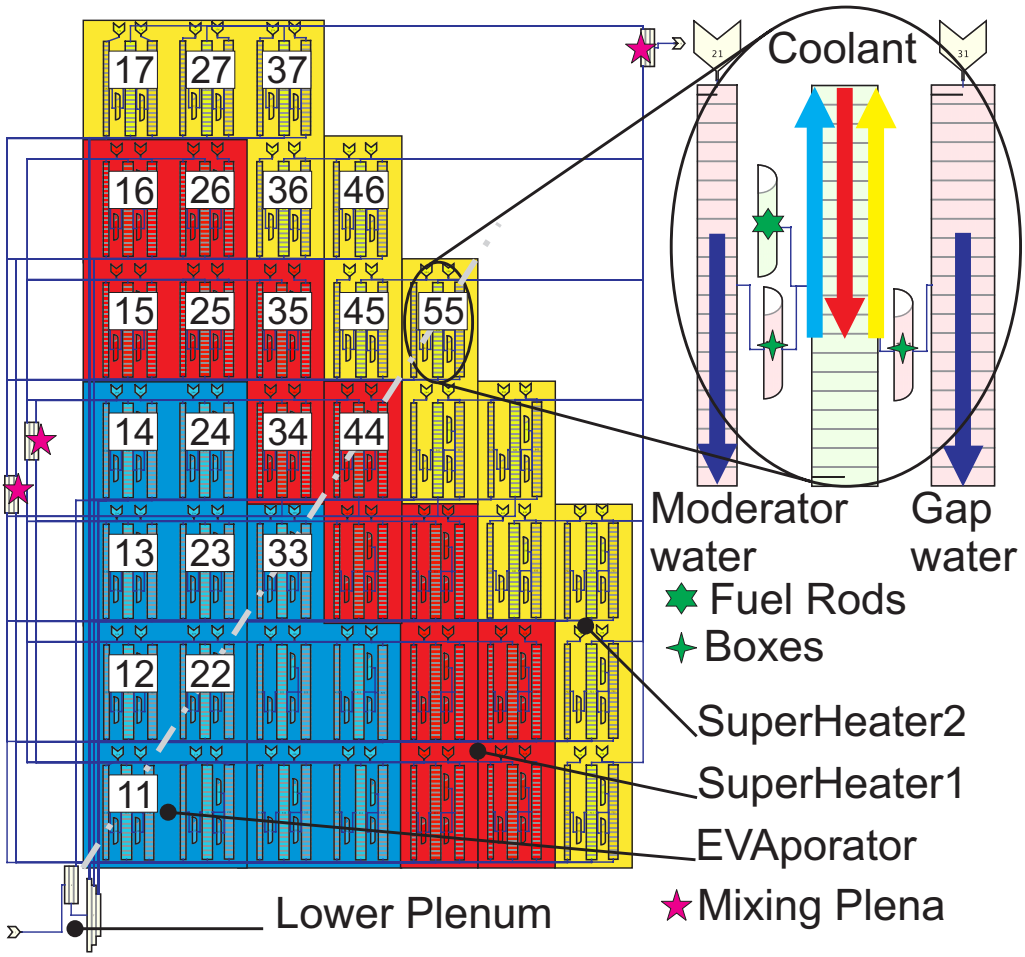

Figure 2.25: Core nodalization in TRACE

Whole core model

When extending the TH model from a single FA to the whole HPLWR core, a pseudo 3D representation is used: 1D components are mapped to a 3D core node position. Only $1/4$ of the core is represented because of the symmetry – $1/8$ symmetry is not considered to avoid modeling only one half of certain FAs – and each fuel cluster is represented only by an average FA to reduce the number of nodes[13]. The FA model described in the previous section is used as a module to represent all the considered CLs or FAs; the resulting parallel pipes in which the coolant flows are connected at the inlet and outlet to the mixing chambers enabling prediction of the coolant mass flow redistribution to balance the pressure drops due to the inlet orifices and the different heat up. The mixing plena, located above and below the core, are modeled as equivalent 1D component assuming a perfect mixing of the coolant. The mass flow of moderator water is split between the moderator channel and the gap region which are both fixed in the input file to be $1/3$ and $2/3$ of the total moderator flow rate[14]. This representation does not allow for moderator mass flow redistribution among the available flow patches and is not suitable to investigate possible flow reversal phenomena which may happen during operational transients. Additional simplifications are introduced by the representation of the gap water which, in the real geometry, flows in the 3D open space while is modeled with 1D parallel channels without any cross flow but only common outlet plenum.

[13]This model has been refined modeling each FA independently. To build this input deck, a dedicated Perl script has been developed and hence it is impractical to provide any graphical representation of this complex model.

[14]These initial investigations were performed assuming a total moderator flow rate equal to 25% of the RPV inlet flow rate.

2.2.3 TRACE limitations and code improvements

During preliminary investigations, difficulties occur when using the build-in IAPWS steam tables [147] and cause TRACE to crash for some test cases; these troubles disappear when using the latest RELAP5 steam tables, with a finer mesh (i.e. `stgh2onew0 3.1-2`), as underlined by Manera and Antoni [86].

A successive and more careful analysis of the TRACE source code revealed the use of approximations which are outside their range of validity when performing HPLWR TH analyses. These are mainly related to two different fields:

- fluid properties [100, Chapter 11];
- heat transfer models [100, Chapter 6].

The first point was the object of independent analyses by Jäger et al. [69], whose modifications of fluid properties have been included in the present analyses because they are of crucial importance for supercritical water applications. The second point is important for an accurate prediction of the heat transfer between adjacent pipes and for the evaluation of clad temperature [94]. It is described here emphasizing the applications to HPLWR.

Heat structure geometry model

The original TRACE version has an internal test to check whether the heat is transferred at the outer or inner surface of a cylindrical HS: in the first case it uses a correlation for rod bundle while in the second case it uses a correlation for tube, more details are provided in [100].

- For rod bundle geometry, TRACE applies El-Genk correlation:

$$Nu_{El-Genk} = C_{EG} \cdot Re^{0.8} \cdot Pr^{0.33}$$
$$C_{EG} = 0.028\frac{p}{d} - 0.006$$

- For tube geometry, TRACE, originally, uses Gnielinski correlation Gnielinski [49]:

$$Nu_{Gnielinski} = \frac{\frac{f}{2} \cdot (Re - 1000) \cdot Pr}{1 + 12.7 \cdot \sqrt{\frac{f}{2}} \cdot \left(Pr^{2/3} - 1\right)} \tag{2.3}$$

  where $f = [1.58 \cdot \ln(Re) - 3.28]^{-2}$ is the Fanning friction factor.

As previously described, cylindrical HSs are used in the HPLWR to model not only the fuel rods, hence this distinction has been eliminated and the same heat transfer correlation is used both at the inner and outer surface of the cylindrical HS.

Heat transfer correlations and wall effects

The described heat transfer correlations are based only on water bulk properties and neglect the effect of the water properties variations at the wall. For supercritical water, these phenomena are more important in heat transfer prediction than in LWRs [115] and hence, should be considered in the analysis.

Modifications in the source code have been introduced to calculate liquid density and enthalpy at the wall temperature, and hence to use more adequate correlations for heat transfer in supercritical water. Among the available ones two have been chosen: Jackson and Hall [67] and Bishop et al. [8], which has been recommended by Cheng and Schulenberg [23] for HPLWR

applications; for sake of completeness they are reported here, together with the well established Dittus-Boelter correlation [33] which has been implemented for comparison.

$$Nu_{Jackson} = 0.0183 \left(\frac{\rho_{wall}}{\rho_{bulk}}\right)^{0.3} \left(\frac{\bar{c_p}}{c_{p,bulk}}\right)^{n} \cdot Re^{0.82} \cdot Pr^{0.5} \tag{2.4}$$

$$Nu_{Bishop} = 0.0069 \left(\frac{\rho_{wall}}{\rho_{bulk}}\right)^{0.43} \cdot Re^{0.9} \cdot \bar{Pr}^{0.66} \left(1 + \frac{2.4}{x/d_H}\right) \tag{2.5}$$

$$Nu_{DB} = 0.023 \cdot Re^{0.8} \cdot Pr^{a} \tag{2.6}$$

$$\text{where } \bar{c_p} = \frac{enthalpy_{wall} - enthalpy_{bulk}}{T_{wall} - T_{bulk}}, \bar{Pr} = \frac{\mu \bar{c_p}}{k} \text{ and } a = \begin{cases} 0.4 \text{ for } T_{wall} > T_{bulk} \\ 0.3 \text{ for } T_{wall} < T_{bulk} \end{cases}$$

The exponent n in Jackson correlation, equation (2.4), assumes different values, close to 0.4, depending on the comparison of T_{wall}, T_{bulk} and the pseudo-critical temperature, [67]. Since this correlation was obtained for heated pipes, the exponent n is not defined for a cooled pipe, i.e. when $T_{wall} < T_{bulk}$. For HPLWR application, also heat transfer coefficients for cooled fluid are necessary: for these cases n has been fixed to 0.4. The inlet effect in Bishop correlation, equation (2.5), $\left(1 + \frac{2.4}{x/d_H}\right)$, being x the distance from the pipe inlet, was *not* implemented into TRACE; for the current HPLWR model this effect is negligible since the hydraulic diameter d_H is less than 5 mm whereas the length of the first axial cell is 20 cm.

Additional modifications of the source code were necessary in order to consider the Hufschmidt and Burck factor, $(Pr_{bulk}/Pr_{wall})^{0.11}$, as originally introduced by Gnielinski [49].

Flow regimes

In the original TRACE version, the wall heat transfer coefficient is calculated by a logic selection algorithm for the different flow regimes. A modification was introduced to ensure that supercritical water is always considered as single-phase fluid. For this case, the heat transfer coefficient is taken to be the maximum among the values calculated for 1) laminar, 2) turbulent forced convection and 3) natural convection (either laminar or turbulent). For natural convection, TRACE uses correlations based on Prandtl and Grashof numbers [100]. For HPLWR application, the low flow velocity of the moderator is responsible for the low value of the calculated Nu number in turbulent forced convection which is of the same order of magnitude of the one calculated for natural convection. Hence the original TRACE version switches among different heat transfer correlations while calculating the heat transfer between coolant and moderator. This is responsible for the sharp axial variations in the heat transfer coefficient, presented later in Figure 2.32. For sake of simplicity and better understanding of the results, it was chosen to avoid changes between heat transfer correlations in the axial length and, hence, the Nu number is always calculated assuming turbulent forced convection which will be the case for the considered HPLWR steady state investigations.

2.2.4 TRACE performance for HPLWR analyses

Single fuel assembly analyses

After having described the limitations found in TRACE, the sensitivity to the introduced improvements is analyzed. For single FA analysis, the thermal power is here assumed to be 3.25 MWth to rise the coolant outlet temperature just above the pseudo-critical one of 657 K, at the nominal pressure of 25 MPa, from 550 K to roughly 665 K. The power axial distribution is plotted in Figure 2.26, and more details are given in [95]. For this power range, it was possible

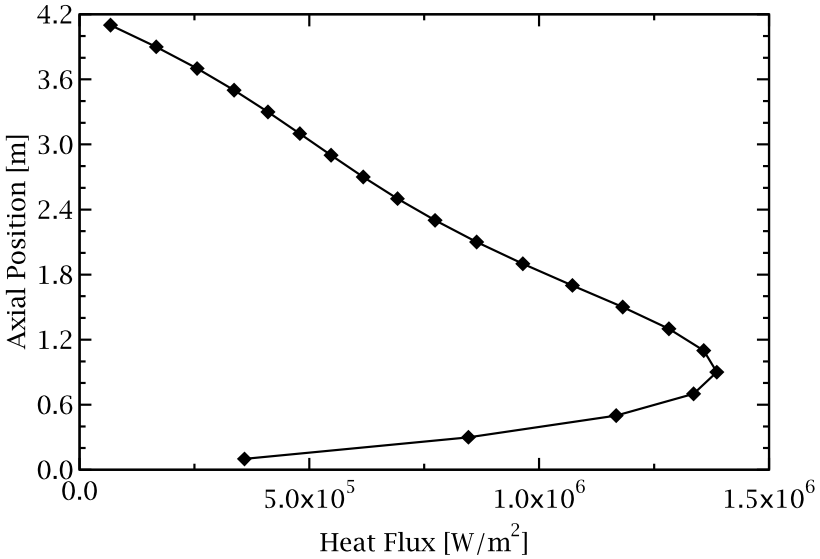

Figure 2.26: Axial distribution of the heat flux

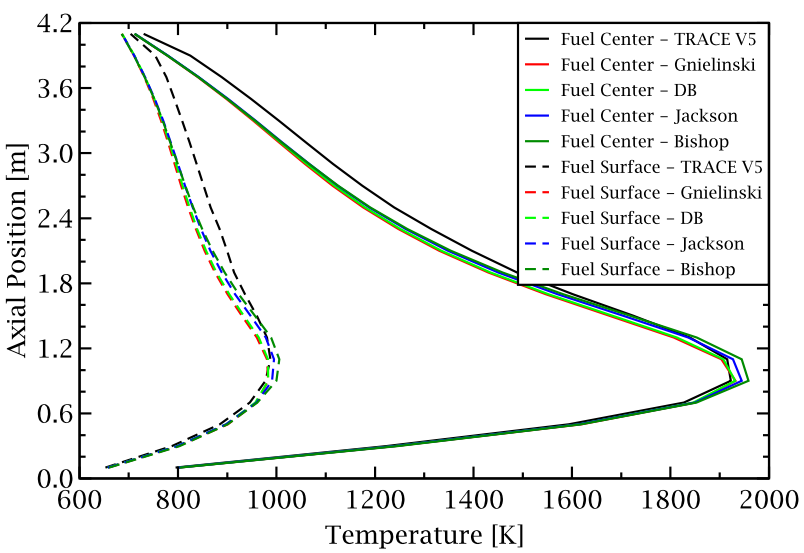

Figure 2.27: Fuel axial temperature distribution

to reach a convergence criterion of 10^{-3} when using the modified TRACE versions whereas the original executable fails in reaching this convergence.

Initially, the sensitivity of the "integral" results is considered, e.g., the temperature of the constituents plotted in Figure 2.27, 2.28 and 2.29. The fuel temperatures, both at the pellet surface and centerline, are important parameters of the coupling with RP analyses, their predicted values are plotted in Figure 2.27: the surface temperature has a moderate sensitivity to the modification introduced in TRACE while the centerline one, for the considered steady state condition, is almost insensitive since its value is mainly determined by the linear power at which the fuel rod is operated. The other key parameters of the coupling with RP analyses are the water temperatures and densities. The coolant temperature is practically not affected by the modifications (less than 1 K in temperature differences) as expected for steady state calculations with fixed total power and mass flow rate. Also the moderator temperature variations show limited sensitivity for the selected boundary conditions since they are changed of no more than 5 K[15]. Higher sensitivity is shown for the clad and moderator box temperatures which undergo more pronounced variations. Even if the moderator box temperature is of no concern for safety

[15]Gap water temperatures are not plotted because they are very similar to those of the moderator water.

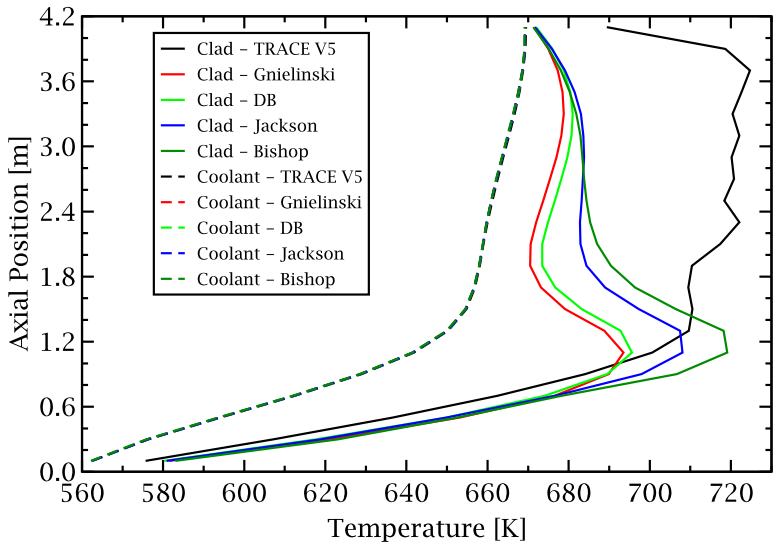

Figure 2.28: Coolant and clad axial temperature distributions

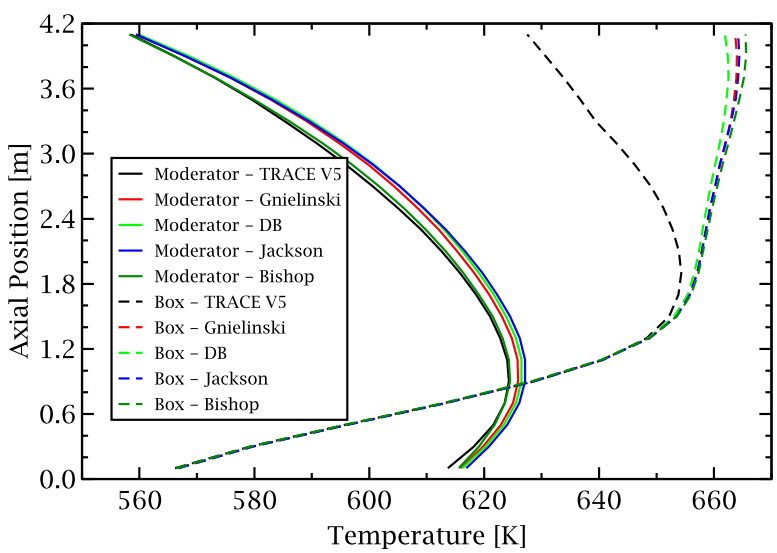

Figure 2.29: Moderator water and box axial temperature distributions

analysis, since it can not reach critical values, it determines the heat transfer between coolant and moderator. The modifications introduced lead to a pronounced rise in its temperature in the upper part of the core. The clad temperature is a crucial value for determining the feasibility of the reactor: its temperature variation obtained with the original TRACE version is not realistic, especially considering the pronounced bottom peak in the power which is well reproduced by the modified TRACE versions both when using Bishop or Jackson correlations. It is quite evident that the original TRACE version does not perform as the improved one in the vicinity of the pseudo-critical temperature, where the differences with sub-critical water are more pronounced.

Better insight into the reasons behind the changes of the constituents temperature can be found considering the predicted HTC for the different HSs of the FA model which are plotted in Figure 2.30, 2.31 and 2.32 as a function of the water (coolant or moderator) bulk temperature.

Using Gnielinski correlation, equation (2.3), with the improved TRACE versions, the calculated HTC shows the same behavior for the heat transfer between the coolant and the fuel rods or the moderator box, Figure 2.30 and 2.31, because this correlation does neither account for the effect of different wall temperatures nor for cooling or heated fluid. The same happens when using Dittus-Boelter correlation, equation (2.6), as far as the coolant is heated whereas differences up to 20% are found in the HTC between cooled and heated conditions: i.e. for heat

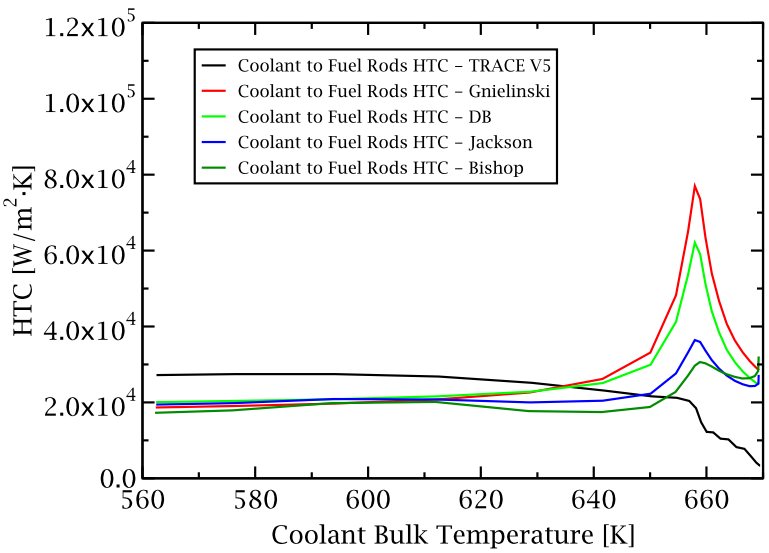

Figure 2.30: Coolant to fuel rods heat transfer coefficient

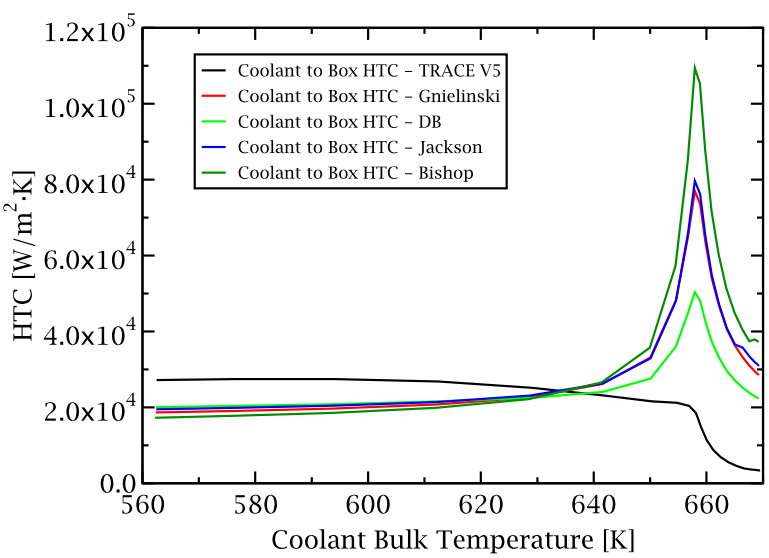

Figure 2.31: Coolant to box heat transfer coefficient

transfer between coolant and fuel rods or moderator box (only in the upper part).

Using both Jackson and Bishop correlations, equation (2.4) and (2.5), different HTC are predicted according to the different temperature of the clad and of the moderator box. Using the original TRACE version, without the improvements in the water properties proposed by Jäger et al. [69], the calculated HTC does not seem to be physical and TRACE fails in reproducing the expected peak in the vicinity of the pseudo-critical temperature [8, 67].

Moderator water temperature does not increase monotonically in the flow direction like the coolant one does, Figure 2.29. For this reason, when plotting the HTC as function of the moderator bulk temperature the curves, which follow the flow direction, have two points for the higher temperatures, as shown in Figure 2.32. Whereas Gnielinski correlation gives exactly the same HTC for the same moderator bulk temperature, despite the different temperature of the moderator box; Bishop and Jackson correlations show similar trends and both predict a different HTC even for the same moderator water bulk temperature but for a different moderator box temperature. Concerning Dittus-Boelter correlation, it predicts almost the same value of the HTC for heated and cooled conditions. The original TRACE version, because of the limitations already underlined, calculates a not smooth variation which does not seem to be physical.

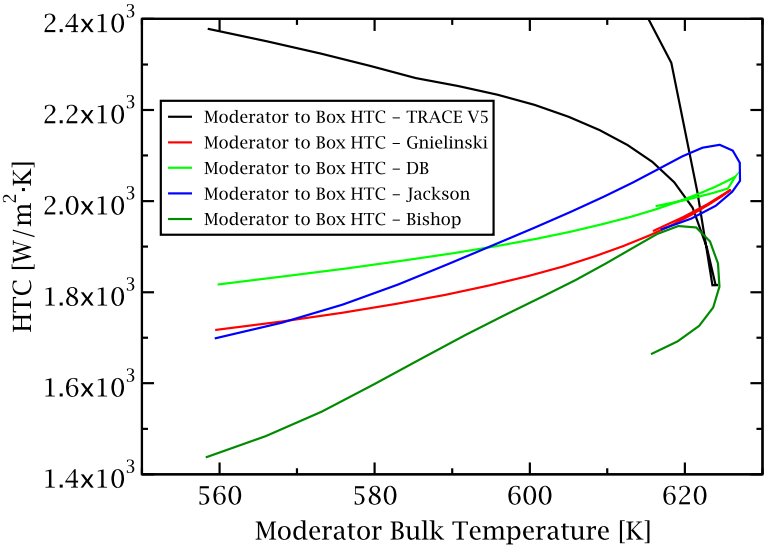

Figure 2.32: Moderator to box heat transfer coefficient

Whole core analyses

Concerning whole core analyses, attention is given to the axial temperature variations of water and structural material. The thermal power of the whole core is here assumed to be 2400 MWth and the RPV inlet flow rate is fixed to 1160 kg/s, resulting in a hot leg average temperature above 800 K. An available core power map obtained for steady state coupled RP/TH analysis of this HPLWR core configuration is used for the following studies [97]. The total moderator flow rate is equal to 25% of the RPV inlet flow rate. For the rather complicated core model and for the high power density in the central core region, the convergence criterion has been slightly relaxed to $5.0 \cdot 10^{-3}$; this value is satisfied by the modified TRACE versions but not by the original one.

The described code improvements lead to variations up to 65 K, 15 K, 20 K and 45 K in the local temperature of, respectively, gap water, moderator, coolant and lumped fuel[16]. To obtain a better understanding of the core results sensitivity, the axial variation of water and clad temperature for selected FA in different core region is plotted in Figure 2.33 to 2.36.

The coolant and the clad temperature, calculated using both the original and the modified TRACE versions, for the FA with highest power density, are plotted in Figure 2.33 and similar considerations to those presented for single FA analysis can be drawn. The clad temperature variation does not seem to be realistic when using the original TRACE version whereas the values obtained with the modified TRACE versions give a better representation of the axial power shape. In addition, the clad temperature at the top of the core is close to the one of the coolant, as expected, since the power generated in this region is lower [97]. The coolant temperature variation predicted using Bishop and Jackson correlations are quite close: the inlet temperature calculated using these correlations is higher than the one predicted by the original TRACE version as the outlet one is lower. This is due to the higher heat transfer between coolant and moderator water obtained using the modified TRACE versions, as shown in Figure 2.35 and 2.36. The coolant temperature predicted using Dittus-Boelter correlation agrees well with those obtained using the correlations dedicated to supercritical water whereas the clad temperature variations shows bigger discrepancies. Also concerning the other selected cluster located in SH1, the clad temperatures variations are affected by the code modifications. The original TRACE version calculates an abrupt jump of clad temperature which does not seem to be physical and which is substantially reduced with the improved TRACE versions, Figure 2.34.

Moderator temperature variations, for both the fraction flowing in moderator channel and that

[16]Calculated using the Rowlands formula, equation (2.1).

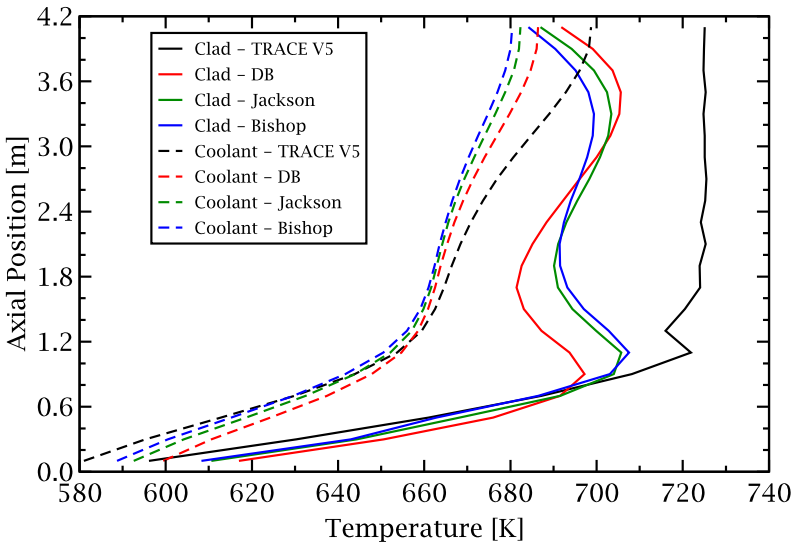

Figure 2.33: Coolant and clad axial temperature distributions in CL 11 (EVA)

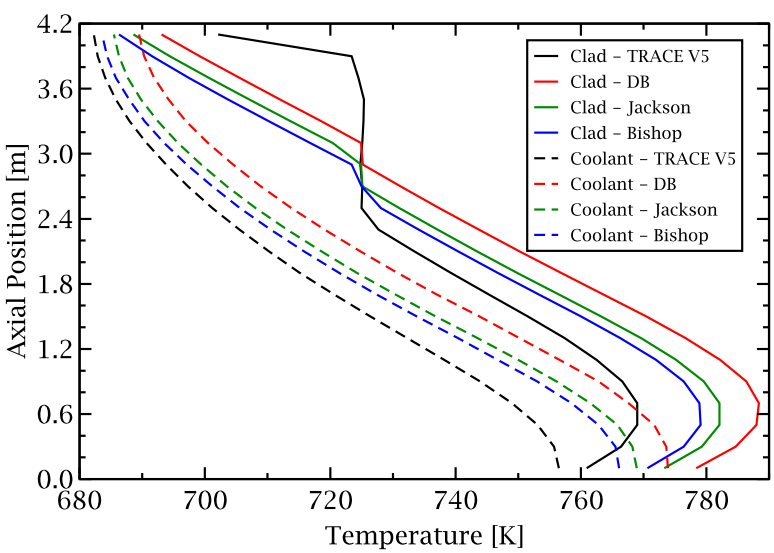

Figure 2.34: Coolant and clad axial temperature distributions in CL 44 (SH1)

in the gap between FAs, are plotted in Figure 2.35 and 2.36 for selected FAs of SH1 and SH2 core regions. These results are remarkable because they show a pronounced difference between the predicted temperature variations of gap water using the original or the improved TRACE versions. The moderator and gap water channels have similar flow conditions and hence they are expected to have similar heat up which is found only when using the improved TRACE versions. The original TRACE version leads to a pronounced underestimation of the gap water temperature rise which explains the different coolant core entrance temperature underlined previously. Since the first node is already heated, this temperature is not the inlet one and hence the various TRACE versions, predicting a different heat transfer, have a different moderator bulk temperature already in the first cell.

The variations in water temperature distribution, changing the heat flux between coolant and moderator, change also the coolant flow rate which is calculated by TRACE according to the chosen orifices map, which has not been changed and hence is not optimized for each of the different heat transfer correlations. Comparing the results obtained with the original TRACE version with those obtained using Bishop correlation, variations up to 20%, 15% and 12% are found in EVA, SH1 and SH2 respectively: e.g., in the core central channel, the flow rate is increased from 2.7 kg/s to 3.3 kg/s.

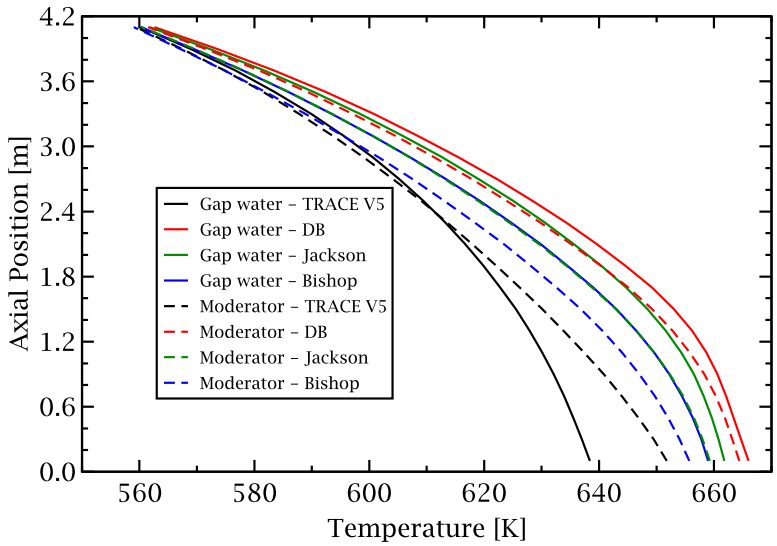

Figure 2.35: Moderator and gap water axial temperature distributions in CL 44 (SH1)

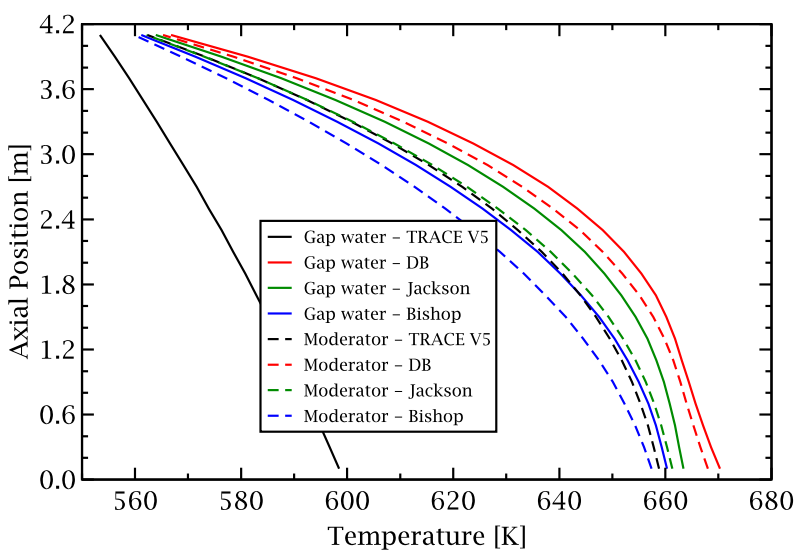

Figure 2.36: Moderator and gap water axial temperature distributions in CL 37 (SH2)

Convergence of the fuel assembly wise core model

The developed FA-wise model requires extremely long CPU time[17] to fulfill selected convergence criterion, because of the high number of components as well as the coupling among the various regions and flow paths provided by the heat transfer between coolant and moderator/gap water together with the multi-pass core design. The convergence of the calculation, whenever the maximum specified simulation time is reached, can be verified plotting the temperature distribution as function of the successive iterations involved in the steady state calculations. This task is easy achievable since TRACE is always run in transient mode and the convergence tests stop the calculations in case of achieved steady state solutions.

Temperatures of selected structural materials are plotted in Figure 2.37 to underline the achieved convergence of the steady state solution. The importance of the initial conditions on TRACE convergence is evident and, hence, to reduce the CPU time needed to perform the successive iterations of the coupled ERANOS/TRACE system, the TRACE run of the previous iteration is used to restart the calculation with the new power map predicted with ERANOS.

[17] The FA-wise core model may take up to 30 hours on a 2.4 GHz Linux PC with 2 GB of RAM, depending on the restart condition, on the selected maximum time step size and convergence criterion, here set to $5.0 \cdot 10^{-4}$.

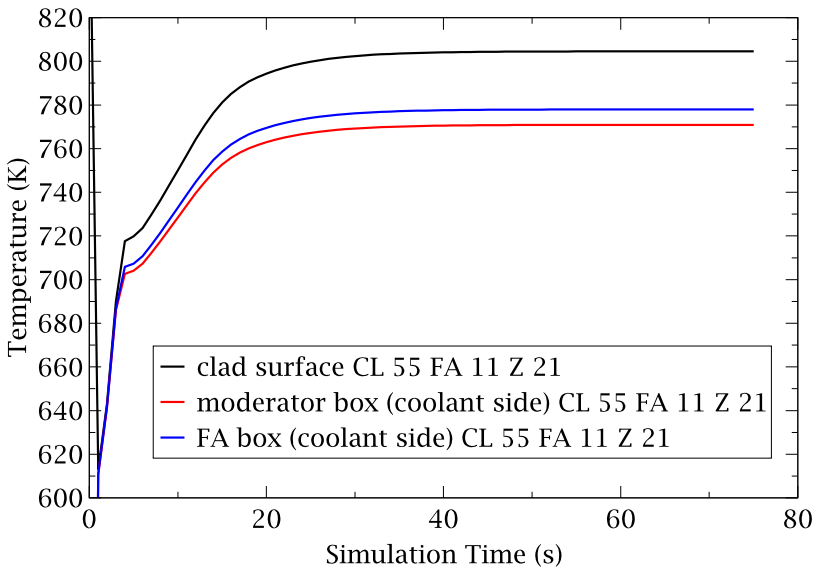

Figure 2.37: Structural material temperature variations during the steady state simulations

2.3 Modeling of the HPLWR fuel assembly with MATRA

2.3.1 Code selection

As described in the introduction, wire-wraps have been selected as fuel rod spacers and mixing devices for the HPLWR FA, Figure 1.2(b) on page 3. They divert the coolant flow within the fuel bundle improving the coolant mixing and reducing the peak - to - average temperature distribution. For this reason they have been extensively studied in the past, especially for liquid metal cooled fast reactor concepts [22, 74, 160].

Within the Working Package 5 of the HPLWR EU-Project [54], the effects of the diverted flow induced by wire on the local HTC is investigated with detailed CFD simulations [18, 76] which aim to estimate local effects such as azimuthal asymmetries in the clad temperature. These kind of simulations are very useful to improve the understanding of the flow field within the fuel bundle but are extremely time consuming and hence can not be applied to even full length single fuel assembly analyses. Fanning et al. [41] showed the importance of having a representation of the wire effects in the sub-channel investigations to determine local peak temperatures using a direct comparison with CFD simulations.

For these reasons, MATRA [71, 75, 168] has been selected for HPLWR applications since it includes a model to represent a wire wrapped fuel bundle, formerly developed for COBRA IIIC by D.S. Rowe [127].

In MATRA it is not possible to represent the heat transfer to thermally, but not hydraulically, connected channels when the relative flow is counter-current. Since the present FA design has thermal insulated boxes [51], this limitation should be acceptable. Considering the present application, the fission power is entirely assigned to the coolant and the heat losses to moderator water are neglected, the calculated coolant temperature is hence higher providing a conservative evaluation. Some more details on this topic will be analyzed later with a direct comparison with TRACE for the bundle average coolant temperature.

2.3.2 Supercritical water steam table

MATRA has been mainly developed to analyze advanced LWRs [168] and it includes several capabilities to represent two-phase flow phenomena. A dedicated steam table is hard coded

in the subroutine TAF of the MATRA source file. It calculates the properties of light water in liquid and vapor states according to the 1967 formulation of properties for water and steam. Unfortunately, this hard coded steam table is not applicable to water at supercritical pressure and hence modifications of the source code are necessary. In MATRA, there are 3 possible calls to the steam table: 1) a property as function of temperature and pressure; 2) the pressure as function of one property and temperature; 3) the temperature as function of pressure and one property. Considered properties may include: specific volume [m^3/kg], specific enthalpy [kJ/kg], specific entropy [kJ/kg/K], thermal expansion coefficient [1/K], specific heat [kJ/kg/K], thermal conductivity [kW/m/K], viscosity [kg/m/s] and surface tension [N/m].

In MATRA there are several fluids available [84], hence the extension to supercritical water can be performed by adding an additional fluid type which has the thermophysical properties of water at 25 MPa. Concerning the desired steady state applications to HPLWR core analyses, the usage of a simple temperature dependent lookup table, similar to the one originally developed for STAFAS by Cheng et al. [24], is acceptable. Hence tabulated values for density, specific enthalpy, specific heat, viscosity and thermal conductivity – based on the current IAPWS format [147] – have been hard coded in the MATRA source file as function of temperature, ranging from 513.5 to 923.15 K. The selected temperature mesh has been chosen keeping in mind that a linear interpolation will be used among the tabulated values: 5 K steps are used in the region far from the pseudo-critical point and are gradually reduced to 2, 1 and 0.25 K to capture the abrupt changes of water properties. The developed subroutine is able to return the required properties for the desired temperature and to determine the temperature corresponding to the input property. The two phase issue has been solved by selecting a high saturation temperature in order to ensure single-phase representation in all the considered conditions.

This approach has been preferred to the usage of approximate analytical functions, as the ones proposed by Laurien et al. [81], because it is more accurate and the CPU time in sub-channel calculations is of no concern.

2.3.3 Description of the wire-wrap model

The HPLWR FA has 60 sub-channels and 40 wires which are wrapped around the 40 fuel rods as depicted in Figure 2.38. A 1.34 mm diameter wire crosses the 1.44 mm gap between adjacent rods; the wire lead is 20 cm and the wire revolution is in counter-clockwise direction when observed from the top [55].

It is important to underline that, despite the provided geometrical representation, the sub-channel approach is far from being a fully 3D representation of the flow and the real XYZ spatial position of the various sub-channels – represented only through flow area, gap width, heated and wetted perimeters – is lost. This is due to the major simplification in the treatment of lateral exchange between adjacent sub-channels: any lateral flow through the gap region between sub-channels loses its sense of direction after leaving the gap region [149, Chapter 6]. For this reason, sub-channels can be connected arbitrarily and, because of the simplifications in the lateral convective terms of the momentum balance equation, the sub-channel approach is most appropriate for predominantly axial flow situations.

The wire-wrap model of D.S. Rowe [43, 127, 160] imposes the cross flow through the gap between adjacent sub-channels only when a wire crosses that gap: the wire is assumed to have no effect on cross flow until it crosses a gap sweeping a portion of the flow from the sub-channel it is leaving into the one it is entering. To model this effect, the user has to provide the relative position of each gap with respect to the wire at the bundle inlet, XCROSS(K,L), and the code has an algorithm, in the subroutine FORCE, to evaluate the wire azimuthal position at each axial level. From the specified wire position at the bundle inlet, the code tracks the wire position relative to the gaps between sub-channels as it proceeds axially through the rod bundle. The axial nodalization has been fixed to 2.5 cm in order to have 8 zones in each wire lead. In this

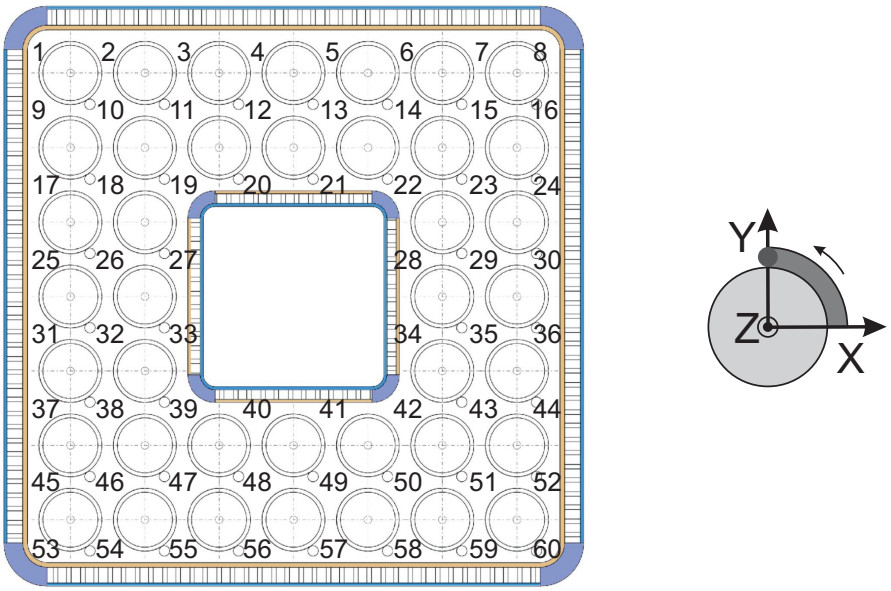

Figure 2.38: The 60 Sub-Channels in the Fuel Assembly

way, every two axial zones, the wire is crossing a gap between adjacent sub-channels forcing cross flow through that gap and, every 8 axial zones, the wire is located in the same azimuthal position around the fuel rod.

The D.S. Rowe model, reported here as coded in the subroutine `FORCE`, is mostly based on geometry and flow consideration. It imposes the cross flow per unit axial lenght `W(K,J)` at the gap `K` crossed by a wire in the axial location `J` as:

```
IF (XCROSS(K,L).LT.0.D0) THEN
W(K,J)=-GAP(K,J)*DUR(K)*PI*(DIA+THICK)/DX(J)*F(JJ,J)/A(JJ,J)
ELSE
W(K,J)=+GAP(K,J)*DUR(K)*PI*(DIA+THICK)/DX(J)*F(II,J)/A(II,J)
END IF
```

where `GAP(K,J)` is the width of the gap `K` between adjacent fuel rods, `DIA` is the fuel rod diameter, `THICK` is the wire thickness, `DX(J)` is the length of the axial nodalization, `F(JJ,J)` and `A(JJ,J)` are the mass flow and flow area of the donor sub-channel (either `II` or `JJ`) at the given axial position. The proportionality constant, `DUR(K)`, is a user specified input parameters which may depend on the considered gap `K`. For all the axial positions in which the gaps are not crossed by a wire, the standard sub-channel approach to calculate the cross flow, based on the lateral pressure differences between adjacent sub-channels, is used. But the cross flow through the gaps not crossed by a wire and bounding the donor/receiver sub-channels are modified accounting for the calculated `W(K,J)` in order to ensure the mass conservation.

2.3.4 Sensitivity of the cross flow to the mixing coefficients for a purely hydraulic case

The qualification of the input parameter `DUR(K)` is rather complex and its value is recommended to be chosen as function of the wire geometry and spatial nodalization [43]:

$$\texttt{DUR(K)} = \frac{\text{axial node length (DX)}}{\text{wire lead}}$$

During intial tests, it was found that this model may lead to negative enthalpy predicitions and hence code crashes. These have been blamed to excessive high cross flow which may results in

negative prediction of the axial mass flow in certain sub-channels. To avoid this trouble, the axial nodalization, and hence `DUR(K)`, has to be kept small: the selected 2.5 cm has never shown such a kind of problem for all considered test cases.

Several test cases have been performed to analyze the wire effect for non-heated cases using nominal flow conditions, the results reported here correspond to an inlet temperature of 382 degrees C and a bundle averaged mass flux of 1814 kg/(s m^2). Sensitivity studies showed a clear dependence of the cross flow on the axial mass flux but the lateral - to - axial velocity ratio was found to be rather insensitive to the selected boundary conditions, as confirmed by Himmel [55]. It is defined as follow:

$$VR = \frac{\text{averaged lateral } \vec{v} \text{ in the gap}}{\text{averaged axial } \vec{v} \text{ in the donor sub-channel}} \tag{2.7}$$

The velocity ratio is selected as a convenient dimensionless quantity to analyze and compare the obtained results.

As suggested by Kiss et al. [76], the 100 gaps have been divided into 6 types, which depends on the crossing direction of the wire:

- 32 gaps between lateral sub-channels or from a lateral to a corner;
- 20 gaps between central sub-channels;
- 32 gaps between a lateral and a central sub-channel;
- 4 gaps from a corner to a lateral sub-channel (FA box);
- 4 gaps from a corner to a lateral sub-channel (moderator box);
- 8 gaps from a corner (at the moderator box) to a central sub-channel.

Initially, `DUR(K)` has been fixed to the recommended value equal to 0.125 for all the 100 gaps. The obtained results for each type of gap are plotted in Figure 2.39 for an axial length equal to one wire lead: for the considered non-heated case, the hydraulic solution has a period of one wire lead. The sign of the cross flow, and hence on VR, respects the following convention: it is positive when it is directed in ascending sub-channel number.

The cross flow through the gap between two lateral sub-channels adjacent to the FA box wall (4 and 5) is unilateral while the one between two central or a central and a lateral sub-channels is bilateral but the cross flow calculated by MATRA between two lateral sub-channels adjacent to the moderator box wall (20 and 21) is bilateral and hence does not represent the expected flow sweeping effect predicted with high fidelity CFD simulations [55, 76]. The unilateral flow in the lateral sub-channels is explainable on basic physical considerations since, per each wire lead, a wire crosses the lateral gaps only in one direction whereas the central gaps in two opposite directions, as explained also in [9, 74, 75]. In particular, since the wire direction is counter-clockwise in the HPLWR FA: the expected unilateral flow is always from sub-channel 5 to 4 (negative cross flow) and from 20 to 21 (positive cross flow).

To overcome this discrepancy, a sensitivity study has been initiated to calibrate the values of `DUR(K)` with an iterative procedure. It was immediately realized that the cross flow through a gap is strongly influenced not only by the input `DUR(K)` of that gap but also by those of the neighboring gaps permitting only a qualitative tuning of these coefficients. For each type of gap defined previously, the value of `DUR(K)` has been adjusted with respect to the recommended one with a try and fail procedure till an acceptable qualitative agreement on the flow field with the high fidelity results is obtained; the selected values are listed in Table C.10 on page 147. To achieve the observed unilateral flow through the gaps between the lateral sub-channels adjacent to the moderator box, the cross flow among two central sub-channels as well as among the lateral

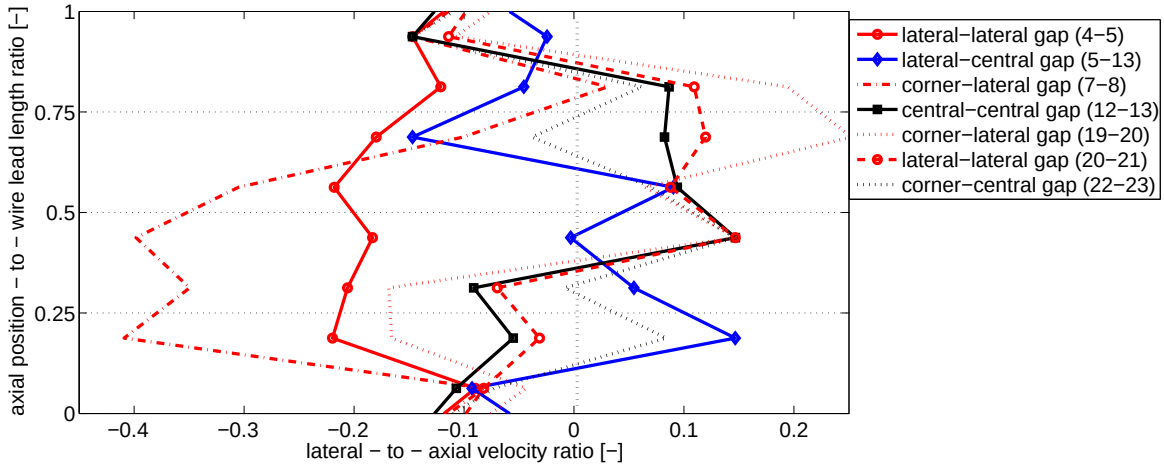

Figure 2.39: Velocity ratio in selected gaps with recommended `DUR(K)`

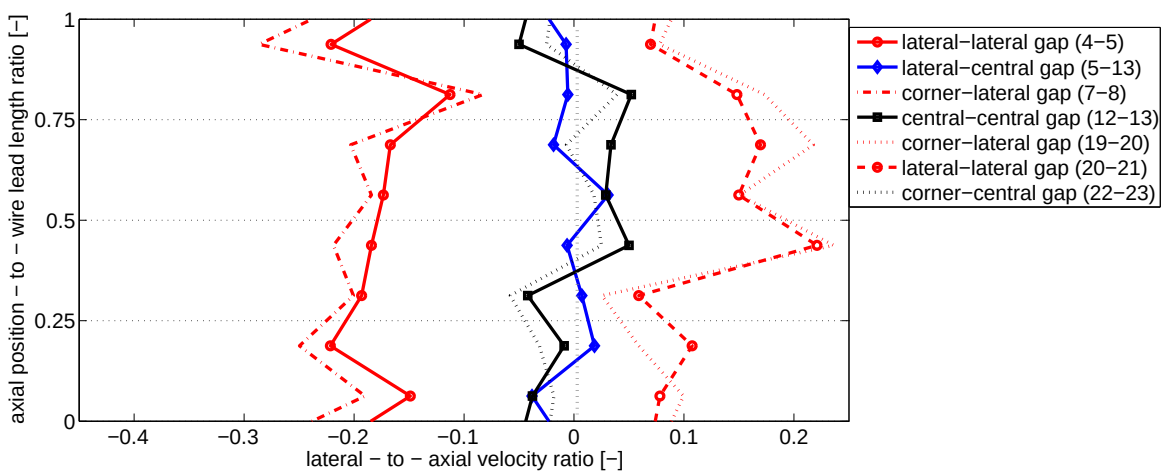

Figure 2.40: Velocity ratio in selected gaps with adjusted `DUR(K)`

and the central one shall be reduced. *VR* obtained with the adjusted `DUR(K)` factors are plotted for selected gaps in Figure 2.40: a unilateral flow is predicted in all the gaps crossed by the wire in only one direction (e.g. between sub-channels 4 and 5, 7 and 8, 19 and 20, or 20 and 21) whereas a bilateral flow occurs when a gap is crossed by two different wire at different axial position (e.g. between sub-channels 5 and 13, 12 and 13 or 22 and 23). The lateral velocity in the gaps bounding a central sub-channels is always smaller than the lateral velocity in gaps between lateral sub-channels ensuring a unilateral flow field.

A direct comparison with the data kindly provided by Himmel [55] is plotted in Figure 2.41:

- in the gap between a lateral and a lateral sub-channel (e.g. between 4 and 5), a good agreement is found since a unilateral flow is observed in both cases with also a similar magnitude, which is a bit over-predicted by MATRA;

- in the gap between a lateral and a central sub-channel (e.g. between 5 and 13), a bilateral flow is observed in both cases which show similar axial trends;

- in the gap between a central and a central sub-channel (e.g. between 12 and 13) only the axial trend is reproduced while the magnitude of the lateral velocity seems to be under-predicted by MATRA but this effect was expected on the basis of the selected coefficients.

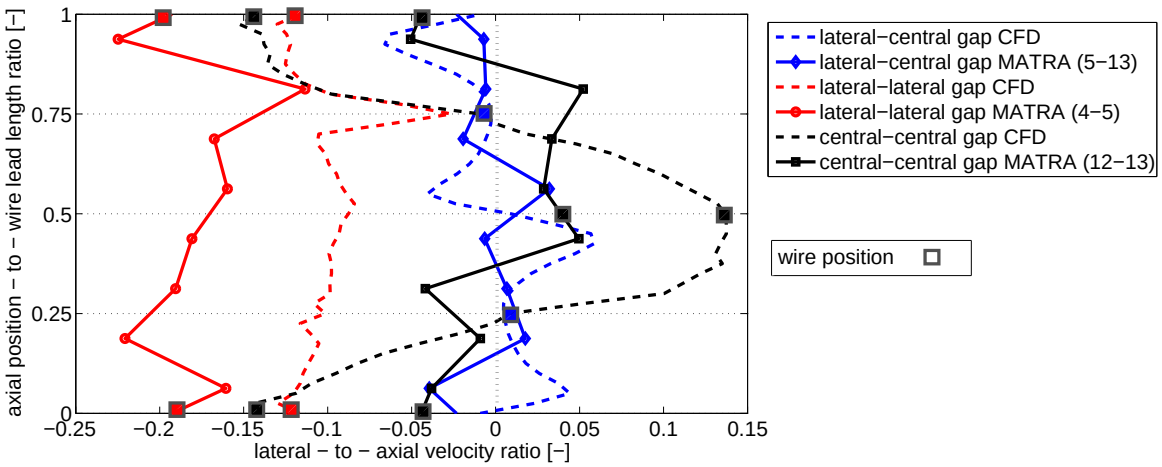

Figure 2.41: Comparison of the velocity ratio between sub-channel and CFD [55] analyses

Considering the differences between the models, due to both boundary conditions and spatial resolution, and the limited amount of data available (only 3 gaps are comparable), this agreement is sufficient for the present applications because it enables to reproduce reasonably well the global flow field within the fuel bundle. As it will be shown later, for a heated case, the changes of the cross flow have only a limited effect on the bundle temperature distribution but additional efforts would be necessary to achieve also a quantitative agreement with high fidelity CFD simulation of the whole bundle.

Chapter 3

Design and development of a coupled multi-physics, multi-scale analysis tool

3.1 Problem statement

The coupling between RP and TH physical models is based on the power map and on the temperature distributions of the constituents as explained in the introduction. For steady state applications, the physical modules can be treated as distinct components and their coupling can be implemented as interactions between them. The dependence of XSs in the linear transport equation (1.1) on the temperature and density of the constituents is the principle source of the non-linear coupling between RP and TH physical modules.

The independent solution of the fundamental steady state equations of RP and TH, equations (1.1) and (1.2, 1.3) respectively, for the HPLWR core requires to use dedicated codes to perform RP and TH core analyses predicting the coupling parameters. The capability of the selected tools to predict these coupling parameters have been verified in the previous chapter permitting to proceed further with the development of the coupled system as interactions between the two physical models.

Since it is impractical with the available computational resources and tools to simulate a full reactor core using fuel rod spatial resolution, the coupled system is applied to a core model based on FA-wise nodalization. To predict the local clad temperatures, the obtained coupled solution is investigated at sub-channel resolution applying pin-power reconstruction techniques and dedicated mapping scheme to realize the desired multi-scale investigations.

3.2 Details of ERANOS/TRACE coupling

3.2.1 Design of the coupling framework

ERANOS and TRACE run successfully in a 32-bit Linux environment which offers the possibility to develop high flexible calculation procedures by means of Bash scripting language, a free software Unix shell written for the GNU Project. In Bash, the automation of the iterative procedure – including successive codes executions and runs of the codes interfaces – can be achieved with few programming lines and the developed supervision script offer high flexibility while maintaining simplicity.

The stand alone codes are coupled with dedicated interfaces; these have been developed from scratch and are responsible for the data extraction (post-processing) and input file preparation (pre-processing). A powerful tool to process and modify ASCII files is Perl language: a high-level, general-purpose, platform independent, interpreted, dynamic programming language. By using

Perl it is possible to scan ASCII files searching for user defined keywords and specified format. This offers the possibility to search in ERANOS and TRACE output files for the data required for the coupling, i.e. the core power map, fuel temperatures as well as water temperatures and densities, and to insert these data, after proper reformatting, in the input file of the other code. The coupling is hence achieved exchanging data between the codes using these Perl processing functions and without requiring any code modifications or frequent user interaction. The coupled system is run from command line without any GUI[1].

ERANOS and TRACE are kept independent, considering the geometrical capabilities and the physical principles within each module.

3.2.2 Mapping scheme

Cluster wise core representation At the beginning, a direct mapping of the computational nodes between the codes has been selected and the same nodalization is used for both RP and TH analyses. This approach simplifies the data exchange and does not pose questions on the kind of interpolation to be used on the data. The mapping schema is based on an XYZ indexing of each CL in the 3D core volume, which is the same for both codes. In this way a one-to-one correspondence between the spatial volumes or nodes in TRACE and ERANOS is established and is used to extract and correctly position the individual data. This mapping schema simplifies substantially the set-up of the input file since the user does not have to respect any predefined order to input the components and specify the geometry since the coupling scripts will search for the specified keywords.

Fuel assembly wise core representation The necessity of an individual representation of each FA in the core is evident when considering the extraction of the boundary conditions necessary for sub-channel investigations. For this reason the model used for TRACE has been refined going from a CL-wise core representation to a FA-wise core representation. The computational cost of such a detailed model with TRACE is acceptable but the one of ERANOS, which would be increased by roughly nine times[2], is impermissibly high on the available single machine. For this reason the ERANOS core model is kept at a CL-wise representation. The complex interpolation of the neutron flux and power gradient is performed using the flux reconstruction function available in ERANOS [130] to represent the 9 FAs in each CL used as computational node. The previous mapping schema is extended by adding the FA position inside each CL to the index used to exchange the data. Using the ERANOS post processing function and the new mapping notation, the coupling schema from ERANOS to TRACE is still a direct one. In ERANOS, data at cluster level are required while TRACE calculates now data at FA level, hence, the TH parameters calculated by TRACE are averaged over the 9 FAs of each CL. A simple arithmetic mean is used to calculate temperatures and densities necessary for the feedbacks on RP calculations.

3.2.3 Automated calculation procedure in ERANOS

To provide an accurate representation of the considered TH feedbacks on RP calculations, a precise representation of the 40-group self-shielded XSs dependence on the temperatures and densities changes is mandatory. As mentioned in the introduction, very advanced coupled

[1]For this reason SNAP, i.e. TRACE GUI, is not used during the coupled analysis but only when preparing the input file, the corresponding core model is given in Figure 2.25, including cluster numbering and flow paths description.

[2]The CPU time in ERANOS is mainly spent in the XSs generation. Hence, resolving the 9 FA of each CL would increase it by a factor of 9 demanding for XSs interpolation scheme which are not available for the current application.

systems use a multi-dimensional XS interpolation among the TH parameters [114, 155], but the complexity of the current application, which considers 7 parameters[3] with pronounced cross term effects, suggested to use an on-line XSs generation technique.

For this reason cell calculations with ECCO are performed at each iteration and for each node in order to generate accurate 40-group, self-shielded, homogenized XSs and P1 scattering matrices needed to perform 3D steady state SP3 analyses with VARIANT. This approach has been verified in section 2.1 for simplified geometries. The ERANOS calculation procedure for the present 3D core application, which requires the generation of a high number of XSs, has been automatized relying both on the ERANOS user language and on Bash scripting as summarized in Figure 3.1.

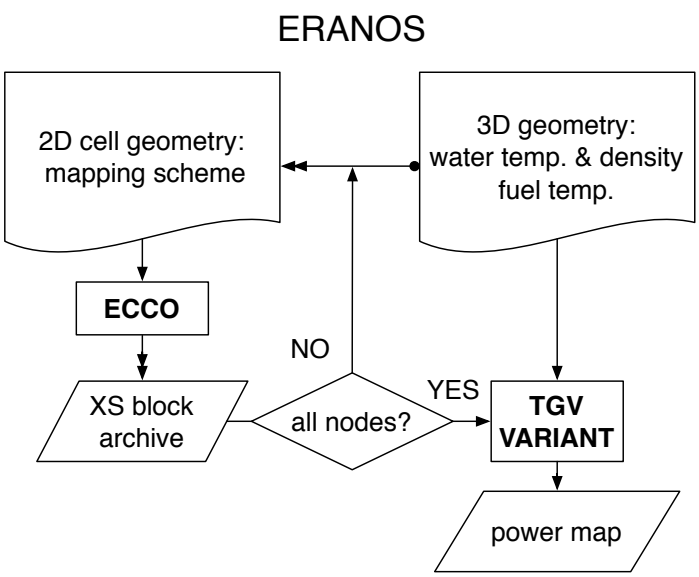

Figure 3.1: Multi-scale neutronic flow chart in the ERANOS system

In addition, the printout of the core power map is formatted respecting the user defined mapping schema with ERANOS dedicated functions for the "edition traverse" [35] as well as nodal flux reconstruction [130], when needed.

3.2.4 Data flow and code interfaces

From TRACE to ERANOS: as defined in the introduction, 7 TH parameters are considered for each individual node. In TRACE a component based representation of the HPLWR core has been represented, hence several components have to be searched for extracting the temperature and density of the coolant, moderator and gap water as well as for the fuel pellet centerline and surface temperature at all axial positions[4]. The fuel lumped temperature, used in the ECCO input file, is calculated according to the Rowlands formula [128], previously described in equation (2.1), which has been implemented in the Perl script, `TRACE2ECCO.pl`, responsible for the generation of the ECCO input files. This script, which fed into the ERANOS system the just calculated TH properties, is also responsible for the mapping of the axial nodes for coolant and moderator/gap water including up- and downward flow[5]. In addition, it calculates the CL-wise arithmetic mean of the TH parameters extracted for each FA.

[3] Fuel temperature plus coolant and moderator/gap water temperature and densities for the current analyses.

[4] The clad temperature should have almost no importance for the coupled solution, hence its value has been selected and kept constant.

[5] Depending on the core region, i.e. EVA, SH1 or SH2, the coolant flow direction is modified.

From ERANOS to TRACE: the in-core power map is calculated by VARIANT using the 40-group, self-shielded, homogenized XSs generated by ECCO and corresponding to the input TH parameters. The volumetric power density is printed in the output file as axial traverses for each CL or FA including the mapping keywords and the ERANOS user language is used to calculate the total power of each CL or FA covering the two kinds of input data necessary for TRACE. A different Perl script, `TGV2TRACE.pl`, has been developed to extract these data and fed them into the TRACE input file respecting the XYZ position of each value.

To mitigate pronounced oscillations among successive iterations experienced in preliminary analyses, a damping factor has been introduced [129]. Among the available parameters, the power map, $P(x,y,z)$, is most sensitive to abrupt changes since it has to satisfy physical limits (e.g. maximum linear power) hence an under-relaxation r has been used for this parameter between successive iterations (index j):

$$P_{(j)'}(x,y,z) = r \cdot P_{(j)}(x,y,z) + (1-r) \cdot P_{(j-1)'}(x,y,z) \tag{3.1}$$

This operation is automatized in the Perl script `TGV2TRACE.pl` which uses the relaxed power map of the previous iteration stored in an ASCII file.

3.2.5 Coupled system

The coupled system for 3D HPLWR analyses consists of 4 blocks: 2 stand alone codes and 2 interfaces. A dedicated Bash supervision tool is responsible for the automation of the successive runs of the codes and interfaces. To provide high flexibility, two nested scripts are used: the outer one is simply responsible for the iteration loop while the inner one for the codes run. Using this approach, it is possible to change the relaxation parameter, the code interfaces[6] or the skeleton input files while the coupled system is in operation. Supervision is added to the main function calls to terminate the coupled system if VARIANT or TRACE failed in calculating the coupling parameters[7]. A graphical representation of the coupled system is provided in Figure 3.2.

The coupled system is run for a user defined number of iterations. The verification of the convergence of the iterative procedure has been delegated to the user, who should inspect the changes of the TH parameters or power map among successive iterations, more details will be provided later in the application to HPLWR core analyses. This can easily be achieved using the output files of the Perl scripts which are formatted to be directly imported in Matlab or Octave using the `load` function. The restart of a terminated run is extremely simple thanks to the developed coupling scripts.

3.2.6 Testing of the coupled system with single fuel assembly analyses

Operating conditions

The coupled system is initially tested for a simple geometry, a single FA, to verify the data exchange and to gain experience with the sensitivity of the different parameters on the coupled solution, [92, 95]. Thanks to the problem simplicity, the computational cost is low and hence several test cases can be performed allowing to get more insight into the physical basis of the coupled analyses. For these initial tests, no under-relaxation has been used, freezing r to 1 in equation (3.1).

The boundary conditions are assumed for a typical EVA FA, which presents the highest coolant density reduction and hence is the most sensitive to the TH feedbacks when compared

[6] For example to exchange only certain feedbacks, as done when first neglecting the fuel temperature variations.

[7] Besides programming errors which can occur in the development stage, code crashes may occur and it is highly desirable to stop immediately the iterative procedure.

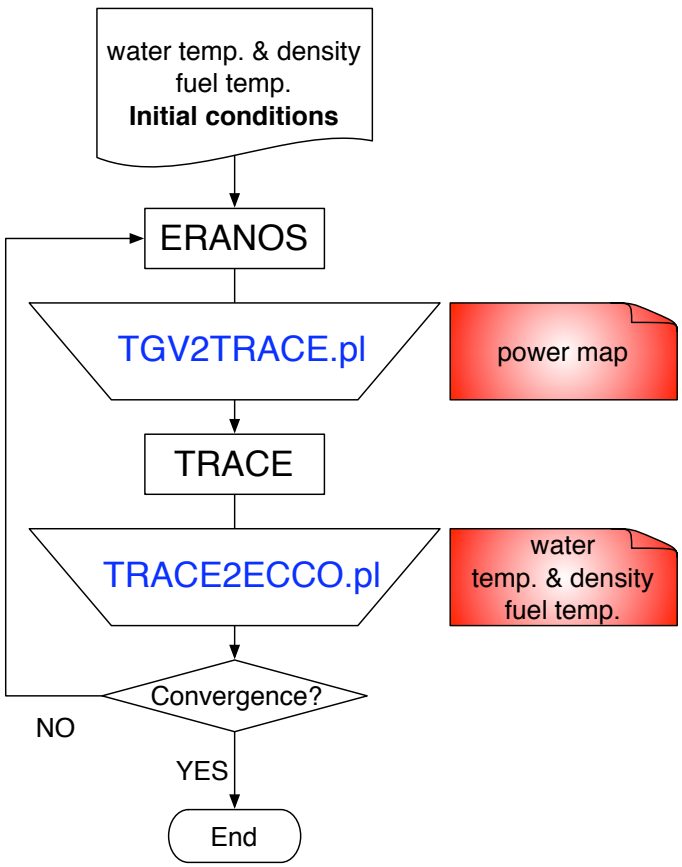

Figure 3.2: Coupled system flow chart

to the other core region (namely SH1 and SH2). They include coolant inlet temperature and flow rate both fixed to nominal values, as well as the power which, being equal to 2.56 MWth, corresponds to a representative EVA FA [137]. The total FA power is kept constant and is not affected by the TH feedbacks. The developed models for ERANOS and TRACE have been described in the previous chapter.

The starting condition used for the the neutronic calculation is uniform TH properties in all the 21 axial cells in which the axial length is divided. This results in the expected cosine power shape at the first iteration [79]. At first, only the density and temperature of coolant and moderator/gap water are exchanged between the codes; successively also the effect of fuel temperature variations is investigated. It is reminded here that the water temperature influences the thermal scattering law and hence RP calculations.

Preliminary coupled investigations exchanging only water properties

Neglecting the effect of the fuel temperature variations on the axial power shape, the initial cosine shape, typical of uniform properties in the axial direction, is distorted immediately presenting a bottom peak which remains with only slight modifications in the successive iterations, as shown in Figure 3.3.

Only few iterations are necessary to obtain a reasonably converged shape which demonstrates the sensitivity of the power generation to the water densities axial distribution, Figure 3.4. It seems that the coolant, being closer to the fuel rods, has more pronounced feedbacks than moderator/gap water. The three different water properties for coolant and moderator/gap water can be combined in a node-wise volume averaged water density distribution which results to be higher where the power density is higher. Since the volume averaged water density neglects the fact that coolant and moderator/gap water, occupying different positions in the FA, affect in a

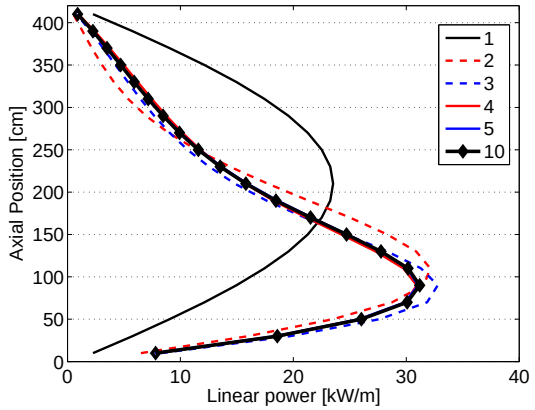

Figure 3.3: Axial power shape in successive iterations varying only water properties

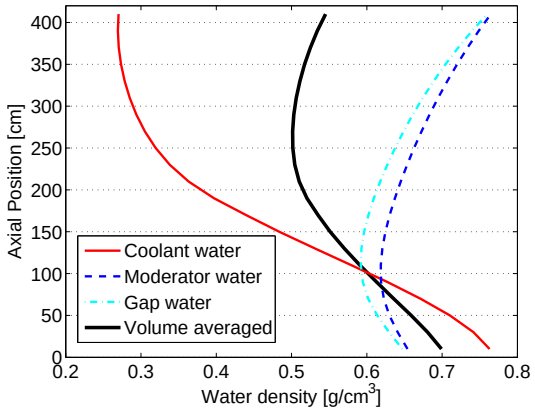

Figure 3.4: Water axial densities distribution in iteration 10 varying only water properties

different way the power shape, it is used only for better and easier understanding of the results while the heterogeneity is preserved both in RP and TH calculations.

Sensitivity of the coupled analysis to fuel temperature variations

Considering also the effect of fuel temperature variations on the coupling and starting from the same initial condition, a completely different power shape evolution has been found, as shown in Figure 3.5. After the initial oscillations, the power shape stabilizes and exhibits a bottom peak which is less pronounced than when neglecting the fuel temperature effect, Figure 3.3, as expected because of the negative feedbacks caused by the resonance broadening, primarily of ^{238}U, in the nodes of higher fuel temperature. The pronounced initial oscillations are more evident when plotting the power generated in selected axial nodes as function of the iteration number, Figure 3.6.

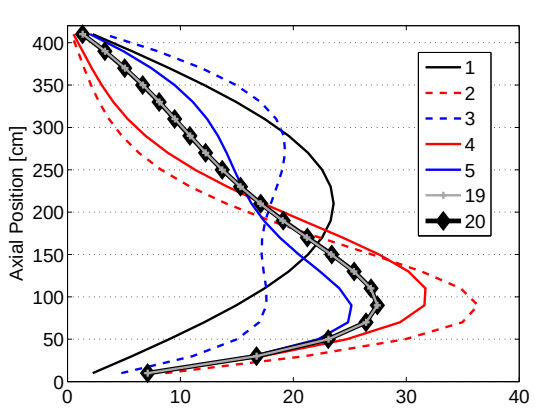

Figure 3.5: Axial power shape in successive iterations including fuel temperature effect

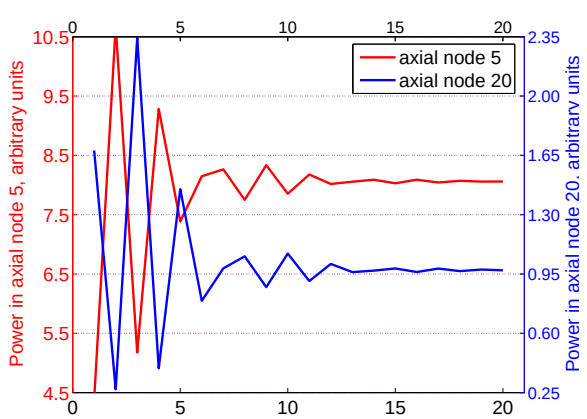

Figure 3.6: Power for selected axial nodes in successive iterations

To understand the changes of the power shape, the axial distribution of the TH parameters in successive iterations is plotted in Figure 3.7 and 3.8. RP calculations exhibit a pronounced power peak in nodes with high coolant density and low fuel temperature (iterations 2 and 4). This leads, in the successive iteration, to a lower coolant density and higher fuel temperature which together suppress the power peak (iteration 3 and 5). This gives rise to the strong oscillations of the power shape in the initial iterations.

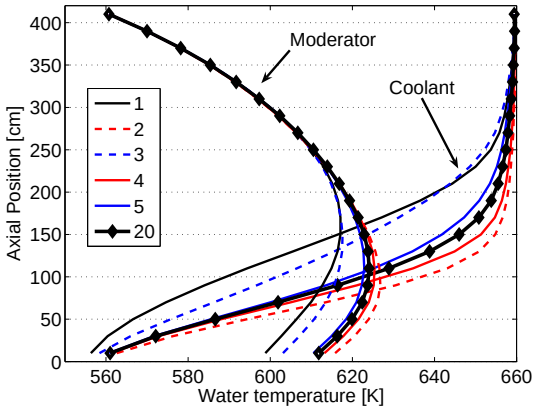

Figure 3.7: Water temperatures in successive iterations including fuel temperature effect

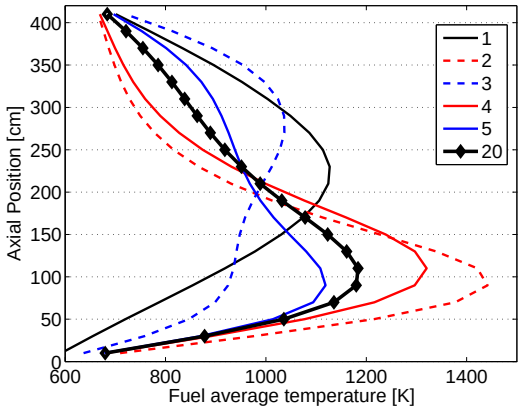

Figure 3.8: Node-wise average fuel temperature in successive iterations

Intermediate conclusions and suggestion for whole core analyses

The coupled system is able to predict physically based results for a typical HPLWR FA. These analyses pointed out the strong amplification which exists among the feedbacks induced by the water properties and by the fuel temperature variations: the two effects are competing in determining the axial power shape.

The coupled analysis converged to a stationary solution after 12-14 iterations, exhibiting pronounced initial oscillations around the final solution. The convergence of the coupled analysis can be accelerated by introducing an under-relaxation in the power, i.e. changing r in equation (3.1) from 1 (no under-relaxation) to values between 0.4 and 0.6 after the second iteration. The relaxed power shape obtained by weighting iterations 2 and 3 is already very close to the one of the final iteration, Figure 3.9, and hence, despite the non-linearity of the problem, the number of iterations required to achieve convergence can be drastically reduced: only 4-5 iterations are necessary for a stationary solution.

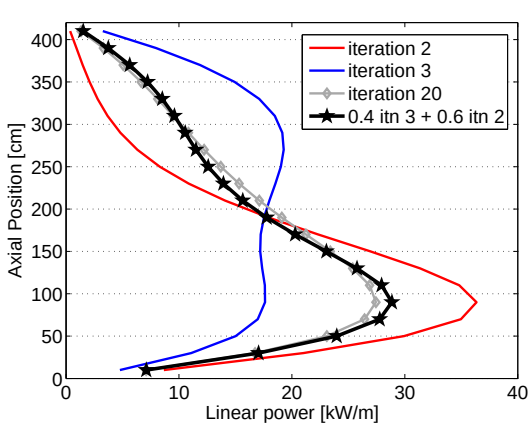

Figure 3.9: Power for selected axial nodes in successive iterations

While the RP/TH coupled solution is independent from the coupling strategy, this can be modified by the user in order to accelerate the convergence or to avoid code failures[8]. Besides the already mentioned under-relaxation factor on the power map r, which can be modified while the coupling system is in operation, the user can choose not to exchange some of the TH parameters, e.g. the fuel temperature, but to keep their value frozen in the initial iterations. These promising results suggest to use an under-relaxation on the power map for whole core

[8]Encountered in TH calculations and attributed to impermissibly high power peaks.

analyses and to de-couple the feedbacks of water properties and fuel temperature. The more pronounced feedbacks are produced by the water density changes and are attenuated by the negative feedbacks provided by the fuel temperature. Hence the proposed approach for whole core coupled analyses, which aims to model the transition from the core power map at "zero power" to "full power"[9], consists of two steps:

1. at first, it is chosen not to exchange the calculated fuel temperature between TH and RP but to keep its value fixed to a constant value uniform for the whole core, modeling only the feedbacks due to water properties variations, until the power map stabilizes to a partially coupled solution; a weak under-relaxation can be used ($r = 0.8$);

2. successively, also the fuel temperature variations are included in the coupling, a stronger relaxation factor has to be chosen ($r = 0.6$) to mitigate the amplifications between water densities and fuel temperature feedbacks observed in preliminary investigations.

The proposed coupling strategy de-couples the water and fuel feedbacks allowing better understanding of both the physics and the sensitivity of these feedbacks. It will be applied to HPLWR core analyses in the next chapter demonstrating how the power map is modified mainly by the water density changes but also by the fuel temperature distribution.

3.3 Pin-power reconstruction

3.3.1 Details

To provide a local evaluation of the clad and fuel temperatures it is necessary to investigate in more detail each individual FA. To do so, the power calculated for whole core analyses in the homogenized FA has to be redistributed within the 40 fuel pins accounting for the effects of both neutron flux spatial gradient and local heterogeneity of the FA lattice. The selected sub-channel code requires the following input data for each FA:

1. axial heat flux distribution;

2. radial power factor of each rod;

3. average heat flux.

While the first and the last parameters are already available from the refined core analysis at FA level, it is unknown how the power is distributed within the 40 fuel pins of each FA. However, this distribution can be calculated applying a methodology to reconstruct the power generated in each fuel pin from the one predicted at FA level. As described in the introduction, equation (1.5) on page 11, pin-power reconstruction techniques require to combine two spatial scales [120]: whole core and heterogeneous FA. The first scale is tackled with ERANOS, using the developed core model for VARIANT, while the second one is covered by MCNP5.

According to the modeling capabilities of MATRA, the axial power shape of each pin in each FA is the same and the pins are differentiated only by the corresponding total power. For this reason it is necessary to extract the total power generated in each homogenized fuel rod cell[10] from whole core calculations and to correct this value accounting for the local heterogeneity of the FA. 2D heterogeneous FA models are hence analyzed with MCNP5. The pronounced changes in water and fuel temperatures, which occur inside the HPLWR core, may change the pin-power distribution depending on the core position and poses questions concerning which

[9] That is from ignoring to taking into full consideration the main TH feedbacks.

[10] Obtained by summing each individual power shape over the active length.

values of the TH parameters should be used. For this reason, several 2D FA models are analyzed with MCNP5 to cover the combination of the TH parameters corresponding to the power peak axial region of each CL in the core. Providing in this way a representation which is believed to be more accurate than using only selected mean values.

3.3.2 Flux and power distribution at pin level from VARIANT

In ERANOS it is possible to refine, with a polynomial function, the nodal flux calculated by VARIANT to a user selected nodalization [130]. In addition, since the nodal flux can be stored for successive usage, it is not necessary to run again VARIANT once that the nodal flux has been archived minimizing the CPU time needed. The nodal flux calculated at CL level can hence be refined to obtain the neutron flux, and power, at smaller scale: since each FA is constituted of a 7 by 7 fuel rod lattice and each CL contains 3 by 3 FAs, refining the nodal flux at CL level in 21 by 21 cells in the horizontal plane it is possible to have the local flux at equivalent fuel pin level, as depicted in Figure 3.10.

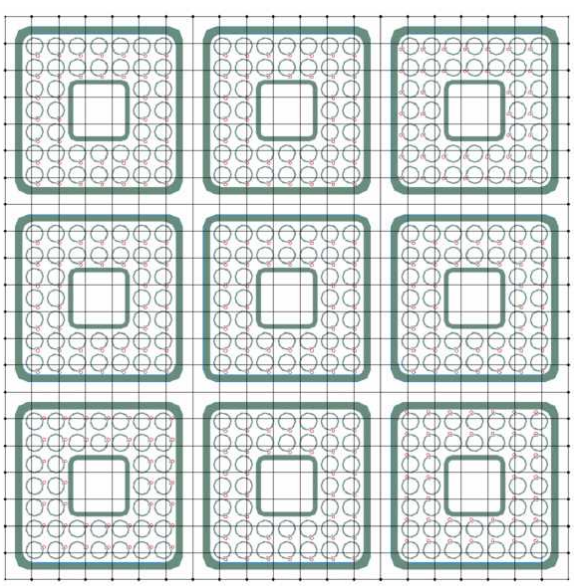

Figure 3.10: Pin level mesh on the cluster node

The fine flux can successively be used to calculate and print power traverses for each equivalent fuel pin cell which accounts for the pronounced flux gradient and for the spatial changes in the fission XSs originated by the TH feedbacks since each CL node uses different 40-group XSs.

In VARIANT calculations each CL is represented as a homogenized medium and hence the effect of the local FA heterogeneity, depicted in Figure 1.2, can not be evaluated and the influence of the moderator box can not be taken into account. To estimate the local heterogeneity of the FA lattice, additional calculations of the heterogeneous FA are necessary.

In MATRA, a normalized axial power traverse is required for each FA but a fine axial nodalization is generally used in sub-channel calculations. The axial nodalization can be refined, once again, with the flux build function of ERANOS used to interpolated the neutron flux within the 20 cm axial nodes each of which is divided into 8 meshes of 2.5 cm selected for MATRA analyses. A Perl post-processing script extracts and normalizes the obtained power density.

3.3.3 Effects of the local heterogeneity of the fuel assembly with MCNP5

The geometrical heterogeneity of the HPLWR FA, increased by the current insulated boxes design [51], can be represented by MCNP5 to predict the power distribution within the 40 fuel rods accounting for the different moderating properties of coolant or moderator/gap water and for the parasitic absorptions in the boxes. For this purpose, 2D models of the FA with reflecting boundary conditions are considered for different combinations of the water and fuel temperature and densities.

In MATRA input, it is required to provide the relative pin-power distribution for the whole FA, which is assumed to be the same in all axial zones. The selection of the TH parameters to be used for these MCNP5 calculations is not unique. It has ben chosen to extract the 7 TH parameters from the axial power peak region of each CL in one eighth of the core, because the power peak region may be the critical one, but other choices are also available, e.g. an axial average.

To improve the consistency of the multi scale tool, it is desirable to use the same nuclear data evaluation in both codes selecting the JEFF 3.1 [103] also for MCNP5 calculations. An accurate representation of TH feedbacks on RP calculations requires to have temperature dependent XSs, the available JEFF 3.1 data are processed at 300, 400, 500, 600, 700, 800, 900, 1000, 1200, 1800 K concerning resonance broadening and at 293, 323, 373, 423, 475, 523, 573, 623, 647, 800, 1000 K concerning bounded hydrogen in water. A material mixing technique has been considered here to refine the available temperatures for the resonance broadening with temperature steps of 100 K. A weighted square root temperature, suggested in [14], has been considered:

$$\Sigma(T) = w_1\Sigma(T_1) + w_2\Sigma(T_2)$$

$$w_1 = 1 - w_2 \qquad w_2 = \frac{\sqrt{T} - \sqrt{T_1}}{\sqrt{T_2} - \sqrt{T_1}}$$

Concerning the $S(\alpha,\beta)$, the direct application of this technique is not possible. The temperatures extracted from TRACE output for each CL are rounded to the closest available temperature. This approach is not desirable in iterative procedures because it may lead to non-continuos variations of the parameters but is of no concern for the present one-way coupling which does not iterate the obtained solution.

The error prone procedure of locating the axial power peak within each CL, extracting the 7 TH parameters and preparing the MCNP5 input files after having rounded the temperatures to the closes value available has been automated with a Perl script, `MCNP5inputmaker.pl`. In this way, other operative conditions can also be analyzed easily.

The normalized power generation in the different fuel rods can be obtained using the dedicated fission energy deposition tallies while the needed relative power distribution requires to post-process the results. Inserting the tally comment card in the MCNP5 input file, the XY position of the printed tally can be directly identified and extracted by the Perl script to automatize the data extraction.

3.3.4 Combined effect: coupling ERANOS and MCNP5

The developed 2D mapping schema established a one to one correspondence between ERANOS and MCNP5 nodes: the total power of each cell is multiplied by the corresponding heterogeneous relative power distribution, as described in equation (1.5). Additional normalization is needed to obtain the normalized relative pin-power ensuring the preservation of the total power of each FA.

3.4 One-way coupling: from fuel assembly to sub-channel investigations

A skeleton input file for MATRA has been prepared and is modified by the Perl script `MATRAinputmaker.pl` which merges the boundary conditions extracted from TRACE, ERANOS and MCNP5 output files. This Perl script, besides performing the described pin-power reconstruction, scans the TRACE output file searching for the inlet mass flow rate of each individual FA and for the temperatures of the 3 mixing chambers retrieving the inlet temperature of EVA, SH1 and SH2, respectively. Only few keywords are necessary and the generation of the 22 input files for the 22 considered CLs in the considered core model are readily generated permitting the simulation of the 198 FAs in the considered one eighth core model.

Once the MATRA input files have been prepared with this automatized procedure, it is simply necessary to execute several times MATRA to obtain the desired results. The `MATRAinputmaker.pl` is a versatile tool which, beside eliminating an error prone data manipulation which is now fully automatized, allows the user to modify the selected empirical factors easily and only in one skeleton file to quickly generate again the several input files required for core analyses.

A triple nesting of XY indexes is used to identify each fuel rod or each sub-channel inside each FA inside each CL. The usage of this mapping schema simplifies the post-processing of MATRA output files and allows to print TH parameters and corresponding XYZ position for plotting purposes.

3.5 Discussion of the proposed approach

3.5.1 Main advantages

Flexibility

The developed codes interfaces, written in Perl language, deal with the coupling among the different physics and scales. They operate by means of uniquely defined keywords in the input/output ASCII files and, hence, they are independent by the codes used and are mainly based on the required data and format which can easily be modified to be applied even to different codes. Having this in mind, it is easy to understand that any modification of the selected codes, which does not affect the output format, does not require to change the coupling scripts allowing to solve the main simplifications/limitations of the physical models listed in the following sections.

The coupling among the codes is problem dependent, but has been developed minimizing the number of constraints which would require modifications to apply it to a different HPLWR design or to different reactor concepts. For example, the number of axial zones and FAs to be considered is not hard coded into the Perl scripts but is extracted from the code outputs. Sánchez Espinoza et al. [134] proved the flexibility of the developed ERANOS/TRACE coupled system which has been applied to a completely different reactor concept even using different coupling parameters.

Visualization capabilities

Advanced visualization capabilities have been added to support and facilitate analyses of whole core results. Since none of the selected codes offers 3D data visualization, Tecplot 360 [146] has been chosen to fulfill this task. A convenient form for data visualization is XYZ scattered data which is consistent with the coupling scheme used to exchange data among the codes. For these reasons, Perl scripts based on the coupling ones are used to extract the data of

interest from the code output files and to print them in a tabulated form which is directly loadable into Tecplot to generate the plots which will be shown in the successive chapter.

3.5.2 Main simplifications

Coupled RP/TH system

The coupled ERANOS/TRACE system relies on node-averaged properties for representing the mutual feedback effects ignoring local temperature/power distributions. In addition, several simplifications are used in the stand alone codes, the most important ones are discussed here.

The geometries used for all codes are input at room temperature ignoring the thermal expansion of the fuel rod lattice, core support plate and other internals.

The water direct heat up, mainly due to neutrons slowing-down and gamma ray absorption, has been neglected because it should depend on the water density and on the fluid type (coolant or moderator) as well as on the core position (EVA, SH1 or SH2). For simplicity, the moderator/gap water flow paths are modeled with 1D components fixing the inlet conditions and, hence, mass flow redistribution or more complex effects like flow reversals can not be investigated but should be of no concern for the considered steady state operative condition. The core mixing plena are modeled as 1D components since more detailed representations are not available with a system code like TRACE. This kind of modeling permits the coolant mass flow redistribution among the several FAs but results in a perfect mixing of the coolant. The former is extremely important for an accurate prediction of the temperatures inside each FA while the latter has only a limited impact thanks to the good mixing obtained in the plena [154].

The heat transfer coefficient of the helium gap between fuel pellet and clad is affected by several parameters, among which the power level and fuel burn-up play a dominant role, making its value dependent on the core position but it is here assumed to be constant in all the fuel rods. The qualification of this quantity is extremely important for the determination of the absolute value of the fuel temperature which influences the whole coupled analysis. The fuel density changes may have marginal impacts on both RP and TH solution, but it may result in fuel-clad interactions which, changing the HTC of the helium gas gap, have pronounced effects on the fuel pellet centerline temperature and, consequently, on the margin to fuel melting. This kind of interactions can be predicted only with adequate fuel behavior model which is not considered since not implemented in the code used. The fuel axial heat conduction has only limited importance for uranium dioxide and hence has not been considered yet.

The difficulties in assessing these effects, which generally require extensive usage of empiricism, suggested to not investigate them in further details since no experimental data are available yet and high fidelity simulations are not practical with the available computational resources. As a matter of fact, the usage of more sophisticated physical models, which have not been verified and validated, does not improve the accuracy of the results.

Multi-scale approach

The evaluation of the errors introduced by the developed pin-power reconstruction technique is rather complex because of lack of experimental data. The effects of local temperature distribution on the node-averaged feedbacks used in the coupled RP/TH analyses have not been quantified since no additional iterations have been performed. On the one hand, the whole core coupled analyses at sub-channel, or even finer, spatial resolution [158] is not practical with the available computational resources and, on the other hand, the alternative usage of averaging techniques would introduce additional sources of uncertainties.

Several main simplification have been introduced in the physical models used in MATRA. Among them it is worth to mention that water properties have been implemented as function

of temperature only, neglecting the effects of pressure drops. The heat transfer from coolant to moderator/gap water is not modeled, resulting in higher coolant temperatures. MATRA offers only a simplified representation of the structural materials whose properties are not dependent on temperature and uses Dittus-Boelter as heat transfer correlation [33]. For the time being, the lack of heat transfer experiments in a wire wrapped bundle under supercritical water conditions does not favor a specific heat transfer correlation. Once suitable experimental data are available, Dittus-Boelter shall be replaced by a new correlation. It is worth to mention that there are other simplifications behind the sub-channel approach which are not accurate for supercritical water, e.g. despite the hydraulic solution is obtained with a sub-channel centered approach, the solution of the conjugate heat transfer problem is based on a fuel rod centered approach and simple arithmetic mean is used to evaluate a representative coolant bulk temperature of the 4 sub-channels. This may affect the accuracy of the calculated solution, especially in the vicinity of the pseudo-critical point, where small temperature variations causes high changes of the water properties like specific heat capacity or density.

3.5.3 Known limitations and sources of uncertainties

The described simplifications will introduce errors or inaccuracy in the predicted results which will be propagated within the coupled system. For the considered steady state applications, in which the solution is iterated several times, the error propagation may result in a biased solution.

Additional sources of uncertainties on the results which will be presented in the successive chapters may lie in the heat transfer correlations for supercritical water in rod bundles for both heating and cooling conditions which is still under investigation [70]. In addition, the sub-channel investigations are strongly dependent on the constitutive equations required for the input parameters, e.g. friction factors and lateral exchange rates between adjacent sub-channels, which are generally based on existing experience and hence can hardly be quantified for this innovative reactor concept. Also the neutronic solution is influenced by the heavy nuclide scattering resonances on neutron slowing down [28] and by the neutrons scattering law, $S(\alpha,\beta)$, in supercritical water but both have not been investigated in detail. The fuel and water stoichiometry at operating conditions may also influence the neutron spectrum.

Sensitivity and uncertainty analyses can help in identifying and ranking the weaknesses in the global model in order to direct the R&D efforts where the effects are most important [161]. Uncertainty assessment is required for a practical use of best-estimate TH computation which can not rely only on expert judgment, especially for such an innovative reactor concept. To the author's knowledge this kind of analyses has not yet been applied consistently to the field of multi-physics and, hence, have not been included in the present work even if it would be a valuable tool.

Chapter 4

Application of the coupled multi-physics, multi-scale analysis tool

4.1 Core model

For the current analyses the thermal power of the whole core is fixed to 2300 MWth while the RPV inlet flow rate is assumed to be 1179 kg/s, 75% of which becomes moderator/gap water and is pre-heated before being mixed with downcomer water to reconstitute the coolant flow rate at the EVA entrance. Since a core loading strategy is not yet available, the current analyses uses a uniform enrichment of the UO_2 both in radial and axial direction and no reactivity control techniques are considered up to now. A preliminary optimization of the FA power distribution [57], lowered the enrichment of the corner fuel pins of each FA, (from 5 wt% to 4 wt% in ^{235}U).

Only one eighth of the core, as shown in Figure 4.1, is considered in these investigations to reduce the CPU time since no asymmetric conditions will be analyzed.

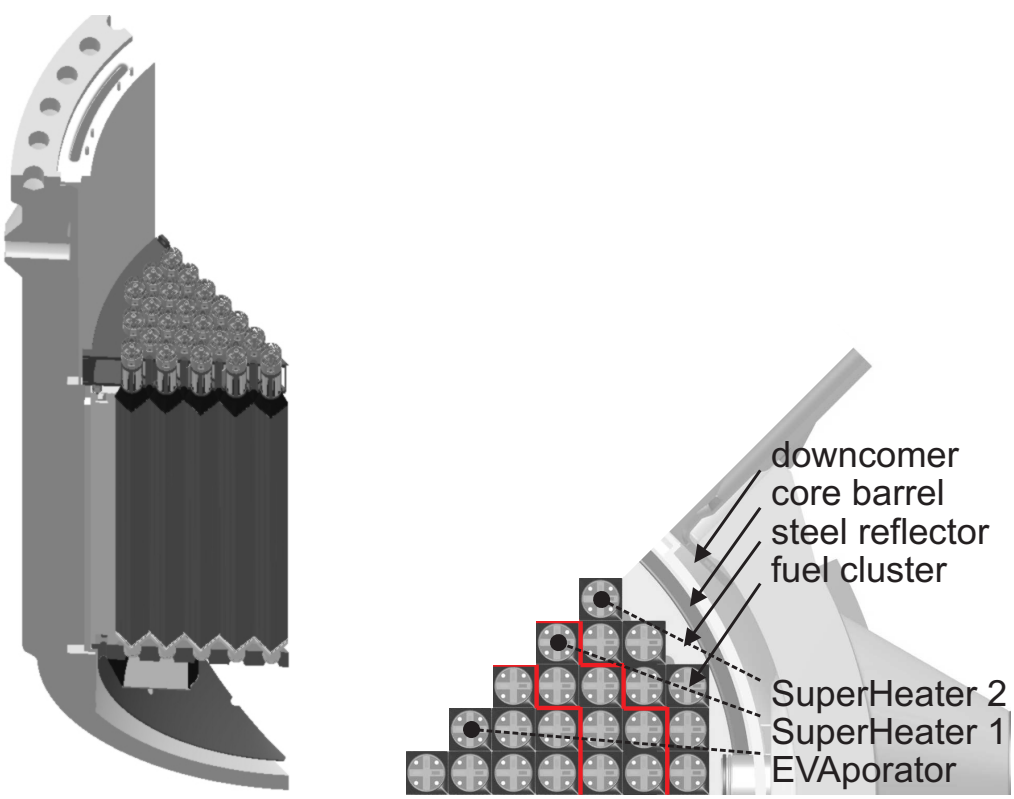

Figure 4.1: Considered core region

With the release of ERANOS 2.1 [131], nuclear data based on JEFF-3.1 [103] are available and will be used for HPLWR applications since they are expected to increase the accuracy and reliability of the results as explained by Jacqmin et al. [68].

4.2 Description of the considered scales

Several spatial scales have been considered for the results presented in this chapter and are here described. One quarter of the core is modeled in TRACE and ERANOS analyses while maintaining the one eighth symmetry for the feedbacks.

A CL-wise core nodalization is used in section 4.3 for the application of the coupled ERANOS/TRACE system, Figure 3.2. This mean that, in TRACE input file description, there is only one average FA representative of each CL, as described previously in Figure 2.25. With this model, the TH parameters, needed for the feedbacks, are calculated for each CL in the quarter core model and in the selected axial nodalization (21 zones).

This solution is refined for a FA-wise core nodalization in section 4.4 where the coupled ERANOS/TRACE sytem, Figure 3.2, is applied to more detailed input files of both TRACE and ERANOS to predict, with additional iterations, the effects of the CL heterogeneity. TRACE calculates TH parameters for all FAs in the considered quarter core model permitting to predict the coolant mass flow redistribution among them. The TH parameters are successively averaged by the code interface to CL-wise values needed by ERANOS to generate the 40-group, self-shielded, homogenized XSs. The neutron flux solution obtained for core analyses with VARIANT is automatically refined within the ERANOS system from CL to FA spatial resolution providing the power level and shape for each FA in the quarter core as needed by TRACE.

The coupled solution obtained for FA-wise core description with the coupled ERANOS/-TRACE system is analyzed at pin level applying a pin-power reconstruction technique. As described in section 4.5, this technique merges ERANOS results, obtained for whole core analyses, with those of MCNP5, obtained for heterogeneous FA analyses. The pin-power distribution is necessary to complete the one-way coupling between the equivalent channel representation of each FA and the sub-channel resolution permitting to predict sub-channel averaged TH properties fore one eight of the core with MATRA, as shown in section 4.6.

4.3 3D coupled analyses at fuel cluster scale

4.3.1 Transition from un-coupled to coupled in-core power map

While the RP/TH coupled solution is independent from the coupling strategy, this can be modified by the user in order to accelerate the convergence or to avoid code failures experienced in TH calculations and attributed to impermissibly high power peaks. Besides the already mentioned under-relaxation factor on the power map, r in equation (3.1), which can be modified while the coupling system is in operation, the user can choose not to exchange some of the TH parameters, e.g. the fuel temperature, but to keep their value frozen in the initial iterations.

The proposed coupling strategy is capable to model the transition from the initial "zero power" condition[1] to the coupled "full power" condition, which includes the feedbacks due to variations of water temperatures and densities as well as fuel temperature. It has been selected on the basis of the results presented for FA analyses in subsection 3.2.6 together with initial investigations and testings.

[1]The one without any TH feedbacks, i.e. constant water and fuel temperature distributions assumed to be 300 K in the whole core.

The selected strategy is described here, referring to Figure 4.2, 4.4 and 4.5 in which the core power map for selected iterations is plotted. Starting with uniform TH data distribution both in axial and radial position, the neutron transport equation is solved for the cold core condition obtaining the 3D power map which shows a typical fundamental mode spatial distribution, Figure 4.2: because of the neutron leakage not compensated by adequate uranium enrichment, more neutrons and hence a higher power level are found in the central regions. An insight into the expected changes of the core power map is given by inspecting the coolant temperature distribution after the first iteration plotted in Figure 4.3. This figure is helpful to better understand the 3 pass core concept: the coolant is heated up in the flow direction, it enters in the core from the bottom of EVA in which it flows upward, then it flows downward in SH1 and finally upward again in SH2. The lower temperature is located in the lower third of EVA and hence a power rise in this region is expected. For the initial iterations, it was decided not to exchange the calculated fuel temperature between TH and RP but to keep its value fixed to a constant value, modeling only the feedbacks due to water properties variations. Ignoring the fuel temperature feedbacks by freezing its value, a weak under-relaxation can be used, $r = 0.8$ in equation (3.1). Four iterations are performed, till the power map stabilizes to a partially coupled solution which exhibits a pronounced peak in the lower region of EVA as shown in Figure 4.4. Then also the fuel temperature variations are included in the coupling, a stronger relaxation factor has to be chosen ($r = 0.6$) to mitigate the amplifications between water densities and fuel temperature feedbacks observed in preliminary investigations. The consistently coupled core power map is plotted in Figure 4.5 and exhibits a less pronounced peak in the lower part of EVA which is consistent with the negative feedbacks given by the resonance broadening of ^{238}U.

The lower power generation in the CLs close to the core periphery is already pronounced for the uncoupled analysis at "zero power" condition, Figure 4.2, and is induced by the radial neutron leakage. For the coupled solution, the gradients of the in-core power distribution are amplified since low coolant densities occur in the SHs, hardening the neutron spectrum in the core periphery and increasing the neutron mean free path as well as their leakage probability, Figure 4.5. The reduced reactivity of the SHs with respect to EVA contributes to the reduction of the neutron flux amplitude in these regions.

The convergence can be evaluated considering a core averaged percentage difference in the power density, f, defined as follow:

$$f = \frac{100}{\text{Core nodes } (462)} \sum_{x,y,z} \left| \frac{\text{Power}_j(x,y,z) - \text{Power}_{j-1}(x,y,z)}{\text{Power}_j(x,y,z)} \right| \tag{4.1}$$

The evolution of this factor in successive iterations is plotted in Figure 4.6: after five iterations, ignoring the fuel temperature effect, the averaged percentage difference f is around 1%. When modeling also the fuel temperature feedbacks, f is initially increased but then is reduced to a value close to 0.01% which persists, with some small oscillations, between the final iterations (11, 12, 13, 14). The corresponding temperature difference for the four constituents, being around 1 K, is satisfactory for the present applications.

The coupled RP/TH analysis permits to estimate how the total power of the three pass core is subdivided in the three regions, as shown in Table 4.1: the power generated in both SHs is decreased by the coolant and moderator/gap water density reduction. The power redistribution is attenuated when considering also the fuel temperature feedbacks which slightly reduce the power fraction generated in EVA.

Extensive sensitivity studies devoted to the optimization of the coupling scheme have not yet been performed, mainly because of the high CPU time requested: around one day per each iteration of the coupled system on a 2.4 GHz Linux PC with 2 Gb of RAM.

The predicted coupled solution is found to be consistent with previously obtained results as well as with those of independent analyses by Maráczy et al. [87].

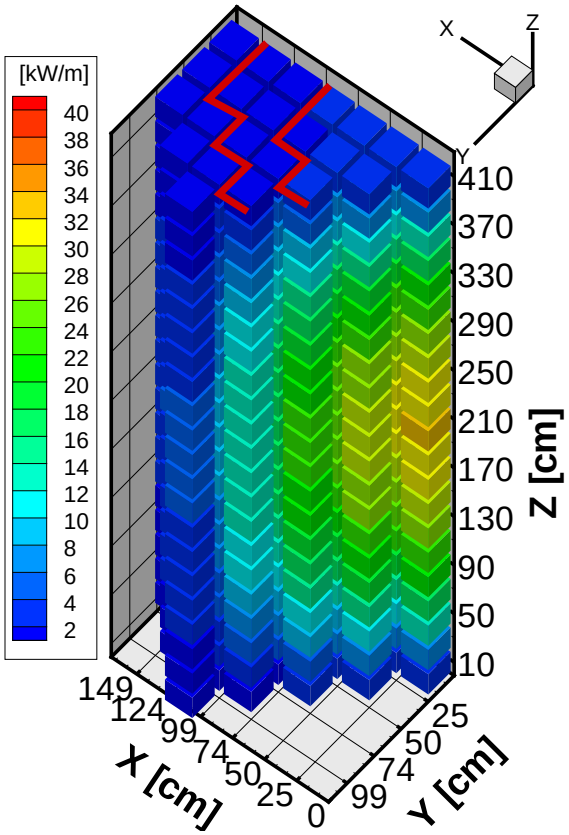

Figure 4.2: Core power map without TH feedbacks (iteration 1)

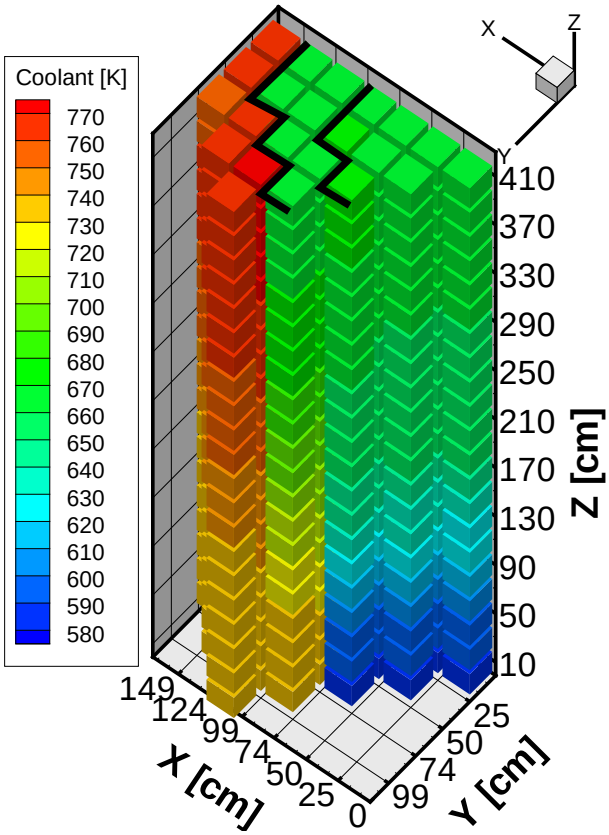

Figure 4.3: Coolant temperature distribution after iteration 1

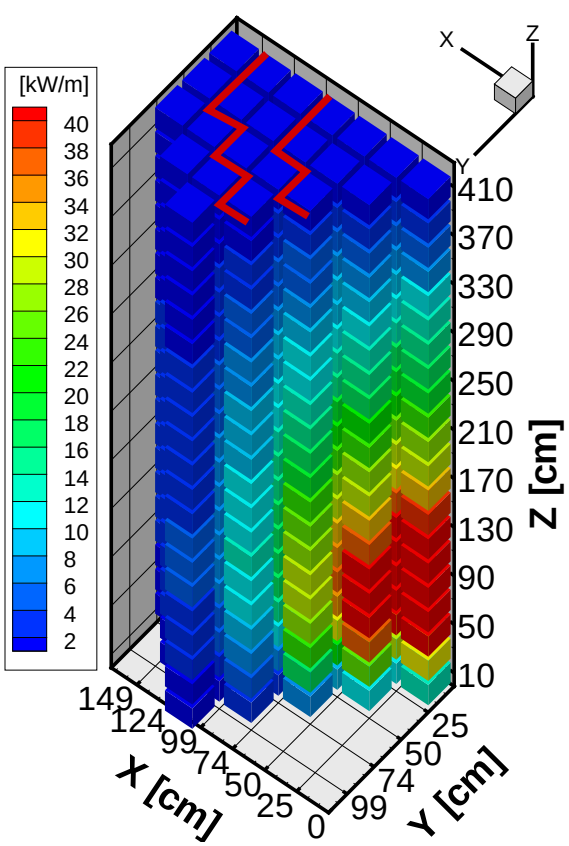

Figure 4.4: Core power map with coolant and moderator feedbacks (iteration 5)

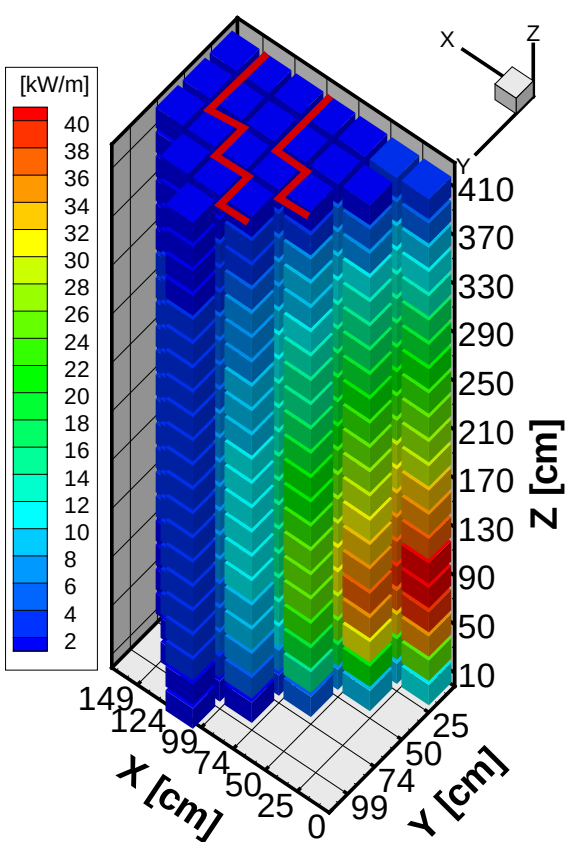

Figure 4.5: Core power map with TH feedbacks for coupled solution (iteration 14)

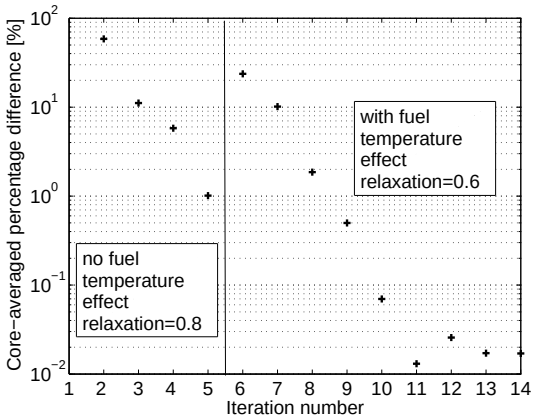

Figure 4.6: Core average percentage difference f in successive iterations

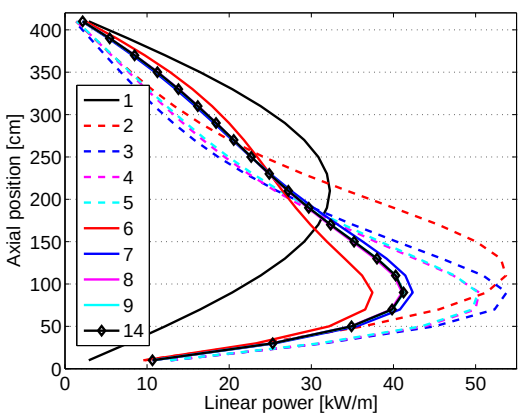

Figure 4.7: Axial power shape of highest power density cluster (CL 11) in successive iterations

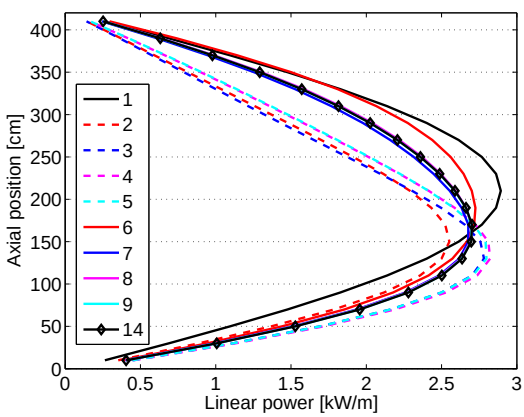

Figure 4.8: Axial power shape of lowest power density cluster (CL 37) in successive iterations

4.3.2 Changes of the axial power shape in selected clusters

The consistency and convergence behavior of the coupled system can be estimated considering the changes of the core power map in the successive iterations. To better understand the results, axial power shapes of the highest and lowest power level CL are considered in Figure 4.7 and 4.8. The CL indexes have been given previously in Figure 2.16 on page 32.

The solution of the 3D core power map for uniform TH data both in axial and radial direction, with both fuel and water temperature equal to 300 K, results in the cosine axial shape typical of an uncoupled analysis [80] (iteration 1). Modeling only the feedbacks due to water properties variations, four iterations are performed (2 to 5) and the power shape stabilizes to a partially coupled solution, as shown in Figure 4.7 for the central CL where a pronounced bottom peak (iteration 4 and 5) is found, as already experienced for FA analysis. When also the fuel temperature variations are included in the coupling, the selected relaxation factor mitigates the amplifications between water densities and fuel temperature feedbacks observed in preliminary investigations and only small oscillations are found (iteration 6 and 7) and the power shape stabilizes already after 3 additional iterations: its shape is almost identical for successive iterations (8, 9 and 14 in the figure). The change of the maximum linear power, always located in the considered high power density CL, is also included in Table 4.1, to underline how this important quantity is sensitive to the coupled analysis.

Beside the reduction of almost one order of magnitude in the linear power between CL 11 and 37, the different evolution of the power shape is quite evident, e.g. the effect of the fuel

Table 4.1: Changes of core properties with the thermal-hydraulics feedbacks

Considered feedbacks (FBs)	itn.	Core regions power percentage			Coolant inlet temperature [K]			k_{eff}	max [kW/m]
		EVA	SH1	SH2	EVA	SH1	SH2		
no FBs	1	57.1	31.0	11.9	588	667	736	1.16798	32.3
water FBs	5	64.7	25.5	9.8	591	679	747	1.14457	50.3
water + fuel FBs	14	63.3	26.3	10.4	590	676	743	1.12307	41.2

temperature variations – iteration 5 and 14 – is much more pronounced in CL 11 than in CL 37. This effect is probably due to the spatial coupling among the FAs.

4.3.3 Sensitivity of k_{eff} to the TH feedbacks

Beside the power map, also k_{eff} is affected by the TH feedbacks, only the 3 k_{eff} values corresponding to different TH feedbacks representation are compared in Table 4.1: cold core condition (water and fuel at 300 K), only water feedbacks (fuel at 300 K) and combined feedbacks of water as well as fuel temperature variations.

Considering only the feedbacks due to water density reduction, k_{eff} if reduced of more than 2000 pcm, being the reactor under-moderated. Also the fuel temperature feedbacks, combined with the additional changes of water properties, result in an additional 2000 pcm reduction of k_{eff}.

These changes may give an idea of the excess reactivity control that should be achieved with the control rods to bring the reactor to "zero power", cold condition.

4.3.4 Thermal-Hydraulics parameters at fuel cluster scale

During the coupled analysis, the coolant inlet temperature of the three core regions changes[2], as shown in Table 4.1 while the core outlet temperature, 766 K, is not affected by the coupled analysis since both the thermal power of the plant and the mass flow rate are fixed. The region wise average coolant outlet temperature is affected by several parameters including, in addition to the input power level, the heat transfer to the moderator/gap water, which varies depending on the flow conditions, and the change in the region inlet temperature which, because of the strong nonlinearity of the enthalpy temperature dependence shown in Figure 1.3, may change the temperature rise corresponding to the same enthalpy rise.

The pronounced heterogeneity of the in-core power distribution, Figure 4.5, results in coolant mass flow redistribution among the parallel pipes representing the CLs of each core region which may lead to high peak temperatures. For this reason, inlet orifices are needed to balance the effect of the different heat up. The orifices have been dimensioned with an iterative procedure in preliminary investigations and are not modified during the coupled analysis. Due to the adequate orifices dimensioning, the calculated mass flow distribution among the parallel channels, which is higher in the higher power density CLs, balances the presented non-uniformity in the power input and the predicted coolant temperature variations within the three regions are quite uniform, as shown in Figure 4.9. More details will be given in the next section for FA-wise investigations. Comparing the coolant temperature distribution for the coupled solution with that obtained at the first iteration, Figure 4.9 and 4.3, respectively, a faster heat up in EVA is found because of the higher power density in this core region.

[2]EVA inlet temperature is determined by the mixing of moderator/gap water with downcomer water.

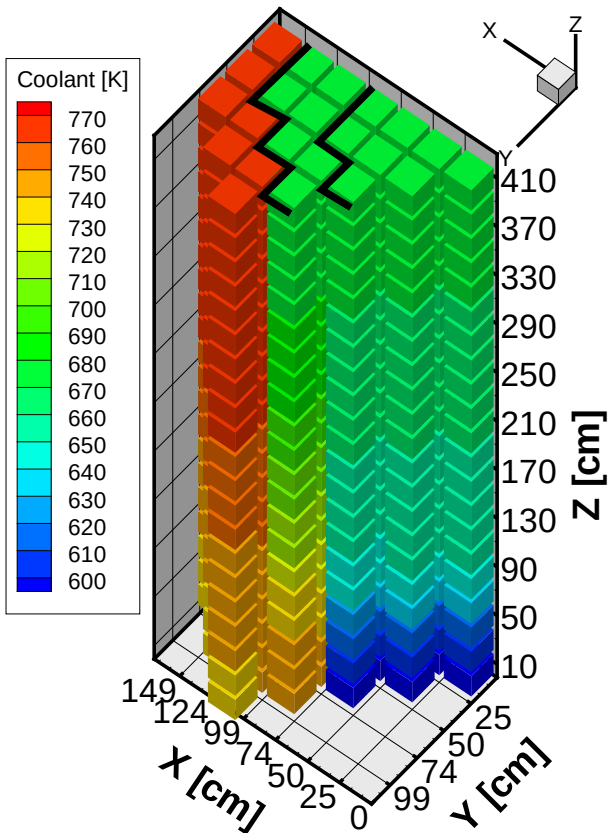

Figure 4.9: CL averaged coolant temperature for coupled solution

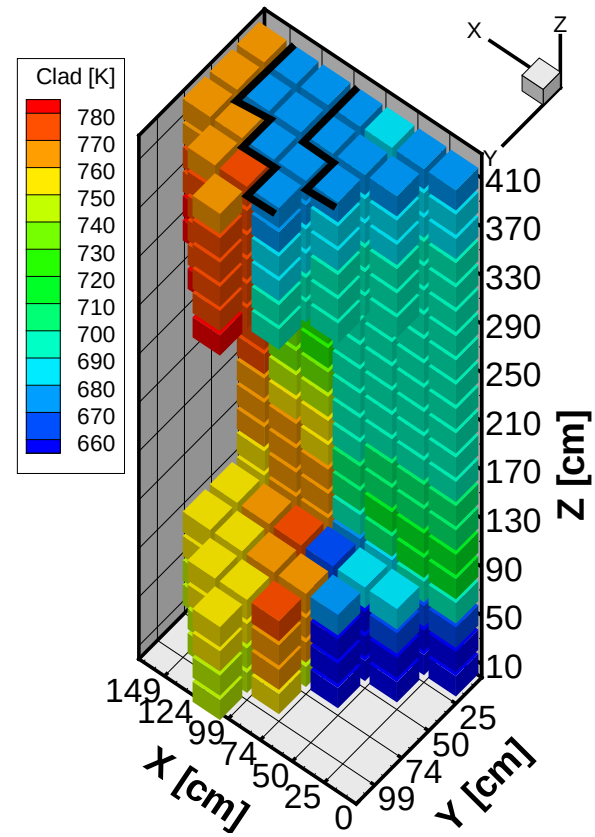

Figure 4.10: CL averaged clad temperature for coupled solution

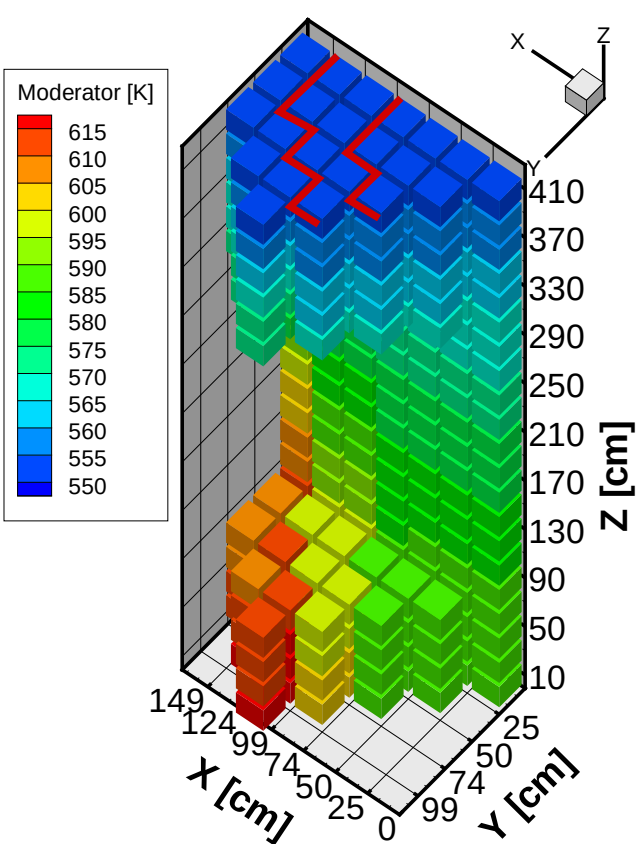

Figure 4.11: CL averaged moderator temperature for coupled solution

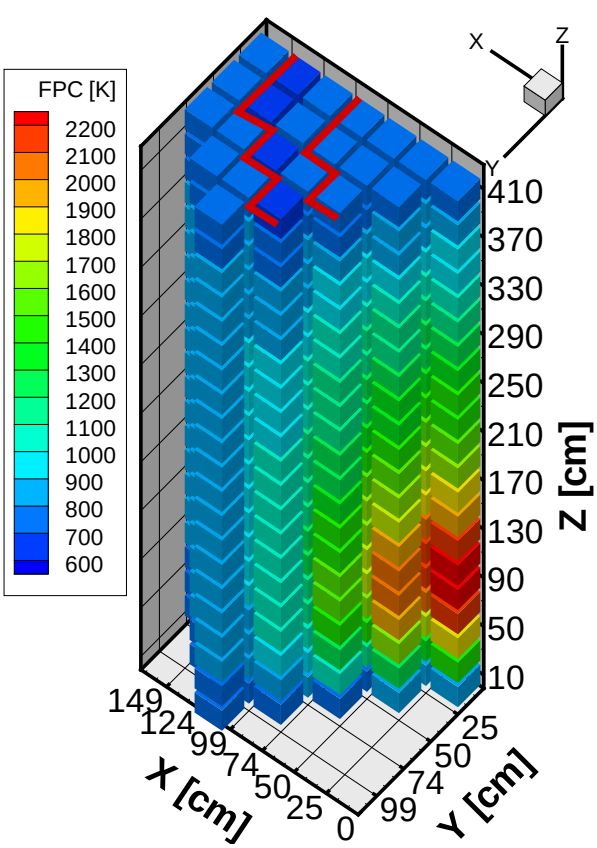

Figure 4.12: CL averaged Fuel Pin Centerline (FPC) temperature for coupled solution

Moderator heat up is higher in the SHs than in EVA since there the coolant temperature is higher, Figure 4.11. Thanks to the current FA design with insulated walls [51] and selected moderator flow rate, the moderator outlet temperature is sufficiently below the pseudo-critical one. Predicted gap water temperatures are not shown, being very similar to the ones of the moderator.

Clad and fuel temperatures are plotted in Figure 4.10 and 4.12. They show sensitivity to both the power map and the coolant temperature distribution. The spatial variations of the fuel temperature resemble well the coupled in-core power map and the spatial dependence of the negative feedback offered by the resonance broadening, primarily of ^{238}U, is the main responsible for the attenuation of the power peaks, as shown in Figure 4.4 and 4.5.

More insight into the physical reasons behind the predicted temperature variations will be given in the next section.

4.4 3D coupled analyses at fuel assembly scale

4.4.1 Additional iterations

The developed coupled system has been successfully applied to HPLWR core analysis to predict power and constituents temperature distributions with values averaged at CL resolution. The pronounced power gradients in the HPLWR core, together with the heterogeneity of the HPLWR CL, depicted in Figure 1.2, can possibly originate pronounced differences between the predicted TH values at CL and FA resolution. For these reasons, the developed coupled system has been extended to provide a FA representation. The graphical representation of the nested mapping scheme which allows to identify individual FAs within each CL is depicted in Figure 4.13.

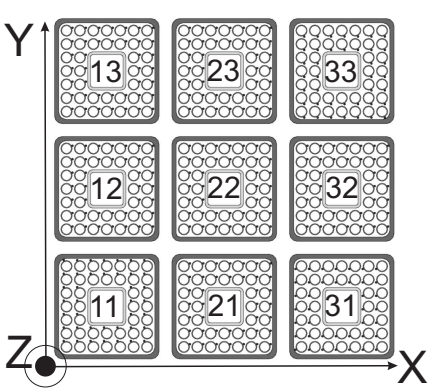

Figure 4.13: Fuel assemblies indexes within each fuel cluster

Because of the high CPU time, of more than two weeks for the presented CL-wise core analyses, the obtained solution is used as starting point for the FA-wise core analyses. In this way only few additional iterations are necessary to achieve a new consistent solution between the calculated power and constituents temperature distributions with the coupled ERANOS/TRACE system Figure 3.2. Thanks to the finer resolution, a new optimization of the coolant inlet orifices became possible justifying a few of additional iterations.

The TH parameters used for the feedbacks on RP are averaged to the same CL-wise nodalization previously used and are now considered to verify the convergence. The temperature difference, in each of the 462 computational nodes used in ERANOS, between the two final additional iterations is below 1 K demonstrating the achieved convergence[3].

[3]It is important to remember that the temperatures calculated by TRACE are rounded to integer numbers by the Perl script `TRACE2ECCO.pl` and then fed into ERANOS.

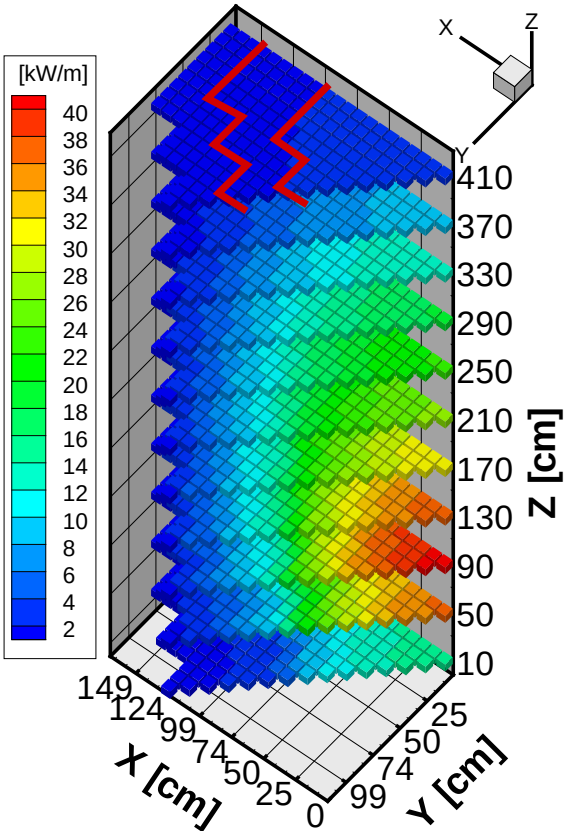

Figure 4.14: FA averaged core power map for coupled solution

4.4.2 Details on the in-core power map

A 3D representation of the core power map at FA scale is given in Figure 4.14[4] and does not present remarkable differences with the one obtained at CL scale previously shown in Figure 4.5. The power distribution is strongly affected by the combined effects of neutron leakage and reduced coolant density in the SHs and in the upper part of EVA.

The FA relative power in each of the three core regions – defined as the power generated in each FA - to - the average power of the corresponding region (EVA, SH1, SH2) ratio – gives an idea of the power heterogeneity and is plotted in Figure 4.19. In SH2, because of the combined effect of TH feedbacks and neutron leakage, larger flux gradients occur: the FAs in CL 45 and 36[5] have higher power density than those of CL 37 mainly because of the vicinity to higher reactivity regions. To estimate the mass flow redistribution among the 9 FAs of each CL, also the CL-wise FA relative power – defined as the power generated in each FA - to - the average power of the corresponding CL ratio – is important and hence is plotted in Figure 4.20: the higher and lower relative power occurs within the SH2, in CLs located close to the steel reflector where the flux gradients are higher, and have power peaking factors above 1.5. Within each CL, the highest power density FA is always the one closer to the center of the core whereas the lowest is the one pointing towards the core periphery, they are marked as 11 and 33, respectively, being positioned in X=1 or 3 and Y=1 or 3 within the cluster itself, Figure 4.13.

4.4.3 Thermal-Hydraulics parameters at fuel assembly scale

The obtained coupled solution at FA resolution allows to have a better insight into the physics which govern the coupling between RP and TH analyses of the HPLWR as well as on

[4]To allow an easier understanding of the plot, only some representative axial positions have been included.

[5]See Figure 2.16 on page 32 for CL indexes.

the sensitivity of the various TH parameters. Predicted TH parameters corresponding to the presented core power map are given in Figures 4.15 to 4.18, providing additional details to those obtained at CL resolution.

The predicted coolant temperature distribution, Figure 4.15, underlines the necessity of splitting the coolant heat up in successive steps with intermediate mixing: peak temperatures are found also in SH1, because of the nonuniform heat up, and occur in the highest power density FA of each CL, Figure 4.20. The coolant temperature rises fast in the lower part of EVA because of the higher power density and of the strong nonlinearity of the enthalpy temperature dependence, Figure 1.3. In EVA the coolant outlet temperatures are rather uniform since this region presents smaller flux gradients in horizontal direction, while in the SHs the coolant temperature distribution has a larger spread. The coolant temperature is strongly influenced both by the power level and by the coolant mass flow in each FA, more details will be given shortly.

The clad temperature is a crucial design criterion for the HPLWR core, its value predicted by the coupled system is plotted in Figure 4.16. The sensitivity of the clad temperature to both the power level and the coolant temperature is evident, more than for the previous CL-wise analysis: peak temperatures occur not only in regions with the maximum coolant temperature (SH2) but also with lower coolant temperature but higher power level (SH1). In the lower part of EVA, where the power peak is located, the clad temperature is higher than in the neighboring regions but, thanks to the lower coolant temperature, its value remains much lower than the peak one. This underlines the importance of operating the 3 heat up steps for the coolant at different power levels. The reduction of the maximum clad temperature, located in SH2, has to rely mainly on adequate coolant mass flow redistribution, which will be presented shortly, since the power level is there already reduced.

The moderator water heat up, Figure 4.17, is closely related to the temperature distribution of the coolant and hence it is not the same for the 9 FAs within each CL. The gap water has a very similar heat up and hence it is not plotted. For both, the effects of possible mass flow redistribution among the parallel channels, originated and justified by the different heat up, have not been investigated but may affect the temperature distribution. Concerning gap water, the mixing which would occur in the real 3D geometry would also influence its temperature.

The fuel pin centerline temperature is also an important design criterion, its spatial distribution is plotted in Figure 4.18. As underlined from the CL-wise analysis, since its value is mainly sensitive to the power level, in contrast to the clad temperature, the peak values occur where the power peak is located, i.e. in the lower part of EVA, even if the cooling is here more efficient as proven by the low clad temperatures. The reduction of the maximum fuel pin temperature can hence be achieved with an optimization of the power map which has not yet been performed.

4.4.4 Coolant mass flow distribution

It is desirable, mainly for economics reasons, to operate all the FAs with similar peak clad temperatures. To achieve this goal, two main parameters can be adjusted: the power level and the coolant mass flow of each FA. Thanks to the 3 pass core design, a quite evident decoupling of these two parameters exists: where the power level is high, EVA, the coolant temperature is low reducing the predicted clad temperature which does not reach critical values, as shown in Figure 4.16. The peak clad temperature occurs in SH2 where the power level is low and the high coolant temperature has a clear effect in determining the clad temperature.

The optimization of the in-core power distribution is not yet available and is not the subject of the current analyses. The coolant mass flow distribution among the 117 parallel pipes representing each individual FA in each of the 3 core regions[6] can be evaluated by TRACE thanks to the developed pseudo 3D core model. Adequate mass flow distribution is required, especially in both

[6]In one quarter of the core there are 3 regions (EVA, SH1 and SH2), each with 13 CLs, each composed of 9 FAs.

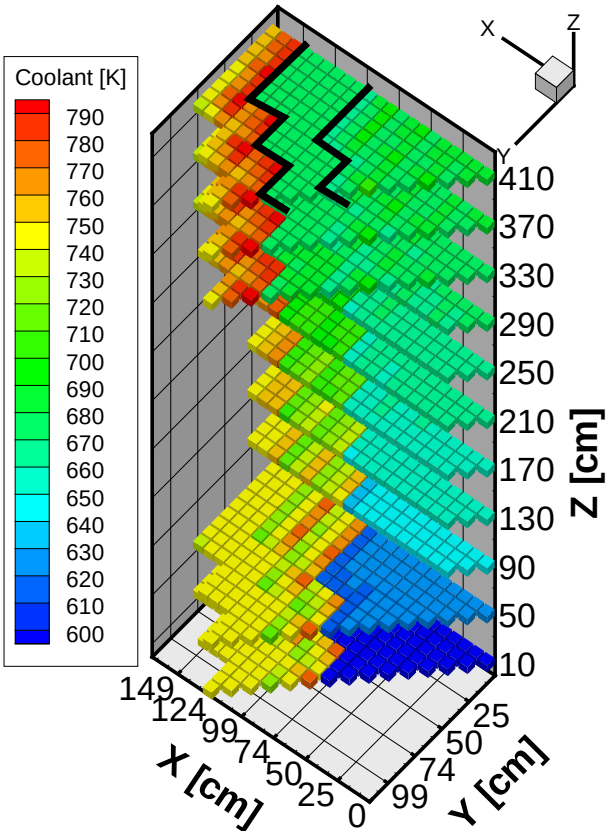

Figure 4.15: FA averaged coolant temperature for coupled solution

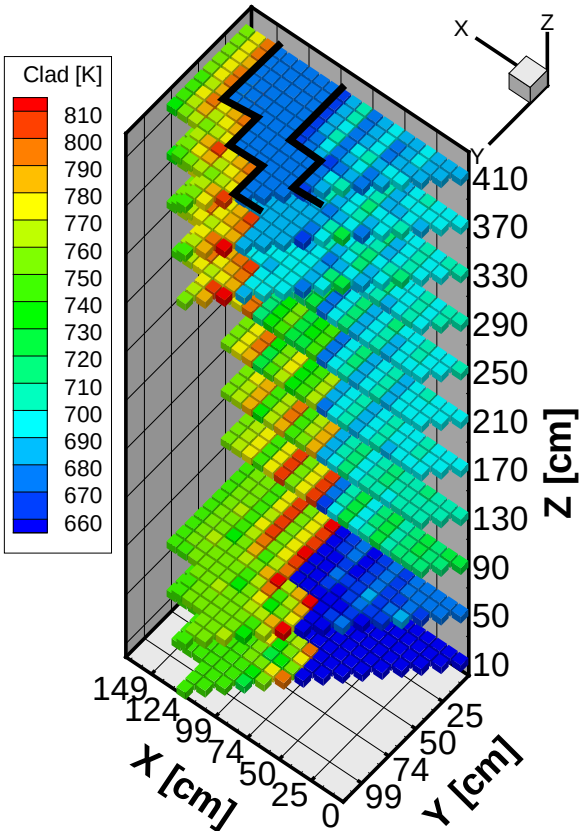

Figure 4.16: FA averaged clad temperature for coupled solution

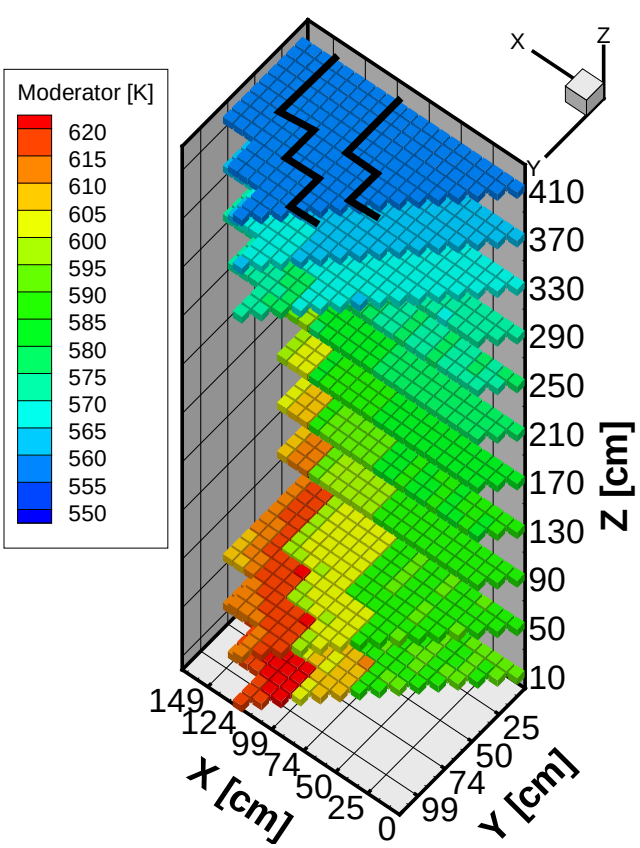

Figure 4.17: FA averaged moderator temperature for coupled solution

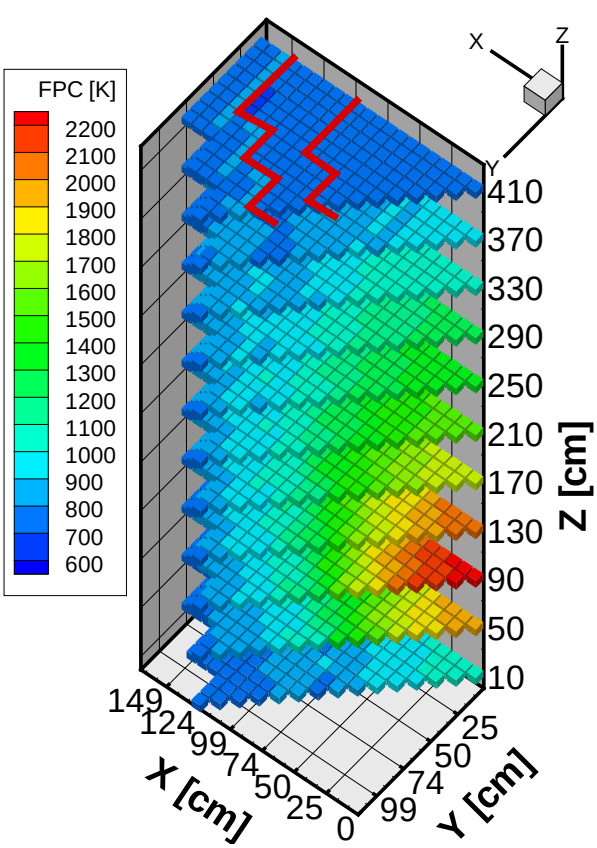

Figure 4.18: FA averaged Fuel Pin Centerline (FPC) temperature for coupled solution

SHs, to reduce the maximum clad temperature.

The coolant mass flow redistribution is mostly affected by the pronounced power heterogeneity which can be balanced using adequate inlet orifices. These are represented in TRACE by means of kfactors [100] used at the inlet of each coolant pipe. Their dimensioning has been obtained with an iterative procedure, based on the power - to - flow ratio and adjusted by trial and error, in order to have similar maximum coolant outlet temperature [7] of each CL in the 3 core regions, as shown in Figure 4.21. This approach has been preferred, for its simplicity, to the development of a functional relationship between the mass flow rate and peak clad temperature of each FA which may be more affected by the coupled analyses.

It was observed that, for the HPLWR operating conditions, a higher heat up would correspond to a higher pressure drop and hence a reduction of the mass flow rate resulting in an even higher coolant heat up. For this reasons, the kfactors have been dimensioned to ensure a higher mass flow rate in the FAs of higher relative power, as shown comparing Figure 4.22 and 4.19.

Inlet orifices are envisioned to be placed on the core support plate at the inlet of EVA and such kind of devices may also be placed at the inlet of both SHs in order to adjust the mass flow distribution among the various CLs. The head- and footpiece of the current fuel element design [44] do not allow to have inlet orifices for each FA within each CL without welding them during fuel element construction. This option is not considered to be practical to allow CL shuffling during plant operation. To represent the unique inlet orifice of each CL with TRACE the 9 FAs belonging to the same CL employ the same inlet kfactor. This representation has been selected to provide a more realistic representation of the flow splitting among the parallel flow paths and allows to optimize the mass flow accordingly to the peak FA of each CL.

The mass flow redistribution among the CLs is mainly influenced by the differences among the kfactors rather than by their absolute values which, indeed, determine how the CL mass flow rate is distributed within the 9 FAs of each CL. To simplify the coupled analyses, the selected kfactors have been dimensioned to ensure a quite stable mass flow rate in the successive iterations despite the modifications of the power map. For this reason, the pressure drop originated by the inlet orifice dominates the one due to the CL-wise power peaks, Figure 4.20, and the mass flow in the 9 FAs of each CL is almost the same, as shown in Figure 4.22.

The orifices optimization is rather complex because of the numerous parameters which have to be checked and is extremely time consuming[8]. The modifications of the coolant mass flow may affect the other TH parameters distribution and hence the coupled solution requiring additional coupled iterations to verify convergence. The determined orifices schema behaves properly and provides differences of around 15 K and less than 5 K in peak coolant temperature of SH2 and SH1, respectively, Figure 4.21, 4.24 and 4.26. The corresponding differences in peak clad temperature, Figure 4.25 and 4.27, are slightly higher but are acceptable for the current application nonetheless further optimization is possible and required.

The power - to - flow ratio[9] is commonly used to identify the critical FAs and is plotted in Figure 4.23. EVA FAs have the highest ratios because of the higher power level of this core region but, concerning clad temperatures, the critical FAs are located in SH2, the CLs indexes are 37, 46 and 55 which are marked in Figure 2.16 on page 32. From these plots it is possible to understand how the biggest differences happens among the FAs of the same CL since the relative flow can not be further adjusted to balance the CL-wise power heterogeneity shown in Figure 4.20. This ratio does not account for the energy transferred to moderator/gap water, which

[7] Thanks to the small size of the FA and to the good mixing provided by the wires used as fuel rod spacers, the average temperature of the FA, predicted by TRACE, is not very different from the one of the hottest sub-channel, as will be shown in the next sections. For this reason, the optimization of the mass flow based on FA average values is adequate for the current applications.

[8] A single TRACE run for the FA-wise core model may take up to 30 hours on a 2.4 GHz Linux PC with 2 GB of RAM, depending on the restart condition, on the selected maximum time step size and convergence criterion.

[9] [W/(kg/s)]=[J/kg].

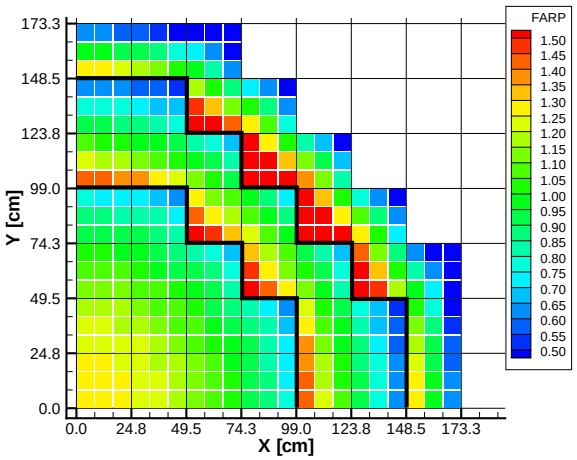

Figure 4.19: Region-wise FA Relative Power (FARP)

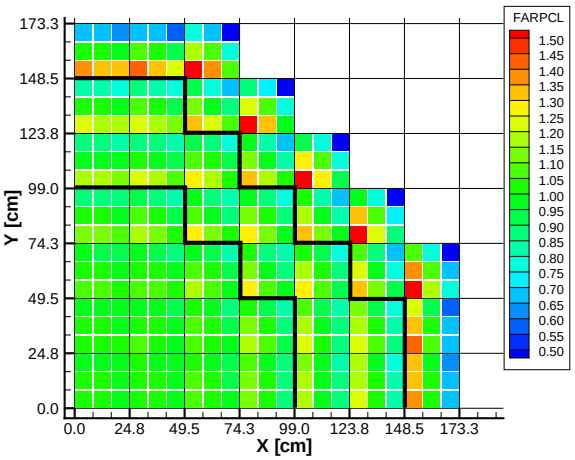

Figure 4.20: CL-wise FA Relative Power (FARPCL)

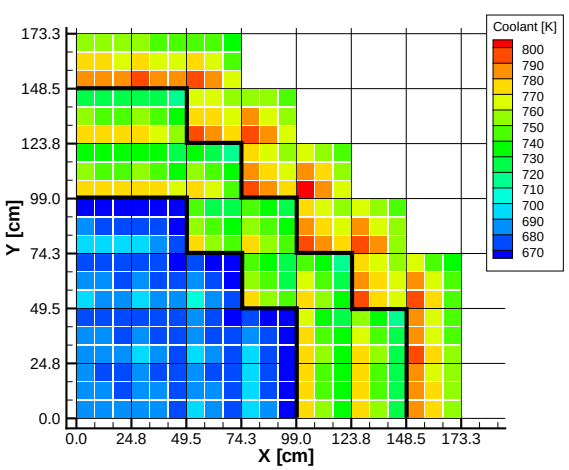

Figure 4.21: Coolant outlet temperature in each FA of the quarter core

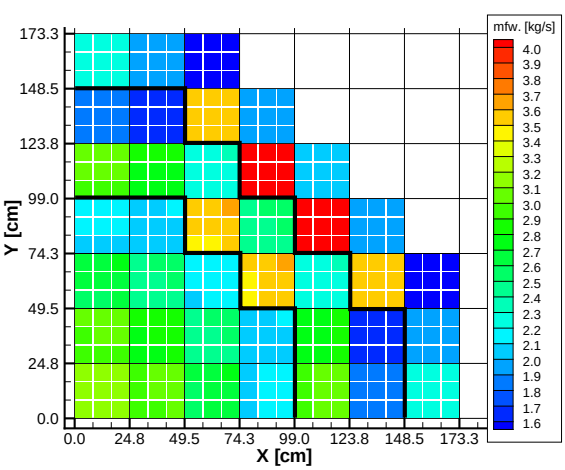

Figure 4.22: Predicted coolant mass flow in each FA of the quarter core

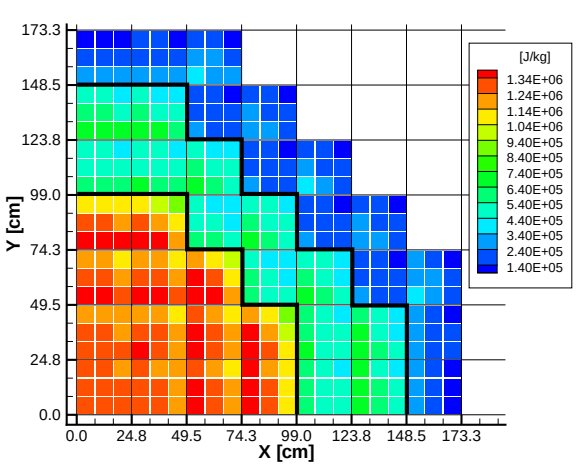

(a) all core

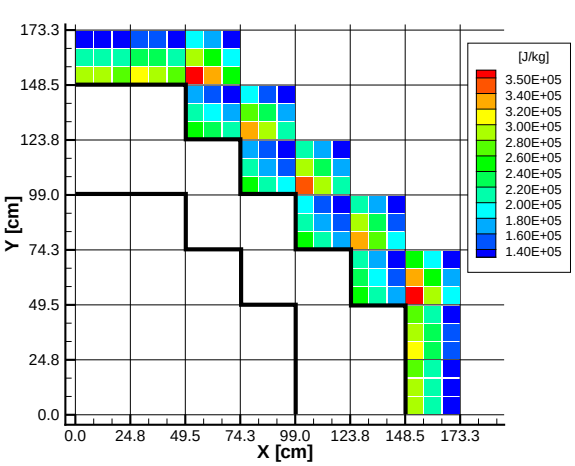

(b) only SH2

Figure 4.23: Power - to - Flow ratio for each FA [J/kg]

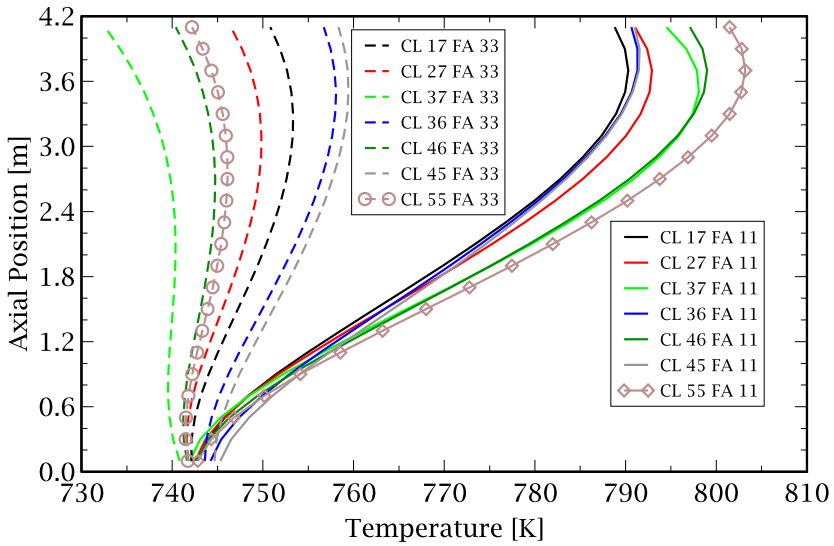

Figure 4.24: Coolant axial temperature distribution in highest (11) and lowest (33) power density FAs of each CL in SH2

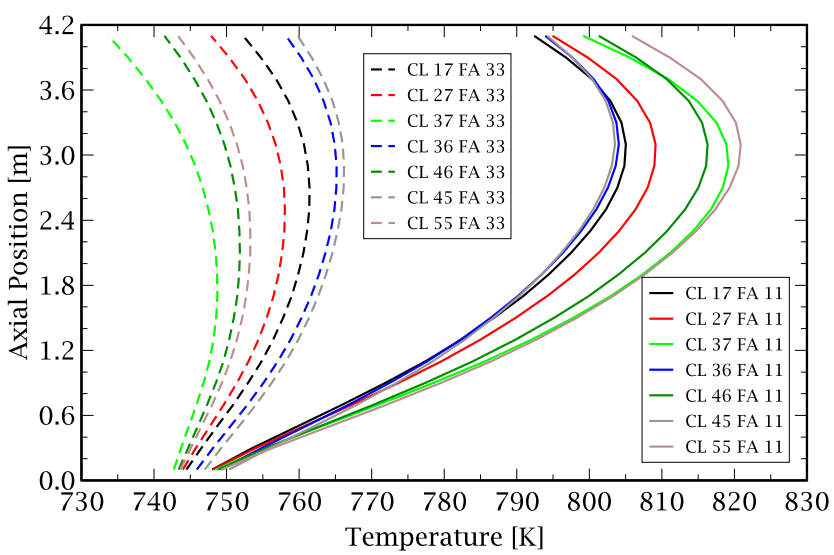

Figure 4.25: Clad axial temperature distribution in highest (11) and lowest (33) power density FAs of each CL in SH2

Table 4.2: Power balance for coolant water

	CL 37 FA 11	CL 37 FA 33	CL 55 FA 11	CL 55 FA 33
Power from fuel rods [W]	$4.86E+5$	$1.50E+5$	$6.93E+5$	$2.17E+5$
Power to moderator [W]	$-7.78E+4$	$-6.68E+4$	$-8.26E+4$	$-7.13E+4$
Power to gap water [W]	$-1.55E+5$	$-1.33E+5$	$-1.63E+5$	$-1.40E+5$
Net power input [W]	$2.53E+5$	$-5.01E+4$	$4.48E+5$	$5.08E+3$
Coolant flow [kg/s]	1.269	1.275	2.006	2.028

is not the same for various FAs since is a function of the coolant flow rate and temperature as shown in Table 4.2. For this reason, considering SH2, which is the critical region for peak clad temperature, the FA of highest power - to - flow ratio (CL 37 FA 11) is not the one with the highest coolant temperature (CL 55 FA 11) as result evident from Figure 4.24.

The axial variation of the coolant temperature in the highest and lowest power density FAs of each CL in SH2, FA 11 and 33 as marked in Figure 4.13, allows better understanding of the

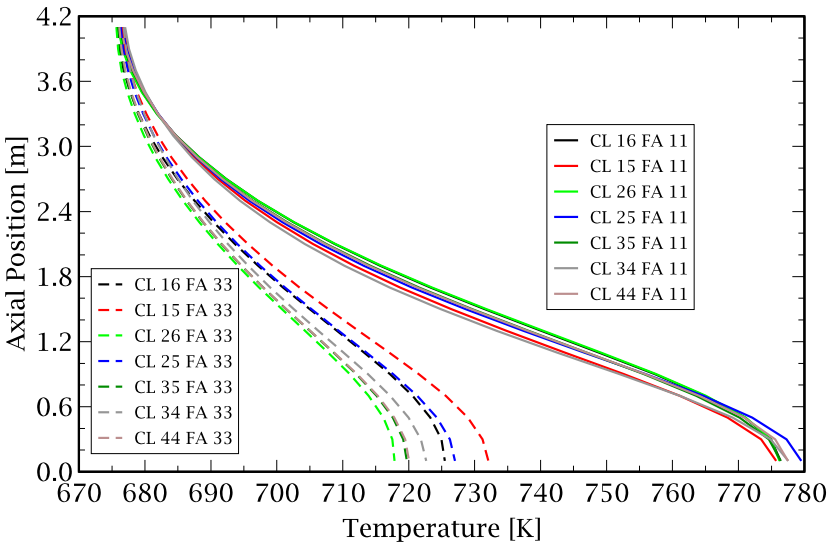

Figure 4.26: Coolant axial temperature distribution in highest (11) and lowest (33) power density FAs of each CL in SH1

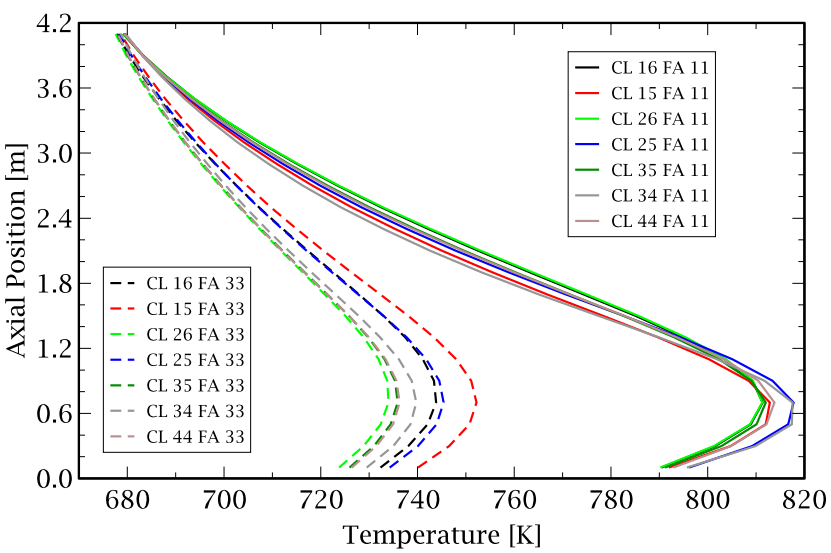

Figure 4.27: Clad axial temperature distribution in highest (11) and lowest (33) power density FAs of each CL in SH1

HPLWR core behavior and is plotted in Figure 4.24. The power gradients present in each CL, Figure 4.20, can not be compensated by mass flow redistribution using only one orifice for each CL and hence the lower power FA has much lower coolant and clad temperatures than the high power one, with differences of the order of 60 K and 80 K, respectively. In certain low power FAs close to the periphery of SH2 (CL 37 FA 33) the power generated by fission is even lower than the heat transferred from the coolant to the moderator/gap water[10], as shown in Table 4.2 and hence the coolant temperature decreases rather than increases in the flow direction. This happens even when using the current FA design with insulated walls [51].

The peak clad temperatures predicted at FA-wise scale in SH1, Figure 4.27, are quite similar to those of SH2 because of the higher power level even if the coolant temperature is there lower. A careful mass flow redistribution is, hence, required also in SH1 to avoid reaching impermissibly high clad temperatures.

[10]Which is calculated by TRACE and depends on the mass flow rate and temperature of both coolant and moderator/gap water.

4.5 Pin-power reconstruction: from fuel assembly to fuel pin scale

4.5.1 Local heterogeneity of the fuel assembly

In addition to fuel rod lattice structure, the local heterogeneity of the FA, due to the presence of the boxes and to the different neutron moderation in the coolant and in the moderator/gap water, may result in non-uniform power distribution within the 40 fuel rods.

The large range of water density and fuel temperature variations within the core may enhance this effect, hence, to provide a more realistic pin-power distribution, it was decided to perform several MCNP5 simulations of a 2D heterogeneous FA considering TH parameters typical of each CL in the considered quarter core. As alredy described in the previous chapter, for each CL, the TH parameters corresponding to the axial power peak zone Z are used for these MCNP5 calculations, they are given in Table 4.3, in which the temperatures of the available XSs are given.

A graphical representation of the 2D FA, modeled with reflecting boundary conditions in MCNP5, is given in Figure 4.28. Since CL-averaged TH values are used for each FA representative of the 22 CLs in the considered core model, all the sub-channels and fuel rods have the same water and fuel properties, respectively. The small geometry allows to easily perform these calculations in a reasonable CPU time without the need to consider existing symmetry planes which would inevitably cut the tallied volumes.

Table 4.3: TH parameters used for MCNP5 calculations

CL	Z	coolant		moderator		gap water		fuel
		[K]	[g/cm^3]	[K]	[g/cm^3]	[K]	[g/cm^3]	[K]
11	5	647	0.51511	573	0.71533	573	0.71726	1600
12	5	647	0.52060	573	0.71579	573	0.71771	1500
13	5	647	0.52498	573	0.71593	573	0.71781	1400
14	5	647	0.54086	573	0.71677	573	0.71854	1200
22	5	647	0.52298	573	0.71590	573	0.71780	1400
23	5	647	0.53082	573	0.71628	573	0.71816	1300
24	5	647	0.55631	573	0.71814	573	0.71990	1100
33	5	647	0.54594	573	0.71718	573	0.71898	1200
15	7	647	0.10826	573	0.70814	573	0.71003	1000
16	8	647	0.11093	573	0.71509	573	0.71647	900
25	7	647	0.10868	573	0.70858	573	0.71041	1000
26	8	647	0.11256	573	0.71582	573	0.71712	900
35	7	647	0.10969	573	0.70959	573	0.71127	900
34	6	800	0.10785	573	0.70308	573	0.70522	1000
44	7	647	0.10972	573	0.70930	573	0.71101	900
17	8	800	0.09090	623	0.68074	623	0.68243	800
27	8	800	0.09100	623	0.68268	623	0.68399	800
37	8	800	0.09150	623	0.68889	623	0.68921	800
36	8	800	0.09099	623	0.67654	623	0.67910	900
46	8	800	0.09101	623	0.68301	623	0.68429	800
45	8	800	0.09116	623	0.67479	623	0.67773	900
55	8	800	0.09065	623	0.68152	623	0.68292	800

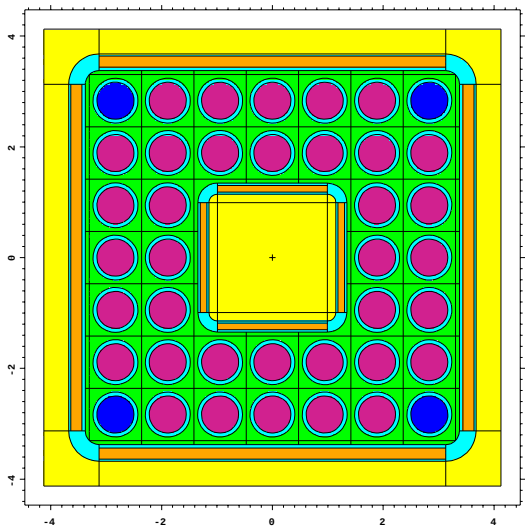

Figure 4.28: Insulated fuel assembly geometry in MCNP5

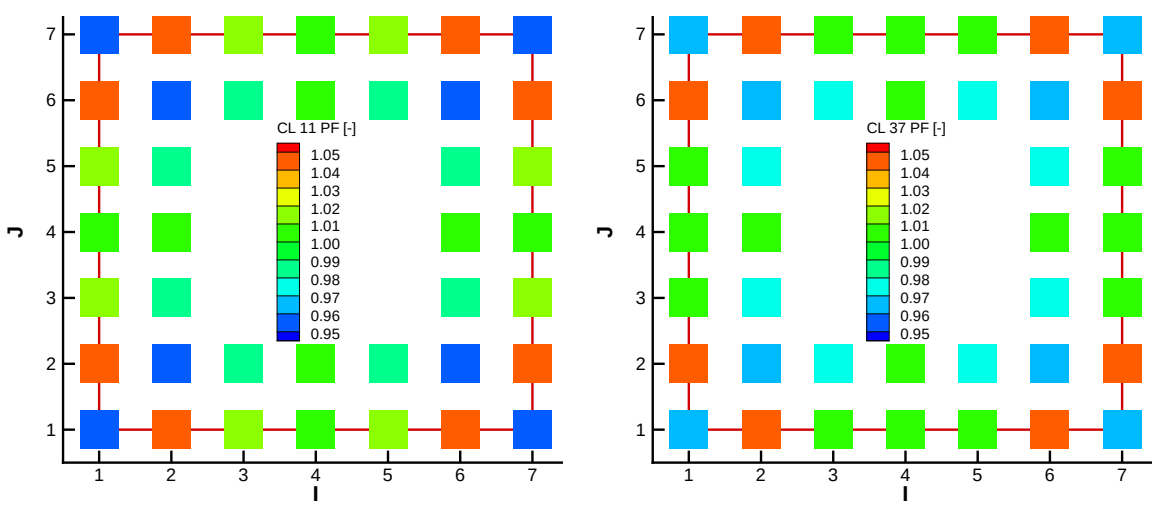

(a) CL 11 (b) CL 37

Figure 4.29: Peak Factor (PF) of each fuel rod as predicted by MCNP5 for selected CLs

Despite these large range of variations of the TH parameters, the resulting relative fuel rod power distribution is rather similar for the considered 22 cases. Two extreme ones have been selected, CL 11 and 37, and have been plotted in Figure 4.29. For a better understanding of the relative fuel rod power, it is important to remember that the 4 fuel rods at the corner of the fuel assembly, in blue in Figure 4.28, have a lower enrichment in ^{235}U with respect to the other 36: 4wt% instead of 5wt%, which has been defined in early stages of the HPLWR project [57] and has not been modified since then. This preliminary optimization of the FA power distribution was finalized to the reduction of pronounced power peaks but more studies will be required in future design stages to flatten the power peaks within each FA, as current practice in BWRs.

The initial neutron source used for the criticality calculations is uniformly distributed within the 40 fuel rods and the number of skipped cycles (300) is well above the first cycle number which has source entropy within 1 standard deviation of the average entropy, i.e. the recommended number of cycles to be skipped, ensuring the satisfaction of source entropy convergence check[11].

[11]It is well known that this condition is only necessary but not sufficient for the establishment of source convergence.

Beside the check on the accuracy of the neutron source, precision of the MCNP5 calculations is inspected considering the relative errors and tally fluctuations charts. For this reason, 8 independent tallies, each with only one bin, are used for the 7 fuel rods, respecting the one eighth symmetry of the geometry, plus the average over all rods. In this way, the statistic of each individual tallied quantity can be better assessed. Sensitivity studies were used to fix the parameters needed by the criticality calculations: 50000 neutrons are followed for 1000 cycles, of which the first 300 are discharged. With this number of histories, the relative errors are extremely small: 0.0001 for the average over all fuel rods and 0.0006 or 0.0007 for the tallies over the single fuel rods. Despite the precision of the tallied quantities, only 7 of the 22 runs passed the 10 statistical checks of the tally fluctuation charts while for the other runs some tallies missed one of the 10 checks[12]. The manual inspection of the tally fluctuation charts found only marginal trends which, together with the high precision of the calculated tallies may not justify additional code runs.

The relative fuel rod power is perfectly symmetric because reflecting boundary conditions are used for these 2D calculations. A refined treatment could be envisaged in order to represent the neutron flux gradient within each FA using group dependent albedos instead of reflecting boundary conditions at the lateral surfaces of the FA but this would require complicated coupling between core and cell calculations, both performed with deterministic methods, which goes well beyond the present studies and would be extremely difficult to assess. In addition, this kind of approach, may lead to an overestimation of the neutron flux gradients.

4.5.2 Combined effect of neutron flux gradients and of local heterogeneity of the fuel assembly on fuel rod power distribution

Using the ERANOS system it is possible to reconstruct the nodal flux calculated by VARIANT for the desired XYZ mesh [130]. To predict the pronounced effects of the flux gradient on the redistribution of the calculated CL power in each fuel rod, a 21×21 refinement of each CL is considered, as shown in Figure 3.10 on page 63. With this refinement, the total power generated in each equivalent cell is available and can be extracted from the ERANOS output, its graphical representation is given in Figure 4.30. The power distribution is largely dominated by the spatial flux gradient but presents a clear discontinuity at the interface between EVA and SH1, where the fission XS is discontinuous because of the abrupt changes in the TH properties.

Once the power at cell level is available, it is necessary to correct it in order to obtain the power generated in each fuel rod. The power generated in the 9 cells which occupy the moderator box has to be relocated to the remaining 40 cells representative of each fuel rod and the predicted local heterogeneity of the FA has to be considered. These tasks have been automatized in a new Perl script whose application to fuel rod power reconstruction results in the detailed power map shown in Figure 4.31. In the figure, it is possible to recognize each individual fuel rod and to see the effects of both the neutron flux gradient and the local heterogeneity of the FA. Because of the radial neutron flux gradient, the fuel rods which are closer to the center of the core have a higher power level than the ones closer to the periphery of the core, also within each FA but, because of the local FA heterogeneity and selected enrichment distribution, the corner fuel rods of each FA have a lower power compared to the others rods. The maximum fuel rod power is higher than the maximum cell power, Figure 4.30, since there are only 40 fuel rods instead of 49 cells.

The difference between the results extracted from VARIANT and those obtained with the developed pin-power reconstruction technique is more evident when considering only a single CL, as done in Figure 4.32 and 4.33.

Since the sub-channel investigations uses a finer axial mesh, an additional nodal flux reconstruction in ERANOS is used to subdivide each of the 21 axial zones used up to now into 8 to

[12]The figure of merit or the estimated mean has a trend during the last half of the problem.

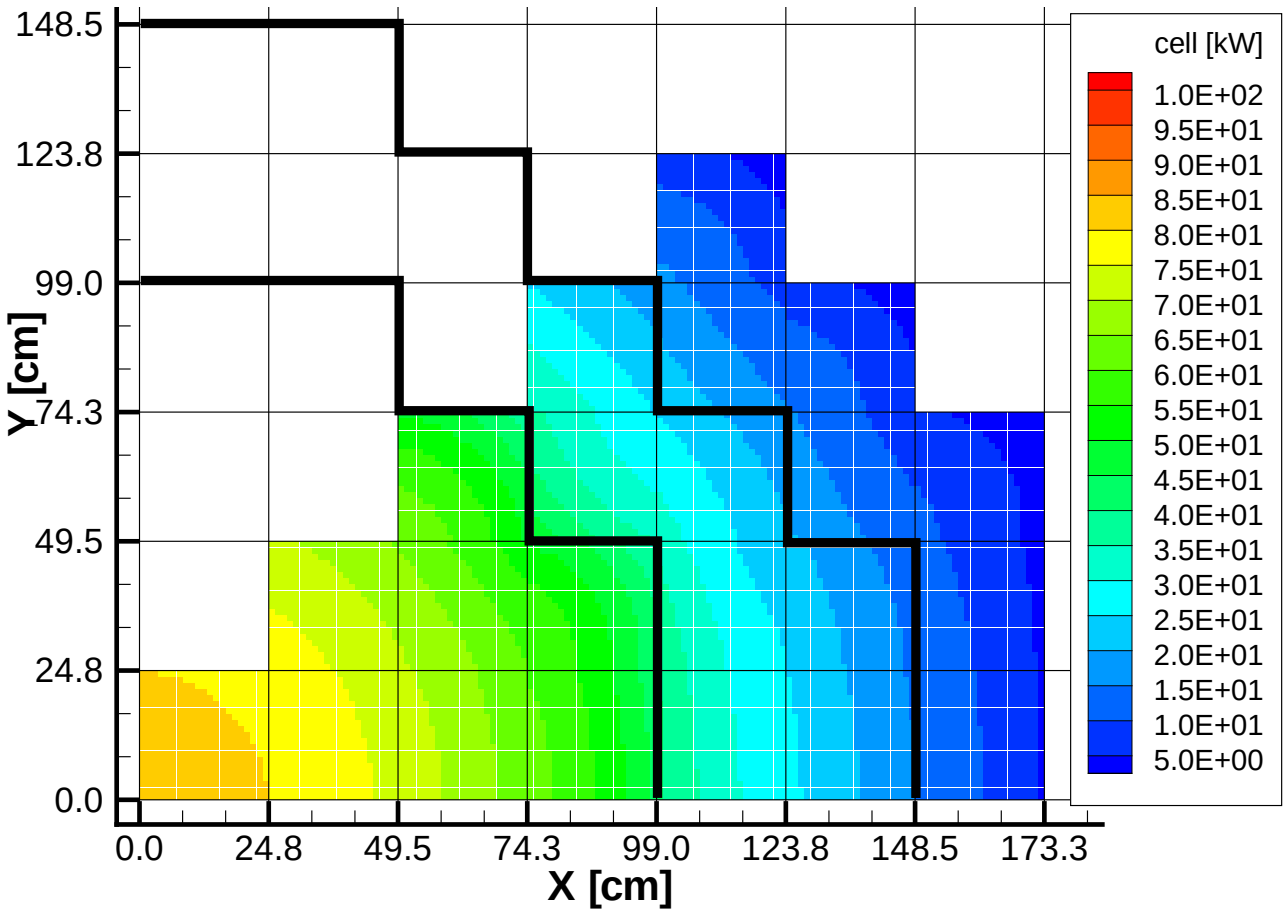

Figure 4.30: Power generated in each cell as extracted from VARIANT

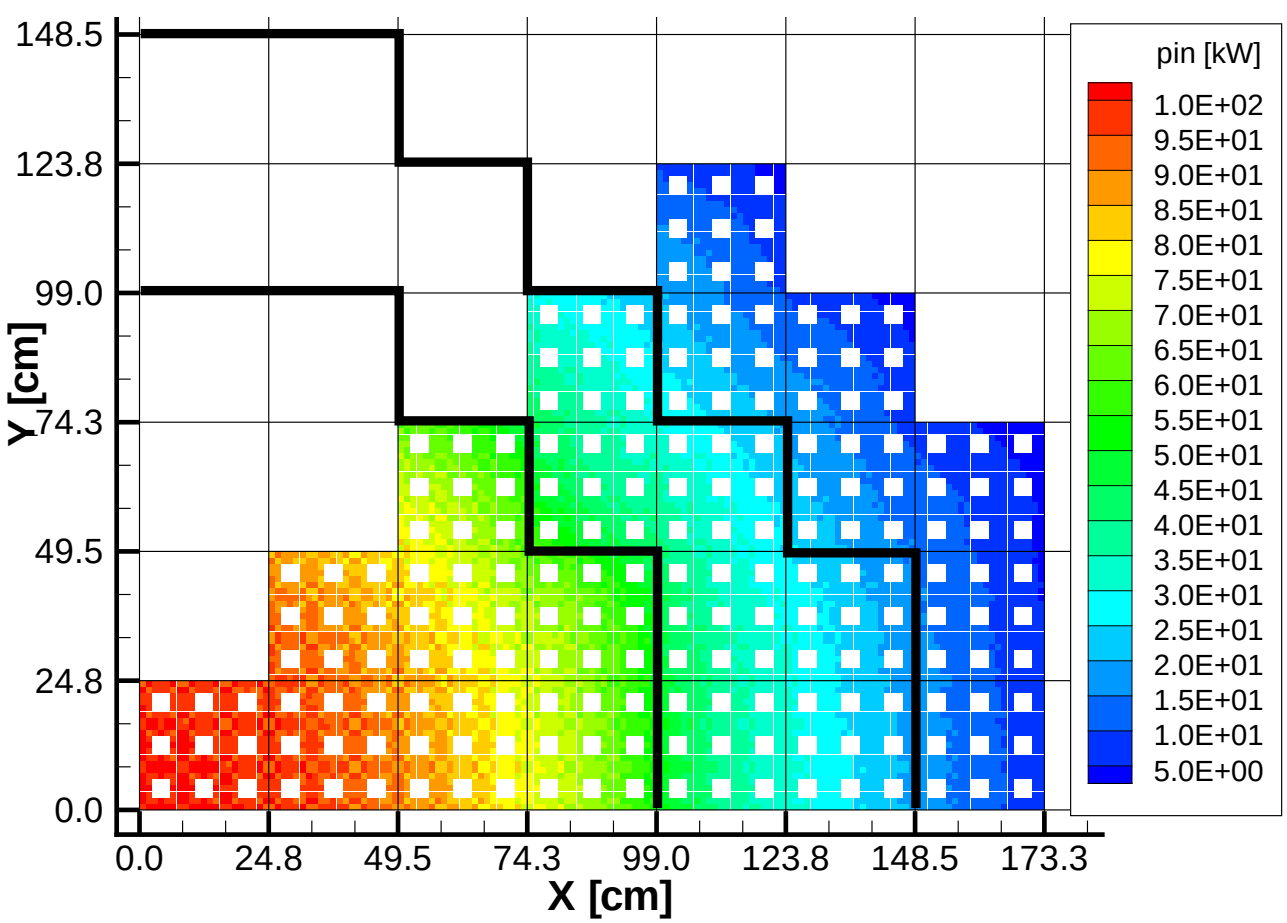

Figure 4.31: Power generated in each fuel rod obtained with pin power reconstruction

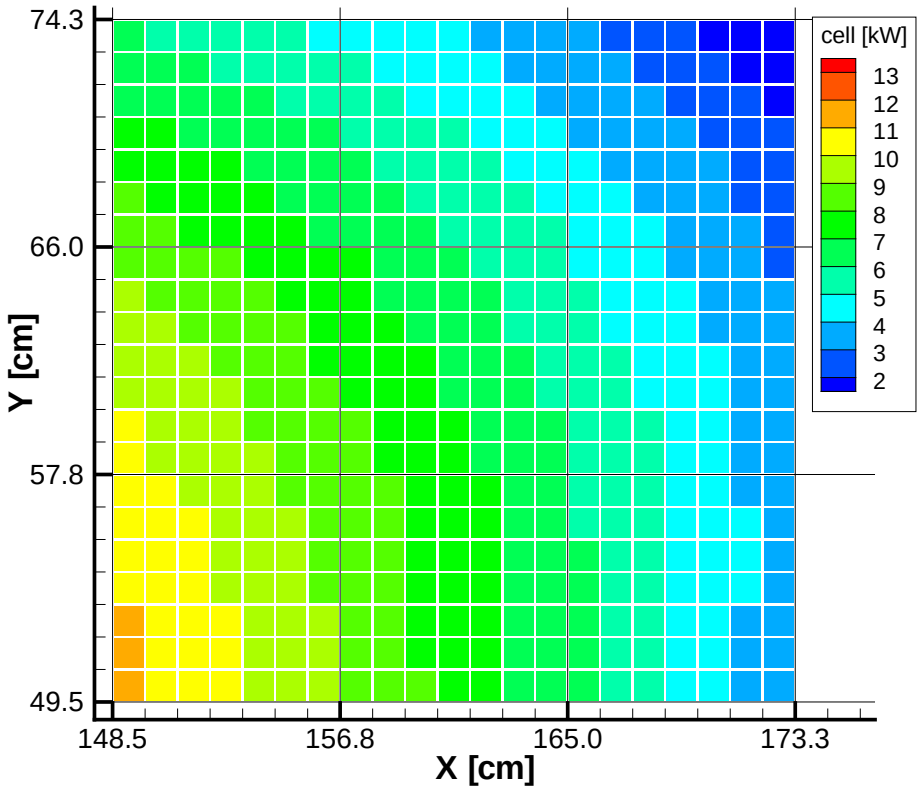

Figure 4.32: Details on CL 37: power distribution obtained with VARIANT

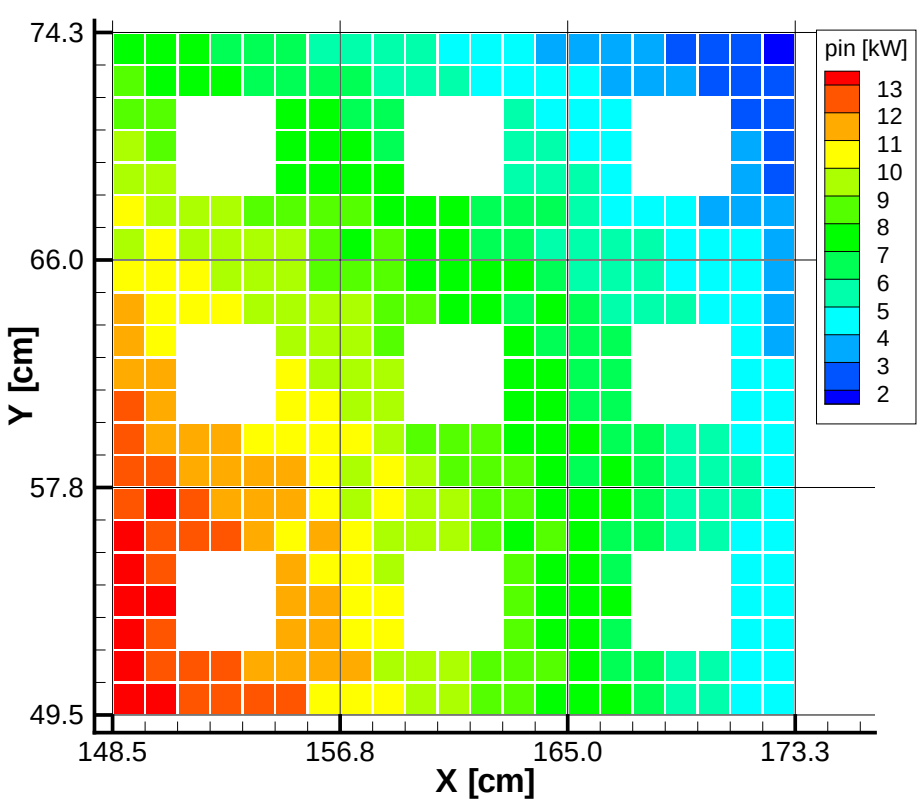

Figure 4.33: Details on CL 37: reconstructed pin-power distribution

have the power generated each 2.5 cm as requested for MATRA. This axial refined power map completes the set of input data which are necessary for sub-channel investigations.

4.6 Investigation of the obtained coupled solution at sub-channel resolution

4.6.1 Whole core results

The procedure to extract and manipulate all the input data, necessary for the sub-channel investigations of the HPLWR core, has been automatized with a Perl script allowing great flexibility and application of the one-way coupling to different operating conditions and using different skeleton files for MATRA[13].

Beside the automation of the repetitive code execution for all considered input files, additional efforts have been devoted to provide a user friendly representation of the huge amount of data calculated at sub-channel level[14]. With the usage of the finer mapping scheme, based on a multiple nesting of each individual fuel pin inside each FA inside each CL, it is possible to locate the results of individual FA sub-channel analyses into the corresponding 3D position, simplifying the interpretation and analysis of the obtained data.

At first, the outlet temperature of each individual sub-channel in the modeled one eighth of the core[15] is considered, its representation is given in Figure 4.34. Since CL 37 is identified as the one with the highest outlet coolant temperature, it is also considered separately in Figure 4.35 using a finer color map. It is possible to recognize that, in most FAs, the effect of the wires leads to a good mixing and to a rather homogeneous outlet temperature despite the pronounced power gradients. The mixing is actually more pronounced, for the selected mixing coefficients, for the lateral sub-channels which have more uniform temperatures with respect to the central sub-channels; this behavior has been observed also by [55] with a completely different computational approach. The higher coolant outlet temperature with respect to the previous FA-wise core analysis, Figure 4.21, is readily explained by having neglected the heat transfer to the moderator/gap water in these sub-channel investigations. For this reason, there is a direct correspondence between the coolant outlet temperature and the power - to - flow ratio, plotted in Figure 4.23, which identified CL 37 FA 11 as the critical FA for the peak coolant and clad temperature. The small dimensions of the HPLWR FA together with the good mixing offered by the wires result in rather uniform outlet temperatures of the sub-channels belonging to the same FA which put the burden of the high peak - to - average coolant outlet temperature on the big differences among the FAs within the same CL. These may be as high as 90 K as already predicted by TRACE, Figure 4.24.

The calculated fuel rod centerline temperature is plotted in Figure 4.36. Using the selected fuel and clad average properties in MATRA, a good qualitative agreement on both the absolute values and the spatial distribution of the temperatures is found with TRACE for FA resolution, Figure 4.18, providing a verification of both scales. As already mentioned, the fuel rod centerline temperature is mostly influenced by the linear power of each rod, plotted in Figure 4.37. This quantity has been calculated by MATRA merging the input radial (pin-wise) and axial (FA-wise) power distributions.

The predicted clad temperature is plotted in Figure 4.38. The results obtained confirm the investigations at FA-scale, in particular the clad temperature for the operative condition in EVA is low and hence has not been included in the plot allowing to see that the clad temperature in the lower part of SH1 is quite high especially in the rods operated at higher power level. Critical

[13] Allowing to change sensible parameters, like the turbulent mixing factor or the fraction of axial flow diverted by the wire, and to easily repeat the whole core analyses.

[14] In one eighth of the core there are 22 CLs, each constituted of 9 FAs with 60 sub-channels and 40 fuel rods while 168 axial node are considered.

[15] The core symmetry is broken by the unilateral sweeping effect originated by the wires but the present investigation is restricted to only one eighth of the core because of the huge amount of data to be handeled and because the effect on the peak clad temperature should not be very pronounced.

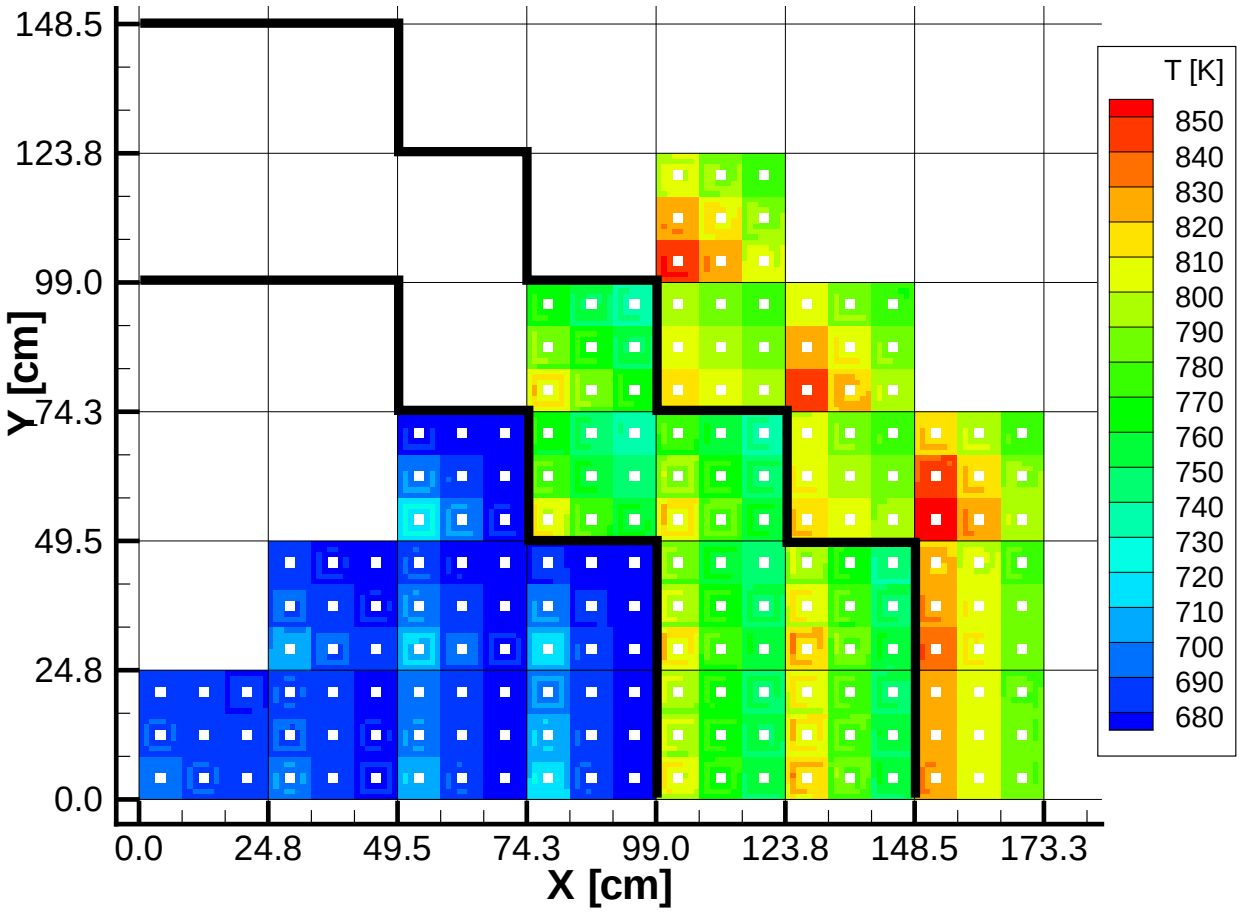

Figure 4.34: Outlet temperature of all considered sub-channels

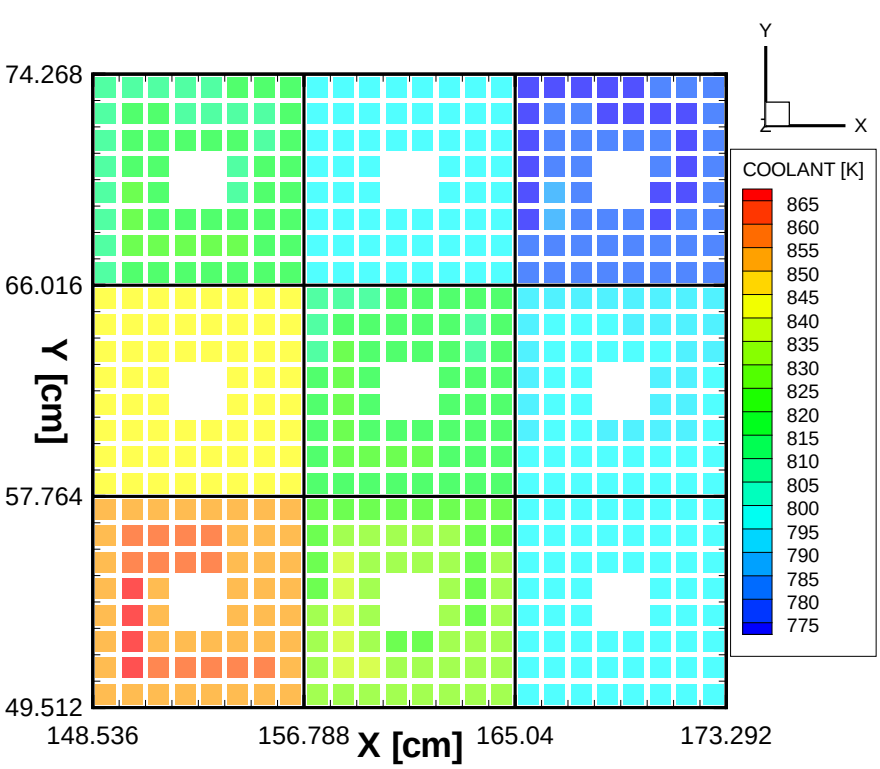

Figure 4.35: Outlet temperature of the hot CL (37)

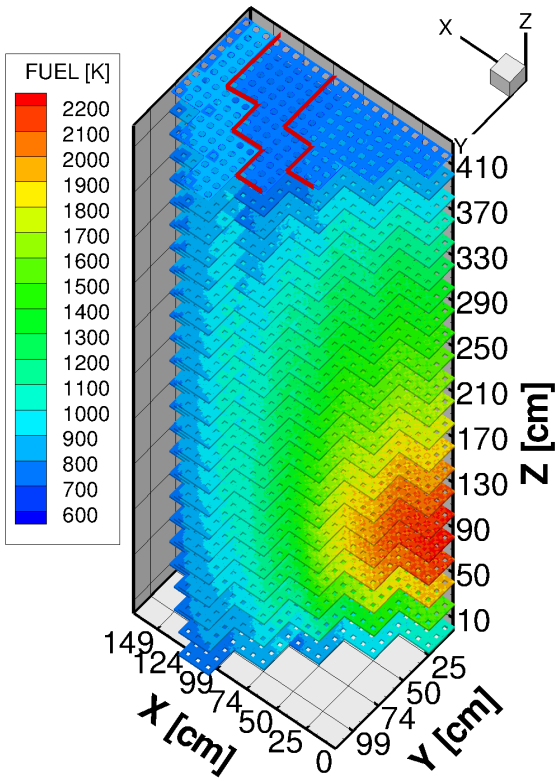

Figure 4.36: Centerline temperature of each individual fuel rod

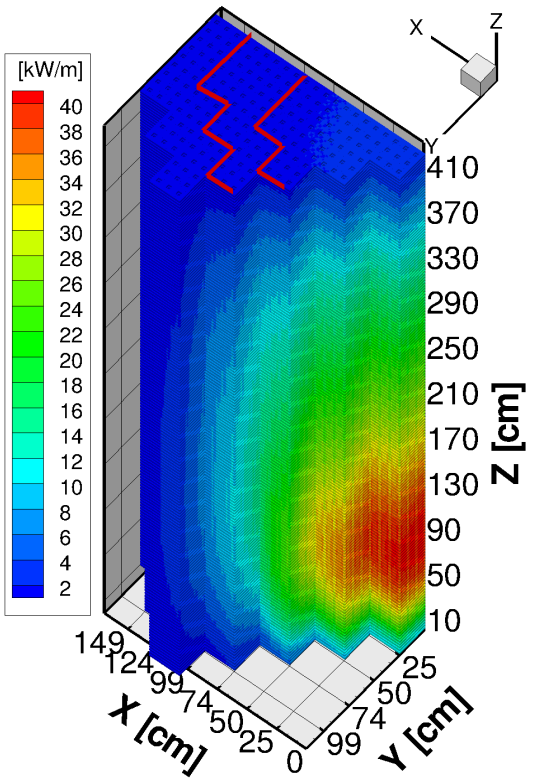

Figure 4.37: Individual fuel rod linear power

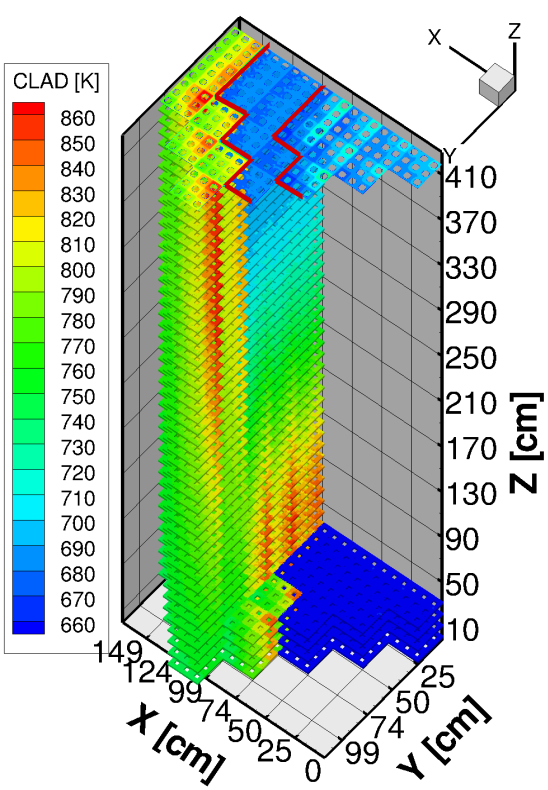

Figure 4.38: Clad temperature of each individual fuel rod

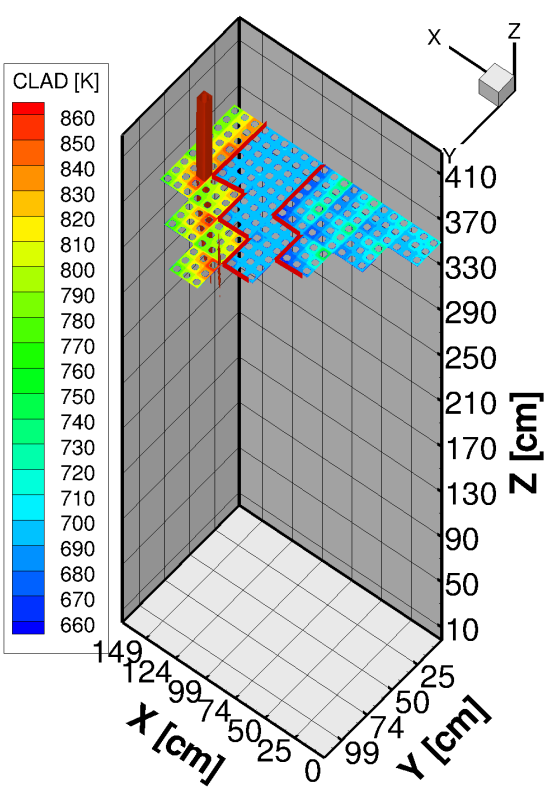

Figure 4.39: Peak clad temperature

values may occur in SH2 and the identification of the peak clad temperature is simplified by the 3D visualization tool: the isosurface corresponding to 860 K, plotted in Figure 4.39, identify CL 37 FA 11 as the one with the highest clad temperature. Also CL 55 has a high clad temperature confirming the previous results obtained for FA-scale in Figure 4.25.

The pronounced power gradient within the FA, ignored at FA-scale, play an important role in the encountered discrepancy in the absolute temperature values between the considered scales. But it is also important to keep in mind the difference in the models and in particular the simplifications involved in the sub-channel wise analyses: the coolant temperatures predicted by MATRA are higher, since the heat transfer to moderator/gap water has been neglected, rising the clad one as well as a different heat transfer correlation[16] and structural material properties have been used.

4.6.2 Details on the hot fuel assembly

More details on the identified hot FA are given in Figure 4.40, where clad and coolant temperatures in each individual rod and sub-channel are plotted in the vicinity of the peak clad temperature axial position. The clad temperature resemble both the pin axial and radial power peaking – which is very pronounced for this peripheral FA Figure 4.41 – and the coolant temperature distribution: its maximum occurs in the power peak pins in axial positions where the coolant temperature is not yet at its maximum.

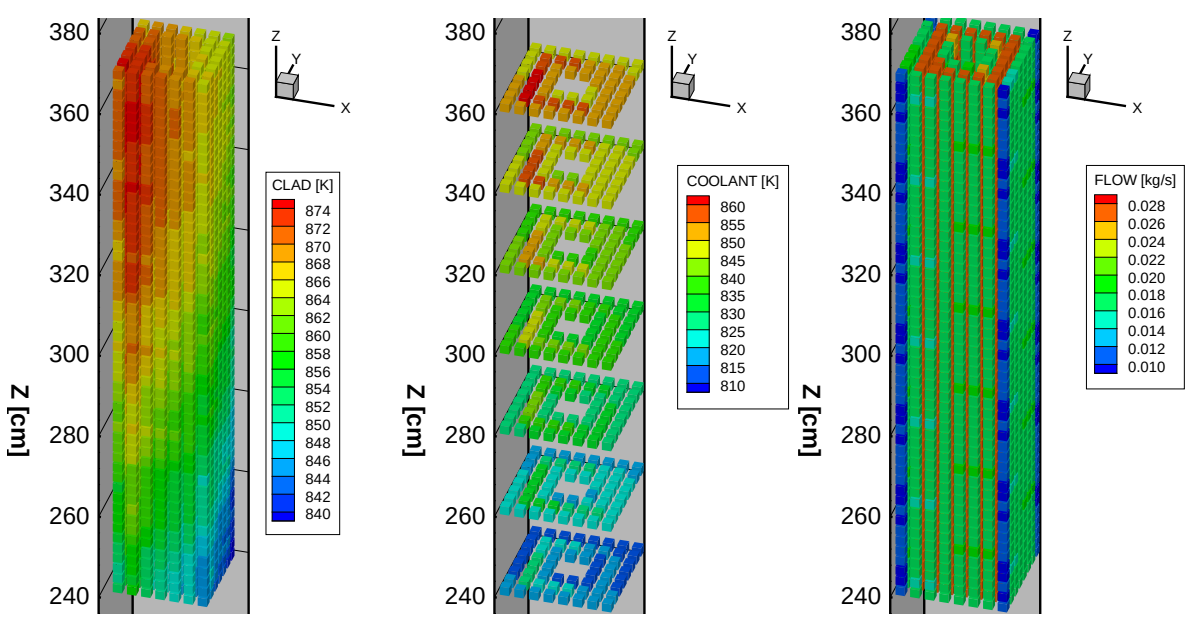

(a) Clad temperature (b) Coolant temperature (c) Coolant mass flow

Figure 4.40: Details of the hot fuel assembly

The axial temperature of the clad has small fluctuations, of the order of 1 K, and it is not monotonically changing till the maximum value as obtained for FA-scale. This effect, which is mainly due to the neglection of the axial conduction, is amplified both by the short nodalization and by the average HTC which is calculated in MATRA: a temperature average of the 4 neighbouring sub-channels of each fuel rod is performed in MATRA in order to have one fluid temperature to compute the clad temperature. Since differences in the fluid condition occur in successive axial nodes – the coolant heat up is not uniform and the presence of the

[16]For the coolant temperature ranges in SH2, well above the pseudo-critical one, the differences between Dittus-Boelter and Bishop heat transfer correlations are marginal [115].

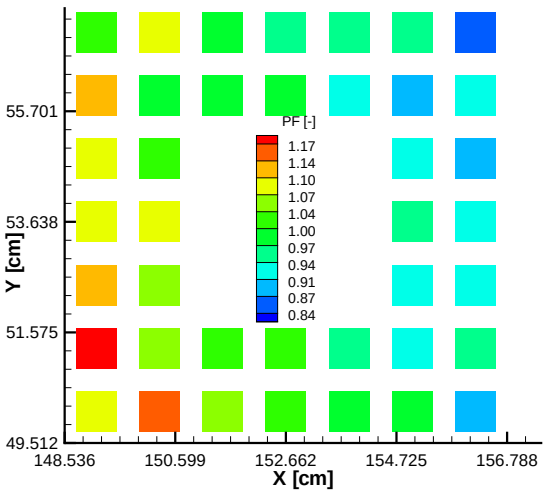

Figure 4.41: Power Peak Factor (PF) in the pins of the hot fuel assembly

wire modifies the axial mass flow in the lateral and corner sub-channels, Figure 4.40(c) – this averaging may results in the observed small clad temperature differences.

The relative pin power distribution, plotted in Figure 4.41, causes the observed non-uniformity in coolant and clad temperature distribution. Comparing the values obtained with the developed pin power reconstruction with those predicted by MCNP5 for a single FA analysis, Figure 4.29(b), it is possible to see how pronounced are the effects of neutron flux gradient on the relative pin power distribution. These rather high values are not the maximum ones encountered: in the FA closer to the steel reflector a power peaking factor of 1.55 is found for the considered operative condition but, thanks to the lower power level, no critical temperatures are found in that region. This demonstrates the importance of obtaining the neutron flux gradient from whole core analyses since the heterogeneous pin power distribution obtained with single FA analyses predicts substantially lower power peaks.

For the selected mixing coefficients, the coolant temperature presents peak values in the central sub-channel which also have a higher mass flow rate because of the larger flow area. This finding is consistent with the unilateral sweeping flow which exists in the lateral sub-channels and helps in smoothing the temperature distribution. For the central sub-channels, the bilateral flow through the gaps seems to be less effective in reducing peaking temperatures but, nonetheless, maximum differences between adjacent sub-channels are below 10 K thanks to the good inter-channel mixing.

4.6.3 Details on the power peak fuel assembly

The current proposal of the HPLWR 3 pass core decouples the region of high power level (EVA) from those of high coolant temperature (SHs). More details on the power peak FA located at the center of EVA, as shown in Figure 4.37, are plotted in Figure 4.42.

The fuel temperature, Figure 4.42 (a) and (b), has its highest values where the power peaks are located, as shown in Figure 4.42(c). The high fuel pin centerline temperature rises the clad one which exhibits peaks in the corresponding regions, Figure 4.42(d) but, thanks to the low coolant temperature in these regions, Figure 4.42(e), the clad temperature is well below the values predicted in the hot fuel assembly shown previously.

As shown in Figure 4.43, despite the very pronounced power peak close to the bottom of the FA, the higher clad temperatures occur where the coolant temperature is closer to its maximum even if there the power level is much lower. This consideration has to be kept in mind when optimizing the axial power shape in EVA: the rise of the power level in the upper part will result

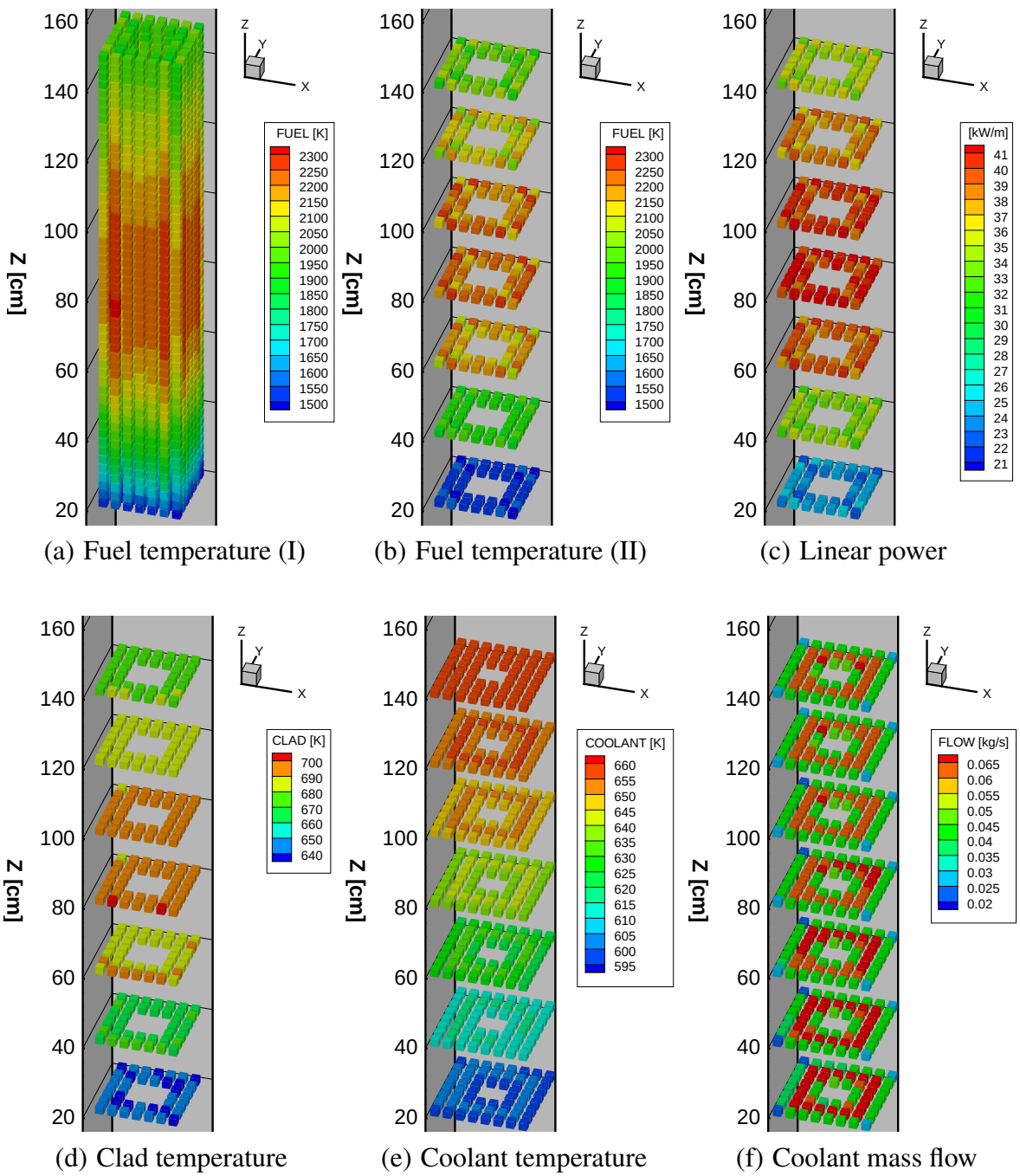

(a) Fuel temperature (I) (b) Fuel temperature (II) (c) Linear power

(d) Clad temperature (e) Coolant temperature (f) Coolant mass flow

Figure 4.42: Details of the power peak fuel assembly

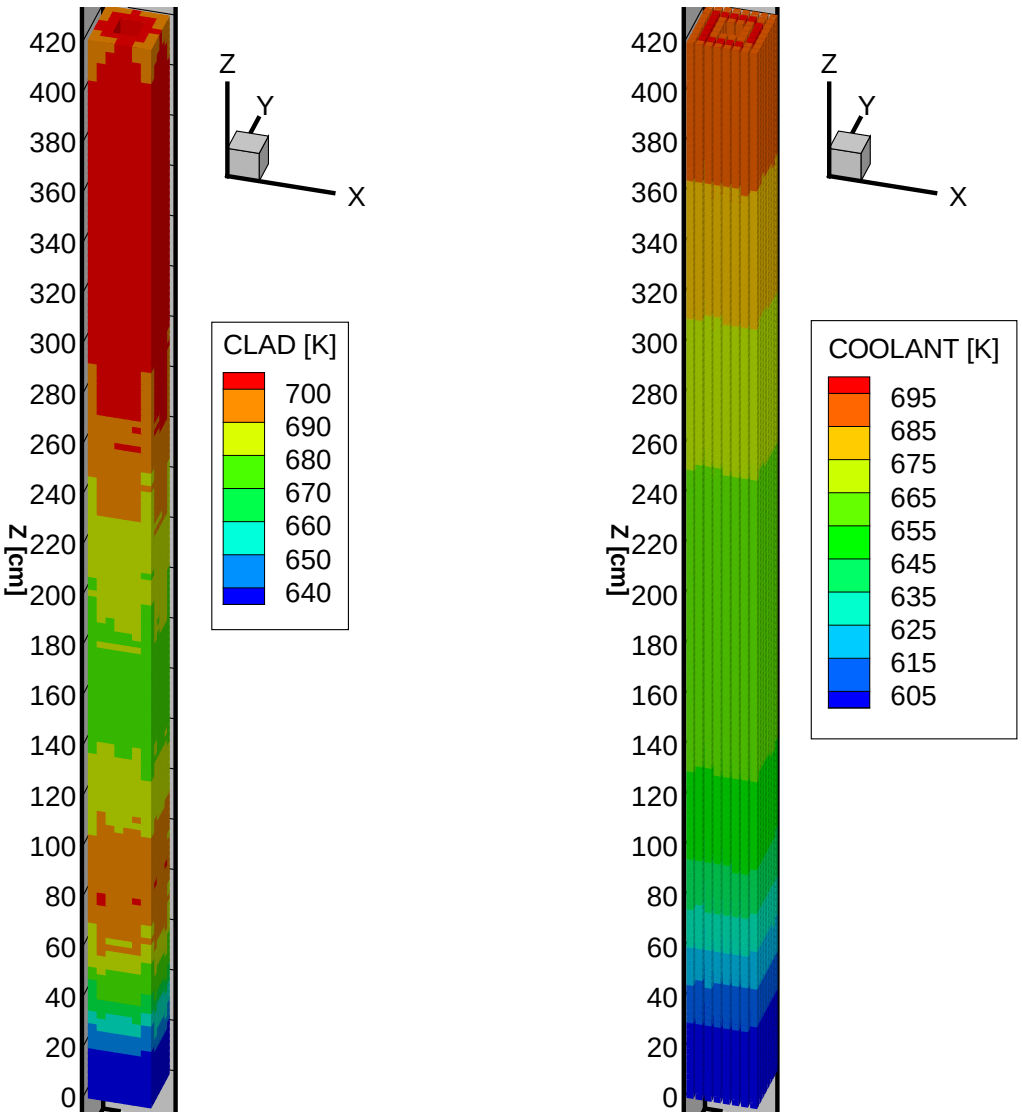

(a) Clad temperature (b) Coolant temperature

Figure 4.43: Axial temperature distributions in the power peak fuel assembly

in an increase of the clad temperature and may require several iterations to achieve a good axial power profile which satisfies constraints on both fuel and clad temperature distribution.

4.6.4 Additional sensitivity studies

Effects of the heat transfer from coolant to moderator water

As discussed in the previous chapter, MATRA can not account for the counter-current heat transfer between coolant and moderator/gap water. This results in an over prediction of the coolant temperatures which can be evaluated by a direct comparison between the axial temperature distribution predicted by TRACE[17] and the bundle average calculated by MATRA. For the two FAs with highest coolant outlet temperature, located in SH2, this comparison is plotted in Figure 4.44 and shows remarkable differences.

These findings are consistent with the presented power - to - flow ratio, Figure 4.23, and power balance for these FAs, Table 4.2: for CL 37 FA 11 the power transferred to moderator/gap water is the 42% of the power generated from nuclear fission while in CL 55 FA 11 is only

[17] Which takes into full consideration the energy transferred to the moderator/gap water.

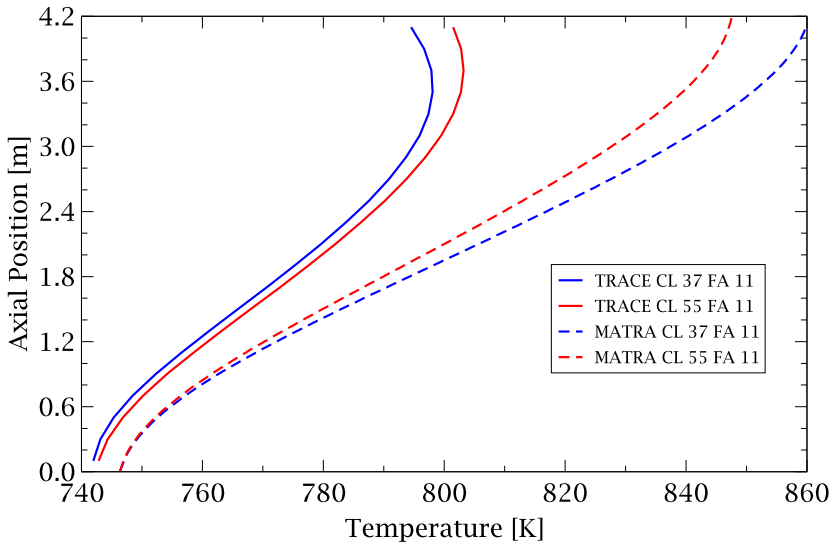

Figure 4.44: Coolant temperatures predicted by TRACE and MATRA

35%. This, together with the different mass flow rate, explains why TRACE predicts higher temperature in CL 55 FA 11 while MATRA in CL 37 FA 11.

The axial profile of the heat flux from the coolant to moderator/gap water differs substantially from the axial power shape and, in addition, the heat transfer to moderator/gap water affects directly only the lateral sub-channels. For these reasons, it would be necessary to model in full details the heat transfer to the moderator/gap water also at sub-channel resolution. This effect may enhance temperature gradients within the HPLWR FA since the lateral sub-channels already exhibit a lower temperature than the central ones.

Sensitivity to different inter-channels mixing coefficients

As discussed in section 2.3, the diversion cross flow coefficients input in MATRA are based on empirical correlations which are difficult to be assessed because of lack of experimental data. In addition, because of the local nature of this quantities, also the direct comparison with high fidelity CFD simulations is quite complex. For these reasons, it is important to evaluate the sensitivity of the coolant temperature distribution to the selected input parameters to estimate a degree of confidence in the obtained results. The identified hot FA (CL 37 FA 11) is selected for these studies in order to have realistic boundary conditions for the power distribution and coolant flow rate.

Four different cases have been considered to represent the inter-channels mixing and to evaluate the sensitivity of the coolant outlet temperature distribution within the adjacent sub-channels, as shown in Figure 4.45:

(a) the wire-wrap model of D.S. Rowe [127, 160] is used to predict the diversion cross flow and the associated enthalphy transfer; the cross flow coefficients have been adjusted as described in section 2.3;

(b) the wire-wrap model of D.S. Rowe [127, 160] is used as in the previous case but recommended values of the diversion cross flow coefficients are used;

(c) the presence of the wire is neglected and the enthalpy mixing among adjacent sub-channels is enhanced by means of the turbulent mixing factor [118] determined using the Miyaguchi correlation as suggested by Heinecke [50];

$$\text{homogeneous mixing coefficient } \beta = 0.66 \frac{\text{fuel rod lattice pitch}}{\text{wire lead}}$$

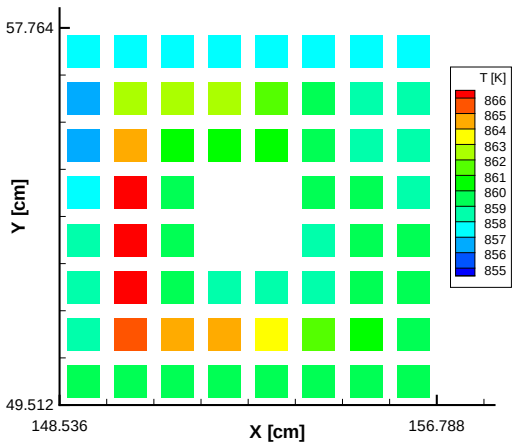

(a) D.S. Rowe model with adjusted `DUR(K)`: max T 868 K

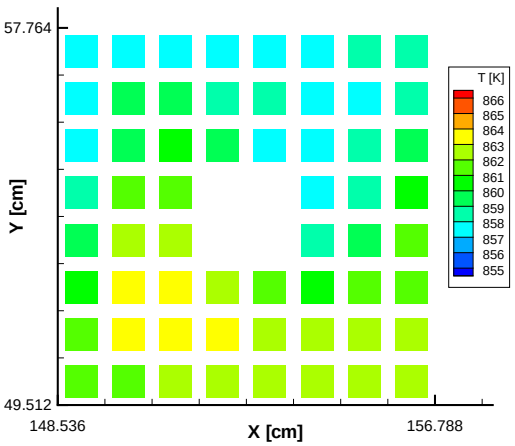

(b) D.S. Rowe model with recommended `DUR(K)`: max T 864 K

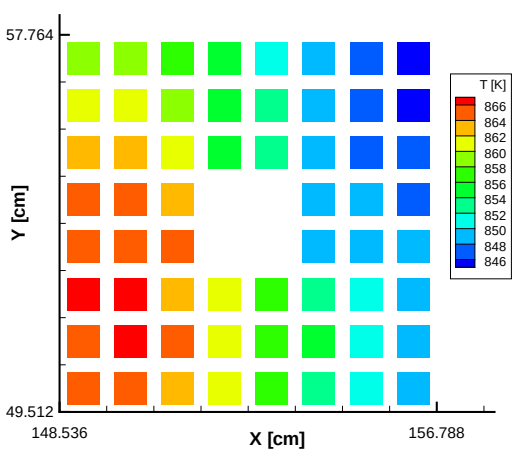

(c) turbulent mixing factor based on the Miyaguchi correlation: max T 866 K

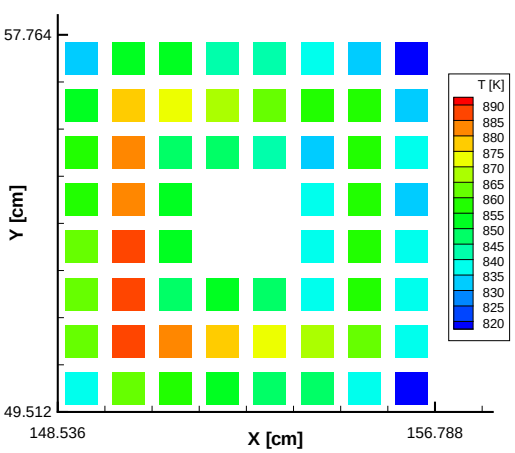

(d) without wire model and without turbulent mixing factor: max T 889 K

Figure 4.45: Sensitivity of the outlet coolant temperature in CL 37 FA 11 to the wire representation (the color maps are different)

(d) the presence of the wire is neglected and the enthalpy mixing among adjacent sub-channels is achieved only through the mass transfer calculated by MATRA to balance the different pressure drops of the various sub-channels.

The effects of the two last cases can be evaluated only for a heated case because they do not influence the mass transfer between adjacent sub-channels and hence have not been considered in section 2.3.

A rather small difference in peak temperature is obtained when comparing cases (a) and (b): despite the changes in cross flow underlined in Figure 2.39 and 2.40 on page 52, the temperature distribution is not changed substantially. As expected, since case (b) predicts higher cross flows, it has slightly lower temperature differences, in particular the one between the central and lateral sub-channels is evidently reduced. The difference between the maximum and minimum outlet temperature for the two models is of only 11 and 6 K, respectively, testifying an excellent inter-channel mixing.

The differences found between case (a) and (c) underline the importance of the sweeping

effects in the lateral sub-channels to achieve a more uniform coolant temperature distribution within the FA. The usage of a turbulent mixing factor seems to provide a better enthalpy balance only among neighboring sub-channels but the input power gradients, shown in Figure 4.41, are visible from the outlet temperature distribution. The usage of the Miyaguchi correlation results in lower maximum and minimum temperatures, the first one by 2 K while the latter ones by 11 K, increasing the difference between the maximum and minimum outlet temperature to 20 K.

Case (d) is considered as term of comparison, it should underestimate the mixing among the sub-channels and hence may provide a conservative upper bound of the temperature differences which are increased up to 75 K, with a maximum temperature higher by 21 K.

These results are encouraging since the presented sensitivity to the inter-channel mixing is not very pronounced, mainly thanks to the small FA size, and hence the results uncertainty should also be limited. The peak - to - average ratio of coolant temperature in the hot FA is close to unity despite the relevant power gradients and, hence, the selected mass flow optimization, based on FA-wise mean values, is adequate for the current application.

Chapter 5

Concluding Remarks

5.1 Remarks on qualification of the separate fields

5.1.1 ERANOS-MCNP5 code-to-code comparison

The verification of the ERANOS modeling, including both the chosen calculation procedure and geometry representation, has been achieved by a comparison with MCNP5 which, thanks to a continuous energy treatment and accurate geometry representation capabilities, offers a powerful tool for validation. At the current design stage, the code assessment has to rely on code-to-code comparison, since no experimental data are available yet. A good agreement is found comparing ERANOS and MCNP5 results, on both "local" multiplication factor (k_∞) and axial power shapes, for the different scales involved in deterministic core calculations, including both cell and 3D analyses [89].

Concerning cell calculations, a FA model has been developed to represent the important heterogeneity effects when generating the multi-group homogenized XSs for successive core analyses; these are due to the combined space and energy dependent resonance self-shielding whose influence is very pronounced in a thermal spectrum reactor, as shown from the comparison between homogeneous and heterogeneous geometry models. A plausible behavior of ECCO results is observed when using appropriate calculation procedures and a good agreement with MCNP5 results is found using the same evaluation of the nuclear data libraries processed at the same temperatures. Concerning FA results, the comparison of MCNP5 and VARIANT shows good agreement in the calculated power shape; the differences are well below 5% in the regions of the power peak and are also influenced by the slightly different boundary conditions as well as different interpolation of the XSs among the available temperatures. For whole core analyses, the results of 3D calculations with VARIANT have been verified with sensitivity studies to the mesh size, the reflector model, the flux angular expansion order as well as with 2D calculations, for RZ geometry, using BISTRO which is based on different solution algorithms of the transport equation.

The developed calculation procedures for deterministic neutronic analyses of the HPLWR core have been verified and demonstrated to be suitable for the current feasibility studies. The effect of fuel temperature variations has been considered only for FA analyses underlining pronounced feedbacks which have to be represented when evaluating the core power distribution. For future core design studies, more extensive assessment will be necessary and accompanied by experimental analyses. In particular attention has to be given to the thermal scattering law of bound hydrogen in supercritical water, i.e. the $S(\alpha,\beta)$ thermal treatment.

The small geometrical and material changes introduced in the current FA with insulated boxes [51] when compared with the one with solid stainless steel [57] does not require to repeat the code-to-code comparison for the modified geometry.

5.1.2 TRACE improvements

The direct application of the system code TRACE to HPLWR thermal-hydraulic analyses is straightforward when using an external steam table in the IAPWS format, originally developed for RELAP5, but a careful analysis of the source code revealed that some of the used approximations are not adequate when applied to supercritical water causing lack of accuracy and convergence difficulties.

Some inconsistencies in the models used by TRACE when the code is applied to HPLWR core analysis have been identified and corrected [94]. The proposed improvements regard both water properties representation and heat transfer models; which are important to extend TRACE capabilities to analyze the thermal-hydraulic performance of the HPLWR core concept.

The code verification focused mainly on the heat transfer models modifying the original representation of cylindrical heat structures, which is not fully applicable to HPLWR analysis, ensuring single-phase representation of supercritical water and introducing two heat transfer correlations which have been specifically developed for supercritical water – Bishop et al. [8], Jackson and Hall [67] – even if for pipe rather than for bundle flow and only for heated conditions. These have been compared with two well established correlations: Dittus-Boelter [33] and Gnielinsky [49], which is used in the original TRACE version.

The studies performed showed pronounced sensitivity to the code modifications: the presented investigations are important in assessing the code capabilities and to ensure its applicability to HPLWR analyses.

5.1.3 MATRA applications

The extension of the sub-channel code MATRA to enable analyses of fuel bundle cooled with supercritical water has been achieved including temperature dependent lookup tables for the required properties. They are based on the IAPWS format.

The model developed by D.S. Rowe [127, 160], already included in the MATRA source code, has been used to successfully represent the effects of the wire-wrap and the available tuning factor has been adjusted to obtain a qualitative agreement with high fidelity CFD simulations available within the HPLWR EU-Project. Nonetheless additional efforts should be devoted to the qualification of the inter-channel mixing and of the wire effect on both mass and energy transfer.

5.2 Remarks on the developed multi-physics, multi-scale core analysis methodology

The initial qualification of the separate fields involved in the envisioned core analyses served as robust basis to develop the coupled multi-physics multi-scale simulation tool. The required level of detail, in which each individual fuel rod is resolved, has been achieved with a two-step approach in which first a consistent coupled reactor physics / thermal-hydraulics solution of the HPLWR core at fuel assembly resolution is obtained and, successively, the core is investigated at sub-channel resolution predicting local, i.e. pin-wise, clad and fuel temperature.

To tackle the coupled reactor physics and thermal-hydraulics analyses of the whole HPLWR core, two state-of-the-art computational codes, ERANOS and TRACE respectively, have been coupled through an iterative procedure in which they are run in series. The physics of the coupling have been represented through data exchange among the codes which do not have to be modified but are kept as independent: in the developed coupled system the communication among ERANOS and TRACE is achieved through the input/output files and is fully automatized by external processing functions, based on Perl scripts, which identify and exchange the data

required for the coupling, i.e. core power map, fuel temperatures as well as water temperatures and densities.

Initially, the coupled ERANOS/TRACE system has been successfully applied to a single fuel assembly analysis, for which various tests indicated the sensitivity and importance of the considered parameters. Based on this experience, a whole core was analyzed by the coupled system obtaining promising results and understanding the physical reasons of the interaction between the two fields. The qualification of the coupled system has been achieved mainly verifying the correctness of the data exchange among the codes and the consistency of the intermediate solutions. Based on the investigations performed with the coupled ERANOS/TRACE system [92], it is shown that a pronounced coupling exists between reactor physics and thermal-hydraulics of the HPLWR core: the neutron flux is strongly influenced by the water density distribution which, in turn, depends on the power map and hence on the neutron flux. In addition, the fuel temperature has appreciable feedbacks, which should not be neglected, on neutronic analyses and, consequently, on the core power map distributions.

The developed coupled system predicted how the core power map is redistributed according to the water density feedbacks and how power peaks are reduced by the fuel temperature variations. The developed pseudo 3D TRACE core model enabled to adjust the coolant mass flow rate among the various fuel assemblies to reduce the peak clad temperature, nonetheless additional optimization of the power - to - flow ratio is desirable. The coarse nodalization used for coupled calculations, based on homogenized fuel assembly geometry and equivalent channel representation, do not have the spatial resolution needed to predict local peak quantities which may differ substantially from the predicted averaged values because of spatial power gradient and abrupt changes of water properties with the heat up. For this reason the HPLWR core was investigated at sub-channel resolution extracting the boundary conditions form the available coupled solution.

Whereas the necessary thermal-hydraulic boundary conditions, namely inlet mass flow and temperature of each fuel assembly, are already available thanks to the developed pseudo 3D TRACE core model, the power distribution of each fuel assembly within the fuel rods require additional modeling. This task has been achieved applying a pin-power reconstruction technique which assumes that the resulting pin-power distribution can be obtained combing the effects of global flux gradients, predicted by the 3D core analyses, and of local heterogeneity of the fuel assembly. This technique has been implemented in an additional data processing tools which has been developed to collect and merge results obtained for the different spatial scales by different codes, ERANOS and MCNP5 respectively. The reconstructed pin-power, beside ensuring conservation of energy, provide a physically sound representation of both the local fuel assembly heterogeneity and the pronounced flux gradients which exist in the not yet optimized HPLWR core. Even though the qualification and quantification of the errors has not been performed, since it would require high fidelity core analyses, e.g. with MCNP5, the results are satisfactory for the present application.

A one-way coupling is used to to zoom in each fuel assembly extracting the operating conditions for the predicted steady state coupled solution. A dedicated processing script merges the pin-power distribution and the flow boundary conditions to generate input files for each fuel assembly which are used to predict with MATRA local temperature distributions for the coolant and structural materials [93]. Because of the small dimensions of the fuel assembly, and thanks to the good mixing offered by the wire-wraps, the fuel assembly wise peak - to - average ratios for coolant, clad and fuel temperature in each horizontal section are not very pronounced and the results obtained at sub-channel resolution confirm the trends of those predicted at fuel assembly level. Higher peak - to - average ratios of various quantities exist both in the axial direction and among the various fuel assemblies of each fuel cluster and would require a carefull optimization of the HPLWR core which can be performed with the developed analysis tool.

The multi-physics, multi-scale core analysis tool has been developed independently from

the stand-alone codes, hence, refinement of the separate models, which will not modify the input/output format, can be easily considered solving some of the discussed simplifications.

5.3 Conclusions

The results achieved confirm the necessity of the present multi-physics, multi-scale analysis of the HPLWR core. The proposed approach may be used as guideline for investigations of modified HPLWR designs as well as of different reactor concepts which exhibit pronounced coupling between reactor physics and thermal-hydraulics and require quantifications of local temperature distributions.

Despite the discussed simplifications, this approach represent a new quality in core analyses which is extremely important in suggesting science-based design improvements. The number of a priori assumptions which were involved in the preliminary design proposal [137] has been drastically reduced going towards a high fidelity core analysis. It is now possible to model all fuel rods and all the sub-channels within the HPLWR core individually and in full detail while taking into full consideration the pronounced coupling between reactor physics and thermal-hydraulics and the relevant 3D spatial effects due to both local heterogeneity of the fuel assembly and multi-pass core design. This is a major achievement as compared with the standard methodologies.

Appendix A

HPLWR core design studies based on the obtained coupled solution

A.1 Disclaimer

While developing the presented computational tool, the coupled ERANOS/TRACE system has been used to support and advance the design of the HPLWR core. During these studies slightly different operating conditions were assumed: the thermal power of the reactor core was 2400 MWth and the RPV inlet flow rate was 1160 kg/s. Having a higher total power and a lower mass flow rate, the resulting coolant outlet temperature was slightly higher than the 770 K achieved with the current design proposal.

The initial FA design proposed by Hofmeister et al. [57] was suitable for a preliminary supercritical water cooled reactor concept, as defined by Vogt et al. [153], in which the moderator/gap water heat up by heat exchange across the FA walls with the coolant was not very significant because of lower operating temperatures. With the current 3 pass core design proposal by Schulenberg et al. [137] higher coolant temperature can be achieved and the moderator/gap water heat up is more pronounced than in the initial reactor concept for which the FA has been designed. This results in reduced neutron moderation and may originate flow reversals driven by buoyancy effects which would interfere with the downward flow direction of moderator/gap water. A thermal insulation of the FA walls is hence necessary, as discussed in section A.2.

For the coupled solution, the in-core power distribution, obtained for the not yet optimized core loading strategy, satisfies partially the required power level in the three core regions (EVA, SH1 and SH2) but exhibits pronounced peaks and flux gradients. A well designed core should have reduced peak - to - average ratios of all sensible quantities including the in-core power map. This kind of optimization requires several parametric studies to account for the pronounced coupling between RP and TH but should also consider the changes of core properties which occur during the burn-up. For this reason, a 3D burn-up investigation of the coupled solution of the HPLWR core has been considered in section A.3.

Discussion on how the several pieces goes together from a design perspective is given in section A.4 together with suggestions for future works.

A.2 Thermal insulation of the fuel assembly walls

A.2.1 Insulated fuel assembly design

To reduce the heat up of moderator/gap water it is reasonable to increase the thermal resistance of both moderator and FA boxes changing their constituent material. With respect to the original

FA design which massive stainless steel [57], Al_2O_3 has been selected as insulating material thanks to its lower thermal conductivity and it behavior in supercritical water is currently studied within the Working Package 4 of the HPLWR EU-Project [54]. Since this ceramic compound does not provide the necessary mechanical resistance, it has to be enclosed in an honey-comb structure delimited by two stainless steel liners [51]. Venting holes in the liners are envisioned to avoid to design a sandwich structure capable to withstand the 25 MPa operative pressure. Through these holes, supercritical water penetrates in the ceramic structure filling the void fraction resulting in an increase of thermal conductivity of the insulating material.

An equivalent thermal conductivity of the heterogeneous material structure has been calculated for several temperatures and has been used to specify a new material in TRACE. Tabulated values are summarized in Table A.1. For intermediate temperatures, TRACE performs a linear interpolation. This equivalent thermal conductivity is a weighted function of the ones of stainless steel, water and Al_2O_3 explaining its strange behavior with temperature which is due to the different temperature dependence of the three materials: the conductivity of steel increases linearly with temperature, the one of water at 25 MPa is slightly decreasing with temperature but has a pronounced reduction in the vicinity of the pseudo-critical temperature (657 K), the one of Al_2O_3 is here assumed to be constant.

Table A.1: Equivalent thermal conductivity $\lambda_{eq.}$(T) [W/mK] of insulated boxes

T [K]	293	550	600	650	700	750	800	900
Mod. box	3.1335	3.5228	3.5586	3.5743	3.5166	3.5816	3.6543	3.8052
FA Box	2.8817	3.2337	3.2649	3.2774	3.2216	3.2803	3.3462	3.4833

A.2.2 Sensitivity studies

This section investigates the sensitivity of the coupled RP/TH whole core analyses to the introduction of the thermal insulation in the box walls without varying neither the thermal power nor the RPV inlet flow rate but permitting the modification of subdivision of the RPV inlet flow rate between moderator water and downcomer water which was initially fixed to 25% and 75% as in previous studies [153].

The sensitivity of moderator/gap water heat up is considered first: the highest and lowest power density fuel clusters of each core region, whose position is clearly marked in Figure 2.16 on page 32, are selected to inspect the obtained results.

Moderator temperature

Moderator water flows downward from the top to the bottom of all three core regions and is heated up only by the temperature difference with respect to the coolant since the direct heat up due to neutrons and gamma rays has not yet been modeled. Figure A.1 shows the sensitivity of moderator water temperature distribution to the FA design and to the moderator water flow rate [96, 97].

At first, only the boxes material has been changed, keeping the same moderator - to - RPV inlet water flow rate ratio. The results show only a limited sensitivity of the moderator water temperature variation to the thermal insulation of the boxes, as can be seen comparing Figure A.1(a) and A.1(b). To understand the physical reason of that small influence, the total heat transfer resistances between coolant and moderator has been split in 3 parts: 1) coolant to wall 2) the wall itself 3) wall to moderator. Because of the low liquid velocity of the moderator, the wall to moderator HTC is small[1] (HTC $\in [1E3; 3E3]$ W/m^2/K) making this the biggest of the

[1]The moderator is substantially heated up because of its low velocity even if the HTC is small.

three thermal resistances and, as a consequence, the increase of the heat transfer resistance in the wall, which is the smallest one, is not effective in reducing the heat transferred.

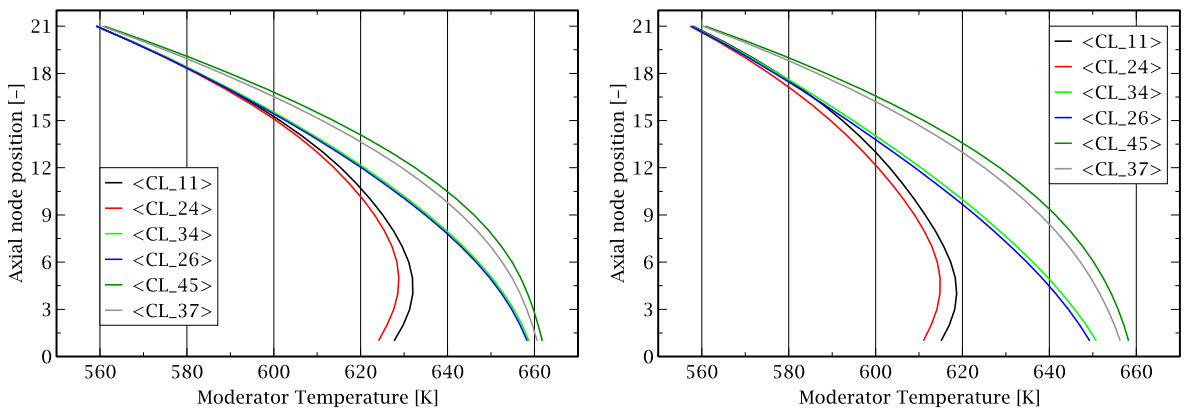

(a) Solid SS boxes – moderator water flow rate: **25%** of RPV inlet water

(b) Insulated boxes – moderator water flow rate: **25%** of RPV inlet water

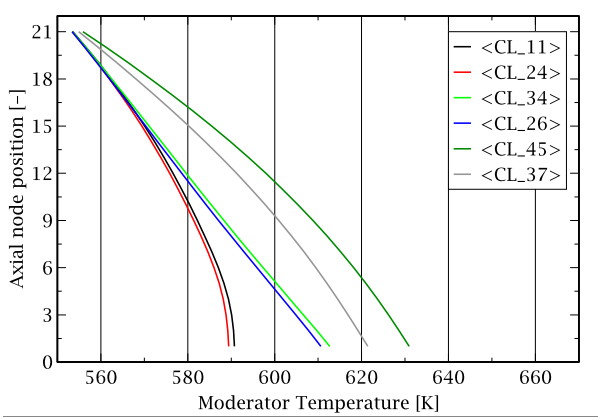

(c) Insulated boxes – moderator water flow rate: **75%** of RPV inlet water

Figure A.1: Sensitivity of the moderator temperature variation in selected core clusters to different design proposals

The increase of the wall thermal resistance becomes important when changing the moderator flow rate: the insulated design allows to increase the flow velocity of the moderator without increasing the global HTC resulting in lower moderator water exit temperature. As initial guess, the total moderator flow rate is assumed to be 75% of RPV inlet flow rate, which results in the same moderator - to - coolant flow rate ratio as that of the single pass core design [152]. This change has proven to be effective in reaching the desired goal as can be seen from the comparison of Figure A.1(a) and A.1(c): the moderator temperature is reduced below the pseudo-critical one (657 K at 25MPa) avoiding the pronounced drop in its density and hence ensuring a more uniform neutron moderation, Table A.2.

Since the moderator/gap water heat up shows only limited sensitivity to the thermal insulation of the FA boxes when its flow rate is not changed, the comparison for the other TH parameters is restricted to two cases:

- FA with solid stainless steel boxes and a total moderator water flow rate equal to 25% of RPV inlet flow rate;
- FA with insulated boxes and a total moderator water flow rate equal to 75% of RPV inlet flow rate.

Table A.2: Moderator water maximum temperature [K]

flow rate†	solid SS boxes **25%**	insulated boxes **75%**
EVA	$\lesssim$ 640 K	$\simeq$ 590 K
SH1	$\simeq$ 660 K	$\simeq$ 610 K
SH2	$\simeq$ 660 K	$\simeq$ 630 K

†given as fraction of RPV inlet flow rate.

Power generation

The pronounced changes in the moderator temperature variation do not result in important feedbacks on the coupled RP/TH solution: the variation in power distribution is not very pronounced as shown in Table A.3 and Figure A.2. The higher moderator density is more important in SHs, whose power fraction is slightly increased reducing the amount of energy generated in EVA.

Table A.3: Region wise power generation

$\left(\frac{\text{Power(region)}}{\text{Power total}}\right)$	EVA	SH1	SH2
solid SS boxes	66%	24%	10%
insulated boxes	63%	26%	11%

The core power map and axial power shape are plotted in Figure A.2 and A.3, respectively. A pronounced bottom peak is found also when having a less pronounced axial reduction of moderator density underlining the sensitivity of the power shape to the coolant density variation and the importance of the spatial coupling among adjacent regions of this rather small core[2].

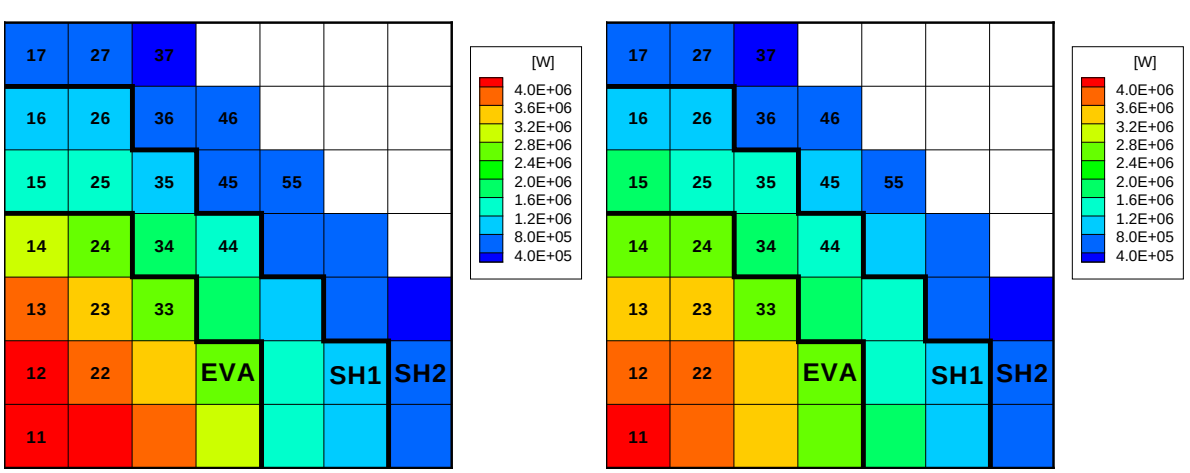

(a) Solid SS boxes – moderator water flow rate: **25%** of RPV inlet water

(b) Insulated boxes – moderator water flow rate: **75%** of RPV inlet water

Figure A.2: Sensitivity of the power map (in the average FA of each CL)

The power generation, obtained as result of whole core coupled analysis, is not substantially modified by the differences in moderator water density, hence only small changes in the other thermal-hydraulic parameters are expected.

[2]The outer diameter of the steel reflector is 3.97 m.

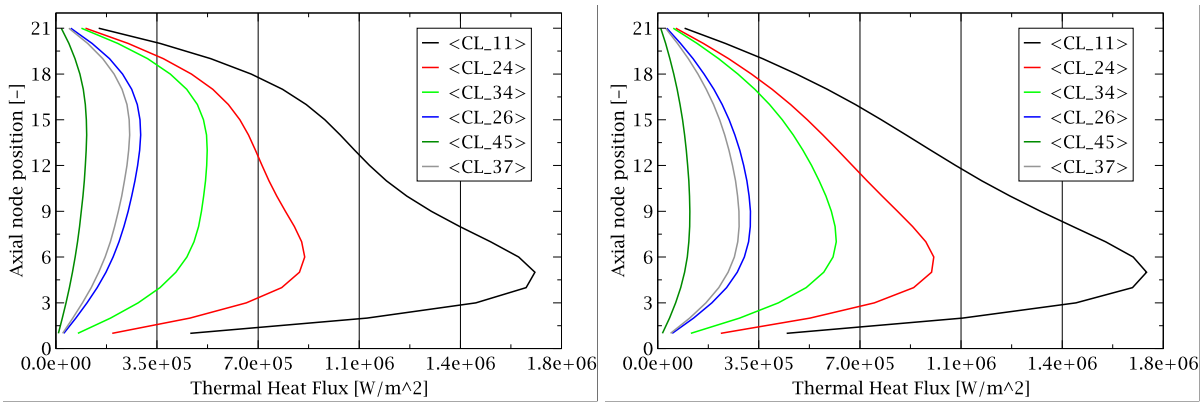

(a) Solid SS boxes – moderator water flow rate: **25%** of RPV inlet water

(b) Insulated boxes – moderator water flow rate: **75%** of RPV inlet water

Figure A.3: Sensitivity of the axial power shape

Coolant temperature

Since moderator water is mixed at the core bottom with the remaining fraction of RPV inlet water, which flows through the downcomer, to re-establish the coolant flow rate, the change in its outlet temperature is supposed to affect the coolant inlet temperature. This effect is found to be compensated by the change in the moderator flow rate and, as a result, the coolant inlet temperature is almost unchanged, as shown in Figure A.4. Once the coolant inlet temperature has been determined, two parameters determine the coolant temperature axial variation: the power generated by fissions and heat transfer to moderator water. The first parameter is almost not changed by the new design, according to the results shown in the previous subsection. Also the total heat transfer to the moderator remains almost the same since rather small changes in the coolant temperature distribution occurs, as shown in Figure A.4. Apparently the heat flux from the coolant to the moderator has not been reduced as much as the specific energy transferred to the moderator, since the moderator flow rate is three times higher than in the original proposal.

The region-wise power relocation required an additional iteration loop in order to dimension the inlet orifices to achieve uniform coolant outlet temperature in the same core regions. This criterion provides a quite straightforward definition of the coolant mass flow but, being based on average values rather than on peak one, should be refined. The definition of inlet orifices is done

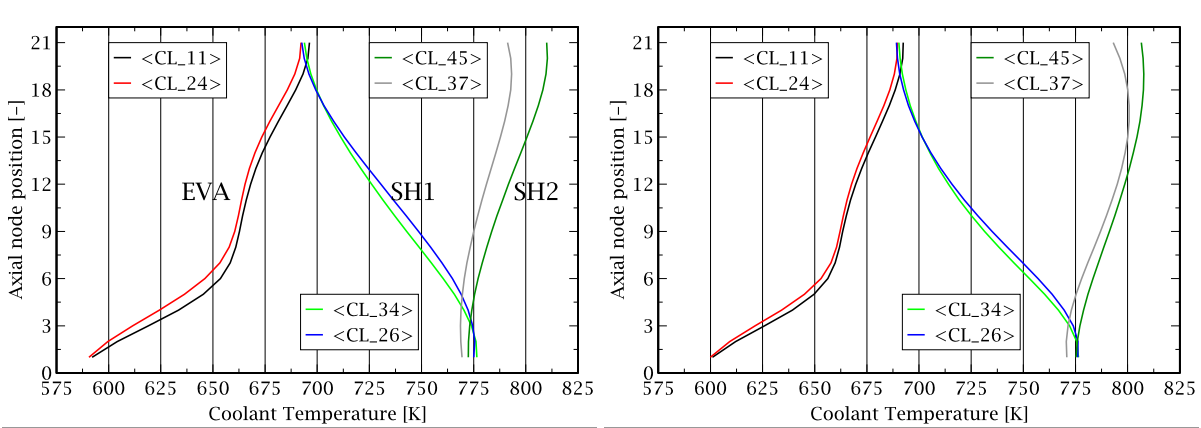

(a) Solid SS boxes – moderator water flow rate: **25%** of RPV inlet water

(b) Insulated boxes – moderator water flow rate: **75%** of RPV inlet water

Figure A.4: Sensitivity of the coolant temperature variation in selected core clusters

using kfactors at the entrance of the coolant pipes. These are dimensioned on the following basis: higher kfactor results in higher inlet pressure drop and hence in a reduction of the coolant flow rate and the corresponding rise in its outlet temperature. This procedure is not exact for HPLWR application because the heat flux from coolant to moderator water is influenced by the coolant flow rate and hence the change in its flow rate will modify the energy transfer from coolant to moderator. Nonetheless this effect is found to be dominated by the heat transfer from the fuel rod to the coolant which, for steady state conditions, results in higher coolant temperature when the flow rate is reduced. The current kfactor map and the resulting coolant mass flow, in the equivalent average FA channel of each fuel cluster, is given in Figure A.5 for the insulated boxes design with a moderator flow rate equal to 75% of RPV inlet flow rate.

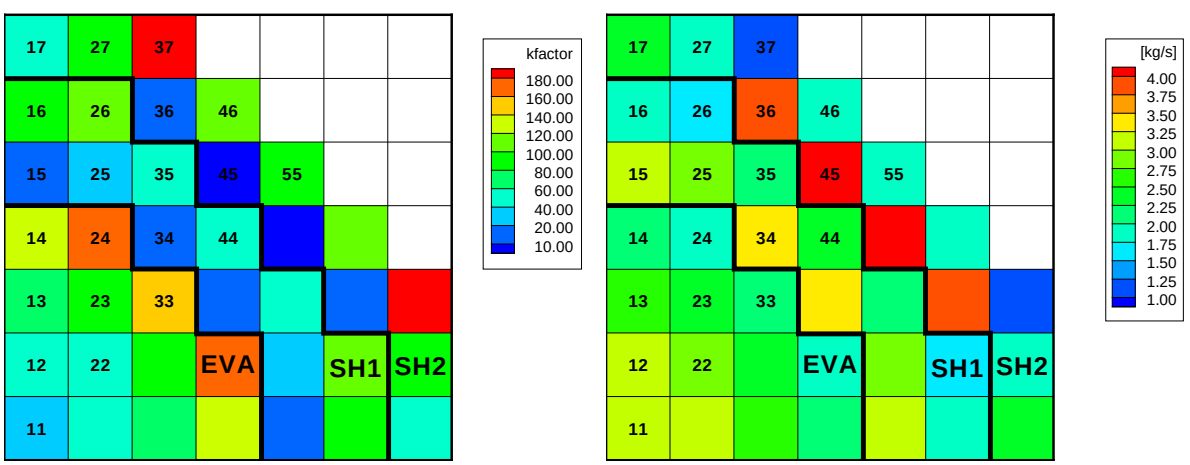

(a) Inlet orifices (b) mass flow rate

Figure A.5: Coolant flow parameters using insulated FA boxes and a moderator flow rate equal to 75% of RPV inlet flow rate

Fuel and clad temperature

It is well known that the fuel pin centerline temperature is influenced mainly by the fission energy deposition whereas the clad temperature follows more closely the temperature variation of the coolant. Since both driving parameters are not changed substantially by the new insulated box design, as shown in previous sections, these temperature will not be substantially modified, they are reported in Figure A.6 and A.7.

Since the FA design with insulated boxes exhibits a slightly more pronounced bottom power peak in CL 11, both fuel and clad temperatures of this CL are increased with respect to the values predicted for the FA design with solid SS boxes. The same happens also for CL 24 and in SH1 where both structural material temperatures are raised by the higher power level in the considered CLs 34 and 26. In SH2, the flatter axial power shape results in a change of the axial position where the clad peak temperature occurs but its value is almost unchanged.

Multiplication factor

The new FA design has two main advantages from point of view of the neutron economy: reduced mass of structural material and higher moderator water density. Since the first one results in a reduction of parasitic absorptions while the second one in a better neutron thermalization, both of them increase the reactivity of the core, as shown in Table A.4: k_{eff} of whole core is increased of $\simeq$ 8600 pcm for the new FA design.

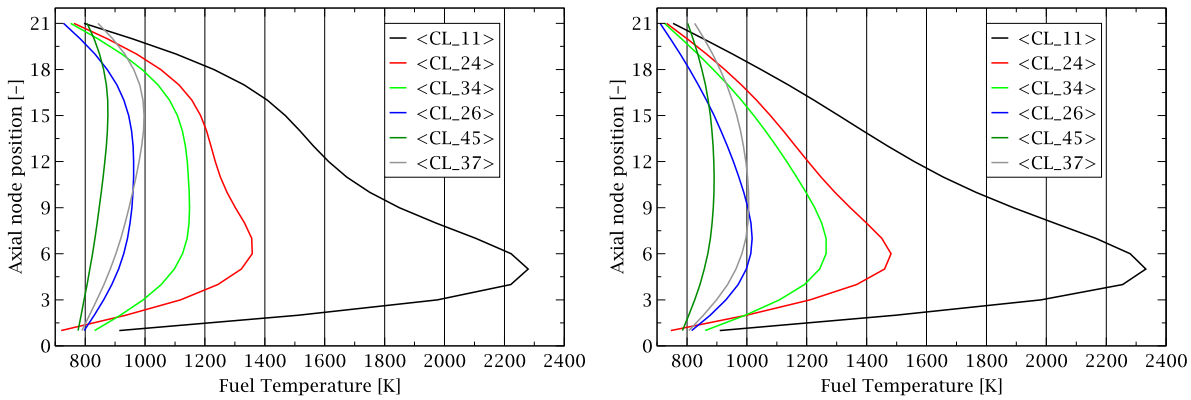

(a) Solid SS boxes – moderator water flow rate: **25%** of RPV inlet water

(b) Insulated boxes – moderator water flow rate: **75%** of RPV inlet water

Figure A.6: Sensitivity of the fuel pin centerline temperature

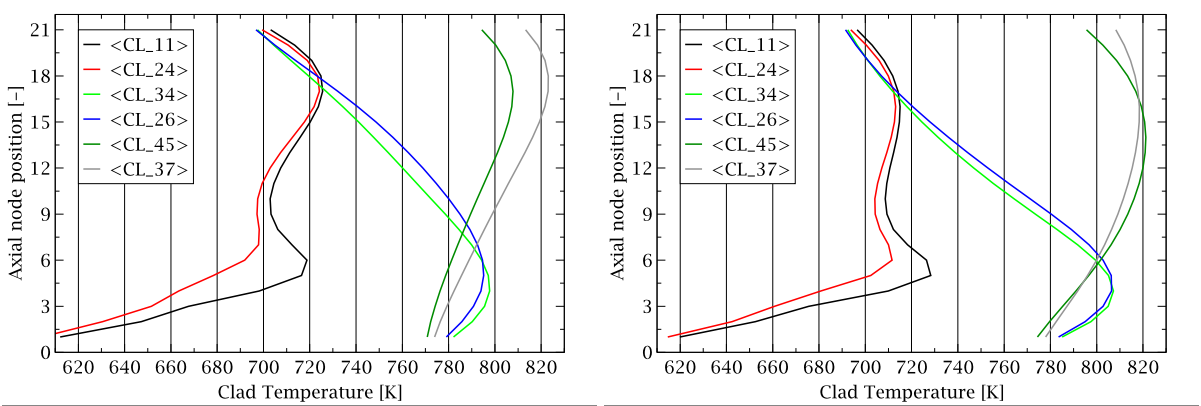

(a) Solid SS boxes – moderator water flow rate: **25%** of RPV inlet water

(b) Insulated boxes – moderator water flow rate: **75%** of RPV inlet water

Figure A.7: Sensitivity of the clad temperature

More insight into the effect of the insulated boxes is obtained by considering the local multiplication factor, i.e. k_∞, obtained for each 2D cell calculation[3]. k_∞ is plotted as a function of the axial position in Figure A.8 for the highest and lowest power density clusters. The pronounced k_∞ rise is due to both points mentioned before whereas the attenuation of k_∞ variations in the axial direction is caused by the reduced axial variation of moderator density which makes the axial distribution of all quantities in the FA more uniform. In addition, the local multiplication factor, when using the new insulated boxes design, does not drop below unity (sub-critical condition) when the moderator density reaches its minimum as it happened for the solid stainless steel boxes.

It is important to mention that the reduction of the SS mass in the insulated FA design results in a lower absorption XS which, modifying the neutron balance, changes the neutron leakage probability not only from the core periphery but also among the various FAs and core regions (EVA, SH1 and SH2). With the insulated FA design there is a more pronounced spatial coupling since neutrons may travel easier from the center to the periphery of the core[4]. This may help in explaining why, despite the pronounced changes in the axial variation of the local multiplication factor (k_∞) in CL 37 (located in SH2), the axial power shape is almost unchanged.

[3]These are performed when calculating the multi-group macroscopic self-shielded XSs.

[4]The effect of the reduced absorption XS with the insulated FA design seems to enhance the 3D spatial coupling even if, because of the better thermalized spectrum, the neutron main free path becomes shorter.

Table A.4: Sensitivity of k_{eff} to the boxes design

	solid SS boxes	insulated boxes
k_{eff}	1.05324	1.12109

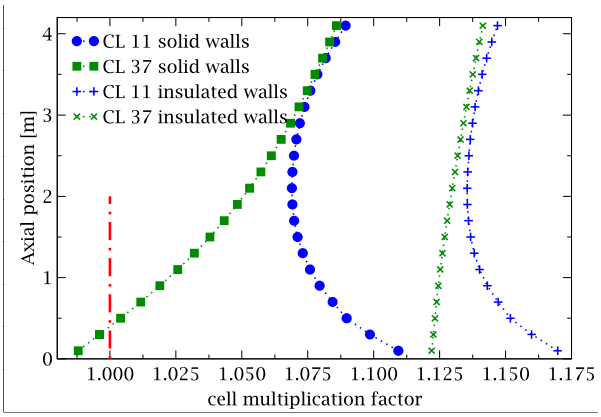

Figure A.8: k_∞ of the 2D fuel assembly calculation for the 21 axial zones of selected core clusters

A.2.3 Effectivity of the insulated fuel assembly design

The selected insulating material for the new fuel assembly design, together with variations of the moderator - to - coolant flow ratio, is effective in reducing the moderator temperature rise with respect to the original fuel assembly design with massive stainless steel boxes. The increase in the moderator water density within the core causes a redistribution of the power map both in axial and radial direction which can be predicted with the usage of the coupled RP/TH system. A compensation between temperature reduction and mass flow rate increase of moderator water occurs and results in a similar core inlet temperature of the coolant: the moderator water is collected after one pass through the core and mixed with the remaining part of the reactor pressure vessel inlet water, which flows in the downcomer, to reconstitute the coolant flow rate. The higher density of the moderator, together with the reduction of the total stainless steel mass in the new FA proposal, contributes to an appreciable increase of the reactivity of the HPLWR core and, hence, may lead to a higher flexibility of core loading strategies and reactivity controls finalized to achieve an higher average discharge burn-up.

It may be worth to underline here that the considered TRACE model, being unable to predict the moderator/gap water mass flow redistribution among the parallel flow paths and having a 1D representation of the gap water region can not be used to investigate possible flow reversals which would require a different approach, as the one showed by Kunik [78].

A.3 3D burn-up investigations of the coupled solution

A.3.1 Necessity of 3D burn-up investigations

The pronounced water density variation, which takes place inside the core where the coolant is heated up from 550 K to 800 K, is supposed to generate pronounced 3D effects during reactor operation because the different core regions have different flux amplitude and neutron spectrum, as shown in Figure 2.23 on page 37. In addition, the pronounced power peaks result in different local burn-up of the various regions which will cause power redistribution during reactor operation. Open questions are how k_{eff} and the power map will change during the burn-up and require a 3D, multi-zone, burn-up analysis of the core.

This goal is achieved using the ERANOS system [131], which includes the necessary modules and calculation procedure to perform this kind of analysis.

The starting condition is the one just presented and obtained with coupled RP/TH core analysis [96]. At present, it includes neither fuel enrichment optimization nor reactivity control systems, i.e. control rods or burnable poisons. The uranium dioxide enrichment is uniform in both axial and radial direction, the ^{235}U contents of the 40 fuel rods in each FA is 5wt% for 36 rods and 4wt% for the remaining four corner pins as described in Figure 4.28 on page 85.

A.3.2 Proposed approach for burn-up analysis

The CL-wise core nodalization used in the coupled system is also adopted for multi-zone burn-up analysis: there are 462 different zones in one eighth of the core, each with a different material composition, 21 in axial direction and 22 CLs in the horizontal plane. A burn-up period of 200 days ($\simeq$6400 MWd/tHM at nominal power[5]) is considered here and has been divided into two different time steps, as described in Figure A.9:

1. an inner time step at which macroscopic XSs and the average normalized flux are calculated according to the change in fuel isotopic composition;

2. an outer time step at which whole core flux calculations are performed to evaluate the changes of the region-wise neutron flux distribution.

The inner time step is important to achieve the expected burn-up: as it will be shown, the depletion of the fissile content in the fuel requires to increase the neutron flux amplitude to maintain the operating power. It is desirable to minimize the number of flux calculations to reduce the necessary CPU time but the length of the outer time step has to be short enough to avoid unphysical power shape oscillations, as underlined by Reiss et al. [119] with a different computational approach: in the given outer time step, the power peak regions, having a higher neutron flux amplitude, experience a higher local burn-up than low power regions which may result in an overprediction of the fuel burning and of the reactivity reduction causing, at the next time step, a tilt of the flux and power. For this reason, sensitivity studies were performed.

To drastically reduce the CPU time required, the 40 groups self-shielded microscopic XSs are not recalculated during the burn-up analysis and the macroscopic XSs are modified only by the changes in the atomic densities of the considered isotopes. This simplifying assumption neglects the effects of spectrum variations due to isotopic changes of the fuel and is generally accepted for these kind of analyses, nonetheless this effect may be investigated in future analyses. Possible dynamic effects, e.g. Xenon oscillations, as well as any modification of the TH feedbacks used at Beginning Of Life (BOL) have not been considered. The main outcomes of these assumptions, which result in a coupled neutronic/burn-up analysis, will be discussed together with the presented results.

Typical LWRs evolution chains for actinides and fission products have been selected in ERANOS calculations. The considered isotopes are listed here:

Actinides ^{234}U ^{235}U ^{236}U ^{238}U ^{237}Np ^{239}Np ^{238}Pu ^{239}Pu ^{240}Pu ^{241}Pu ^{242}Pu ^{243}Pu ^{244}Pu ^{241}Am ^{242g}Am ^{242m}Am ^{243}Am ^{242}Cm ^{243}Cm ^{244}Cm ^{245}Cm ^{246}Cm ^{247}Cm ^{248}Cm,

Fission products ^{87}Rb ^{91}Zr ^{92}Zr ^{93}Zr ^{94}Zr ^{95}Zr ^{96}Zr ^{95}Nb ^{95}Mo ^{97}Mo ^{98}Mo ^{99}Mo ^{100}Mo ^{99}Tc ^{101}Ru ^{102}Ru ^{103}Ru ^{104}Ru ^{109}Ag ^{127}I ^{131}I ^{129}I ^{133}Cs ^{134}Cs ^{135}Cs ^{136}Cs ^{137}Cs ^{138}Ba ^{143}Nd ^{144}Nd ^{145}Nd ^{146}Nd ^{147}Nd ^{147}Sm ^{149}Sm ^{150}Sm ^{151}Sm ^{152}Sm ^{154}Sm ^{150}Nd ^{153}Eu ^{154}Eu ^{155}Eu ^{86}Sr ^{88}Sr ^{89}Sr ^{90}Sr ^{121}Sb ^{125}Sb, no lumped fission products have been used.

[5] The core average burn-up is not very representative for the considered pronounced power peaks.

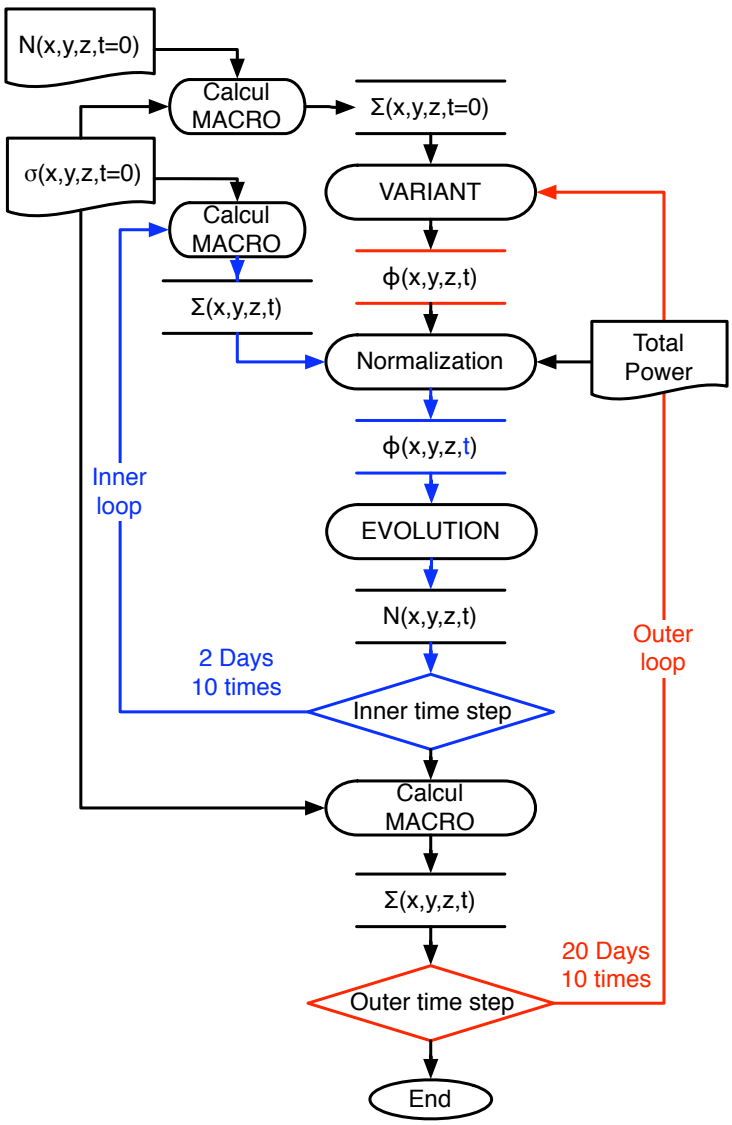

Figure A.9: ERANOS calculation procedure for bun-up analysis

A.3.3 Selected results of burn-up analysis

The usage of a multi-zone 3D burn-up tool allows to estimate how the power map is redistributed during reactor operation, taking advantage of the developed 3D visualization tool.

Figure A.10 shows the spatial distribution of the power density in the HPLWR core during the first two months of operation. The power density at BOL is not homogeneous because of the combined effects of neutron leakage and TH feedbacks, as discussed in the previous sections and shown in Figure A.10(a): the core central regions have a higher power level than the peripheral ones. As a consequence, being the power generation rate roughly proportional to the flux amplitude[6], the various core regions will experience different burn-up levels and the central regions will burn faster than the peripheral ones. The power peak located in the lower third of the central core region, caused by the TH feedbacks, identify the region of higher flux amplitude which will experience a higher burn-up. Because of the well thermalized neutron spectrum in EVA, in this region the reactivity is reduced by the fuel burning and, to maintain the 2400 MWth thermal power of the whole core, a pronounced power relocation occurs, rising power level of the peripheral regions. This leads, after few outer steps, to an almost flat axial power distribution,

[6]Since the fission XSs are region dependent because of the TH feedbacks, the power - to - flux ratio is different in the 462 considered zones.

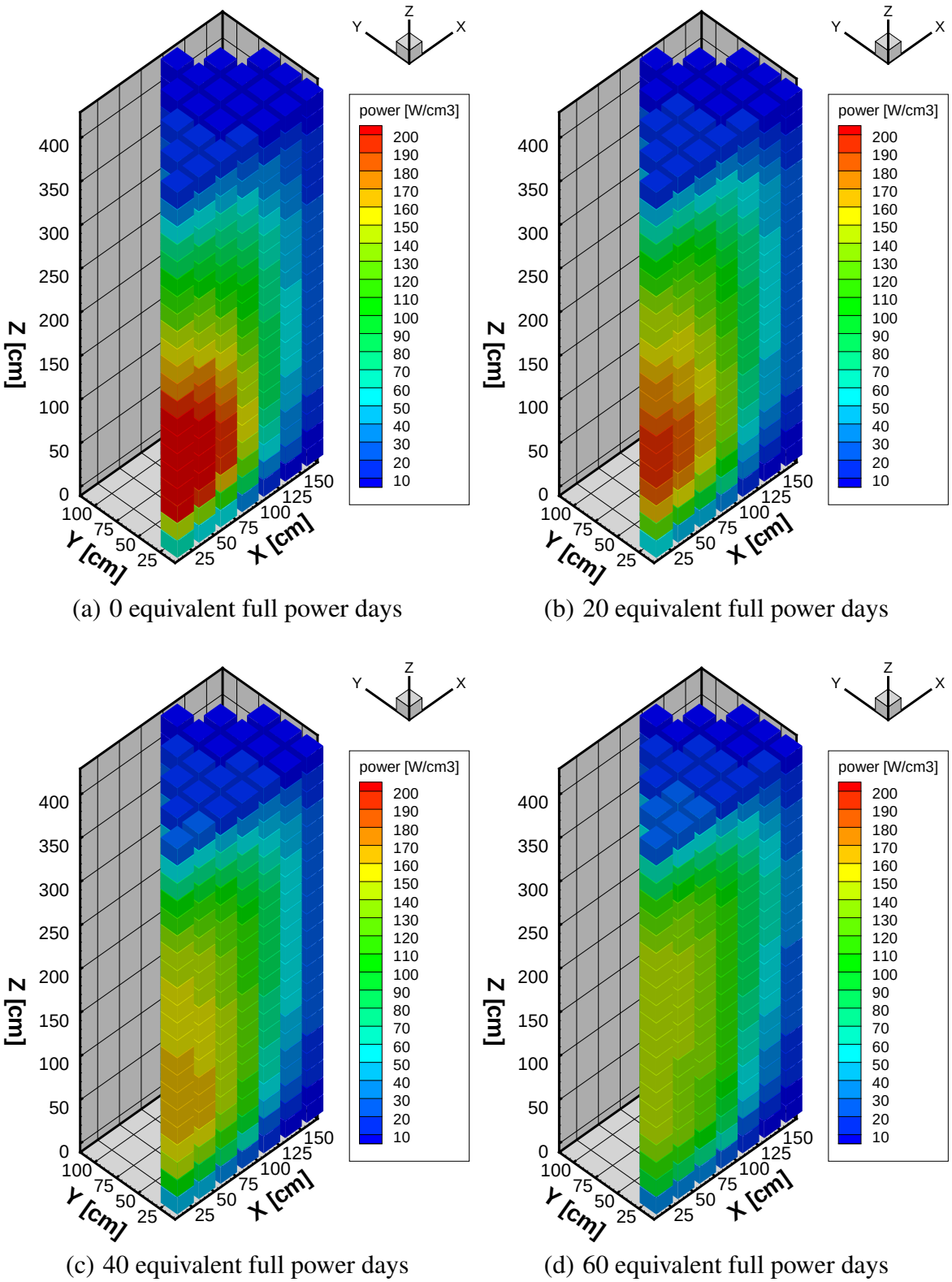

(a) 0 equivalent full power days

(b) 20 equivalent full power days

(c) 40 equivalent full power days

(d) 60 equivalent full power days

Figure A.10: Power density changes with burn-up (I)

as shown also later in Figure A.13. The selected 20 days outer time step has been chosen on the basis of several tests, e.g. big oscillations of the axial power shape which presents tilts between bottom and top peak were found using a step of 100 days.

The performed burn-up analysis, which does not account for modifications of the TH feedbacks during the investigated reactor operation time, shows pronounced power relocations which lead to a rather homogeneous distribution already after 60 equivalent full power days, as shown

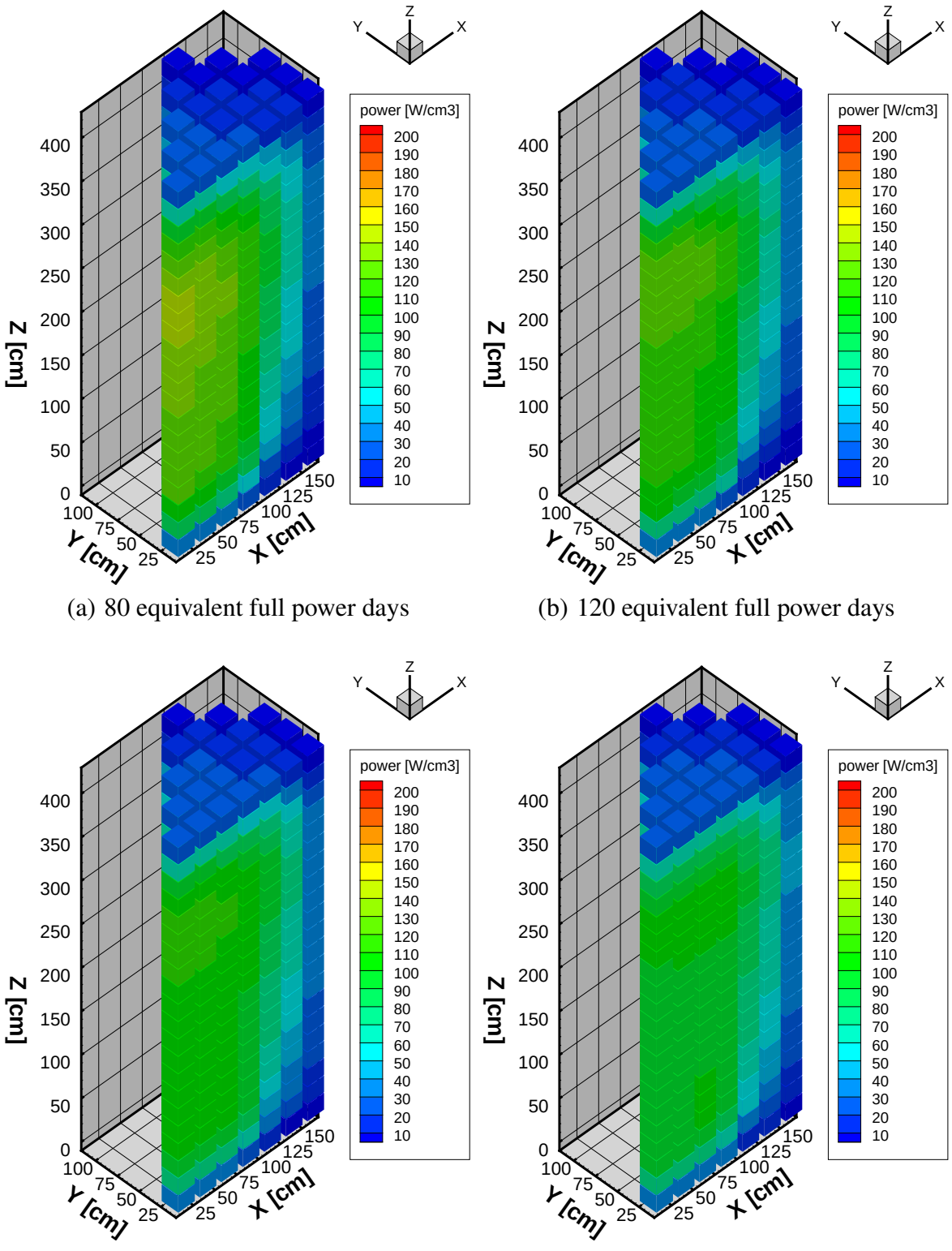

(a) 80 equivalent full power days

(b) 120 equivalent full power days

(c) 160 equivalent full power days

(d) 200 equivalent full power days

Figure A.11: Power density changes with burn-up (II)

in Figure A.11. It is quite clear that the power map after few outer steps is no more consistent with the TH data which characterize the associated 40 groups, self-shielded microscopic XSs used for these neutronic calculations. Therefore additional coupled RP/TH calculations would be necessary.

The total power generated in the average FA of each CL is plotted in Figure A.12 at the first and last time step to provide a graphical representation of the power redistribution within the 3

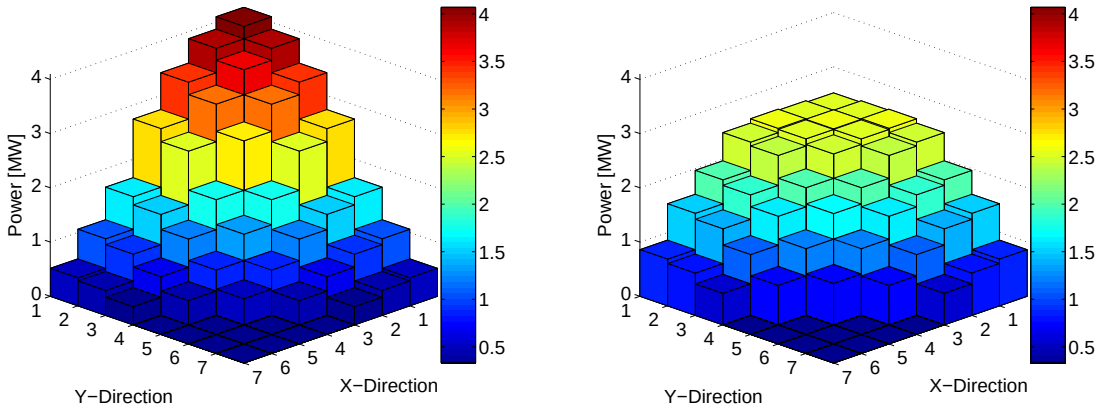

(a) 0 days (b) 200 days

Figure A.12: Quarter core power map changes with burn-up (in the average FA of each CL)

Table A.5: Changes of the region-wise power percentage with burn-up

	equivalent full power days	
	0	200
EVA	63%	49%
SH1	26%	34%
SH2	11%	17%

core regions described in Table A.5.

For the highest and lowest power density clusters of the fresh core analysis, the evolution of the axial power shapes is considered in Figure A.13. The highest power density cluster is the one located at the center of the core and hence it can be considered to be one of the most important in determining the whole core power map because of the spatial coupling among the various FAs. The strong space dependence in the flux amplitude, amplified by TH feedbacks, results in different fuel burning at the various axial zones. In particular the pronounced bottom peak in the axial power shape at BOL can not be maintained: in this part of the core the quick burning of ^{235}U is not compensated by the conversion of ^{238}U, and hence the higher neutron fluence reduces progressively the reactivity of these regions causing axial (and radial) power relocation as shown in Figure A.13(a). For the selected periphery cluster, the understanding of

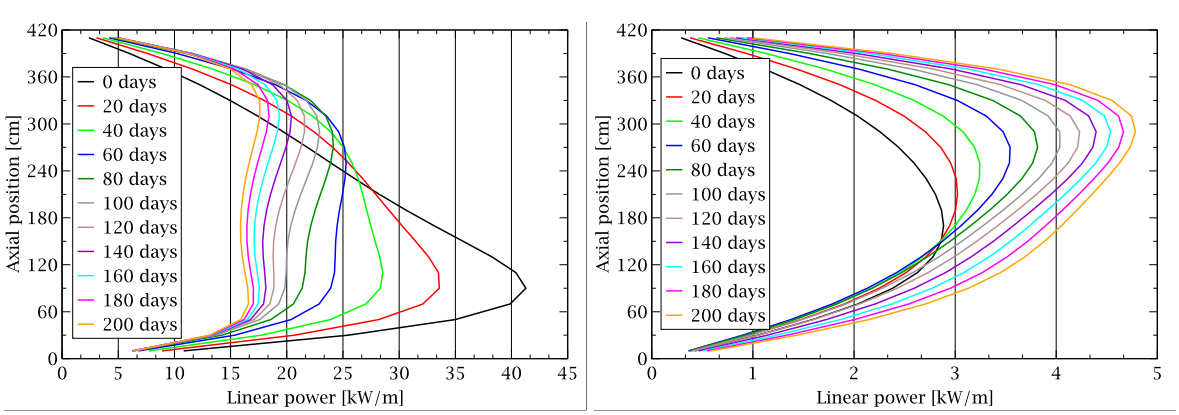

(a) Highest power density cluster (CL 11) (b) Lowest power density cluster (CL 37)

Figure A.13: Axial power shape changes with burn-up in selected core clusters

the power shape evolution is more complex: its value at BOL is strongly influenced by the radial neutron leakage from the center of the core which interacts with the axial reactivity distribution, previously showed in Figure A.8, determining the power shape. When the bottom peak in the axial power shape of the central cluster disappears, the peaking of the neutron flux in the lower part is substantially reduced and, hence, the power generation is shifted towards the top because of the BOL TH feedbacks: in the upper part the high density of moderator water, which is flowing downward, is the dominant contribution to neutron thermalization and, hence, the upper regions have higher reactivity than the lower ones.

The evolution of the two most important fissile isotopes for the HPLWR core, i.e. ^{235}U and ^{239}Pu , is considered as a function of the burn-up in Figure A.14 to understand the changes in the axial power shape. Different axial zones of the highest and lowest power clusters are considered, being zone 1 the bottom and 21 the top of the active length. The pronounced difference in the evolution of these isotopes for the two selected clusters is mainly due to the difference, of almost one order of magnitude, in the neutron fluence. In addition, the various axial zones of the same cluster have different isotopes evolution, as expected by the changes found in the axial power shape.

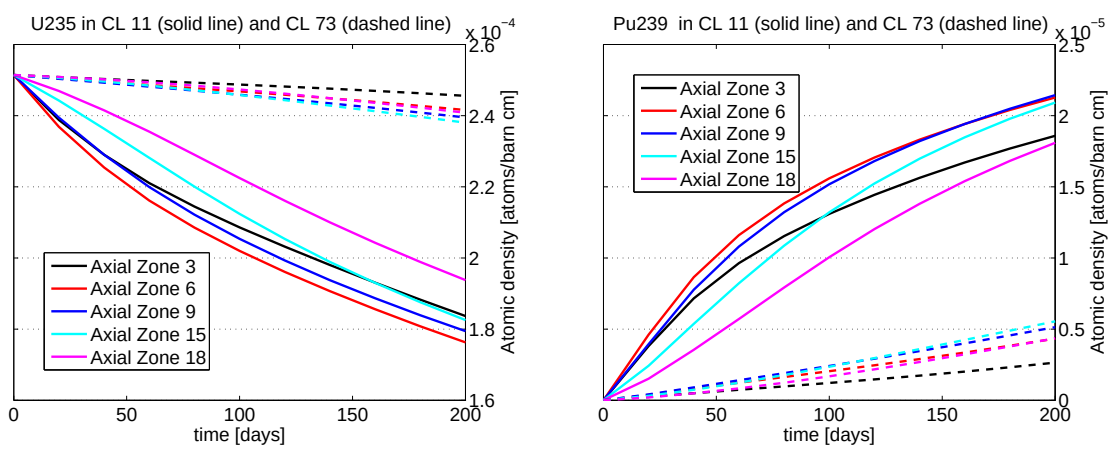

(a) ^{235}U (b) ^{239}Pu

Figure A.14: Fissile isotopes evolution in the highest (solid line) and lowest (dashed line) power density clusters

Besides the local effect of fuel isotopic changes on the power distribution, also the variation of the core k_{eff} is important and will be considered next. Because of its innovative design, the HPLWR 3 pass core has both thermal and epi-thermal regions and hence it is interesting to analyze which is the combined effect of the burn-up on k_{eff}. Its value at different time steps is given in Table A.6 and shows a quite pronounced reactivity reduction. This will hence require compensation to maintain the reactor in critical condition which can be achieved both using burnable poisons and control rods movement; also fuel shuffling can play an important role when considering longer burn-up intervals and reloading operations.

Table A.6: Reactivity variation with burn-up

days	0	20	40	60	80	100	...	180	200
MWd/tHM	0	639	1278	1918	2557	3196	...	5753	6392
$\Delta\rho$ [pcm]	0	−326	−601	−952	−1344	−1759	...	−3467	−3887

A.3.4 Lessons learned

A reasonable approach for 3D burn-up analysis of the HPLWR core has been presented showing results which are important in understanding the behavior of the HPLWR core during operation and fuel burn-up [90].

The axial power shape is one of the parameters which determine the maximum length of the outer time step used for core flux calculation. The flux amplitude in each region is kept constant during the outer time step, hence, if this time step is too long, there will be an excessive burning of the power peak regions and an underestimation of the burning of low power density regions; since the burn-up reduces the reactivity of the zones, when the time step is too long, the negative reactivity introduced in the power peak region is overestimated causing the flipping or tilting of the power peaks to the regions where the negative reactivity insertion has been underestimated. Oscillating behavior of the power peaks among lower and upper regions is clearly not physical and can be avoided by selecting a short enough time step for whole core flux calculations: the chosen value of 20 days fulfills this requirement and the power shape varies smoothly from the initial, pronounced bottom peak to the final, flatter shape.

The effect of the burn-up on both the core power map and on the axial power shape is very pronounced: because of the initial strong space dependence in the power distribution together with the differences in microscopic XSs originated by the TH feedbacks, the isotopic evolution of each core zone is different and hence the power distribution changes during burn-up. This would result in a variation of the TH feedbacks which can be predicted only by introducing coupled RP/TH analyses during the burn-up intervals with an additional time step. For the current status of the coupled procedure, this additional requirement is extremely time consuming and hence has not yet been taken into consideration.

The conversion of fertile material is not sufficient to compensate the fissile burning and the accumulation of fission products causing a monotonic reduction of k_{eff} with the burn-up and requiring, besides the introduction of burnable poisons to compensate for the initial excess reactivity, to account for control rods movements in order to produce accurate results. The control rods movement introduces further modifications of the power distribution which would affect the RP/TH coupled solution. Core re-loading strategy as well as re-shuffling of partially burned CLs will be a challenging task for accurate design calculations.

The power shape changes rather quickly during the initial time steps while later it approaches a more stable behavior which is typical of the equilibrium cycle. This condition is desired to provide better design optimization of the HPLWR core but its determination requires to go beyond this preliminary analysis based on the general approach used for current LWRs and to take into account, besides the effect of fuel isotopic changes, the important feedbacks due to the changes in TH feedbacks, reactivity control devices and 3D space coupling effects among the different core regions.

A.4 Suggestions for core design optimization

On the basis of the results presented in chapter 4, together with the studies summarized in this chapter, suggestions for future core design optimization are proposed.

Since the peak clad temperature is a critical design criterion for this kind of nuclear reactor, the obtained results underlines the effectivity of the “3 pass core” concept in separating the regions of high power density (EVA) from those of low margins on local clad temperature (SH2). The presented hot, full power condition of the HPLWR core is far from being optimized and it has been analyzed to test the developed coupled system which can now be used to suggest design improvements. These regard both reactor physics and thermal-hydraulics characteristics of the core, which are closely coupled.

Obtained results showed the importance of adequate mass flow redistribution among the individual fuel assemblies, which acts as parallel channels with common inlet and outlet plena. This is important in EVA because of the strong density reduction but also in the SHs because of the pronounced neutron flux gradient and hence is recommended to account for inlet orifices for all fuel assemblies. Due to the appropriate selection of the inlet orificing scheme and to the corresponding mass flow distribution, the region wise (EVA, SH1 and SH2) coolant and clad peak temperatures are rather uniform among the various fuel clusters but further optimization is desirable. The main source of the high peak - to - average ratio for the coolant outlet temperature lies in the differences among the 9 fuel assemblies of each single fuel cluster, especially in the SHs, and are caused by the pronounced flux gradient combined with the impossibility to perform independent adjustment of the coolant mass flow rate among the 9 fuel assemblies of each fuel cluster, as already discussed by Vogt [152] in a previous work. It is worth to mention here that the proposed mass flow adjustment by means of inlet orifices is surely dependent on the flow condition and hence on the load of the reactor. All the presented studies assumed a full power condition, but during reactor startup, transient or also part load operation, the different combination of power level and mass flow may affect the efficiency of the orifices and hence the flow distribution.

The optimization of the axial power profile in EVA will rise the power generated in the top part of the fuel assembly and, hence, may result in elevate local clad temperature also in this core region. These can be predicted with the developed coupled system.

The pronounced axial and radial power peaks can be reduced by varying the enrichment of the fuel rods and introducing burnable poisons. The strong neutron flux gradients at the interfaces between the core regions and close to the axial and radial reflectors may require optimization of the enrichment distribution within the fuel rods of each fuel assembly challenging the selected computational tools and leading to complicated control of core loading. The carried out 3D burn-up analysis [90] showed that evident changes in the in-core power distribution happen during few months of operation demanding consistent coupled reactor physics, thermal-hydraulics and burn-up analyses with fine spatial and time resolution.

The high temperature differences between the fuel assemblies, especially within the same fuel cluster, might result in thermal deformations, which have to be considered at the design stage. Thermo-mechanical analyses are desired to evaluate the relative thermal expansions of core components and the associated stresses. A particular attention should be given to alignment of the single FA with the corresponding control rod driver.

The developed system has been applied only to steady state investigations since it was mainly devoted to design studies. The extension to dynamic investigations, as needed for safety analyses, is not straightforward since it would require to take into considerations several new aspects. Among these, the most important is the coupling in time among the different physics which involves several time scales. In addition it would be necessary to use a different ERANOS module for the solution of the time dependent 3D transport equation as well as to development a XS lookup table to reduce the CPU time needed by the coupled system. In this framework, additional coupling with fuel performance tools will be extremely useful to improve the accuracy of the results.

Appendix B

Coupling methodology: 3D core mapping scheme and Perl scripts

B.1 General considerations and mapping scheme

The developed multi-physics, multi-scale computational tool is based on the usage of stand-alone codes which have been connected only by data exchange among them. This task, achieved developing new code interfaces, is mainly based on pre- and post-processing of ASCII files and relies on Perl language which offers great flexibility and portability. The proposed two-step methodology uses different approaches:

1. The two-way coupling between RP and TH analyses requires an iterative procedure in which the stand-alone codes and the interfaces are repetitively executed. This tasks has been automated with the usage of Bash scripting language which acts as a supervision tool.

2. The one-way coupling between full core analysis at FA- and pin-level does not require any iteration but automated interfaces are highly desirable to allow repetition of the multi-scale investigations.

The automation of these error prone activities is highly desirable especially from a qualification point of view: removing user dependencies and permitting results repeatability is the first step towards assessment of the developed coupled system.

The key behind the coupling (either one- or two-way) is the unique identification of each considered parameter which is moved from one code to the other. This task has been achieved using a developed mapping schema which associates each parameter to its 3D spatial position without relying on an arbitrary order of the considered elements.

The mapping schema has been initially developed for CL-wise spatial representation of the HPLWR core. The geometry of the HPLWR core allows to considered a rectangular grid with XYZ indexes to identify each cell center. As shown in Figure 2.16 on page 32, there are up to 7 cluster in X or Y direction and 21 zones are considered in Z direction. The XY index, e.g. 35, is uniquely defined in all the core positions and has been selected to locate each CL. Thanks to the assumed symmetry XY=YX, e.g. CLs 35 and 53 have the same TH properties and power level.

When going to FA-wise spatial representation of the HPLWR core, two additional indexes, I and J, are used to identify the 9 FA within each CL. They are still based on rectangular considerations, as shown in Figure 4.13 on page 76, I is in x direction while J in y direction and both range between 1 and 3.

When going further deep to pin-wise or cell-wise spatial resolution, within each FA two more indexes are introduced, A and B, to cover all the possible cells, Figure 3.10 on page 63. They

both range between 1 and 7 when considering the fuel rods or between 1 and 8 when considering the sub-channels.

This multiple nesting results in a clear mapping schema in which first the CL is identified, then the FA within the selected CL is located and finally the fuel rod is found.

B.2 Execution of the coupled ERANOS/TRACE system

The automated execution of the coupled ERANOS/TRACE system has been achieved with a sequential process executed by an outer loop, both written in Bash and described here.

The developed sequential process, `Coupled_TRACE_ERANOS.run`, has been described previously in Figure 3.2 on page 59. It starts with the execution of ERANOS – assigned to an additional script `ERANOSrun.run` which ensures generation of all the 462 necessary 40-group self-shielded homogenized XSs and execution of the successive 3D core calculation, as described in Figure 3.1 on page 57 – followed by `TGV2TRACE.pl`, which creates the necessary input file for TRACE execution and, finally the ECCO input files are produced, with the call to `TRACE2ECCO.pl`, closing the iteration loop.

`Coupled_TRACE_ERANOS.run`

```
#! /bin/bash
#
#      Author: Lanfranco.Monti@iket.fzk.de
#        Date: 10/31/2008
#
itn=$1 # read iteration number
#
echo -e "\n
-------------------------------------------------------------------------------------------"
echo -e " $0 -- Beginning of coupled iteration number ${itn} -- $(date '+%D %k:%M')"
echo -e "
-------------------------------------------------------------------------------------------\n"
#run ERANOS (generate XS and core analysis)
ERANOSrun.run ${itn}
#build TRACE input file from ERANOS data
r=0.55
echo -e " *** Under-relaxation in the power of $r\n"
perl -w TGV2TRACE.pl ${itn} skeleTRACE_FA_restart.inp $r || exit
#clean the directory
cd iteration${itn}
mkdir ECCO_files
mv FA_CL_* ECCO_files/
echo -e "\n TRACE -- calculating trace${itn} \n"
#copy steam table
ln -s ../tpfh2onew .
#copy restart file
let p=itn-1
ln -s ../iteration$p/trace$p.dmp trace${itn}.rst
#run trace
trace_Bishop_i5 -p trace${itn}
# echo -e "\n plotting TH variables \n"
# demux trace xtv file
xtv2dmx.sh -r trace${itn}.xtv -d trace${itn}.dmx -s
rm trace${itn}.xtv
## get the problem time when solution converged, to plot the data in aptplot NB time is
integer
# time=$(grep "steady state converged at problem time" trace${itn}.msg | awk '{printf "%5.0f",
 $7}')
# let time=time-1
# echo -e "time in msg file $time \n"
## prepare aptplot script file
# sed -e "s/FILENAME/trace${itn}/" -e"s/10.0/$time/" ../apt05.gr > apt_${itn}.gr
## run aptplot for the considered itn
# aptplot -noscreen -nowin -nosafe -batch apt_${itn}.gr
cd ..
# build ECCO input files from TRACE data
perl -w TRACE2ECCO.pl ${itn} skeleECCO_CL || exit
```

Within this sequential process, it is possible to add additional calls, e.g. to analyze TRACE results after each iteration with an available command line plotting tool, or even to insert a process to verify achieved convergence.

`Coupled_TRACE_ERANOS.run` is called from a the outer loop process, `CTHN.run`, which uses the iteration number as index.

`CTHN.run`

```
#!/bin/bash
#
#      Author: Lanfranco.Monti@iket.fzk.de
#        Date: 06/24/2008
# Description: coupled analisys, for loop
#
echo -e "\n $0 -- Starting of the coupled analysis $(date '+%D %k:%M')"
for (( itn=1 ; itn<=15 ; itn=itn+1 ))
do
Coupled_TRACE_ERANOS.run ${itn} || exit
done
echo -e "\n
-------------------------------------------------------------------------------------------"
echo -e " $0 -- End of the coupled analysis $(date '+%D %k:%M')\n"
```

It may be mentioned that the first iteration requires special attention since a previous power shape is not available to apply an under-relaxation. The commenting of some lines of the `TGV2TRACE.pl` script solve this issue. In addition, an assumption on the TH data distribution within the core has to be made. The repetitive calls to `Coupled_TRACE_ERANOS.run` allow execution flexibility, e.g. it is possible to change the relaxation parameter `$r` or the skeleton input files between successive iterations.

All scripts, both in Bash and in Perl languages, have been developed with attention to debugging and problem identification: each key action is preceded by a print to the standard output[1] which allows to easily locate the cause of any possible trouble occurred. Several tests have been performed and the developed supervision tool has always stopped immediately the iteration loop whenever any code or interface failure occurred. In addition, this command line tool permits remote execution.

B.3 TRACE2ECCO.pl

The post-processing of the TRACE output and the preparation of the needed ECCO input files is performed by the `TRACE2ECCO.pl` Perl script.

When processing the TRACE output file, the first thing to keep in mind is that more than one `trac large edit`, i.e. the print out of all components, exists in the output file. The one of interest it the last one because it contains the converged temperature distributions. For this reason, with a **`while`** loop, each line of the output file is searched for the `trac large edit` keyword, using the `$line =~ / /` expression, and, when the pattern is found, the file position is recorded and a counter is incremented. The TRACE output file is processed line by line till the end, then a test is performed to verify that more than one `trac large edit` has been found. If not, a problem during execution had occurred and the script is terminated with a `fatal error` message. If the test is passed, the TRACE output file is rewinded till the position of the last encountered `trac large edit`. In this way, the extracted TH data are always corresponding to the last edit.

```
# get the position of /trac large edit/ in the output file
my $count=0 ;
while(my $line = <TRACE_OUT>){
   if ($line =~ /^ trac large edit/){
      $currentpos=tell(TRACE_OUT);
      #print "The current position is $currentpos \n";
```

[1] Which can be redirected to a text file for a more convenient inspection.

```
        $count++;
      }
   }
   # print "$count $currentpos \n";
   die "X" x 15 ."   fatal error!!!   "."X" x 15 . "\n $0 Can't find more than $count trac large
edit!\n" if ($count<=1);
   seek(TRACE_OUT, $currentpos, 0); # Sets FILEHANDLE's position.
```

It is now possible to start the data extraction: the output file is processed line by line, from the beginning of the `trac large edit`, checking for the necessary keywords. The different components are coolant, moderator, gap water and fuel rod HS and each title card include the CL and FA number, according to the previously described mapping schema, which are extracted directly from the output file.

Once that the component has been identified, a nested **`while`** loop continues to process line by line the output file searching for the user specified format and for the end keyword which returns to the component search. The data needed for the coupling are identified using some of the so called Regular Expression: `\s` identifies a whitespace characters (either space or tab), `\S` identifies any non-whitespace character (alphanumeric, punctuation, etc.), `\d` identifies digits only, the + means that the previous pattern has to be present one or more time avoiding the need to know exactly the format, e.g. `\S+` will match `1.1234E+01`. The parenthesis are used to store the matched expression in memory allowing to recall it later. A powerful feature of Perl is that the variables do not have to be declared: if the matched expression is a string or a number it does not matter.

With such a detailed, but easy, specification of the line format only the desired data are extracted from the output file minimizing coding errors. Processing line by line, all the axial position of the identified component are read till the examined line contains the exit keyword, which is independent from the number of considered axial regions. At this point the script search for the next component exiting from this inner loop with the command **`last`**. Since there is no relation between the input and the output order of the components, this approach is necessary being unknown which component will appear first. The output file is processed only once, checking each line for all interesting component.

The TH data of each component are saved in a specified *hash*, or associative array, in which each value has a corresponding *key*: the index used for the mapping, i.e. `$CL._.$FA._.$z`.

The densities in TRACE are printed in kg/m^3 while in the ERANOS input file the units are g/cm^3, hence the data are automatically converted. The Rowlands [128] formula has also been implemented to calculate the fuel lumped temperature used in ERANOS from the calculated pellet surface and centerline ones (the position of these values, together with the format of the output, depend on the selected nodalization of the fuel rod and hence is problem dependent).

```
   while( $line = <TRACE_OUT>){
     # get the coolant temperature and density
     if ($line =~ / coolant channel CL (\d\d) FA (\d\d)/){ # starting key word
       $CL = $1 ;
       $FA = $2 ;
       print " $0 -- in CL $CL FA $FA found coolant channel\n";
       my $z = 1 ;
       while( $line = <TRACE_OUT>){
         if ($line =~ /dis.sol. p.o.sol. fr.new if.drag   temp.ss.  evap.     cond.    mfw.liq.
mfw.vap.   velt.liq   velt.gas  wf.gas/){ # ending key word
           $axial = $z - 1 ; # assign number of axial zones
           # read two more lines to get mass flow rate mfw
           $line = <TRACE_OUT> ;
           $line = <TRACE_OUT> ;
           # search for the lines with the proper format
           if ($line =~ /^\s+(\d+)\s(\S+)\s+(\S+)\s+(\S+)\s+(\S+)\s+(\S+)\s+(\S+)\s+(\S+)\s+(\S+)\s+(\S+)
\s+(\S+)\s+(\S+)\s+(\S+)/){
             $mfw{$CL._.$FA}  = $9 ;
             last;
           }
         }
         # search for the lines with the proper format
```

```
          elsif ($line =~ /^\s+(\d+)\s(\S+)\s+(\S+)\s+(\S+)\s+(\S+)\s+(\S+)\s+(\S+)\s+(\S+)\s+(\S
+)\s+(\S+)\s+(\S+)\s+(\S+)$/){
            $tempCtmp{$CL._.$FA._.$z}    = $6 ;
            $densityCtmp{$CL._.$FA._.$z} = $8/1000.0 ; # [g/cm3]
            $z++;
          }
        }
      }
      # get the moderator water temperature and density
      elsif ($line =~ / moderator channel CL (\d\d) FA (\d\d)/){ # starting key word
        $CL = $1 ;
        $FA = $2 ;
        print " $0 -- in CL $CL FA $FA found moderator channel\n";
        my $z = 1 ;
        while( $line = <TRACE_OUT>){
          if ($line =~ /^ total power/){               # ending key word
             last;
          }
          # search for the lines with the proper format
          elsif ($line =~ /^\s+(\d+)\s(\S+)\s+(\S+)\s+(\S+)\s+(\S+)\s+(\S+)\s+(\S+)\s+(\S+)\s+(\S
+)\s+(\S+)\s+(\S+)\s+(\S+)$/){
            $tempMusd{$CL._.$FA._.$z}    = $6 ;
            $densityMusd{$CL._.$FA._.$z} = $8/1000.0 ; # [g/cm3]
            $z++;
          }
        }
      }
      # get the gap water temperature and density
      elsif ($line =~ / gap water channel CL (\d\d) FA (\d\d)/){ # starting key word
        $CL = $1 ;
        $FA = $2 ;
        print " $0 -- in CL $CL FA $FA found gap water channel\n";
        my $z = 1 ;
        while( $line = <TRACE_OUT>){
          if ($line =~ /^ total power/){         # ending key word
             last;
          }
          # search for the lines with the proper format
          elsif ($line =~ /^\s+(\d+)\s(\S+)\s+(\S+)\s+(\S+)\s+(\S+)\s+(\S+)\s+(\S+)\s+(\S+)\s+(\S
+)\s+(\S+)\s+(\S+)\s+(\S+)$/){
            $tempGusd{$CL._.$FA._.$z}    = $6 ;
            $densityGusd{$CL._.$FA._.$z} = $8/1000.0 ; # [g/cm3]
            $z++;
          }
        }
      }
      # get the fuel T at the pin centerline and surface
      elsif ($line =~ /  fuel rod HS CL (\d\d) FA (\d\d)/){ # starting key word
        $CL = $1 ;
        $FA = $2 ;
        print " $0 -- in CL $CL FA $FA found fuel rod\n";
        my $z = 1 ;
        while( $line = <TRACE_OUT>){
          if ($line =~ /idi   hliqi       tliqi       hvapi       tvapi/){ # ending key word
            last;
          }
          # search for the lines with the proper format
          elsif ($line =~ /^\s+(\d+)\s+(\d+)\s+(\S+)\s+(\S+)\s+(\S+)\s+(\S+)\s+(\S+)\s+(\S+)\s+(\S
+)\s+(\S+)\s+(\S+)\s+(\S+)$/){ # ( ){10}/){ #
            $tempClad{$CL._.$FA._.$z} = $12 ;
            $tempF0{$CL._.$FA._.$z}   = $4  ; # field  4 is fuel centerline temperature
            $tempFR{$CL._.$FA._.$z}   = $10 ; # field 10 is fuel surface temperature
            # calculate the average T using the Rowlands formula
            $tempF{$CL._.$FA._.$z} = 4.0/9.0*$tempF0{$CL._.$FA._.$z}+5.0/9.0*$tempFR{$CL._.$FA._.
$z} ;
            $z++;
          }
        }
      }
    }
    close TRACE_OUT ;
```

All the TH data have been extracted and are associated with their core position according to the mapping schema. It is now necessary to adjust them accounting for both up- and downward flow. In TRACE is possible to specify arbitrarily the flow direction but the output is always

printed in ascending order of the cell numbers. For the prepared input specification, it is necessary to flip upside down the data extracted for moderator/gap water in all the core and for coolant in SH1 only. This task has been achieved using temporary variables (hashes), and flipping the axial index. Concerning the fuel temperature, since the HS have been defined as oriented from bottom to top, there is no need to flip the data. In SH1 the first axial cell of the fuel rod HS is connected to the last cell of the coolant pipe.

```
# flip moderator and gap water
my $zz = $axial ;
#print "$zz \n" ;
for ($z = 1; $z <= $axial; $z++){
  for ($y = 1; $y <= 7; $y++){
    for ($x = 1; $x <= 7; $x++){
      for ($j = 1; $j <= 3; $j++){
        for ($i = 1; $i <= 3; $i++){
          my $index = $x.$y._.$i.$j ;
          $tempG{$index._.$z} = $tempGusd{$index._.$zz} ;
          $tempM{$index._.$z} = $tempMusd{$index._.$zz} ;
          $densityG{$index._.$z} = $densityGusd{$index._.$zz} ;
          $densityM{$index._.$z} = $densityMusd{$index._.$zz} ;
          # the coolant temperature is not flipped but initialized
          $tempC{$index._.$z} = $tempCtmp{$index._.$z} ;
          $densityC{$index._.$z} = $densityCtmp{$index._.$z} ;
        }
      }
    }
  }
  # the coolant temperature in SH1 is flipped
  foreach $CL (@SH1,@SH1symmetric) {
    for ($j = 1; $j <= 3; $j++){
      for ($i = 1; $i <= 3; $i++){
        $tempC{$CL._.$i.$j._.$z} = $tempCtmp{$CL._.$i.$j._.$zz} ;
        $densityC{$CL._.$i.$j._.$z} = $densityCtmp{$CL._.$i.$j._.$zz} ;
      }
    }
  }
$zz-- ;
}
```

The next step is the insertion of the TH data in the provided ECCO skeleton input file. It is now necessary to average the TH parameters from the FA-wise spatial resolution used in TRACE to the CL-wise selected in ERANOS. As described in chapter 3 on page 55, an arithmetic mean has been used for this purpose.

One ECCO input file is prepared for each CL and it is placed in a new directory for the successive iteration, keeping a more ordered file structure. It include a loop, written in the ERANOS user language, to calculate all axial zones, it is described later. Selected keyword are inserted to identify each input file and to check the data exchange. The formated data are inserted in an identified position of the ECCO skeleton file; all temperatures are rounded to integers: `%4.0f`.

Finally, a user friendly print out of the TH data is provided to allow convergence checking. This file can be directly loaded in Matlab or Octave.

```
# make directory for new iteration
my $itnx = $itn + 1 ;
mkdir ( "iteration${itnx}", 0755 ) or die "mkdir failed $!\n";
foreach $CL (@EVA, @SH1, @SH2) { # for each cluster in 1/8 of the core
  # initialize the strings to be printed in ECCO file
  $stringC = sprintf("%8s", "-> tempC");
  $stringM = sprintf("%8s", "-> tempM");
  $stringG = sprintf("%8s", "-> tempG");
  $stringF = sprintf("%8s", "-> tempF");
  $stringCC = sprintf("%7s", "-> denC");
  $stringMM = sprintf("%7s", "-> denM");
  $stringGG = sprintf("%7s", "-> denG");
  # calculate algebraic mean among the 9 FAs of each CL for each TH parameter
  for ($z=1; $z<=$axial; $z++){
    $tempC_CL{$z} = 0.0 ; # coolant temperature for CL average
    $tempM_CL{$z} = 0.0 ; # moderator temperature for CL average
    $tempG_CL{$z} = 0.0 ; # gap water temperature for CL average
```

```
        $tempF_CL{$z} = 0.0 ; # fuel equivalent temperature for CL average
        $densityC_CL{$z} = 0.0 ;
        $densityM_CL{$z} = 0.0 ;
        $densityG_CL{$z} = 0.0 ;
        for ($j = 1; $j <= 3; $j++){
          for ($i = 1; $i <= 3; $i++){
              $tempC_CL{$z}= $tempC_CL{$z} + $tempC{$CL.'_'.$i.$j.'_'.$z}/9 ;
              $tempM_CL{$z}= $tempM_CL{$z} + $tempM{$CL.'_'.$i.$j.'_'.$z}/9 ;
              $tempG_CL{$z}= $tempG_CL{$z} + $tempG{$CL.'_'.$i.$j.'_'.$z}/9 ;
              $tempF_CL{$z}= $tempF_CL{$z} + $tempF{$CL.'_'.$i.$j.'_'.$z}/9 ;
              $densityC_CL{$z}= $densityC_CL{$z} + $densityC{$CL.'_'.$i.$j.'_'.$z}/9 ;
              $densityM_CL{$z}= $densityM_CL{$z} + $densityM{$CL.'_'.$i.$j.'_'.$z}/9 ;
              $densityG_CL{$z}= $densityG_CL{$z} + $densityG{$CL.'_'.$i.$j.'_'.$z}/9 ;
          }
        }
        # fill the strings containing the TH data
        $stringC = $stringC.sprintf(" %4.0f", "$tempC_CL{$z}");
        $stringM = $stringM.sprintf(" %4.0f", "$tempM_CL{$z}");
        $stringG = $stringG.sprintf(" %4.0f", "$tempG_CL{$z}");
        $stringF = $stringF.sprintf(" %4.0f", "$tempF_CL{$z}");
        $stringCC = $stringCC.sprintf(" %7.5f", "$densityC_CL{$z}") ;
        $stringMM = $stringMM.sprintf(" %7.5f", "$densityM_CL{$z}") ;
        $stringGG = $stringGG.sprintf(" %7.5f", "$densityG_CL{$z}") ;
        # set the format of the strings (max 80 characters in ERANOS input)
        if ( $z % 14 == 0 ){
          $stringC = $stringC.sprintf("%s", "\n        ");
          $stringM = $stringM.sprintf("%s", "\n        ");
          $stringG = $stringG.sprintf("%s", "\n        ");
          $stringF = $stringF.sprintf("%s", "\n        ");
        }
        if ( $z % 9 == 0 ){
          $stringCC = $stringCC.sprintf("%s", "\n       ");
          $stringMM = $stringMM.sprintf("%s", "\n       ");
          $stringGG = $stringGG.sprintf("%s", "\n       ");
        }
      }
       # generate one ECCO files for each CL: it contains a loop to consider the 21 axial zones
       print " $0 -- opening ECCO skeleton file \n" ;
       open(SKELETON ,"<${skele}") or die "Can't open ECCO SKELETON: ${skele} $!" ;
        # open the new ECCO files to be written
       open(OUT, ">iteration${itnx}/FA_CL_$CL") or die "Can't open ECCO new input file FA_CL_$CL:
$!";
       seek(SKELETON, 0, 0 ) ; # Sets FILEHANDLE's position.
          while (<SKELETON>) {
             # replace key word in skeleton file with TH data
             s/regione/CL_$CL/; # \_ is used to escape (and print)
             s/ITN/$itnx/;
             print OUT;
             if ( $_ =~/Define vectors of Thermal Hydraulic conditions/){
             # insert an array of TH data to be read by ERANOS
               print OUT "$stringC ;\n" ;
               print OUT "$stringM ;\n" ;
               print OUT "$stringG ;\n" ;
               print OUT "$stringF ;\n" ;
               print OUT "$stringCC ;\n" ;
               print OUT "$stringMM ;\n" ;
               print OUT "$stringGG ;\n" ;
             }
          }
          close OUT;
          print " $0 -- building ECCO input files -- CL $CL COMPLETED\n";
          # print the array with all the TH data in the proper format and position
       print TH_DATA_CL "%      Coolant    Moderator      Gap Water     Fuel -- in CL $CL\n" ;
       for ($z=1; $z<=$axial; $z++){
       printf TH_DATA_CL "%6.0f %7.5f %6.0f %7.5f %6.0f %7.5f %6.0f \n",  $tempC_CL{$z},
$densityC_CL{$z}, $tempM_CL{$z}, $densityM_CL{$z}, $tempG_CL{$z}, $densityG_CL{$z}, $tempF_CL{$z};
       }
    }
   print "-" x 80 ."\n $0 execution completed!!!\n"."-" x 80 ."\n" ;
```

B.4 TGV2TRACE.pl

The post-processing of the ERANOS output and the preparation of the TRACE input files is performed by the `TGV2TRACE.pl` Perl script.

Also the VARIANT output file is checked for the existence of the printed power shapes with a similar procedure to the one used for the TRACE output file.

```
print " $0 -- opening and processing current iteration ($itn) VARIANT output file \n" ;
open(TGV_OUT, "<iteration${itn}/full_core_FA.OUT") or die "Can't open output file: iteration${
itn}/full_core_JEFF31.OUT $!";
# verify the existance of the edition traverse in VARIANT file
my $count = 0 ;
while( $tgv = <TGV_OUT>){
  if ($tgv =~ /^ PRINT_CL_POWER/){
    $currentpos=tell(TGV_OUT);
    #print "The current position is $currentpos \n";
    $count++;
  }
}
# print "$count $currentpos \n";
die "X" x 15 ."   fatal error!!!   "."X" x 15 . "\n $0 Found $count PRINT_CL_POWER in TGV-
VARIANT output file!\n" if ($count ne 1);
```

It the test is passed, the VARIANT output file is rewinded till the position of the edition traverses and each successive line is processed with a **`while`** loop searching for the power shape and total power of each individual FA in the considered one eighth core model. Despite the CL-wise core analysis with ECCO and VARIANT, the power map, calculated using the nodal flux reconstruction available in ERANOS, is at FA resolution and no external data interpolation is needed. As for TRACE, the index of the CL and FA as well as the number of the axial zone are extracted directly from the output file. In this way the script does not have to be modified if these parameters are changed (as far as the keywords are the same).

```
# for each line in VARIANT output after the keyword EDIT_POWER extract the
# power-shape and the total power (obtained with LU in ERANOS)
seek(TGV_OUT, $currentpos, 0); # Sets FILEHANDLE's position.
while( $tgv = <TGV_OUT>){
  if ($tgv =~ /^\s+\$\$\$\s+POWER_CL_(\d\d)_FA_(\d\d)/){ # starting key word
    my $CL = $1 ; # the CL number is obtained directly form the output file
    my $FA = $2 ; # the FA number is obtained directly form the output file
    print " found CL $CL FA $FA in VARIANT output\n" ;
    while( $tgv = <TGV_OUT>){
      if ($tgv =~ /^ ' end '\s+'POWER_CL_${CL}_FA_$FA'/){ # ending key word
        $axialzones = $z ; # the number of axial zones is assigned to a dedicated variable
        last;
      }
      elsif ($tgv =~ /\.\s+(\d+)\s+\.\s+\s+([\d\.])+\s+\.\s+(\S+)/){
        $z = $1 ;
        $powershape{$CL._.$FA._.$z} = $3 ;
      }
      elsif ($tgv =~ /^ ->TOTAL_POWER\s+(\S+) $/){
        $power{$CL._.$FA} = $1 ;
        #print "in CL $region total power equal to $power{$CL._.$FA} W \n" ;
      }
    }
  }
}
close TGV_OUT ;
```

The current power map has been extracted and properly mapped, it is now necessary to apply the under-relaxation. Since the relaxation factor `$r` can be changed, it is printed on the standard output to allow successive checking. The power map of the previous iteration has been stored in an ASCII file which can now be accessed to calculate the relaxed power map. The relaxed values are printed in an ASCII file to be used at the successive iteration, this file can be directly loaded in Matlab or Octave to check the convergence of the coupled solution.

```
# load the power-shape of previous iteration ${prev} (it is already a relaxed value)
my $prev = $itn - 1 ; # number of previous iteration
my $oldpower = "iteration$prev/powershape$prev.dat" ;
print " $0 -- opening power-shape file of previous iteration: $oldpower \n" ;
```

```
open(DATA, "<$oldpower") or die "Can't open power-shape file: $oldpower $!";
while($data = <DATA>){
  if ($data =~ /^% in CL (\d\d) FA (\d\d) total power equal to (\S+) W/){
    my $CL = $1 ; # the CL number is obtained directly form the output file
    my $FA = $2 ; # the FA number is obtained directly form the output file
    $ppower{$CL._.$FA} = $3 ;
    print " CL $CL FA $FA  found -- total power equal to $ppower{$CL._.$FA} W\n" ;
    for ($z=1; $z<=$axialzones; $z++){
      $data = <DATA> ;
      $ppowershape{$CL._.$FA._.$z} = $data ;
      #print "CL $CL FA $FA  axial $z power $ppowershape{$CL._.$FA._.$z}\n";
    }
  }
}
close DATA ;
# calculate and print relaxed power for current iteration ${itn}
print " $0 -- calculating relaxed power, relaxation factor $r\n";
open(POWER_RELAX, ">iteration${itn}/powershape${itn}.dat") or die "Can't open dat file: $!";
foreach $CL (@EVA, @SH2, @SH1) {
  for ($j=1; $j <= 3; $j++){
    for ($i=1; $i <= 3; $i++){
      $FA=$i.$j ;
      $powerrelax{$CL._.$FA}=$r*$power{$CL._.$FA}+(1-$r)*$ppower{$CL._.$FA} ;
      $rpow = sprintf("%11.5e","$powerrelax{$CL._.$FA}") ;
      print POWER_RELAX "% in CL $CL FA $FA total power equal to $rpow W\n" ;
      for ($z=1; $z<=$axialzones; $z++){
        $powershaperelax{$CL._.$FA._.$z}=$r*$powershape{$CL._.$FA._.$z}+(1-$r)*$ppowershape{
$CL._.$FA._.$z} ;
        printf POWER_RELAX "%11.5e\n", "$powershaperelax{$CL._.$FA._.$z}" ;
      }
    }
  }
}
close POWER_RELAX ;
```

The TRACE skeleton file is now modified to update the power map. Only the power components which are included in the skeleton file are modified, and this is done independently from the file structuring: it is possible to apply it to a full TRACE input file or to a restart input file which should contain all the power components but not the pipes and HSs. Since the TRACE model is representative of the quarter core, it is necessary to set the core symmetry because in VARIANT output only one eight of the core is printed. The selected XY mapping schema simplify this task since it is just necessary to exchange the X and Y indexes when Y is bigger than X. Once that each power component in TRACE skeleton file has been mapped to the corresponding VARIANT one, the FA total power and axial power shape are inserted replacing the values originally present in the skeleton file. Again, there is no predefined order which has to be respected and all power components are automatically identified by their index. When one component is terminated, the control is returned to the outer **`while`** loop (`LOOP`) to search for the next FA.

When the whole TRACE skeleton file has been processed, the input file with the updated power map is available.

```
# prepare new trace input file from skeleton one
print " $0 -- opening TRACE skeleton file: ${sktr} \n" ;
open(TR_INP ,"<${sktr}") or die "Can't open TRACE input file: ${sktr} $!" ;
my $traceinp="iteration${itn}/trace${itn}.inp";
print " $0 -- opening new TRACE input file $traceinp\n" ;
open(TR_OUT ,">$traceinp") or die "Can't open TRACE output file: $traceinp $!";
seek(TR_INP,0,0);
# for each line in TRACE skeleton file search for the power component and replace
# both the total power rpowri and the axial shape zpwtb
LOOP: while($trace=<TR_INP>){
  if ($trace =~ /^power\s+\d+\s+\d+\s+fission energy CL (\d)(\d) FA (\d)(\d)/){
    $x = $1 ;
    $y = $2 ;
    $i = $3 ;
    $j = $4 ;
    # set core symmetry XY = YX
    if    ( $y > $x ){ $CL = $y.$x ; $FA = $j.$i ; }
    elsif ( $y < $x ){ $CL = $x.$y ; $FA = $i.$j ; }
    else             { $CL = $x.$y ; $FA = $i.$j ; } ;
```

```
      print " found fission E - CL $x$y FA $i$j - mapped to $CL $FA\n" ;
      print TR_OUT $trace;
      while($trace = <TR_INP>){
        if ($trace =~ /rpowri/){ # keyword
          print TR_OUT $trace;
          # read one more line after keyword
          $trace = <TR_INP> ;
          $rpowri = sprintf("%11.5e","$powerrelax{$CL._.$FA}") ;
          $trace =~ s/^\s+\S+/   $rpowri/;
        }
        elsif ( $trace =~ /\* zpwtb1\*         0\.0s/){
          print TR_OUT $trace;
          # for loop to print the new power-shape
          # same number of axial zones used in VARIANT (flux build)
          # remember that the last entry must have the "e" keyword
          for ($z=1; $z<$axialzones; $z++){
            my $zpwtb = sprintf("%18s%11.5e%1s\n","* zpwtb1*         ","$powershaperelax{$CL._.
$FA._.$z}","s");
            print TR_OUT $zpwtb;
          }
          my $zpwtb21 = sprintf("%18s%11.5e%1s\n", "* zpwtb1*         ","$powershaperelax{$CL._.
$FA._.$axialzones}","e");
          print TR_OUT $zpwtb21;
          # now remove the original power-shape from trace skeleton file:
          # read a line from trace skeleton untill the "e" keyword is found
          do {chomp($trace = <TR_INP>);} until ($trace =~ /^\* zpwtb1\*[ \.\S]+e\Z/);
          # goto the outer while loop (to not print current line ($trace)
          next LOOP ;
        }
        print TR_OUT $trace;
      }
    }
    print TR_OUT $trace;
  }
  print " $0 -- closing new TRACE input file $traceinp\n" ;
  close TR_OUT ;
  close TR_INP ;
  print "-" x 80 ,"\n $0 execution completed!!!\n"."-" x 80 ,"\n" ;
```

B.5 MCNP5inputmaker.pl

The post-processing of the ERANOS and TRACE output files to prepare one MCNP5 input file for each CL is performed by the `MCNP5inputmaker.pl` Perl script. The script has pronounced problem dependencies and it is reported here for completeness since it can be used as guideline for future applications.

The axial position of the power peak has to be located for each CL (it was decided to use a CL-wise spatial resolution) and has to be stored for future usage.

```
  foreach $CL (@EVA, @SH1, @SH2) {
      $zeta{$CL} = 1 ;
      $max{$CL}  = $ppower{$CL._1} ;
#     print " first value for CL $CL is $max{$CL}\n" ;
    for ($z=2; $z<=21; $z++){ # modify if change number of axial zones
      if ( $ppower{$CL._.$z} > $max{$CL}){ $max{$CL} = $ppower{$CL._.$z} ; $zeta{$CL}=$z ;}
    }
    print "MAX z for CL $CL is $max{$CL} at zeta $zeta{$CL}\n";
  }
```

The CL-wise TH data are available in the Perl script and the axial position index of the peak region has just been identified `$zeta{$CL}`. The temperatures have to be rounded to the closest value in which MCNP5 XS are available. The material identification number in the MCNP5 input has been chosen as the rounded temperature of the available XS in K, to ease the input file preparation. To account for the free gas treatment, the original temperature has to be converted from K into MeV while the densities are already in the correct units.

```
  @H2Otmp = (523 , 573 , 623 , 647 , 800 , 1000 );
  @UO2tmp = (500 , 600 , 700 , 800 , 900 , 1000 , 1100 , 1200 , 1300 , 1400 , 1500 , 1600 , 1700
 , 1800 );
```

```
    foreach $CL (@EVA, @SH1, @SH2) {
      $i = $CL._.$zeta{$CL} ;
    # Determine rounding of the temperatures to the closest available XS
      $minC = 500 ;
      $minM = 500 ;
      $minG = 500 ;
      $minF = 500 ;
      for ($j = 0; $j <= @H2Otmp-1 ; $j++){
        if (abs($tempC{$i}-$H2Otmp[$j]) <= $minC){ $minC = abs($tempC{$i}-$H2Otmp[$j]) ;
$tempCmcnp{$i} = $H2Otmp[$j] ; }
        if (abs($tempM{$i}-$H2Otmp[$j]) <= $minM){ $minM = abs($tempM{$i}-$H2Otmp[$j]) ;
$tempMmcnp{$i} = $H2Otmp[$j] ; }
        if (abs($tempG{$i}-$H2Otmp[$j]) <= $minG){ $minG = abs($tempG{$i}-$H2Otmp[$j]) ;
$tempGmcnp{$i} = $H2Otmp[$j] ; }
      }
      for ($j = 0; $j <= @UO2tmp-1 ; $j++){
        if (abs($tempF{$i}-$UO2tmp[$j]) <= $minF){ $minF = abs($tempF{$i}-$UO2tmp[$j]) ;
$tempFmcnp{$i} = $UO2tmp[$j] ;}
      }
      $MeV_C{$CL} = 8.617*10**(-11)*$tempC{$i};
      $MeV_M{$CL} = 8.617*10**(-11)*$tempM{$i};
      $MeV_G{$CL} = 8.617*10**(-11)*$tempG{$i};
      $MeV_F{$CL} = 8.617*10**(-11)*$tempF{$i};
      # print to verify temperature rounding
      printf( "%s %s %6.0f %7.5f %6.0f %7.5f %6.0f %7.5f %6.0f \n",  $CL, $zeta{$CL}, $tempC{$i},
     $densityC{$i}, $tempM{$i},     $densityM{$i}, $tempG{$i},     $densityG{$i}, $tempF{$i});
      printf( "%s %s %6.0f %7.5f %6.0f %7.5f %6.0f %7.5f %6.0f \n",  $CL, $zeta{$CL}, $tempCmcnp{
$i}, $densityC{$i}, $tempMmcnp{$i}, $densityM{$i}, $tempGmcnp{$i}, $densityG{$i}, $tempFmcnp{$i});
    }
```

Once the materials and temperatures are identified, the skeleton file for MCNP5 is processed for each considered CL modifying the TH data originally included with the same approach used for the ERANOS/TRACE coupling. An additional Regular Expression has been used, the full stop . which identify any character (whitespace or non).

```
    foreach $CL (@EVA, @SH1, @SH2) {
      open(MCNP, "<$mcnp") or die "Can't open file: $!";
      open(OUT, ">FA_$CL") or die "Can't open new input file FA_$CL for MCNP: $!";
      LOOP:while($line=<MCNP>){
        $line =~ s/HPLWR FA exact geometry  with insulated boxes -- tests!!!!/HPLWR FA CL_z $i
$tempC{$i} $densityC{$i} $tempM{$i} $densityM{$i} $tempG{$i} $densityG{$i} $tempF{$i}/;
        $line =~ s/(7)\s+\d+\s+\S+ (.+tmp=)\S+\s+(lat=1.+)/$1 $tempCmcnp{$i} -$densityC{$i}
$2$MeV_C{$CL} $3/ ;
        print OUT $line;
        if ( $line =~ /c -- Moderator channel/){
          while($line=<MCNP>){
            if ( $line =~ /c/){next LOOP;}
            elsif ( $line =~ /(\d+)\s+\d+\s+\S+ (.+tmp=)\S+/ ) {
            $cell = $1 ;
            $geometry = $2 ;
            print OUT "$cell $tempMmcnp{$i} -$densityM{$i} $geometry$MeV_M{$CL}\n";
            }
          }
        }
        if ( $line =~ /c -- gap between fuel assembly/){
          while($line=<MCNP>){
            if ( $line =~ /c/){next LOOP;}
            elsif ( $line =~ /(\d+)\s+\d+\s+\S+ (.+tmp=)\S+/ ) {
            $cell = $1 ;
            $geometry = $2 ;
            print OUT "$cell $tempGmcnp{$i} -$densityG{$i} $geometry$MeV_G{$CL}\n";
            }
          }
        }
        if ( $line =~ /c -- fuel pin 5wt%/){
          while($line=<MCNP>){
            if ( $line =~ /c/){next LOOP;}
            elsif ( $line =~ /(1)\s+\d+\s+(\S+)\s+(.+tmp=)\S+/ ) {
            $cell = $1 ;
            $density = $2 ;
            $geometry = $3 ;
            print OUT "$cell $tempFmcnp{$i}5 $density $geometry$MeV_F{$CL}\n";
            }
            elsif ( $line =~ /(3)\s+\d+\s+\S+\s+(.+tmp=)\S+/ ) {
            $cell = $1 ;
            $geometry = $2 ;
```

```
        print OUT "$cell $tempCmcnp{$i} -$densityC{$i} $geometry$MeV_C{$CL}\n";
        }
        else {print OUT $line; } # print clad line
      }
    }
    if ( $line =~ /c -- fuel pin 4wt%/){
      while($line=<MCNP>){
        if ( $line =~ /c/){next LOOP;}
        elsif ( $line =~ /(4)\s+\d+\s+(\S+)\s+(.+tmp=)\S+/ ) {
        $cell = $1 ;
        $density = $2 ;
        $geometry = $3 ;
        print OUT "$cell $tempFmcnp{$i}4 $density $geometry$MeV_F{$CL}\n";
        }
        elsif ( $line =~ /(6)\s+\d+\s+\S+\s+(.+tmp=)\S+/ ) {
        $cell = $1 ;
        $geometry = $2 ;
        print OUT "$cell $tempCmcnp{$i} -$densityC{$i} $geometry$MeV_C{$CL}\n";
        }
        else {print OUT $line; } # print clad line
      }
    }
  }
}
```

B.6 MATRAinputmaker.pl

The pin-power reconstruction and preparation all MATRA input files for whole HPLWR core analysis at sub-channel resolution is performed by the `MATRAinputmaker.pl` Perl script, completing the requirements for the one-way coupling. Also this script has pronounced problem dependencies, nonetheless it is discussed here for completeness.

Several spatial scales have to be considered with MATRA and several output files have to be processed to perform the desired one-way coupling.

```
#!/usr/bin/perl -w
use strict "refs" ;
# ------------------------------------------------------------------------------
#      Author: Lanfranco.Monti@iket.fzk.de
#        Date: 02/19/2009
# Description: Part 1: exctract the peaking factors from MCNP5 output
#              Part 2: exctract the core power gradient from VARIANT output (cell scale)
#              Part 3: exctract the axial power shape and fuel assembly power
#                      from VARIANT output (fuel assembly scale)
#              Part 4: exctract mass flow rate for each fuel assembly and
#                      inlet temperature for each core part in trace output
#              Part 5: modify MATRA skeleton file
# Usage: run the script with six arguments: file names without extension
#        1- MCNP output
#        2- VARIANT output for cell scale (flux build 21)
#        3- VARIANT output for fuel assembly scale (flux build 3)
#        4- trace output file
#        5- skeleton MATRA file for EVA and SH2
#        6- skeleton MATRA file for SH1 (downward flow)
# ------------------------------------------------------------------------------
print "-" x 80 ,"\n $0 execution started!!!\n"."-" x 80 ,"\n" ;
# ------------------------------------------------------------------------------
# read variables
my $mcnp      = $ARGV[0] ; # MCNP root file name
my $tgvpin    = $ARGV[1] ; # TGV/VARIANT file name for cell scale
my $tgvFA     = $ARGV[2] ; # TGV/VARIANT file name for fuel assembly scale
my $trace     = $ARGV[3] ; # TRACE file name
my $matra     = $ARGV[4] ; # MATRA file name
my $matraSH1  = $ARGV[5] ; # MATRA file name
```

The tallied quantities are extracted form the 22 MCNP5 output files representative of the 22 CL in one eighth of the core, each file is named using the described mapping schema and is identified by its XY position. The assumed symmetry of the considered 2D FA model allows to tally only 7 fuel rods: these values are extracted and normalized using the averaged one. Then the symmetry of the FA has to be set, assigning the normalized value to the corresponding fuel

rods, this procedure is not reported here because it has been done individually for each fuel rod and a mapping scheme to go from the one eighth to the full FA has not been developed.

```
# ------------------------------------------------------------------------------
# Part 1: exctract the peaking factors from MCNP5 output
# there is one output for each CL in 1/8 of the core
foreach $CL (@EVA, @SH1, @SH2) {
print " $0 -- opening and processing MCNP5 output file: ${mcnp}${CL}o\n" ;
open(MCNP_OUT, "<${mcnp}${CL}o") or die "Can't open output file: ${mcnp}${CL}o $!";
# flip XY index in CL notation for graphical representation
if ($CL =~ /(\d)(\d)/){
$i=$1;
$j=$2;
$LC=$j.$i;
}
# initialize the array with all 0 to have a full 7x7 matrix (including moderator channel)
for ($b=1; $b <= 7; $b++){
  for ($a=1; $a <= 7; $a++){
    $index = $CL._.$a.$b ;
    #print "$index\n" ;
    $peak{$index} = 0.0 ;
  }
}
while( $line = <MCNP_OUT>){
  if ( $line =~ /^\+\s+average fission energy deposition/){ # starting key word
    while( $line = <MCNP_OUT>){
      if ( $line =~ /^\s+(\d.\d\d\d\d\dE\S\d\d) (0.\d+)/){
         $average=$1 ;
         print " average power in CL $CL $average\n" ;
         last ;
      }
    }
  }
  if ( $line =~ /^\+\s+pin (\d\d) fission energy deposition/){
    $pin = $1 ;
      if ( $line =~ /^\s+(\d.\d\d\d\d\dE\S\d\d) (0.\d+)/){
         $peak{$CL._.$pin}=$1/$average ; # this normalizatio is not exact since the average
value calculated by MCNP is not the aritmetic mean
         print " pin $pin power in CL $CL: $peak{$CL._.$pin}\n" ;
         last ;
      }
    }
  }
}
close MCNP_OUT ;
```

The relative pin-power distribution is obtained combining the results extracted from the 22 MCNP5 outputs with the ERANOS one where the cell-wise power is calculated (using the 21 by 21 nodal flux reconstruction).

```
# ------------------------------------------------------------------------------
# Part 2: exctract the 2D core power gradient from VARIANT output (cell scale)
print " $0 -- opening and processing VARIANT output file: $tgvpin.OUT\n" ;
open(TGV_OUT_PIN, "<$tgvpin.OUT") or die "Can't open output file: $tgvpin.OUT $!";

# initialize the array with all 0
# this is needed to print the XY core power map with 0 in the non-fuel regions (as needed in
tecplot or matlab)
# it is also used for having a 0 power in the cell corresponding to the water rods.
for ($y=1; $y <= 7; $y++){
  for ($x=1; $x <= 7; $x++){
    for ($j=1; $j <= 3; $j++){
      for ($i=1; $i <= 3; $i++){
        $FApower{$x.$y._.$i.$j} = 0.0 ;
        for ($b=1; $b <= 7; $b++){
          for ($a=1; $a <= 7; $a++){
            $index = $x.$y._.$i.$j._.$a.$b ;
            #print "$index\n" ;
            $cell_power{$index} = 0.0 ;
            $pin_radial{$index} = 0.0 ;
            $pin_powerNN{$index} =0.0 ;
          }
        }
      }
    }
  }
```

```
    }
    my $countvv = 0 ;
    while( $tgv = <TGV_OUT_PIN>){
       if ($tgv =~ /^ PINRECONSTUCTION/){
          $currentpos=tell(TGV_OUT_PIN);
          #print "The current position is $currentpos \n";
          $countvv++;
       }
    }
    # print "$countv $currentpos \n";
    die "X" x 15 ."   fatal error!!!   "."X" x 15 . "\n $0 Can't find more than $countvv
PRINT_FA_POWER_MATRA in TGV-VARIANT output file!\n" if ($countvv ne 1);
    # for each line in VARIANT output after the keyword EDIT_POWER extract the
    # power-shape and the total power (obtained with LU in ERANOS)
    seek(TGV_OUT_PIN, $currentpos, 0); # Sets FILEHANDLE's position.
    while( $tgv = <TGV_OUT_PIN>){
      if ($tgv =~ /^ 'CL_(\d\d)_FA_(\d\d)_PIN_(\d\d)'\s+(\S+) $/){
         $CL = $1 ;
         $FA = $2 ;
         $lattice = $3 ;
         # the hash peak has 0 in the position of the moderator box so the hash cell_power
contains only the fuel pins!
         $cell_power{$CL._.$FA._.$lattice}  = $4 / 10**3 ;
         $pin_powerNN{$CL._.$FA._.$lattice} = $4*$peak{$CL._.$lattice}  ; # this pin power is Not
Normalized (NN)
         #print "in CL $CL, FA $FA, lattice cell $lattice power generated [W] equal to $cell_power
{$CL._.$FA._.$lattice}\n" ;
      }
    }
    close TGV_OUT_PIN ;

    # calculate radial power factor for each rod as needed in MATRA
    # normalize pin power within each FA
    foreach $CL (@EVA, @SH1, @SH2) {
      for ($j=1; $j <= 3; $j++){
        for ($i=1; $i <= 3; $i++){
          $FA_total = 0.0 ;
          for ($b=1; $b <= 7; $b++){
            for ($a=1; $a <= 7; $a++){
              $FA_total = $FA_total + $pin_powerNN{$CL._.$i.$j._.$a.$b}  ;
            }
          }
          $FA_ave = $FA_total / 40 ; # 40 is number of fuel rods to calculate average fuel rod
power in each fuel assembly
          for ($b=1; $b <= 7; $b++){
            for ($a=1; $a <= 7; $a++){
              $pin_radial{$CL._.$i.$j._.$a.$b} = $pin_powerNN{$CL._.$i.$j._.$a.$b} / $FA_ave ;
            }
          }
        }
      }
    }
```

The FA-wise heat flux and axial power shape are obtained from another ERANOS output where only the axial direction has been refined while maintaining FA-wise representation.

```
    # ------------------------------------------------------------------------------
    # Part 3: exctract the axial power shape  and fuel assembly power from VARIANT output (fuel
assembly scale)
    print " $0 -- opening and processing VARIANT output file: $tgvFA.OUT\n" ;
    open(TGV_OUT_FA, "<$tgvFA.OUT") or die "Can't open output file: $tgvFA.OUT $!";
    my $countv = 0 ;
    while( $tgv = <TGV_OUT_FA>){
       if ($tgv =~ /^ PRINT_FA_POWER_MATRA/){
          $currentpos=tell(TGV_OUT_FA);
          #print "The current position is $currentpos \n";
          $countv++;
       }
    }
    # print "$countv $currentpos \n";
    die "X" x 15 ."   fatal error!!!   "."X" x 15 . "\n $0 Can't find more than $countv
PRINT_FA_POWER_MATRA in TGV-VARIANT output file!\n" if ($countv ne 1);
    # for each line in VARIANT output after the keyword EDIT_POWER extract the
    # power-shape and the total power (obtained with LU in ERANOS)
    seek(TGV_OUT_FA, $currentpos, 0); # Sets FILEHANDLE's position.
    while( $tgv = <TGV_OUT_FA>){
       if ($tgv =~ /^\s+\$\$\$\s+POWER_CL_(\d\d)_FA_(\d\d)/){        # starting key word
```

```
        my $CL = $1 ; # the CL number is obtained directly form the output file
        my $FA = $2 ; # the FA number is obtained directly form the output file
        print " found CL $CL FA $FA in VARIANT output\n" ;
        while( $tgv = <TGV_OUT_FA>){
           if ($tgv =~ /^ ' end '\s+'POWER_CL_${CL}_FA_$FA'/){ # ending key word
             $axialzones = $z ; # the number of axial zones is assiged to a dedicated variable
             last;
           }
           elsif ($tgv =~ /\.\s+(\d+)\s+\.\s+\s+([\d\.])+\s+\.\s+(\S+)/){
              $z = $1 ;
              $powershape{$CL._.$FA._.$z} = $3 ;
           }
           elsif ($tgv =~ /^ ->TOTAL_POWER\s+(\S+) $/){
              $FApower{$CL._.$FA} = $1 ;
              $FAheatflux{$CL._.$FA} = $1  / ($pi * $COD * $length * $rods * 1000) ;
              #print "in CL $region total power equal to $FApower{$CL._.$FA} W \n" ;
           }
        }
      }
   }
   close TGV_OUT_FA ;
```

MATRA needs an average power shape, which has to be normalized to sum to unity, and the relative axial position. In addition, in SH1 it is necessary to flip the axial power shape to account for downward flow.

```
   # ------------------------------------------------------------------------------
   # calculate the axial power shape and axial position formated for MATRA
   # calculate local to average heat flux ratio in EVA and SH2 needed for MATRA
   foreach $CL (@EVA, @SH2) {
     for ($j = 1; $j <= 3; $j++){
       for ($i = 1; $i <= 3; $i++){
         # calculate sum of powershape over the axial zones
         # to normalize, the sum of the power densities is needed while the FA power is available
         my $tmp = 0.0 ;
         for ($z = 1; $z <= $axialzones; $z++){
             $tmp = $tmp + $powershape{$CL._.$i.$j._.$z} ;
         }
         # local to average power ratio (the ratio is independent of the units: power density,
heat flux or power)
         for ($z = 1; $z <= $axialzones; $z++){
           $powerratio{$CL._.$i.$j._.$z} = $powershape{$CL._.$i.$j._.$z} / $tmp * $axialzones ;
           #printf(" %9.7f\n","$powerratio{$CL._.$i.$j._.$z}") ;
         }
        #print "\n";
        }
      }
   }
   # calculate local to average heat flux ratio in SH1 (flip axial power shape) needed for MATRA
   foreach $CL (@SH1) {
     for ($j = 1; $j <= 3; $j++){
       for ($i = 1; $i <= 3; $i++){
         # calculate sum of powershape over the axial zones
         my $tmp = 0.0 ;
         for ($z = 1; $z <= $axialzones; $z++){
             $tmp = $tmp + $powershape{$CL._.$i.$j._.$z} ;
         }
         # local to average power ratio (the ratio is independent of the units: power density,
heat flux or power)
         # flip the axial power shape
         my $zz = $axialzones ;
         for ($z = 1; $z <= $axialzones; $z++){
           $powerratio{$CL._.$i.$j._.$z} = $powershape{$CL._.$i.$j._.$zz} / $tmp * $axialzones ;
           #printf(" %9.7f\n","$powerratio{$CL._.$i.$j._.$z}") ;
           $zz-- ;
         }
        #print "\n";
        }
      }
   }
   $SETRI31{1}=0 ; # Y(L) in SETRI 3.1 must include 0 and 1
   for ($z = 2; $z <= $axialzones; $z++){
     my $zz = $z -1 ;
     $SETRI31{$z} = $SETRI31{$zz} + (1 /($axialzones-1));
   }
```

The TRACE output file has to be processed to locate, beside the mass flow rate of each FA, the inlet temperatures of the 3 core regions, i.e. of the mixing chambers, which have to be assigned to the respective FAs.

```
   # ------------------------------------------------------------------------------
   # Part 4: find mass flow rate for each FA and inlet temperature for each core part (EVA, SH1,
SH2) in trace output
   print " $0 -- opening and processing TRACE ouptut file: $trace.out \n" ;
   open(TRACE_OUT, "<$trace.out")  or die "Can't open output file: $trace.out $!";
   # get the position of /trac large edit/ in the output file
   my $countt=0 ;
   while(my $line = <TRACE_OUT>){
      if ($line =~ /^ trac large edit/){
         $currentpos=tell(TRACE_OUT);
         #print "The current position is $currentpos \n";
         $countt++;
      }
   }
   # print "$countt $currentpos \n";
   die "X" x 15 ."   fatal error!!!   "."X" x 15 . "\n $0 Can't find more than $countt trac large
 edit!\n" if ($countt<=1);
   # search for each cluster in 1/8 of the core and extract TH data from TRACE out
      seek(TRACE_OUT, $currentpos, 0); # Sets FILEHANDLE's position.
      # for each line of TRACE output search the key words
      while( $line = <TRACE_OUT>){
         # get the coolant temperature and density
         if ($line =~ / coolant channel CL (\d\d) FA (\d\d)/){ # starting key word
            $CL = $1 ;
            $FA = $2 ;
            #print " $0 -- in CL $CL FA $FA found coolant channel\n";
            my $z = 1 ;
            while( $line = <TRACE_OUT>){
               #if ($line =~ /^ total power/){          # ending key word
               if ($line =~ /dis.sol. p.o.sol. fr.new if.drag   temp.ss.  evap.     cond.    mfw.
liq.  mfw.vap.   velt.liq   velt.gas  wf.gas/){
                 # read two more lines
                 $line = <TRACE_OUT> ;
                 $line = <TRACE_OUT> ;
                 # search for the lines with the proper format
                 if ($line =~ /^\s+(\d+)\s(\S+)\s+(\S+)\s+(\S+)\s+(\S+)\s+(\S+)\s+(\S+)\s+(\S+)\s+(\S+)\
s+(\S+)\s+(\S+)\s+(\S+)\s+(\S+)/){
                 #  print $line ;
                 $mfw{$CL._.$FA}  = $9 / $flowarea ; # [kg/m2 s]
                 printf(" inlet mass flow of CL %s FA %s is %7.2f\n","$CL","$FA","$mfw{$CL._.$FA
}") ;
                 last;
                 }
               }
            }
         }
         if ($line =~ /mixing chamber ([ES][VH][A12]) inlet/){
           $part=$1 ;
           while( $line = <TRACE_OUT>){
             # get temperature in cell 2: for EVA this is the only cell with the correct
temperature!
             if ($line =~ /^\s+2\s(\S+)\s+(\S+)\s+(\S+)\s+(\S+)\s+(\S+)\s+(\S+)\s+(\S+)\s+(\S+)\s
+(\S+)\s+(\S+)\s+(\S+)$/){
               # print $line ;
               $inlettemp{$part}    = $6 - 273.15 ; # temperature in degree C
               printf(" inlet temperature in %s is %7.2f\n","$part","$inlettemp{$part}") ;
               last ;
             }
           }
         }
   }
   close TRACE_OUT ;
   # associate to hashes the inlet temperature of the various regions
   foreach $CL (@EVA) {
           $inlettemp{$CL} =$inlettemp{EVA} ;
   }
   foreach $CL (@SH1) {
           $inlettemp{$CL} =$inlettemp{SH1} ;
   }
   foreach $CL (@SH2) {
           $inlettemp{$CL} =$inlettemp{SH2} ;
   }
```

The prepared skeleton file for MATRA has to be modified including the necessary data. In the present implementation, an input file for each CL has been prepared, it contains 9 parts (kase).

A different skeleton file is used for SH1 to provide correct representation of the wire effect for downward flow changing the `DUR(K)` parameters, the axial power shape has to be flipped as shown before.

The skeleton file modification is generally achieved replacing user selected keywords but also with dedicated formatting which is highly problem and code dependent.

```
# ------------------------------------------------------------------------
# Part 5: modify MATRA skeleton file
print " $0 -- opening MATRA skeleton file \n" ;
open(SKELETON ,"<$matra") or die "Can't open MATRA SKELETON: $matra $!" ;
foreach $CL (@EVA, @SH2) {
  seek(SKELETON, 0, 0 ) ; # Sets FILEHANDLE's position.
  open(OUT, ">matra_CL_$CL.inp") or die "Can't open  MATRA new input file: matra_$CL.inp $!";
  for ($j = 1; $j <= 3; $j++){
    for ($i = 1; $i <= 3; $i++){
      while( <SKELETON> ){
         if (/^!/){ # skip commented lines
           print OUT ;
           next ;
         }
         if (/^0/){ # end of case in matra input => end of fuel assembly
           print " Finished CL $CL FA $i$j\n" ;
           print OUT ;
           last ;
         }
         s/KASE/$CL$i$j/ ;
         s/zone/CL_$CL\_FA$i$j/ ;
         s/     HIN/sprintf("%8.1f",$inlettemp{$CL})/e ;
         s/     GIN/sprintf("%8.3f",$mfw{$CL._.$i.$j})/e ;
         s/   AFLUX/sprintf("%8.3f",$FAheatflux{$CL._.$i.$j})/e ;
         s/RADIAL  1/sprintf("%9.6f",$pin_radial{$CL._.$i.$j.'_17'})/e;
         s/RADIAL  2/sprintf("%9.6f",$pin_radial{$CL._.$i.$j.'_27'})/e;
         s/RADIAL  3/sprintf("%9.6f",$pin_radial{$CL._.$i.$j.'_37'})/e;
         s/RADIAL  4/sprintf("%9.6f",$pin_radial{$CL._.$i.$j.'_47'})/e;
         s/RADIAL  5/sprintf("%9.6f",$pin_radial{$CL._.$i.$j.'_57'})/e;
         s/RADIAL  6/sprintf("%9.6f",$pin_radial{$CL._.$i.$j.'_67'})/e;
         s/RADIAL  7/sprintf("%9.6f",$pin_radial{$CL._.$i.$j.'_77'})/e;
         s/RADIAL  8/sprintf("%9.6f",$pin_radial{$CL._.$i.$j.'_16'})/e;
         s/RADIAL  9/sprintf("%9.6f",$pin_radial{$CL._.$i.$j.'_26'})/e;
         s/RADIAL 10/sprintf("%9.6f",$pin_radial{$CL._.$i.$j.'_36'})/e;
         s/RADIAL 11/sprintf("%9.6f",$pin_radial{$CL._.$i.$j.'_46'})/e;
         s/RADIAL 12/sprintf("%9.6f",$pin_radial{$CL._.$i.$j.'_56'})/e;
         s/RADIAL 13/sprintf("%9.6f",$pin_radial{$CL._.$i.$j.'_66'})/e;
         s/RADIAL 14/sprintf("%9.6f",$pin_radial{$CL._.$i.$j.'_76'})/e;
         s/RADIAL 15/sprintf("%9.6f",$pin_radial{$CL._.$i.$j.'_15'})/e;
         s/RADIAL 16/sprintf("%9.6f",$pin_radial{$CL._.$i.$j.'_25'})/e;
         s/RADIAL 17/sprintf("%9.6f",$pin_radial{$CL._.$i.$j.'_65'})/e;
         s/RADIAL 18/sprintf("%9.6f",$pin_radial{$CL._.$i.$j.'_75'})/e;
         s/RADIAL 19/sprintf("%9.6f",$pin_radial{$CL._.$i.$j.'_14'})/e;
         s/RADIAL 20/sprintf("%9.6f",$pin_radial{$CL._.$i.$j.'_24'})/e;
         s/RADIAL 21/sprintf("%9.6f",$pin_radial{$CL._.$i.$j.'_64'})/e;
         s/RADIAL 22/sprintf("%9.6f",$pin_radial{$CL._.$i.$j.'_74'})/e;
         s/RADIAL 23/sprintf("%9.6f",$pin_radial{$CL._.$i.$j.'_13'})/e;
         s/RADIAL 24/sprintf("%9.6f",$pin_radial{$CL._.$i.$j.'_23'})/e;
         s/RADIAL 25/sprintf("%9.6f",$pin_radial{$CL._.$i.$j.'_63'})/e;
         s/RADIAL 26/sprintf("%9.6f",$pin_radial{$CL._.$i.$j.'_73'})/e;
         s/RADIAL 27/sprintf("%9.6f",$pin_radial{$CL._.$i.$j.'_12'})/e;
         s/RADIAL 28/sprintf("%9.6f",$pin_radial{$CL._.$i.$j.'_22'})/e;
         s/RADIAL 29/sprintf("%9.6f",$pin_radial{$CL._.$i.$j.'_32'})/e;
         s/RADIAL 30/sprintf("%9.6f",$pin_radial{$CL._.$i.$j.'_42'})/e;
         s/RADIAL 31/sprintf("%9.6f",$pin_radial{$CL._.$i.$j.'_52'})/e;
         s/RADIAL 32/sprintf("%9.6f",$pin_radial{$CL._.$i.$j.'_62'})/e;
         s/RADIAL 33/sprintf("%9.6f",$pin_radial{$CL._.$i.$j.'_72'})/e;
         s/RADIAL 34/sprintf("%9.6f",$pin_radial{$CL._.$i.$j.'_11'})/e;
         s/RADIAL 35/sprintf("%9.6f",$pin_radial{$CL._.$i.$j.'_21'})/e;
         s/RADIAL 36/sprintf("%9.6f",$pin_radial{$CL._.$i.$j.'_31'})/e;
         s/RADIAL 37/sprintf("%9.6f",$pin_radial{$CL._.$i.$j.'_41'})/e;
         s/RADIAL 38/sprintf("%9.6f",$pin_radial{$CL._.$i.$j.'_51'})/e;
         s/RADIAL 39/sprintf("%9.6f",$pin_radial{$CL._.$i.$j.'_61'})/e;
         s/RADIAL 40/sprintf("%9.6f",$pin_radial{$CL._.$i.$j.'_71'})/e;
  #        the axial subdivision is highly problem dependent, it is necessary to rewrite it when
changing axial nodalization
```

```
            if (/      Y\(L\)  Axial\(L\)/){
              for ($z = 1; $z <= $axialzones-3; $z=$z+5){
                my $z1= $z + 1 ;
                my $z2= $z + 2 ;
                my $z3= $z + 3 ;
                my $z4= $z + 4 ;
                $SETRI31_line = sprintf("    %6.4f %9.7f    %6.4f %9.7f    %6.4f %9.7f    %6.4f
%9.7f    %6.4f %9.7f\n", $SETRI31{$z}, $powerratio{$CL._.$i.$j._.$z}, $SETRI31{$z1}, $powerratio{
$CL._.$i.$j._.$z1}, $SETRI31{$z2}, $powerratio{$CL._.$i.$j._.$z2}, $SETRI31{$z3}, $powerratio{$CL.
_.$i.$j._.$z3}, $SETRI31{$z4}, $powerratio{$CL._.$i.$j._.$z4});
                print OUT $SETRI31_line  ;
              }
              $z =$axialzones-2 ;
              my $z1= $z + 1 ;
              my $z2= $z + 2 ;
              $SETRI31_line = sprintf("    %6.4f %9.7f    %6.4f %9.7f    %6.4f %9.7f\n", $SETRI31
{$z}, $powerratio{$CL._.$i.$j._.$z}, $SETRI31{$z1}, $powerratio{$CL._.$i.$j._.$z1}, $SETRI31{$z2},
 $powerratio{$CL._.$i.$j._.$z2});
              print OUT $SETRI31_line  ;
            next ;
            }
            print OUT ;
          }
    #    print " next FA \n" ;
        }
      }
     print OUT "\n"  ; # the input file must include a final empty line
     close OUT ;
    }
```

B.7 Loops in the ERANOS user language

The extraction of the power traverses in the considered 22 CL times 9 FA (times 49 when going to cell spatial resolution) may be extremely tedious and error prone. For this reason it was decided to apply the ERANOS user language to loop over the considered rectangular mesh. This procedure allow great flexibility, covering different spatial scales and permitting, changing only few lines, to extract other data of interest, e.g. the total flux. In addition, post-processing keywords can easily be printed using the mapping schema and the total power of each FA (in this example) is automatically calculated summing all axial power densities.

It was decided to print only one eighth of the core, hence the Y index is incremented from 1 to 5 (less than 6) and the X index is incremented from 1 to XMAX being XMAX dependent on Y. Once the position of each of the 22 CLs has been identified, an inner for loop is used to span the 3 by 3 FA. The content of the power traverse is assigned to a temporary array DATA, and the total power of each FA is obtained summing the power traverse and multiplying by the volume of one axial mesh.

```
->EDIT_POWER ;
->Y 1 ;
!   extract the flux traverse in each  fuel cluster
TANTQUE (Y<6) ;
  ->X (Y) ;
  SI (Y<4) ;         ->XMAX 8 ;
    SINONSI (Y=4) ; ->XMAX 7 ;
    SINONSI (Y=5) ; ->XMAX 6 ;
  FINSI ;
  TANTQUE (X<XMAX) ;
    * ' printing fuel assemblies in cluster ' (CAR(X)/CAR(Y)) ;
    !   extract the flux traverse in each fuel assembly
    POUR ->J 1 2 3;
    POUR ->I 1 2 3;
      ->JJ (J-1);
      ->II (I-1);
      EXTRACTION_TRAVERSE_FLUX
      FLUX (FLUX_BUILT) GEOMETRIE (CORE_GEOM)
           ->CL Z (24.756*(X-1)+8.252*(II)) (24.756*(Y-1)+8.252*(JJ))   0.0
                  (24.756*(X-1)+8.252*(I))  (24.756*(Y-1)+8.252*(J))  420.0 ;
      !   calculate the power traverse
```

```
      TRAITEMENT_TRAVERSE TRAVERSE_EXTRAITE (CL)
           ->CL_POWER TAUX MACRO (MACRO_ECCO) 'POWER' TOTAL ;
      !   print the axial power traverse
 EDITION_TRAVERSE ('POWER_CL_'/CAR(X)/CAR(Y)/'_FA_'/CAR(I)/CAR(J)) (CL_POWER) ;
      !   calculate the total power generated in each Fuel Assembly
      (CL_POWER) PTRCD TRVAL ->DATA;
      ->TOTAL_POWER ((SOMME(DATA))*(8.252*8.252*20)) ;
      * TOTAL_POWER ;
      !   print keyword for post-processing
      * ' end ' ('POWER_CL_'/CAR(X)/CAR(Y)/'_FA_'/CAR(I)/CAR(J));
      !   delete the temporary variables
      / (CL) (CL_POWER) ; / DATA TOTAL_POWER ;
    FINPOUR;
    FINPOUR;
    * ' end fuel assemblies in cluster ' (CAR(X)/CAR(Y)) ;
    ->X (X+1) ;
  FINTANTQUE ;
  ->Y (Y+1) ;
FINTANTQUE ;

(EDIT_POWER) ;
```

To reduce the number of files handled in the coupled solution, a procedure has been developed with the ERANOS user language to include all axial zones of each CL in one input file. This procedure is listed here: it passes the combination of the TH parameters for each axial zones to the procedure `HPLWR`, which contains the ECCO calculation procedure, and is obtained with the presented print statements of the `TRACE2ECCO.pl` script.

```
PROC ->EXECUTION
       ECCO_HPLWR
;

* ' Define vectors of Thermal Hydraulic conditions ';
-> tempC  600  611  625  638  647  654  657  658  659  661  662  664  666  668
          670  673  675  678  679  681  681 ;
-> tempM  590  590  590  589  588  587  585  584  582  580  579  577  575  573
          571  569  566  564  561  559  556 ;
-> tempG  589  589  589  588  587  586  584  583  581  580  578  576  574  572
          570  568  566  564  561  559  556 ;
-> tempF  875 1176 1405 1538 1570 1533 1463 1384 1313 1249 1194 1145 1100 1059
         1018  977  933  888  838  787  735 ;
-> denC 0.68971 0.66104 0.62089 0.57161 0.51511 0.45462 0.39591 0.34368 0.30343
        0.27013 0.24386 0.22284 0.20582 0.19199 0.18072 0.17168 0.16450 0.15900
        0.15506 0.15259 0.15156 ;
-> denM 0.71049 0.71089 0.71179 0.71326 0.71533 0.71783 0.72070 0.72372 0.72689
        0.73012 0.73346 0.73688 0.74039 0.74400 0.74773 0.75162 0.75562 0.75974
        0.76398 0.76837 0.77278 ;
-> denG 0.71249 0.71289 0.71379 0.71526 0.71726 0.71972 0.72250 0.72542 0.72849
        0.73160 0.73482 0.73813 0.74150 0.74502 0.74863 0.75242 0.75627 0.76029
        0.76437 0.76860 0.77292 ;

POUR ->I REP(tempC());
ECCO_HPLWR
       denC(I)
       denM(I)
       denG(I)
       tempC(I)
       tempM(I)
       tempG(I)
       tempF(I)
       (I)
;
FINPOUR;
FINPROC;
! ------------------------------------------------------------------------

EXECUTION;
```

B.8 Scripts for graphical representation

To easily generate the 3D plots shown in the thesis, few additional lines have been added to the Perl script `TRACE2ECCO.pl` to generate the XYZ scattered data required by Tecplot 360 [146] including also a dedicated header. The XYZ indexes are converted to the corresponding dimensions in cm.

```
# set geometrical dimension
$meshxy = 8.252  ;
$meshz  = 20 ;
# print tecplot header
print TH_DATA_3D 'TITLE     = "TH parameters" '."\n";
print TH_DATA_3D 'FILETYPE  = FULL '."\n";
print TH_DATA_3D 'VARIABLES = "X [cm]" "Y [cm]" "Z [cm]" "Coolant [K]" "Moderator [K]" "Gap
water [K]" "FPC [K]" "Clad [K]" "[kW/m]"'."\n";
print TH_DATA_3D 'ZONE T="HPLWR CORE", ZONETYPE=ORDERED, DATAPACKING=POINT'."\n";
print TH_DATA_3D "     I=21, J=21, K=$axial \n";
# print axial slices of all TH data
$ZZ = $meshz / 2 ;  # set ZZ position
for ($z=1; $z <= $axial ; $z++){
  $YY = $meshxy / 2 ; # set YY position
  for ($y = 1; $y <= 7; $y++){
    for ($j = 1; $j <= 3; $j++){
      $XX = $meshxy / 2  ; # set XX position
      for ($x = 1; $x <= 7; $x++){
        for ($i = 1; $i <= 3; $i++){
          printf TH_DATA_3D "%6.2f %6.2f %6.2f %6.1f %6.1f %6.1f %6.1f %6.1f %5.2f\n", "$XX",
"$YY", "$ZZ", "$tempC{$x.$y.'_'.$i.$j.'_'.$z}", "$tempM{$x.$y.'_'.$i.$j.'_'.$z}", "$tempG{$x.$y.'_
'.$i.$j.'_'.$z}", "$tempF0{$x.$y.'_'.$i.$j.'_'.$z}", "$tempClad{$x.$y.'_'.$i.$j.'_'.$z}", "$power{
$x.$y.'_'.$i.$j.'_'.$z}" ;
          $XX = $XX + $meshxy; # increment XX counter
        }
      }
      $YY = $YY + $meshxy ; # increment YY counter
    }
  }
$ZZ = $ZZ + $meshz ; # increment ZZ counter
print TH_DATA_3D "\n"  ; # print blanck line between axial slices
}
close TH_DATA_3D ;
```

Also the Perl script which extract the TH data of all considered fuel rods from the 22 MATRA output files and print them in the XYZ scattered data format is given below. This kind of tool is extremely important for the qualitative analyses of the obtained results and to identify the position of critical parameters, e.g. clad temperature or linear power, for a successive, quantitative analysis of the corresponding output file.

```
#!/usr/bin/perl -w
# ------------------------------------------------------------------------
#      Author: Lanfranco.Monti@iket.fzk.de
#        Date: 06/26/2009
# Description: this script extracts clad and fuel temperature as well as
#              heat flux (converted to linear power) for all fuel rods
#              the code process the 22 output files for the 22 clusters
#              they are named MATRA_CL_xy.out
# Usage: no argument are given to the perl script!
#
# ------------------------------------------------------------------------

print "-" x 50 ."\n $0 execution started!!!\n"."-" x 50 ."\n" ;

# subdivision of CL numbers in the 3 regions - XY indexes
my @EVA = ( 11, 21, 31, 41, 22, 32, 42, 33);
my @SH1 = ( 51, 61, 52, 62, 53, 43, 44);
my @SH2 = ( 71, 72, 73, 63, 64, 54, 55) ;
my @FAS = (11, 12, 13, 21, 22, 23, 31, 32, 33);
# geometrical dimension and parameters
my $pi       = 3.141593 ;  # from open office
my $COD      = 0.008 ;     # [m] Clad Outside Diameter
my $rods     = 40 ;        # number of fuel rods
my $length   = 4.2 ;       # [m] active length
my $flowarea = 1830.9e-6 ; # [m2] flow area (nominal value - no wire)
my $meshxy = 8.252 / 7 ;
```

```
my $meshz  = 2.5 ;


foreach $region (@EVA, @SH1, @SH2) {
  print " $0 -- opening MATRA ouptut file: matra_$region.out \n";
  open(MATRA_OUT, "<matra_CL_$region.out") or die "Can't open  MATRA output file:
matra_$region.out $!";
  seek(MATRA_OUT,0,0);
  CASE: while( $line = <MATRA_OUT>){
    if ( $line =~ / R O D     R E S U L T S/) {
      print " R O D     R E S U L T S found \n" ;
      while( $line = <MATRA_OUT>){
        if ( $line =~ /^ Case  \d\d\d\d                CL_(\d\d)_FA(\d\d)/) {
          my $CL = $1 ;
          my $FA = $2 ;
          print "CL $CL FA $FA found \n" ;
          ROD: while( $line = <MATRA_OUT>){
            if ( $line =~ /^ Results for Rod\s+(\d+)/){
              my $rod = $1 ; # identify rod number
              $z = 1 ;    # initialize axial position to 1
            while( $line = <MATRA_OUT>){
              if ($line =~ /End of Case/){ # end of fuel assembly output
                print " exiting FA $FA in CL $CL\n";
                next CASE ;                # go to next "R O D  R E S U L T S" for next fuel
assembly
              }
              if ($line =~ /^ Case/){      # end of individual rod output
                print " exiting rod $rod in FA $FA in CL $CL\n";
                next ROD ;                 # go to next "Results for Rod" for the same fuel
assembly
              }
              elsif ($line =~ /^\s+(\S+)\s-\s+\S+\s+(\S+)\s+1\s+0\s+\S+\s+(\S)+\s+(\S+)\s+\S+\
s+(\S+)/){
                                  #     1          2     3      4   5    6     7       8       9
    10
    #   Axial Zone     Heat Flux   Type   Mode    Hsurf  |  Fluid     Clad    T( 1)    T( 2)
    #       (mm)         (kW/m2)                (kW/m2-C)                  (1.0000) (0.0000)
    #  0.00 -   25.00    151.27      1      0     22.721   317.30   323.95   394.09   522.83
    #  1        2         3          4      5     6        7        8        9        10
                    $heatfl{$CL._.$FA._.$rod._.$z} = $2 * $pi * $COD  ; # is linear power [kW/m
]
                   $cladtmp{$CL._.$FA._.$rod._.$z} = $4 + 273.15 ;
                   $fueltmp{$CL._.$FA._.$rod._.$z} = $5 + 273.15 ;
                   $z = $z + 1;
                 }
              }
            }
          }
        }
      }
    }
  }
  close MATRA_OUT ;
  }
  $axial = $z - 1 ;

  # initialize the array with all 0
  # this is needed to print the XY core power map with 0 in the non sub-channel nodes (as needed
 in tecplot or matlab)
  # it is also used for having a temperature 0 in the points which do not represent a sub-
channel
  for ($y=1; $y <= 7; $y++){
    for ($x=1; $x <= 7; $x++){
      for ($j=1; $j <= 3; $j++){
        for ($i=1; $i <= 3; $i++){
          for ($b=1; $b <= 8; $b++){
            for ($a=1; $a <= 8; $a++){
              for ($z=1; $z <= $axial ; $z++){
                $index = $x.$y.'_'.$i.$j.'_'.$a.$b.'_'.$z ;
                $heatflux{$index} = 0.0 ;
                $fueltemperature{$index} = 0.0 ;
                $cladtemperature{$index} = 0.0 ;
              }
            }
          }
        }
      }
```

```
96    }
97  }
98
99  # move from rod index  in [1;40] to ab position a,b in [1,7] Cartesian geometry
100 for ($z = 1; $z <= $axial; $z++){
101   foreach $CL (@EVA, @SH2) {
102     foreach $FA (@FAS) {
103       $rod = 1 ;
104       for ($b = 7; $b >= 1; $b--){
105         if ( $b < 3 or $b > 5)    { @A = (1, 2, 3, 4, 5, 6, 7); }
106         if ( $b >= 3 and $b <= 5) { @A = (1, 2,          6, 7); }
107         foreach $a (@A) {
108                 #print "$a$b associated to $rod \n";
109                       $heatflux{$CL._.$FA._.$a.$b._.$z} =  $heatfl{$CL._.$FA._.$rod._.$z} ;
110                 $fueltemperature{$CL._.$FA._.$a.$b._.$z} = $fueltmp{$CL._.$FA._.$rod._.$z} ;
111                 $cladtemperature{$CL._.$FA._.$a.$b._.$z} = $cladtmp{$CL._.$FA._.$rod._.$z} ;
112                 $rod = $rod+1 ;
113         }
114       }
115     }
116   }
117 }
118 # for SH1 flip the data upside down (downward flow)
119 my $zz = $axial ;
120 for ($z = 1; $z <= $axial; $z++){
121   foreach $CL (@SH1) {
122     foreach $FA (@FAS) {
123       $rod = 1 ;
124       for ($b = 7; $b >= 1; $b--){
125         if ( $b < 3 or $b > 5)    { @A = (1, 2, 3, 4, 5, 6, 7); }
126         if ( $b >= 3 and $b <= 5) { @A = (1, 2,          6, 7); }
127         foreach $a (@A) {
128                 #print "$a$b associated to $rod \n";
129                       $heatflux{$CL._.$FA._.$a.$b._.$z} =  $heatfl{$CL._.$FA._.$rod._.$zz} ;
130                 $fueltemperature{$CL._.$FA._.$a.$b._.$z} = $fueltmp{$CL._.$FA._.$rod._.$zz} ;
131                 $cladtemperature{$CL._.$FA._.$a.$b._.$z} = $cladtmp{$CL._.$FA._.$rod._.$zz} ;
132                 $rod++ ;
133         }
134       }
135     }
136   }
137 $zz-- ;
138 }
139
140 # set geometrical dimension
141 open(OUT, ">fuelrods_tec360.dat") ;
142 print OUT 'TITLE     = "STRUCTURE TEMPERATURE" '."\n";
143 print OUT 'FILETYPE  = FULL '."\n";
144 print OUT 'VARIABLES = "X [cm]" "Y [cm]" "Z [cm]" "CLAD [K]" "FUEL [K]" "[kW/m]"'."\n";
145 print OUT 'ZONE T="HPLWR CORE", ZONETYPE=ORDERED, DATAPACKING=POINT, VARLOCATION=([4,5,6]=
NODAL) '."\n";
146 print OUT '      I=147, J=105, K=168 '."\n";
147
148 # print a column with the power in CL xy FA ij fuel pin ab at position z
149 # print axial slices
150 # print only 1/8 of the core (y<=5)
151 $ZZ = $meshz / 2 ;  # set ZZ position
152 for ($z=1; $z <= $axial ; $z++){
153   $YY = $meshxy / 2 ; # set YY position
154   for ($y = 1; $y <= 5; $y++){
155     for ($j = 1; $j <= 3; $j++){
156       for ($b = 1; $b <= 7; $b++){
157           $XX = $meshxy / 2  ; # set XX position
158         for ($x = 1; $x <= 7; $x++){
159           for ($i = 1; $i <= 3; $i++){
160             for ($a = 1; $a <= 7; $a++){
161               printf OUT ("%7.3f %7.3f %6.2f %6.1f %6.1f %5.2f\n", "$XX", "$YY", "$ZZ", "
$cladtemperature{$x.$y.'_'.$i.$j.'_'.$a.$b.'_'.$z}", "$fueltemperature{$x.$y.'_'.$i.$j.'_'.$a.$b.'
_'.$z}", "$heatflux{$x.$y.'_'.$i.$j.'_'.$a.$b.'_'.$z}");
162               $XX = $XX + $meshxy; # increment XX counter
163             }
164           }
165         }
166         #print "\n";
167       $YY = $YY + $meshxy ; # increment YY counter
168       }
169     }
```

```
170   }
171 $ZZ = $ZZ + $meshz ; # increment ZZ counter
172 #print OUT "\n"  ; # print blanck line between axial slices
173 }
174
175 print "-" x 50 ."\n $0 execution completed!!!\n"."-" x 50 ."\n" ;
176
177 __END__
```

Appendix C

Geometrical and material data

A detailed list of geometrical and material data used for the presented simulations is essential to permit results reproducibility and, hence, it is provided here. The precision of all dimensions is only associated to the numerical models used and is not based on design requirements.

Only one core geometry has been considered while two different FA designs have been used: solid stainless steel [57] and insulated boxes [51], Figure C.1 and C.2, respectively. The limited modeling capabilities of the selected codes required to develop several models introducing assumptions and simplifications which are described in the following sections.

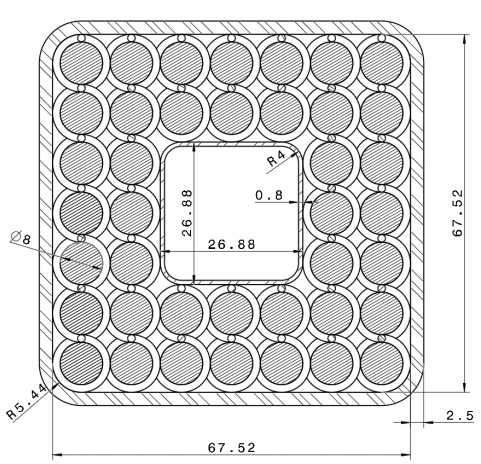

Figure C.1: FA with solid SS boxes

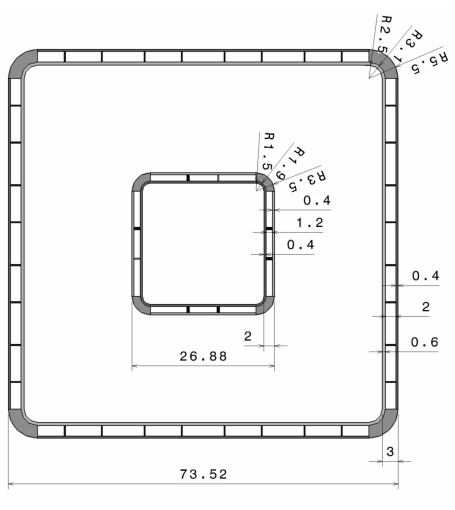

Figure C.2: FA with insulated boxes

C.1 Fuel assembly model

ERANOS

The cell geometry used with ECCO/ERANOS has been described previously in Figure 2.5 on page 23. One half of the gap region between adjacent FAs is included in the considered FA cell model whose lateral dimension is 8.252 cm. All results presented in section 2.1 have been obtained using the solid stainless steel boxes whereas those in chapter 4 are for the insulated boxes. Both geometries are used in Appendix A.

The two design proposals use the same fuel rod lattice, the exact dimensions are given in Table 2.1 on page 19 while the modeled one in Table C.1, and only the material compositions and dimensions of the water rods and of the FA box are modified in the ECCO input files. The

fuel used is UO_2 with two different enrichments of ^{235}U: 4 wt% for the four pins at the corners of the assembly and 5 wt% for the other 36 pins [57].

The presence of the wire wraps, evident in Figure C.1, reduces the amount of coolant and increases that of structural material in the fuel assembly and hence should be taken in account. To do so, an equivalent clad outside diameter is introduced: to have the proper structural material volume fraction in the assembly, the area obtained by adding to the clad cross section area that of the wire (there is one wire for each fuel rod and its XY area is not a circle) must be preserved: hence the clad outside diameter is increased to 8.113 mm.

The gas-filled gap between the fuel pellet and the clad is not represented because it has a negligible effect on the neutronics but it further complicates the geometry and hence the computational time required. Assuming the clad inside diameter equal to the fuel pellet diameter, 6.7 mm, the increase of the clad volume requires to introduce a clad smear density equal to 80.36% of the nominal one.

Table C.1: Modeled fuel rods lattice (summary)

	Fuel	Clad	Coolant
inside diameter [mm]	0.0	6.70	
outside diameter [mm]	6.70	8.113	
material	UO_2	SS-316	H_2O
density [g/cm^3]	10.97	6.43	depends on TH feedbacks

The uranium dioxide density is assumed equal to 10.97 g/cm^3 [156] and independent of fuel temperature because the total mass of the fuel pellet is given and hence the thermal expansion does not cause any reduction of the fuel material in the core. The clad and solid stainless steel boxes material is the SS-316 alloy which has a nominal mass density of 8.0 g/cm^3, its atomic composition is given in Table C.2. Also the mass density of SS-347, used in the insulated boxes, is assumed to be 8.0 g/cm^3, its atomic composition is given in Table C.3. All elements have natural isotopic composition [156]. The isotopic composition of uranium dioxide, water and Al_2O_3 is stoichiometric. The mass density of Al_2O_3 is assumed to be 6.0 g/cm^3, i.e. the nominal density of 2.1 g/cm^3 divided by a porosity of 0.35.

Table C.2: SS-316 Atomic Composition [wt%]

Manganese	1.860
Iron	68.327
Silicon	0.650
Copper	0.240
Nickel	10.120
Chromium	16.620
Molybdenum	2.060

Table C.3: SS-347 Atomic Composition [wt%]

Manganese	2.0
Iron	69.0
Silicon	1.0
Nickel	11.0
Chromium	17.0

Some elements with extremely small concentration have been omitted.

The FA box is modeled as a rectangular one without representing the round corners, as shown in Figure 2.5 on page 23. For this reason, the dimensions the FA box should be slightly adjusted with respect to the real geometry to preserve the total mass of structural material, Table C.4.

The insulated boxes are composed of SS-347, Al_2O_3 and water, their fraction depends on the considered region of the boxes. The density of the water is a function of its temperature and is changed by the TH feedbacks during the coupled analysis. The solid corners of the FA box and the two liners, depicted in Figure C.2, are made of SS-347 and are smeared together with the honeycomb structure; this results in the following volume fractions: SS-347 is 39.42% while the

Table C.4: Adjusted dimensions of the rectangular FA boxes to preserve the volume fraction of the components, Figure 2.5 on page 23

	SS-316 boxes	insulated boxes
Inner side length [mm]	67.33	67.48
Box thickness [mm]	4.82	5.86
Gap between assemblies [mm]	10.37	9.18

honeycomb structure is 60.58%. The honeycomb structure is further divided in the following volume fractions: 60.45% is Al_2O_3, 7.0% is SS-347 and the remaining 32.55% is gap water.

The "Mixed Geometry" model, Figure 2.5 on page 23 and 2.2(e) on page 21, has been applied also to represent the moderator box of both FA geometries, the dimensions are listed in Table C.5. The material corresponding to the "lateral box rod" region has the following volumetric composition: 60.0% honeycomb structure and 40.0% SS-347. The one of the "corner box material" region is composed as follow: 43.6% honeycomb structure and 56.4% SS-347.

Table C.5: Radius of the water rods for the "Mixed Geometry" Figure 2.2(e) on page 21

	SS-316 boxes	insulated boxes
Coolant water rod (lateral cells) [mm]	1.471	1.471
Lateral box rod (lateral cells) [mm]	2.137	2.859
Moderator water (lateral cells)	smeared	smeared
Moderator water rod (corner cells) [mm]	4.389	3.771
Coolant water (corner cells) [mm]	smeared (57.75%)	4.3840
Corner box material (corner cells)	smeared (42.25%)	smeared

The regions which are "smeared" occupy the remaining portion of the lattice cell, which is a square of 9.44 mm side length. In parentheses is given the volume fraction for the smearing.

TRACE

The 3 water flow paths (for coolant and moderator water, which is flowing both in the moderator channel and in the gap between adjacent FAs) are modeled with 3 equivalent pipes whose dimensions are given in Table C.6. The dimensions of the coolant pipe have been calculated accounting for the wire wrap presence, evident in Figure C.1, which reduces the coolant flow area and increases the wetted perimeter.

Table C.6: FA representation: pipes geometry

	solid SS boxes			insulated boxes		
	coolant	moderator	gap	coolant	moderator	gap
flow area [m^2]	1.7571E-3	6.303E-4	1.605E-3	1.7739E-3	5.216E-4	1.430E-3
d_H [m]	4.5757E-3	2.636E-2	2.322E-2	4.6020E-3	2.346E-2	2.010E-2
node length [m]	0.2	0.2	0.2	0.2	0.2	0.2

The flow boundary conditions used for FA calculations are given in Table C.7, all flow rates for FA calculations correspond to the core averaged ones. The thermal power used in subsection 3.2.6 is 2.56 MW.

Table C.7: FA representation: boundary conditions

	inlet T [K]	inlet mass flow [kg/s]	outlet P [MPa]
Coolant	mixing chamber	mixing chamber	25
Moderator channel	550	0.0689	mixing chamber
Gap water	550	0.1377	mixing chamber
Feed water	550	2.2720	mixing chamber

The material composition of the HSs representing the boxes is SS-316 (already available in TRACE source code [100]) for the FA with solid stainless steel boxes while the insulating material is represented with a thermal conductivity dependent on temperature as given in Table A.1 on page 104 (the other properties like density and specific heat capacity are copied from those of SS-316 since they are not important for the considered steady state applications). The geometrical dimensions of the HSs are given in Table C.8.

Table C.8: FA representation: HSs geometry

	solid SS boxes		insulated boxes	
	moderator box	FA box	moderator box	FA box
inner radius [mm]	15.2	41.5	14.2	42.3
outer radius [mm]	16.0	44.0	16.2	45.3
thickness [mm]	0.8	2.5	2.0	3.0

The fuel rods are represented with one HS and, to reach the correct heat transfer area from the fuel to the coolant, a surface multiplier is introduced to reproduce the 40 fuel rods which exist in each FA. The same model is used for both FA designs. The geometry represents the pellet, gas gap and clad material whose properties are available in TRACE [100]. The exact geometry of one fuel rod is represented in TRACE using a series of concentric cylinders: from the center of the cylinder till a radius of 3.35 mm the material is “Mixed Oxide” (this region is divided into 6 equal length parts), then till a radius of 3.5 mm the material is “Gap Gas” and finally, till the outer clad radius of 4.0 mm, the material is “SS-316”. The gas gap HTC is fixed to 6300 W/(m^2 K).

MATRA

With MATRA only the FA with insulated boxes have been modeled. The geometrical parameters of each type of sub-channel are calculated in nominal conditions without accounting for the wire presence since the code algorithm automatically subtracts the wire area from the flow area when the wire is in the sub-channel, they are listed in Table C.9.

Table C.9: Sub-channels geometry

sub-channel	Flow area [mm^3]	wetted perimeter [mm]	heated perimeter [mm]
lateral	26.2209	22.0064	12.5664
central	38.8481	25.1327	25.1327
corner (mod. box)	38.0434	28.3473	18.8496
corner (FA box)	15.6860	14.1267	6.2832

The implicit solution algorithm with inlet flow boundary conditions has been used and the Gauss-Seidel with successive over-relaxation has been selected, among the available ones, for

the solution of the diversion cross flow equation. Additional user specified parameters includes: Crossflow Resistance Coefficient (KIJ) equal to 0.5, Transverse Momentum Parameter (S/L) equal to 0.5, Turbulent Momentum Factor (FTM) equal to 1.0. The single phase turbulent mixing coefficient has been set to zero since the wire model is used. The pressure drop correlation developed by Rehme [116, 117] for wire wrapped fuel bundle geometry is available in MATRA and has been selected.

The wire wrap is described in the SETRI 7.0 card: the wire wrap crossing data are specified for each of the 100 gaps and the wire wrap inventory in each of the 60 sub-channels at the bundle inlet is also required. It is assumed that the wire starts at 12 hours (i.e. between sub-channel 1 and 2 in Figure 2.38). The wire crossing angle XCROSS(K,L) is a required input parameter, it is a dimensionless number obtained dividing the angle, in the horizontal plane, between the wire initial location and the gap by 360 deg: for a square lattice, following the wire in counter-clockwise direction from the starting azimuthal position, assumed here to coincide with the gap above the fuel rod (the wire starts at 12 hours), the 4 gaps have XCROSS(K,L) equal to -1.0, 0.25, 0.5 and -0.75 (the sign is positive when the wire is moving from lower to higher sub-channel number and vice versa). For the FAs in SH1, where the flow is downward, the input parameters XCROSS(K,L) have to be switched as if the wire direction would be clockwise because of the pseudo 3D FA representation. For the considered geometry, the recommended fractions of forced cross flow DUR(K) is 0.125 while the calibrated ones for the six type of gaps are listed in Table C.10.

Table C.10: Adjusted values of DUR(K)

type of gap (accounting for wire crossing direction)	DUR(K)
between lateral sub-channels or from a lateral to a corner	0.188224
between central sub-channels	0.042622
between a lateral and a central sub-channel	0.015816
from a corner to a lateral sub-channel (FA box)	0.244132
from a corner to a lateral sub-channel (moderator box)	0.201128
from a corner (at the moderator box) and a central sub-channel	0.021310

In MATRA only a rude representation of the structural material properties is available. The user should provide, in the input file specification, the thermophysical properties (density, specific heat and thermal conductivity) of the fuel, clad and gas-filled gas which are assumed to be constant and not depending on the temperature. It is possible to specify only the temperature dependence of the fuel thermal conductivity and to assume axial variations of fuel properties. This representation differ substantially from that used in TRACE which has hard coded functions to account for the temperature dependence of the structural material properties.

Reference average values for the structural material properties are available within the HPLWR EU-Project [50] and have been chosen for the present application, they are summarized in Table C.11. Another important value to be input is the fuel-clad gap conductance, i.e. the HTC of the gas-filled gas gap between the fuel pellet and the clad. For the considered uncoupled,

Table C.11: Average structural material properties used in MATRA

	Fuel	SS-clad	
Thermal conductivity	4	20	[W/(m K)]
Heat capacity	0.3	0.5	[kJ/(kg K)]
Density	10.4	7.6	[g/cm^3]

steady state applications of MATRA only the fuel temperature is changed by the variation of the gas HTC. It is clear that, because of the discrepancies in the properties of the structural materials as well as the different heat transfer correlation used in MATRA, selecting the same value chosen for TRACE may not be justified and that this value can be tuned in order to match the fuel pin centerline temperature predicted by TRACE. For this reason, considering the wide range of variation of this quantity [42, 50], sensitivity studies have been performed leading to the selection of the gas gap HTC equal to 3150 W/(m^2 K). This selection gives a quite good agreement with the fuel temperature distributions predicted by TRACE, even if it is half of the corresponding value.

C.2 Core model

TRACE

The considered pseudo 3D core model developed for TRACE relies on the described FA model which is used as module to represent each CL or FA in the core depending on the selected nodalization. The mixing chambers, used as common inlet and outlet plena for the coolant flow, are represented with 1D components (namely pipes) whose flow area is the sum of those of the connected pipes to minimize flow velocity changes and the length of each node is 0.2 m like those of the connected pipes. With these plena it is possible to predict the coolant mass flow distribution among the several flow paths of each core region (13 for CL-wise core model and 117 for FA-wise core model). The coolant mass flow distribution is predicted by TRACE using the kfactor map defined in Figure C.3 and corresponding to the results shown in chapter 4. An

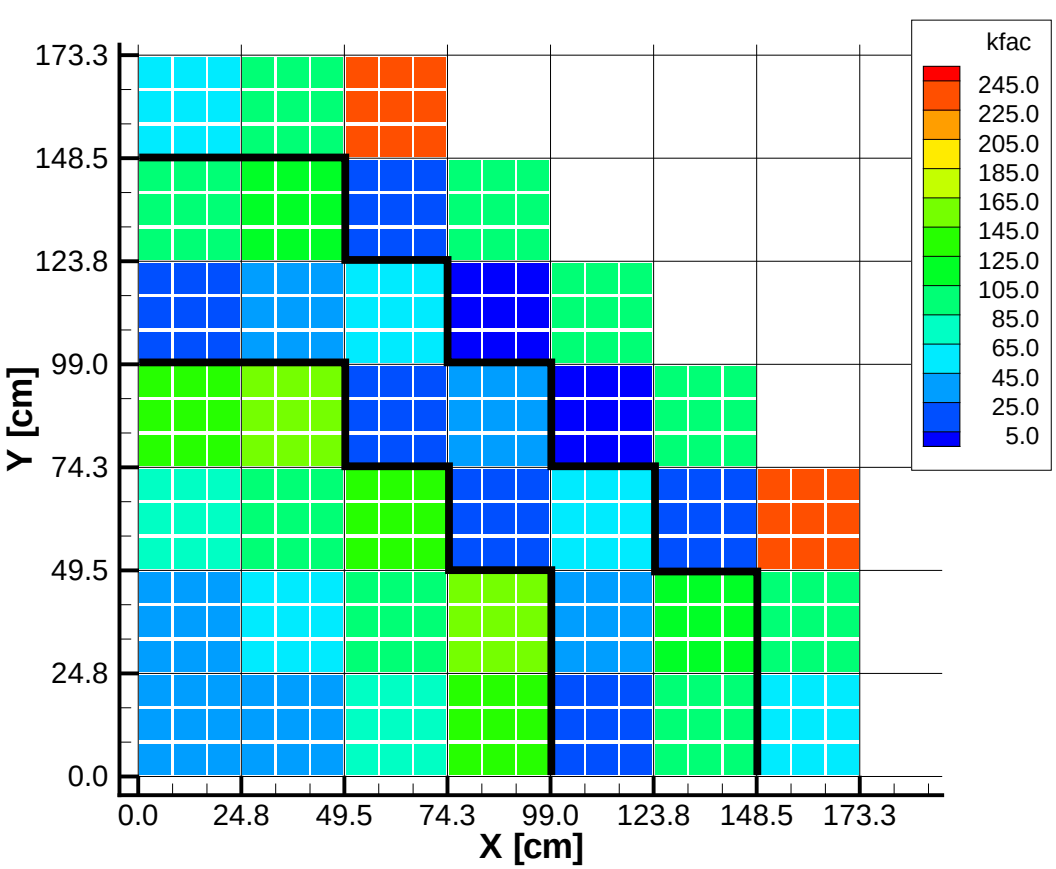

Figure C.3: kfactor (inlet orifices) map

additional pipe is used to model a plenum where the moderator and gap water is collected at the bottom of the core and is successively mixed with the downcomer water.

The inlet water flow rate and temperature of downcomer water, moderator and gap water as well as the outlet pressure, represent the boundary conditions used for TRACE calculations and are fixed using dedicated TRACE components. The inlet temperature of downcomer water, moderator and gap water is always assumed to be 550 K while the one of the coolant is given by the mixing of downcomer water and heated moderator and gap water; for this reason it is not an input parameter. The outlet pressure is fixed to 25 MPa for the preliminary results shown in section 2.2 and Appendix A and to 24 MPa for the results shown in chapter 4. The splitting of RPV inlet water between total moderator water, flowing up-ward to the vessel closure head, and downcomer is not represented since individual inlet conditions are given for each moderator and gap water channel. To have the correct coolant flow rate, the downcomer water fraction is added directly in the lower plenum where is mixed with the outlet of moderator/gap water to reconstitute the coolant mass flow which coincides with the RPV inlet mass flow. The total moderator mass flow is always split in the fraction 1/3 and 2/3 between the moderator channel and the gap between adjacent FAs. The total moderator mass flow is 25% of the RPV inlet mass flow (1160 kg/s) when using the solid SS boxes in section 2.2 and 75% of the RPV inlet mass flow (1179 kg/s) when using the insulated boxes in chapter 4. The remaining fraction of the RPV inlet mass flow is used as downcomer water.

Also the thermal power of the reactor is slightly different among the various chapters: in section 2.2 and Appendix A is 2400 MWth while is reduced to 2300 MWth in chapter 4.

ERANOS

For all considered applications, all FAs in the core have the same enrichment, which is constant in axial direction, since no core loading strategy is available yet. It has been described for the FA cell geometry. Reactivity control systems, including both control rods and burnable poisons, are not modeled and the excess reactivity is not compensated: k_{eff} is well above unity for fresh core analyses as shown in Table 4.1 on page 74 and A.4 on page 110.

The considered quarter core model is constituted of 39 CLs, which are square and have a side length of 24.756 cm (equal to 3 times the FA side length of 8.252 cm which is not modified by the boxes design). These are used to mesh the core in the horizontal plane while the 4.2 m axial length is divided into 21 axial zones of equal length (20 cm)[1]. Each zone has a different homogenized self-shielded 40-group XS which is calculated depending on the TH feedbacks with ECCO.

The model used for the coupled analyses is the one described in Figure 2.16 on page 32; it includes a radial reflector which is constituted of two parts: the blue region represent the downcomer water assumed to be at 550 K and with a density of 0.7769931 g/cm^3 (reduced to one quarter in the upper right corner of the XY geometry to preserve the total mass of downcomer water) while the gray region represents the smearing of steel reflector and core barrel. The density of the steel reflector is 7.90 g/cm^3 while that of the core barrel is 7.70 g/cm^3 and their volume fraction in the smeared material is 79.4% and 20.6%, respectively. Their atomic composition is given in Table C.12 and C.13, all elements have natural isotopic composition [156].

The length of the core in X direction on the X axis is equal to 173.292 cm (24.756 times 7 CLs), the width of the reflector on the X axis (25.178 cm) is determined to preserve its total volume since the in-core meshes are fixed to not introduce additional mesh points within each CL. The thickness of the downcomer water, on the X axis, is preserved; it is 17.7 cm determining the smear density of the downcomer water in the upper right corner of the XY geometry. The neutron

[1] As mentioned, this coarse nodalization can be used thanks to the selected nodal code (VARIANT), while finer meshes are necessary when using finite difference codes like BISTRO.

Table C.12: Steel reflector atomic Composition [wt%]

Manganese	2.000
Iron	68.165
Silicon	0.750
Nickel	10.000
Chromium	19.000

Table C.13: Core barrel Atomic Composition [wt%]

Manganese	0.450
Iron	89.146
Silicon	0.280
Copper	0.170
Nickel	0.210
Chromium	8.370
Molybdenum	0.900
Vanadium	0.216

source necessary for these non-multiplying calculations is the one obtained for the ECCO cell calculation of a typical SH2 CL: coolant at 752 K, moderator and gap water at 600 K, fuel at 835 K.

Also the fission gas plenum above and below the active length of the fuel rods is modeled, with smeared components concentrations, to give a better representation of the axial boundary condition: their length amounts to 25.5 cm each. The assumed water densities and temperatures are given in Table C.14 and correspond to inlet and outlet condition of the selected core regions. The fuel temperature is used only when determining the corresponding neutron sources needed for these non-multiplying calculations.

Table C.14: TH data for the axial surrounding regions and neutron source

plenum	coolant		moderator		gap water		fuel
	[K]	[g/cm^3]	[K]	[g/cm^3]	[K]	[g/cm^3]	[K]
EVA	595	0.7003	587	0.7163	586	0.7182	784
EVA-SH1	675	0.1591	553	0.7779	553	0.7780	691
SH1-SH2	739	0.0965	616	0.6468	616	0.6490	751
SH2	766	0.0871	554	0.7753	554	0.7754	774

Bibliography

[1] M. ANDOH, T. MISAWA, and K. NISHINA. Measurement of flux tilt and eigenvalue separation in axially decoupled core. *Journal of Nuclear Science and Technology*, 34(5): 445–453, May, 1997. (Cited on page 3)

[2] S. ANIEL-BUCHHEIT. Simulation of the VVER-1000 pump start-up experiment in the OECD/DOE/CEA V1000CT benchmark by the FLICA4/CRONOS2 coupled code system. *Progress in Nuclear Energy*, 48:773–789, 2006. (Cited on pages 8 and 21)

[3] S. ANIEL-BUCHHEIT, A. PUILL, R. SANCHEZ, and M. COSTE. Plutonium recycling in a full-MOX 900-MW(electric) PWR: Physical analysis of accident behaviors. *Nuclear Technology*, 128(2):245–256, 1999. (Cited on page 6)

[4] J. R. ASKEW, F. J. FAYERS, and P. B. KEMSHELL. A general description of the lattice code WIMS. *British Nuclear Energy Society*, 5:564–589, October, 1966. (Cited on page 18)

[5] Y. Y. BAE, J. JANG, H. Y. KIM, H. Y. YOON, H. O. KANG, and K. M. BAE. Research activities on a supercritical pressure water reactor in Korea. *Nuclear Engineering and Technology*, 39(4):273–286, August, 2007. (Cited on page 8)

[6] G. I. BELL and S. GLASSTONE. *Nuclear Reactor Theory*. Robert E. Krieger Publishing Company, Malabar, Florida, 1970. (Cited on page 5)

[7] W. BERNNAT, D. LUTZ, E. SARTORI, G. SCHLOSSER, S. CATHALAU, and M. SOLDEVILA. PWR benchmarks from OECD working party on physics of plutonium recycling. In *GLOBAL*, Paris, France, September 11-14, 2005. (Cited on page 13)

[8] A. A. BISHOP, R. O. SANDBERG, and L. S. TONG. Forced convection heat transfer to water at near-critical temperature and supercritical pressures. *A.I.CH.E.-I.Chem.E. Symposium Series*, 2:77–85, 1965. (Cited on pages 37, 40, 44 and 100)

[9] A. BISHOP and N. TODREAS. Hydraulic characteristics of wire-wrapped rod bundles. *Nuclear Engineering and Design*, 62:271 – 293, 1980. (Cited on page 51)

[10] O. BOULAND, V. KOLESOV, and J. L. ROWLANDS. The effect of approximations in the energy distributions of scattered neutrons on thermal reactor Doppler effects. In *International Conference on Nuclear Data for Science and Technology*, pages 1006–1008, Gatlinburg, Tennessee, USA, May 9-13, 1994. (Cited on page 21)

[11] A. BOUSBIA-SALAH and F. D'AURIA. Use of coupled code technique for best estimate safety analysis of nuclear power plants. *Progress in Nuclear Energy*, 49:1–13, 2007. (Cited on page 8)

[12] C. H. M. BROEDERS, V. H. SÁNCHEZ ESPINOZA, E. STEIN, and A. TRAVLEEV. Validation of coupled neutron physics and thermal-hydraulics analysis for HPLWR. In *International Congress on Advances in Nuclear Power Plants (ICAPP)*, Cordoba, Spain, May 4-7, 2003. (Cited on pages 8 and 9)

[13] F. B. BROWN, R. F. BARRETT, T. E. BOOTH, J. S. BULL, L. J. COX, R. A. FORSTER, J. T. GOORLEY, R. D. MOSTELLER, S. E. POST, R. E. PRAEL, E. C. SELCOW, A. SOOD, and J. SWEEZY. MCNP Version 5. In *American Nuclear Society Winter Meeting*, LA-UR-02-3935, Washington, DC, November 17-21, 2002. (Cited on page 13)

[14] F. B. BROWN, B. KIEDROWSKI, W. MARTIN, and G. YESILYURT. Advances in Monte Carlo criticality methods. In *International Conference on Advances in Mathematics, Computational Methods, and Reactor Physics (M&C)*. LA-UR-09-02442 (`mcnp.lanl.gov`), May 3-7, 2009. (Cited on pages 11, 19, 26 and 64)

[15] J. BUONGIORNO. An alternative SCWR design based on vertical power channels and hexagonal fuel assemblies. In *GLOBAL*, New Orleans, Lousiana, November 16-20, 2003. (Cited on page 8)

[16] M. D. CARELLI, L. E. CONWAY, L. ORIANI, B. PETROVIC, C. V. LOMBARDI, M. E. RICOTTI, A. C. O. BARROSO, J. M. COLLADO, L. CINOTTI, N. E. TODREAS, D. GRGIC, M. M. MORAES, R. D. BOROUGHS, H. NINOKATA, D. T. INGERSOLL, and F. ORIOLO. The design and safety features of the IRIS reactor. *Nuclear Engineering and Design*, 230 (1-3):151–167, 2004. (Cited on page 6)

[17] M. D. CARELLI and A. J. FRIEDLAND. Hot channel factors for rod temperature calculations in LMFBR assemblies. *Nuclear Engineering and Design*, 62:155–180, 1980. (Cited on page 11)

[18] L. CHANDRA, J. A. LYCKLAMA À NIJEHOLT, D. C. VISSER, and F. ROELOFS. CFD analyses on the influence of wire wrap spacers on heat transfer at supercritical conditions. In 4^{th} *International Symposium on Supercritical Water-Cooled Reactors*, Heidelberg, Germany, March 8-11, 2009. (Cited on page 48)

[19] C. CHAULIAC, J. M. ARAGONÉS, D. BESTION, D. G. CACUCI, P. CODDINGTON, and L. DADA. NURESIM: a European platform for nuclear reactor simulation. In *International Conference on Nuclear Engineering (ICONE) 14, Workshop on advanced LWR*, Miami, Florida, July 17-20, 2006. (Cited on page 7)

[20] C. CHAULIAC, J. M. ARAGONÉS, D. BESTION, D. G. CACUCI, N. CROUZET, F. P. WEISS, and M. ZIMMERMANN. NURESIM: a European software platform for nuclear reactor simulation. In *International Conference on Advances in Mathematics, Computational Methods, and Reactor Physics (M&C)*, Saratoga Springs, New York, USA, May 3-7, 2009. (Cited on page 7)

[21] H. CHELEMER, J. WEISMAN, and L. TONG. Subchannel thermal analysis of rod bundle cores. *Nuclear Engineering and Design*, 21:35–45, 1972. (Cited on page 11)

[22] S. CHENG. *Constitutive Correlations for Wire-Wrapped Subchannel Analysis Under Forced and Mixed Convection Conditions*. PhD thesis, Massachusetts Institute of Technology. Dept. of Nuclear Engineering, 1984. (Cited on page 48)

[23] X. CHENG and T. SCHULENBERG. Heat transfer at supercritical pressures, literature review and application to HPLWR. Technical Report FZKA 6609, Forschungszentrum Karlsruhe, 2001. (Cited on page 40)

[24] X. CHENG, T. SCHULENBERG, D. BITTERMANN, and P. RAU. Design analysis of core assemblies for supercritical pressure conditions. *Nuclear Engineering and Design*, 223: 279–294, 2003. (Cited on page 49)

[25] N. Z. CHO. Fundamentals and recent developments of reactor physics methods. *Nuclear Engineering and Technology*, 37(1):25–78, February, 2005. (Cited on page 6)

[26] P. CODDINGTON, K. MIKITYUK, S. PELLONI, M. PLASCHY, and R. CHAWLA. Swiss activities related to the analysis of experimental accelerator driven systems. In *International Workshop on P&T and ADS development*, Mol, Belgium, October 6-8, 2003. `http://wwwold.sckcen.be/sckcen_en/activities/conf/conferences/20031006/cd/introduction.html`. (Cited on page 13)

[27] D. CUERVO, M. AVRAMOVA, K. IVANOV, and R. MIRÓ. Evaluation and enhancement of COBRA-TF efficiency for LWR calculations. *Annals of Nuclear Energy*, 33(9):837 – 847, 2006. (Cited on page 11)

[28] R. DAGAN. On the use of S(α,β) tables for nuclides with well pronounced resonances. *Annals of Nuclear Energy*, 32:367–377, 2005. (Cited on page 67)

[29] W. J. M. D KRUIJF and A. J. JANSSEN. The effective fuel temperature to be used for calculating resonance absorption in a $^{238}UO_2$ lump with nonuniform temperature profile. *Nuclear Science and Engineering*, 123:121–135, 1996. (Cited on page 21)

[30] B. DE MARSAC, D. BITTERMANN, J. STARFLINGER, and T. SCHULENBERG. Containment design proposal with active and passive safety systems for a High Performance Light Water Reactor. In 4^{th} *International Symposium on Supercritical Water-Cooled Reactors*, Heidelberg, Germany, March 8-11, 2009. (Cited on page 2)

[31] K. DIETZE, M. ISHIKAWA, and G. RIMPAULT. Integral test of neutron data and comparison of codes by re-analysis of the SEG and STEK experiments. In *JEFF Working Group Meeting*, JEFF / DOC 861, Aix-en-Provence, France, May 16-18, 2001. (Cited on page 13)

[32] I. DILBER and E. E. LEWIS. Variational nodal method for neutron transport. *Nuclear Science and Engineering*, 91:132–142, 1985. (Cited on page 18)

[33] F. W. DITTUS and L. M. K. BOELTER. Heat transfer in automobile radiators of the tubular type. *Publications on Engineering, University of California at Berkeley*, 2:443–461, 1930. (Cited on pages 41, 67 and 100)

[34] K. DOBASHI, A. KIMURA, Y. OKA, and S. KOSHIZUKA. Conceptual design of a high temperature power reactor cooled and moderated by supercritical light water. *Annals of Nuclear Energy*, 25(8):487–505, May, 1998. (Cited on page 1)

[35] J. Y. DORIATH, J. M. RUGGIERI, and G. BUZZI. Calcul de réacteurs par une méthode nodale variationnelle implémentée dans le système de codes ERANOS - reactor analysis using a variational nodal method implemented in the ERANOS system. In *Reactor Physics Faces 21^{st} Century*, Knoxville, TN, USA, 1994. ANS topical meeting. (Cited on pages 18 and 57)

[36] T. DOWNAR, A. SIEGEL, and C. UNAL. White paper on integrated performance and safety codes. In *Science Based Nuclear Energy Systems Enabled by Advanced Modeling and Simulation at the Extreme Scale*, Washington, DC, May 11-12, 2009. `https://www.cels.anl.gov/events/workshops/extremecomputing/nuclearenergy/agenda.php`. (Cited on pages 5 and 7)

[37] J. J. DUDERSTADT and L. J. HAMILTON. *Nuclear Reactor Analysis*. John Wiley & Sons, New York, 1976. (Cited on pages 5, 6 and 12)

[38] EURATOM 5TH FRAMEWORK PROGRAMME. Neutronics/thermal-hydraulics coupling in LWR technology vol. 1. CRISSUE-S – WP1: Data requirements and databases needed for transient simulations and qualifications ISBN 92-64-02083-7, OECD/NEA, 2004. (Cited on page 6)

[39] EURATOM 5TH FRAMEWORK PROGRAMME. Neutronics/thermal-hydraulics coupling in LWR technology vol. 2. CRISSUE-S – WP2: State-of-the-art Report ISBN 92-64-02084-5, OECD/NEA, 2004. (Cited on page 6)

[40] EURATOM 5TH FRAMEWORK PROGRAMME. Neutronics/thermal-hydraulics coupling in LWR technology vol. 3. CRISSUE-S – WP3: Achievement and Recommendations Report ISBN 92-64-02085-3, OECD/NEA, 2004. (Cited on page 6)

[41] T. H. FANNING, W. D. POINTER, and J. W. THOMAS. Multi-resolution modeling of subassembly pin bundlesfor advanced fast reactor safety simulations. In *International Conference on Mathematics, Computational Methods, and Reactor Physics (M&C)*, Saratoga Springs, New York, May 3-7, 2009. (Cited on pages 7, 11 and 48)

[42] H. FENECH. *Heat Transfer and Fluid Flow in Nuclear Systems*, chapter General Consideration on thermal design and performance requirements of nuclear reactor cores. Pergamon Press, Oxford, 1981. (Cited on pages 38 and 148)

[43] H. FENECH and F. BENNET. Axial static pressure variations in inner and side subchannels of a 61-tube wire-wrap bundle. *Nuclear Engineering and Design*, 104:83–92, 1987. (Cited on pages 49 and 50)

[44] K. FISCHER, T. SCHNEIDER, T. REDON, T. SCHULENBERG, and J. STARFLINGER. Mechanical design of core components for a High Performance Light Water Reactor with a three pass core. In *GLOBAL*, Boise, Idaho, USA, September 9-13, 2007. (Cited on pages 2 and 80)

[45] M. FRATONI and E. GREENSPAN. Neutronic design of hydride fuelled BWRs. *Nuclear Engineering and Design*, In Press, Corrected Proof, 2009. (Cited on page 6)

[46] Gen-IV. Generation IV International Forum (`http://www.gen-4.org/index.html`) Generation IV Technology Roadmap (`http://gif.inel.gov/roadmap/`), 2001. (Cited on page 1)

[47] G. GIRARDIN, G. RIMPAULT, F. MORIN, J. BOSQ, P. CODDINGTON, K. MIKITYUK, and R. CHAWLA. Development and characterization of the control assembly system for the large 2400 MWth Generation IV gas-cooled fast reactor. *Annals of Nuclear Energy*, 35(12):2206–2218, 2008. (Cited on pages 3 and 6)

[48] M. GLÜCK. Sub-channel analysis with F-COBRA-TF – code validation and approaches to CHF prediction. *Nuclear Engineering and Design*, 237:655–667, 2007. (Cited on page 11)

[49] V. GNIELINSKI. New equations for heat and mass transfer in turbulent pipe and channel flow. *International Chemical Engineering*, 16(2):359–368, April, 1976. (Cited on pages 40, 41 and 100)

[50] J. HEINECKE. Personal communication at HPLWR progress meeting, Karlsruhe, March 4-6, 2009. AREVA NP GmbH. (Cited on pages 96, 147 and 148)

[51] H. HERBELL, S. HIMMEL, and T. SCHULENBERG. Mechanical analysis of an assembly box with honeycomb structure. In 16^{th} *Pacific Basin Nuclear Conference (16PBNC)*, Paper 1150, Aomori, Japan, October 13-18, 2008. (Cited on pages 4, 48, 64, 76, 83, 99, 104 and 143)

[52] H. HERBELL, M. WECHSUNG, and T. SCHULENBERG. A turbine design concept for the High Performance Light Water Reactor. In 4^{th} *International Symposium on Supercritical Water-Cooled Reactors*, Heidelberg, Germany, March 8-11, 2009. (Cited on page 2)

[53] N. HFAIEDH. *Nouvelle Méthodologie de Calcul de l'Absorption Résonnante*. PhD thesis, Université Louis Pasteur Strasbourg, 21 Septembre, 2006. (Cited on page 18)

[54] High Performance Light Water Reactor EU-Project. `http://www.hplwr.eu/`, 2006. (Cited on pages 1, 2, 13, 48 and 104)

[55] S. HIMMEL. *Modellierung des Strömungsverhaltens in einem HPLWR-Brennelement mit Drahtwendelabstandshaltern*. PhD thesis, Universität Stuttgart, December, 2008. (Cited on pages 4, 49, 51, 52, 53 and 89)

[56] A. HOFFMANN, F. JEANPIERRE, A. KAVENOKY, M. LIVOLANT, and H. LORAIN. APOLLO: Code multigroupe de résolution de l'équation du transport pour les neutrons thermiques et rapides. Technical Report N-1610, Commissariat à l'Énergie Atomique (CEA), Saclay, France, 1973. (Cited on page 18)

[57] J. HOFMEISTER, C. WAATA, J. STARFLINGER, T. SCHULENBERG, and E. LAURIEN. Fuel assembly design study for a reactor with supercritical water. *Nuclear Engineering and Design*, 237:1513–1521, 2007. (Cited on pages 4, 19, 20, 38, 69, 85, 99, 103, 104, 143 and 144)

[58] Y. HU, T. J. DOWNAR, T. KOZLOWSKI, and K. IVANOV. Multi-physics coupled code reactor analysis with the US NRC code system TRACE/PARCS. In *ANS Reactor Physics Topical Meeting - International Conference on the Physics of Reactors (PHYSOR)*, Vancouver, BC, Canada, September 10-14, 2006. (Cited on pages 8, 14 and 36)

[59] B. D. IVANOV, S. ANIEL, P. SILTANEN, E. ROYER, and K. N. IVANOV. Impact of cross-section generation procedures on the simulation of the VVER-1000 pump startup experiment in the OECD/DOE/CEA V1000CT benchmark by coupled 3D thermal-hydraulics/neutron kinetics models. *Progress in Nuclear Energy*, 48:746–763, 2006. (Cited on page 9)

[60] K. IVANOV. Coupled thermo-hydraulics and neutronics simulations. Lectures at the FJ/OH Summer School, Cadarache, August 23 - September 1, 2006. (Cited on page 7)

[61] K. IVANOV and M. AVRAMOVA. Challenges in coupled thermal-hydraulics and neutronics simulations for LWR safety analysis. *Annals of Nuclear Energy*, 34:501–513, 2007. (Cited on page 8)

[62] K. IVANOV, E. SARTORI, E. ROYER, S. LANGENBUCH, and K. VELKOV. Validation of coupled thermal-hydraulic and neutronics codes for safety analysis by international cooperations. *Nuclear Technology*, 157(2):177–195, 2007. (Cited on pages 5 and 14)

[63] K. N. IVANOV, R. MACIAN-JUAN, A. IRANI, and A. J. BARATTA. Features and performance of a coupled three-dimensional thermal-hydraulic/kinetics TRAC-PF1/NEM pressurized water reactor (PWR) analysis code. *Annals of Nuclear Energy*, 26:1407–1417, 1999. (Cited on page 8)

[64] K. N. IVANOV and E. SARTORI. Special issues on the OECD / US NRC BWR Turbine Trip (TT) benchmark. *Nuclear Science and Engineering*, 148(2), October, 2004. (Cited on page 8)

[65] K. N. IVANOV and E. SARTORI. Special issues on the OECD / US NRC PWR Main Steam Line Break (MSLB) benchmark. *Nuclear Technology*, 142(2), May, 2003. (Cited on page 8)

[66] C. J. JACKSON, D. G. CACUCI, and H. B. FINNEMANN. Dimensionally adaptive neutron kinetics for multidimensional reactor safety transients - I: New features of RELAP5/PANBOX. *Nuclear Science and Engineering*, 131(2):143–163, February, 1999. (Cited on page 8)

[67] J. D. JACKSON and W. B. HALL. Forced convection heat transfer to fluids at supercritical pressure. *Kakac S., Spalding D.B., (Eds.), Turbulent Forced Convection in Channels and Bundles*, 2:563–612, 1979. (Cited on pages 37, 40, 41, 44 and 100)

[68] R. JACQMIN, J. TOMMASI, D. BERNARD, and A. SANTAMARINA. Improved reactor core calculations with JEFF-3.1 data. In *International Conference on the Physics of Reactors (PHYSOR)*, Interlaken, Switzerland, September 14-19, 2008. (Cited on page 70)

[69] W. JÄGER, V. H. SÁNCHEZ ESPINOZA, and A. HURTADO. Investigations of experiments with supercritical water with the system code TRACE. In *NUTHOS-7*, Seoul, Korea, October 5-9, 2008. (Cited on pages 14, 40 and 44)

[70] W. JÄGER, V. H. SÁNCHEZ ESPINOZA, N. SCHNEIDER, and A. HURTADO. Assessment of heat transfer correlation for supercritical water in the frame of best-estimate code validation. In *International Congress on Advances in Nuclear Power Plants (ICAPP)*, Tokyo, Japan, May 10-14, 2009. (Cited on pages 14 and 67)

[71] H. Y. JEONG, K. S. HA, Y. M. KWON, Y. B. LEE, and D. HAHN. Analysis of three different types of blockage in a sodium flow path with the MATRA-LMR-FB code. *Annals of Nuclear Energy*, 2009. (Cited on page 48)

[72] J. JIMÉNEZ, M. AVRAMOVA, D. CUERVO, and K. IVANOV. Comparative analysis of neutronics/thermal-hydraulics multi-scale coupling for LWR analysis. In *International Conference on the Physics of Reactors (PHYSOR)*, Interlaken, Switzerland, September 14-19, 2008. (Cited on pages 11 and 13)

[73] A. KARAHAN, J. BUONGIORNO, and M. S. KAZIMI. An evolutionary fuel assembly design for high power density BWRs. In *International Congress on Advances in Nuclear Power Plants (ICAPP)*, Nice, France, May 13-18, 2007. (Cited on page 6)

[74] E. KHAN, W. ROHSENOW, A. SONIN, and N. E. TODREAS. A porous body model for predicting temperature distribution in wire-wrapped fuel rod assemblies. *Nuclear Engineering and Design*, 35:1–12, 1975. (Cited on pages 48 and 51)

[75] W. S. KIM, Y. G. KIM, and Y. J. KIM. A subchannel analysis code MATRA-LMR for wire wrapped LMR subassembly. *Annals of Nuclear Energy*, 29:303–321, 2002. (Cited on pages 14, 48 and 51)

[76] A. KISS, E. LAURIEN, A. ASZÓDI, and Y. ZHU. Improved numerical simulation of a HPLWR fuel assembly flow with wrapped wire spacers. In 4^{th} *International Symposium on Supercritical Water-Cooled Reactors*, Heidelberg, Germany, March 8-11, 2009. (Cited on pages 48 and 51)

[77] Y. KOZMENKOV, S. KLIEM, U. GRUNDMANN, U. ROHDE, and F. P. WEISS. Calculation of the VVER-1000 coolant transient benchmark using the coupled code systems DYN3D/RELAP5 and DYN3D/ATHLET. *Nuclear Engineering and Design*, 237:1938–1951, 2007. (Cited on page 8)

[78] C. KUNIK. Berechnung der Mischkonvektion im Moderatorspalt eines Kernereaktors mit einem Ansatz für poröse Medien. Master thesis, Universität Karlsruhe (TH), 2007. (Cited on page 110)

[79] J. R. LAMARSH. *Introduction to Nuclear Reactor Theory*. Addison-Wesley, Reading, Massachusetts, 1966. (Cited on pages 5 and 59)

[80] J. R. LAMARSH and A. J. BARATTA. *Introduction to Nuclear Engineering*. Addison-Wesley, Reading, Massachusetts, 2001. (Cited on pages 6 and 73)

[81] E. LAURIEN, M. RASHID, and D. M. MCELIGOT. Heat capacity model for turbulent heat transfer at supercritical pressure. In *International Conference on Multiphase Flow (ICMF)*, Leipzig, Germany, July 9-13, 2007. (Cited on page 49)

[82] E. E. LEWIS, C. B. CARRICO, and G. PALMIOTTI. Variational nodal formulation for the spherical harmonics equations. *Nuclear Science and Engineering*, 122:194–203, 1996. (Cited on page 18)

[83] E. E. LEWIS, M. SMITH, and G. PALMIOTTI. A new paradigm for local-global coupling in whole-core neutron transport. *Nuclear Science and Engineering*, 161:279–288, 2009. (Cited on page 17)

[84] K. LITFIN and R. STIEGLITZ. Sub-channel analysis of heavy liquid metal cooled fuel assemblies. In *Jahrestagung Kerntechnik*, Aachen, Germany, May 16-18, 2006. (Cited on page 49)

[85] P. MACDONALD, J. BUONGIORNO, J. W. STERBENTZ, C. DAVIS, and R. WITT. Feasibility study of supercritical light water cooled reactors for electric power production. Final report – 12^{th} quarterly report, Nuclear Energy Research Initiative Project 2001-001 Westinghouse Electric Co. Award Number: DE-FG07-02SF22533, Idaho National Engineering and Environmental Laboratory Bechtel BWXT Idaho, LLC, January, 2005. (Cited on pages 8 and 9)

[86] A. MANERA and O. ANTONI. Code-to-code comparison for blowdown transients at supercritical conditions. In *Jahrestagung Kerntechnik*, Paper 772, Hamburg, Germany, May 27-29, 2008. (Cited on pages 14 and 40)

[87] C. MARÁCZY, G. HEGYI, G. HORDÓSY, E. TEMESVÁRI, C. HEGEDÜS, and A. MOLNÁR. High Performance Light Water Reactor core design studies. In 16^{th} *Pacific Basin Nuclear Conference (16PBNC)*, Aomori, Japan, October 13-18, 2008. (Cited on pages 8, 9, 13, 26, 28, 29, 31, 33 and 71)

[88] M. MATTES and J. KEINERT. Thermal Neutron Scattering Data for the Moderator Materials H2O, D2O and ZrHx in ENDF-6 Format and as ACE Library for MCNP(X) Codes. `http://www-nds.iaea.org/indltsl/`, INDC(NDS)-0470, 2006. (Cited on pages 19 and 26)

[89] L. MONTI, F. GABRIELLI, W. MASCHEK, and T. SCHULENBERG. Assessment of ERANOS for HPLWR core analyses. In *International Conference on Advances in Mathematics, Computational Methods, and Reactor Physics, M&C*, Saratoga Springs, New York, May 3-7, 2009. (Cited on pages 34 and 99)

[90] L. MONTI, F. GABRIELLI, and T. SCHULENBERG. Preliminary 3d burn-up analysis of the HPLWR core. In *Jahrestagung Kerntechnik*, Paper 1203, Dresden, Germany, May 12-14, 2009. (Cited on pages 117 and 118)

[91] L. MONTI, K. B. LEE, M. FRATONI, M. SUMINI, and E. GREENSPAN. Recycling-independent core design for the ENHS fuel self-sustaining reactor. *Nuclear Science and Engineering*, 161:1–21, 2009. (Cited on page 6)

[92] L. MONTI and T. SCHULENBERG. Coupled ERANOS/TRACE system for HPLWR 3 pass core analyses. In *International Conference on Advances in Mathematics, Computational Methods, and Reactor Physics, M&C*, Saratoga Springs, New York, May 3-7, 2009. (Cited on pages 34, 58 and 101)

[93] L. MONTI and T. SCHULENBERG. Preliminary sub-channel wise analyses of the HPLWR 3 pass core. In 13^{th} *International Topical Meeting on Nuclear Reactor Thermal Hydraulics (NURETH-13)*, Kanazawa, Japan, September 27 - October 2, 2009. (Cited on page 101)

[94] L. MONTI, T. SCHULENBERG, W. JÄGER, and V. H. SÁNCHEZ ESPINOZA. Application and improvements of the system code TRACE for HPLWR core analyses. In 7^{th} *International Topical Meeting on Nuclear Reactor Thermal Hydraulics, Operation and Safety (NUTHOS-7)*, Seoul, Korea, October 5-9, 2008. (Cited on pages 40 and 100)

[95] L. MONTI, T. SCHULENBERG, and J. STARFLINGER. Coupled analysis of the HPLWR fuel assembly. In *Jahrestagung Kerntechnik*, Paper 1004, Hamburg, Germany, May 27-29, 2008. (Cited on pages 41 and 58)

[96] L. MONTI, J. STARFLINGER, and T. SCHULENBERG. Effectiveness of an insulated fuel assembly to improve HPLWR core performance. In 4^{th} *International Symposium on Supercritical Water-Cooled Reactors*, Paper 46, Heidelberg, Germany, March 8-11, 2009. (Cited on pages 104 and 111)

[97] L. MONTI, J. STARFLINGER, and T. SCHULENBERG. Coupled neutronic / thermal-hydraulic analysis of the HPLWR three pass core. In 16^{th} *Pacific Basin Nuclear Conference (16PBNC)*, Paper 1149, Aomori, Japan, October 13-18, 2008. (Cited on pages 45 and 104)

[98] M. MORI. *Core design analysis of the supercritical water fast reactor*. PhD thesis, Universität Stuttgart, 2005. (Cited on pages 8 and 9)

[99] C. MURRAY and J. STAUDENMEIER. *TRACE V5.0 User's Manual*. Division of Risk Assessment and Special Projects Office of Nuclear Regulatory Research U. S. Nuclear Regulatory Commission, Washington, DC 20555-0001, 2007. (Cited on pages 14 and 36)

[100] C. MURRAY and J. STAUDENMEIER. *TRACE V5.0 Theory Manual Field Equations, Solution Methods and Physical Models*. Division of Risk Assessment and Special Projects Office of Nuclear Regulatory Research U. S. Nuclear Regulatory Commission, Washington, DC 20555-0001, 2007. (Cited on pages 14, 36, 37, 40, 41, 80 and 146)

[101] D. G. NABEREJNEV, G. IMEL, G. PALMIOTTI, and M. SALVATORES. Physics study of the TRADE: TRIGA Accelerator Driven Experiment. Technical Report ANL-AFCI-091, Argonne National Laboratory, 9700 South Cass Avenue Argonne, IL, 60439, USA, September, 2003. (Cited on page 13)

[102] NEA DATA BANK. The JEF-2.2 Nuclear Data Library. JEFF Report 17, NEA/OECD, Paris, France, April, 2000. http://www.nea.fr/html/dbdata/nds_jefreports/jefreport-17/Table_of_content.pdf. (Cited on page 19)

[103] NEA DATA BANK. The JEFF-3.1 Nuclear Data Library. JEFF Report 21, NEA/OECD, November, 2006. http://www.nea.fr/html/dbdata/nds_jefreports/jeffreport-21/index.html. (Cited on pages 64 and 70)

[104] NEA DATA BANK. LWR pin cell benchmark intercomparisons. JEFF Report 15, NEA/OECD, September, 1999. http://www.nea.fr/html/dbdata/nds_jefreports/jefreport-15.pdf. (Cited on page 13)

[105] NEA DATA BANK. NEA/OECD Reactor Physics Benchmarks. http://www.nea.fr/html/science/projects/benchmarks.html. (Cited on page 5)

[106] NEAMS. Nuclear Energy Advanced Modeling and Simulation http://computing.ornl.gov/workshops/neams/, 2009. (Cited on page 7)

[107] Y. OKA. Review of high temperature water and steam cooled reactor concepts. In 1st *International Symposium on SCWR, Design and Technolgy*, Tokyo, Japan, November 6-9, 2000. (Cited on page 7)

[108] Y. OKA and S. I. KOSHIZUKA. Concept and design of a supercritical pressure direct cycle light water reactor. *Nuclear Technology*, 103(3):295–302, September, 1993. (Cited on page 1)

[109] R. ORSI, M. PESCARINI, A. I. BLOKHIN, and V. SINITSA. A JEF-2.2 cross section library for the MCNP Monte Carlo code. ZZ-MCJEF22NEA.BOLIB NEA-1616/003. (Cited on page 19)

[110] T. ORTEGA GÓMEZ, A. CLASS, R. T. LAHEY, and T. SCHULENBERG. Stability analysis of a uniformly heated channel with supercritical water. *Nuclear Engineering and Design*, 238(8):1930–1939, 2008. (Cited on page 4)

[111] G. PALMIOTTI, C. B. CARRICO, and E. E. LEWIS. Variational nodal method for the solution of the diffusion and transport equation in two and three dimensional geometries. Technical Report 91-208, Commissariat à l'Énergie Atomique (CEA), 1991. (Cited on pages 18 and 34)

[112] G. PALMIOTTI, J. M. RIEUNIER, C. GHO, and M. SALVATORES. BISTRO Optimized Two Dimensional Sn Transport Code. *Nuclear Science and Engineering*, 104:26–33, 1990. (Cited on page 33)

[113] G. PALMIOTTI and M. SALVATORES. Use of integral experiment in the assessment of large liquid-metal fast breeder reactor basic design parameters. *Nuclear Science and Engineering*, 87:333–348, 1984. (Cited on page 3)

[114] A. PAUTZ and A. BIRKHOFER. Coupling of time-dependent neutron transport theory with the thermal hydraulics code ATHLET and application to the research reactor FRM-II. *Nuclear Science and Engineering*, 145:320–341, 2003. (Cited on pages 9 and 57)

[115] I. L. PIORO and R. B. DUFFEY. *Heat transfer and hydraulic resistance at superctirical pressure in power-engineering applications*. American Society of Mechanical Engineers press, 2007. (Cited on pages 37, 40 and 92)

[116] K. REHME. Pressure drop correlations for fuel element spacers. *Nuclear Engineering and Design*, 17:15–23, 1972. (Cited on page 147)

[117] K. REHME. Turbulent momentum transport in rod bundles. *Nuclear Engineering and Design*, 62:137–146, 1980. (Cited on page 147)

[118] K. REHME. The structure of turbulence in rod bundles and the implications on natural mixing between the subchannels. *International Journal of Heat and Mass Transfer*, 35(2): 567–581, 1992. (Cited on page 96)

[119] T. REISS, S. FEHÈR, and S. CZIFRUS. Coupled neutronics and thermohydraulics calculations with burn-up for HPLWRs. *Progress in Nuclear Energy*, 50:52–61, January, 2008. (Cited on pages 8, 9 and 111)

[120] K. R. REMPE and K. S. SMITH. SIMULATE-3 pin-power reconstruction: Methodology and benchmarking. *Nuclear Science and Engineering*, 103:334–342, 1989. (Cited on pages 11 and 62)

[121] G. RIMPAULT. Algorithmic features of the ECCO cell code for treating heterogeneous fast reactor assemblies. In *Mathematics and Computations, Reactor Physics and Environmental Analyses (M&C)*, Portland, Oregon, May 1-5, 1995. (Cited on pages 18 and 22)

[122] G. RIMPAULT. Physics documentation of ERANOS: the ECCO cell code. Technical Report 97-001, Commissariat à l'Énergie Atomique (CEA), 1997. (Cited on pages 22, 31 and 34)

[123] G. RIMPAULT. Deterministic calculation scheme for a fast spectrum core of a supercritical water reactor. Technical Report 07-408, Commissariat à l'Énergie Atomique (CEA), 2007. (Cited on pages 8 and 9)

[124] G. RIMPAULT, C. MARÁCZY, R. KYRKI-RAJAMÄKI, Y. OKA, and T. SCHULENBERG. Core design feature studies and research needs for high performance light water reactors. In *International Congress on Advances in Nuclear Power Plants (ICAPP)*, Paper 3194, Cordoba, Spain, May 4-7, 2003. (Cited on page 13)

[125] G. RIMPAULT, D. PLISSON, J. TOMMASI, J. M. RIEUNIER, and R. JACQMIN. The ERANOS code and data system for fast reactor neutronic analyses. In *International Conference on the Physics of Reactors (PHYSOR)*, Seoul, Korea, October 7-10, 2002. (Cited on pages 13 and 17)

[126] G. RIMPAULT, P. SMITH, R. JACQMIN, F. MALVAGI, J. M. RIEUNIER, D. HONDE, G. BUZZI, and P. J. FINCK. Schéma de calcul de référence du formulaire ERANOS et orientations pour le schéma de calcul de projet. Technical Report 96-220, Commissariat à l'Énergie Atomique (CEA), 1996. (Cited on pages 18, 31 and 35)

[127] D. ROWE. COBRA IIIC: a digital computer program for steady state and transient thermal-hydraulic analysis of rod bundle nuclear fuel elements. Technical Report BNWL-1695, Pacific Northwest Laboratory, March, 1973. (Cited on pages 14, 48, 49, 96 and 100)

[128] G. ROWLANDS. Resonance absorption and non-uniform temperature distributions. *Nuclear Energy*, Parts A and B 16:235, 1962. (Cited on pages 21, 28, 57 and 122)

[129] E. ROYER. Multi-physics and LWR transient analysis. In *International Conference on the Physics of Reactors (PHYSOR)*, Interlaken, Switzerland, September 14-19, 2008. (Cited on pages 4, 7, 14 and 58)

[130] J. M. RUGGIERI. ERANOS manuel des méthodes: Reconstruction fine d'un flux nodal. Technical Report 99-217, Commissariat à l'Énergie Atomique (CEA), 1999. (Cited on pages 18, 56, 57, 63 and 86)

[131] J. M. RUGGIERI, J. TOMMASI, J. F. LEBRAT, C. SUTEAU, D. PLISSON-RIEUNIER, C. D. S. JEAN, G. RIMPAULT, and J. C. SUBLET. ERANOS 2.1: International code system for GEN IV fast reactor analysis. In *International Congress on Advances in Nuclear Power Plants (ICAPP)*, Paper 6360, Reno, Nevada, June 4-8, 2006. (Cited on pages 13, 17, 70 and 111)

[132] V. H. SÁNCHEZ ESPINOZA, A. AL-HAMRY, and C. H. M. BROEDERS. Development and qualification of the coupled code system COBRATF/THREEDANT for the pin-by-pin power calculation. In *International Congress on Advances in Nuclear Power Plants (ICAPP)*, Paper 8269, Anaheim, CA USA, June 8-12, 2008. (Cited on page 10)

[133] V. H. SÁNCHEZ ESPINOZA, B. BECKER, C. H. M. BROEDERS, and P. VINSON. A procedure for coupled neutron physics / thermal hydraulic calculation of the pinwise power distribution within a fuel assembly. In *Jahrestagung Kerntechnik*, Aachen, Germany, May 16-18, 2006. (Cited on page 10)

[134] V. H. SÁNCHEZ ESPINOZA, W. JÄGER, A. TRAVLEEV, L. MONTI, and R. DOERN. Neutronics and thermal hydraulics coupling scheme for design improvements of liquid metal fast systems. In 13^{th} *International Topical Meeting on Nuclear Reactor Thermal Hydraulics (NURETH-13)*, Kanazawa, Japan, September 27 - October 2, 2009. (Cited on page 65)

[135] M. SCHLAGENHAUFER, J. STARFLINGER, and T. SCHULENBERG. Plant control of the High Performance Light Water Reactor. In *GLOBAL*, Paris, France, September 6-11, 2009. (Cited on page 2)

[136] T. SCHULENBERG and J. STARFLINGER. Core design concepts for High Performance Light Water Reactors. *Nuclear Engineering and Technology*, 39(4), August, 2007. (Cited on page 1)

[137] T. SCHULENBERG, J. STARFLINGER, and J. HEINECKE. Three pass core design proposal for a High Performance Light Water Reactor. *Progress in Nuclear Engineering*, 50(2-6): 526–531, March-August, 2008. (Cited on pages 1, 2, 4, 59, 102 and 103)

[138] W. T. SHA. An overview on rod-bundle thermal-hydraulic analysis. *Nuclear Engineering and Design*, 62:1–24, 1980. (Cited on page 11)

[139] A. SIEGEL, T. TAUTGES, A. CACERES, D. KAUSHIK, P. FISCHER, G. PALMIOTTI, M. SMITH, and J. RAGUSA. Software design of SHARP. In *Joint International Topical Meeting on Mathematics & Computation and Supercomputing in Nuclear Applications (M&C + SNA)*, Monterey, California, April 15-19, 2007. (Cited on page 7)

[140] D. SQUARER, T. SCHULENBERG, D. STRUWE, Y. OKA, D. BITTERMANN, N. AKSAN, C. MARÁCZY, R. KYRKI-RAJAMÄKI, A. SOUYRI, and P. DUMAZ. High Performance Light Water Reactor. *Nuclear Engineering and Design*, 221(1-3):167–180, April, 2003. (Cited on page 1)

[141] W. M. STACEY. *Nuclear Reactor Physics*. John Wiley & Sons, New York, 2001. (Cited on pages 5 and 22)

[142] J. STARFLINGER, T. SCHULENBERG, P. MARSAULT, D. BITTERMANN, C. MARÁCZY, E. LAURIEN, J. A. LYCKLAMA À NIJEHOLT, H. ANGLART, N. AKSAN, M. RUZICKOVA, and L. HEIKINHEIMO. European research activities within the project: High Performance Light Water Reactor Phase 2 (HPLWR Phase 2). In *International Congress on Advances in Nuclear Power Plants (ICAPP)*, Paper 7146, Nice, France, May 13-18, 2007. (Cited on page 1)

[143] J. STARFLINGER, T. SCHULENBERG, P. MARSAULT, D. BITTERMANN, C. MARÁCZY, E. LAURIEN, J. A. LYCKLAMA À NIJEHOLT, H. ANGLART, N. AKSAN, M. RUZICKOVA, and L. HEIKINHEIMO. Progress within the European project: "High Performance Light Water Reactor Phase 2" (HPLWR Phase 2). In *International Congress on Advances in Nuclear Power Plants (ICAPP)*, Paper 8247, Anaheim, CA USA, June 8-12, 2008. (Cited on page 1)

[144] J. STARFLINGER, T. SCHULENBERG, P. MARSAULT, D. BITTERMANN, C. MARÁCZY, E. LAURIEN, J. A. LYCKLAMA À NIJEHOLT, H. ANGLART, M. ANDREANI, M. RUZICKOVA, and L. HEIKINHEIMO. Results of the mid-term assessment of the High Performance Light Water Reactor Phase 2 Project. In *International Congress on Advances in Nuclear Power Plants (ICAPP)*, Tokyo, Japan, May 10-14, 2009. (Cited on page 1)

[145] K. TADA, A. YAMAMOTO, Y. KITAMURA, and Y. YAMANE. Application of pin-by-pin fine mesh calculation method to BWR core analysis. In *International Conference on the Physics of Reactors (PHYSOR)*, Vancouver, BC, Canada, September 10-14, 2006. (Cited on page 10)

[146] Tecplot 360. `http://www.tecplot.com/`, Last checked May, 2009. (Cited on pages 65 and 138)

[147] Thermodynamic and Transport Properties of Water and Steam IAPWS. `http://www.iapws.org/`. `http://www.cheresources.com/iapwsif97.shtml`. (Cited on pages 14, 40 and 49)

[148] N. E. TODREAS and M. S. KAZIMI. *Nuclear Systems I Thermal Hydraulic Fundamentals*. Taylor and Francis, Levittown, Pennsylvania, 1993. (Cited on pages 5, 10 and 21)

[149] N. E. TODREAS and M. S. KAZIMI. *Nuclear Systems II Elements of Thermal Hydraulic Design*. Taylor and Francis, Levittown, Pennsylvania, 1993. (Cited on pages 11 and 49)

[150] M. TOHJOH, M. WATANABE, and A. YAMAMOTO. Three-dimensional pin power reconstruction for the axially heterogeneous region in BWR. *Annals of Nuclear Energy*, 33: 242–251, 2006. (Cited on page 11)

[151] S. VAN CRIEKINGEN. On spatial approximation orders in the VARIANT code. In *Jahrestagung Kerntechnik*, Hamburg, Germany, May 27-29, 2008. (Cited on page 18)

[152] B. VOGT. *Analyse eines Druckwasserreaktors mit überkritischem Wasser als Kühlmittel*. PhD thesis, Universität Stuttgart, July, 2008. (Cited on pages 13, 105 and 118)

[153] B. VOGT, J. STARFLINGER, and T. SCHULENBERG. Near term application of supercritical water technologies. In *International Conference on Nuclear Engineering (ICONE) 14*, Miami, Florida, July 17-20, 2006. (Cited on pages 8, 9, 11, 25, 103 and 104)

[154] A. WANK, T. SCHULENBERG, and A. CLASS. Coolant mixing in the plenum of the HPLWR three pass core. In *International Congress on Advances in Nuclear Power Plants (ICAPP)*, Paper 8100, Anaheim, CA USA, June 8-12, 2008. (Cited on pages 2 and 66)

[155] J. K. WATSON and K. N. IVANOV. Improved cross-section modeling methodology for coupled three-dimensional transient simulations. *Annals of Nuclear Energy*, 29:937–966, 2002. (Cited on pages 10, 35 and 57)

[156] WebElements Periodic Table. `http://www.webelements.com/`. (Cited on pages 144 and 149)

[157] D. WEBER, T. SOFU, D. POINTER, A. TENTNER, Z. ZHONG, T. DOWNAR, J. THOMAS, S. LO, and A. SPLAWSKI. Extension of integrated neutronic and thermal-hydraulic analysis capabilities of the Numerical Nuclear Reactor software system for BWR applications. In *International Conference on the Physics of Reactors (PHYSOR)*, Vancouver, BC, Canada, September 10-14, 2006. (Cited on pages 6 and 7)

[158] D. P. WEBER, T. SOFU, W. S. YANG, T. J. DOWNAR, J. W. THOMAS, Z. ZHONG, J. Y. CHO, K. S. KIM, T. H. CHUN, H. G. JOO, and C. H. KIM. High-fidelity light water reactor analysis with the Numerical Nuclear Reactor. *Nuclear Science and Engineering*, 155(3):395–408, 2007. (Cited on pages 7 and 66)

[159] U. WENDE, R. MÜLLER, and J. HEINECKE. Pin-by-pin full-core subchannel analyses with COBRA 3-CP. In *Jahrestagung Kerntechnik*, Nuremberg, Germany, May 10-12, 2005. (Cited on page 11)

[160] C. WHEELER, D. ROWE, and J. SMIT. An experimental study of axial and crossflow velocity in a 7-pin wire wrapped bundle. Technical Report BNWL-1804, Pacific Northwest Laboratory, February 4, 1984. (Cited on pages 48, 49, 96 and 100)

[161] T. WICKETT, D. SWEET, A. NEILL, F. D'AURIA, G. GALASSI, S. BELSITO, M. INGEGNERI, P. GATTA, H. GLAESER, T. SKOREK, E. HOFER, M. KLOOS, E. CHOJNACKI, M. OUNSY, C. LAGE-PEREZ, and J. I. SÁNCEZ-SANCHIS. Report of the uncertaintly methods study for advanced best estimate thermal hydraulic code applications. Technical Report csni-r1997-35 `http://www.nea.fr/html/nsd/docs/1997/csni-r1997-35.pdf`, Nuclear Energy Agency (NEA) / Committee on the Safety of Nuclear Installations (CSNI), February, 1998. (Cited on page 67)

[162] xmas. ZZ GROUPSTRUCTURES, VITAMIN-J, XMAS, ECCO-33, ECCO2000 Standard Group Structures, January 15, 1991. NEA-1344 `http://www.nea.fr/abs/html/nea-1344.html`. (Cited on page 18)

[163] A. YAMAJI, Y. OKA, and S. KOSHIZUKA. Three-dimensional core design of SCLWR-H with neutronic and thermal-hydraulic coupling. In *GLOBAL*, New Orleans, Lousiana, November 16-20, 2003. (Cited on page 8)

[164] A. YAMAJI, T. TANABE, Y. OKA, J. YANG, J. LIU, Y. ISHIWATARI, and S. KOSHIZUKA. Evaluation of the nominal peak cladding surface temperature of the Super LWR with subchannel analyses. In *GLOBAL*, Tsukuba, Japan, October 9-13, 2005. (Cited on page 10)

[165] A. YAMAMOTO and T. IKENO. Impact of pin-by-pin thermal-hydraulic feedback modeling on steady-state core characteristics. *Nuclear Technology*, 149(2):175–188, 2005. (Cited on pages 11 and 12)

[166] J. YOO, Y. ISHIWATARI, Y. OKA, and J. LIU. Conceptual design of compact supercritical water-cooled fast reactor with thermal hydraulic coupling. *Annals of Nuclear Energy*, 33 (11-12):945–956, August, 2006. (Cited on page 8)

[167] J. YOO, Y. OKA, Y. ISHIWATARI, J. YANG, and J. LIU. Subchannel analysis of supercritical light water-cooled fast reactor assembly. *Nuclear Engineering and Design*, 237(10): 1096–1105, May, 2007. (Cited on page 10)

[168] Y. J. YOO, D. H. HWANG, and D. S. SOHN. Development of a subchannel analysis code MATRA applicable to PWRs and ALWRs. *Journal of the Korean Nuclear Society*, 31(3): 314–327, 1999. (Cited on pages 14 and 48)

Acronyms

3D	three dimensional
BOL	Beginning Of Life
CFD	Computational Fluid Dynamics
CL	fuel CLuster
COBRA	computer program for COolant Boiling in Rod Arrays
COD	Clad Outside Diameter
ERANOS	European Reactor ANalysis Optimized System
EVA	EVAporator
FA	Fuel Assembly
FARP	region-wise Fuel Assembly Relative Power
FARPCL	CLuster-wise Fuel Assembly Relative Power
FPC	Fuel Pin Centerline (temperature)
GIF	Generation IV International Forum
HM	Heavy Metal
HPLWR	High Performance Light Water Reactor
HS	Heat Structures
HTC	Heat Transfer Coefficient
IAPWS	International Association for the Properties of Water and Steam
LWR	Light Water Reactor
MATRA	Multichannel Analyzer for steady state and Transients in Rod Arrays
MCNP	Monte Carlo N Particles
RP	Reactor Physics
RPV	Reactor Pressure Vessel
SCWR	SuperCritical Water cooled Reactor
SH1	SuperHeater 1
SH2	SuperHeater 2
TH	Thermal-Hydraulics
TRACE	TRAC/RELAP Advanced Computational Engine
US NRC	United States Nuclear Regulatory Commission
XS	Cross Section